ÉCOLE DOCTORALE D'ASTRONOMIE ET D'ASTROPHYSIQUE D'ÎLE-DE-FRANCE

THÈSE DE DOCTORAT DE L'OBSERVATOIRE DE PARIS
Spécialité : ASTRONOMIE ET ASTROPHYSIQUE MENTION GÉODÉSIE

Présenté par

Álvaro SANTAMARÍA GÓMEZ

ESTIMATION DES MOUVEMENTS VERTICAUX DE L'ÉCORCE TERRESTRE PAR GPS DANS UN REPÈRE GÉOCENTRIQUE, DANS LE CADRE DU PROJET TIGA

à Paris le 11 Octobre 2010 devant le jury composé de

Nicole CAPITAINE	Président
Eric CALAIS	Rapporteur
Jim RAY	Rapporteur
Félix PÉROSANZ	Examinateur
Marie-Noëlle BOUIN	Directrice de thèse
Guy WÖPPELMANN	Co-directeur de thèse
Jesús GÓMEZ GONZÁLEZ	Invité

Travaux effectués au Laboratoire de Recherche en Géodésie (LAREG)
de l'Institut Géographique National (IGN)
6-8 avenue Blaise Pascal, cité Descartes, Champs Sur Marne
77455 Marne La Vallée cedex 2
FRANCE

DOCTORAL SCHOOL OF ASTRONOMY AND ASTROPHYSICS OF ÎLE-DE-FRANCE

DOCTORAL DISSERTATION OF THE OBSERVATOIRE DE PARIS
Specialty : ASTRONOMY AND ASTROPHYSICS, GEODESY MENTION

by

Álvaro SANTAMARÍA GÓMEZ

ESTIMATION OF CRUSTAL VERTICAL MOVEMENTS WITH GPS IN A GEOCENTRIC FRAME, WITHIN THE FRAMEWORK OF THE TIGA PROJECT

in Paris on October 11th 2010 before the committee constituted by

Nicole CAPITAINE	President
Eric CALAIS	Reviewer
Jim RAY	Reviewer
Félix PÉROSANZ	Examiner
Marie-Noëlle BOUIN	Thesis supervisor
Guy WÖPPELMANN	Joint thesis supervisor
Jesús GÓMEZ GONZÁLEZ	Guest

Research carried out at the Laboratoire de Recherche en Géodésie (LAREG)
of the Institut Géographique National (IGN)
6-8 avenue Blaise Pascal, cité Descartes, Champs Sur Marne
77455 Marne La Vallée cedex 2
FRANCE

Acknowledgments

"We must, however, acknowledge as it seems to me,
that a man with all his noble qualities...still bears in
his bodily frame the indelible stamp of his lowly origin."
Charles Darwin (1809 - 1882)

There are many people that I would like to thank for helping me to make this work possible. Maybe, some of them could end being unnoticed or unsung here. I will try to do my best to avoid this to happen. If I did not succeed, I apologize for those who deserve to be mentioned here and were not.

I thank Jesús Gómez for that short interview in spring 2006. Although I thought it did not come out very well, it finally ended with one of my dreams being realized. I also thank all those people, mainly unknown to me, for making possible the collaboration agreement between both Spanish and French IGN. Especially, I thank Oliver Jamet for his pleasant welcome to the LAREG. Also thanks to Anita Gómez and Danielle Michoud from the Observatoire de Paris for all advice and for helping me with the formalities concerning this doctoral thesis.

Arriving in France without speaking French is not an easy way to start exchanges, so I heartfelt thank all people that kindly helped me at that stage. Sincere thanks to all of you for your patience.

I thank Marie-Noëlle Bouin and Guy Wöppelmann for accepting me and for relying on me to make this work. I sincerely acknowledge them for the dedication and guidance received through this research work. They were very important for introducing me in the scientific GPS processing and for transmitting me the pleasure for geophysics. I appreciate they shared with me their experience, knowledge and also, their scientific point of view. I am grateful for all the opportunities they have offered to me to take part in the international scientific community.

I thank all the scientific and administrative members of the IGN/LAREG which I can proudly call my 'alma mater'. Special thanks to Xavier Collilieux for being a great person, a fantastic colleague and the best geodesy teacher I have ever had. Several discussions with Zuheir Altamimi, David Coulot, Arnaud Pollet and Samuel Nahmani are also gratefully acknowledged. Plenty of discussions with all of them have increased my passion for geodesy and have let me see the tip of the iceberg about reference frames. Also, I appreciate the discussions with Jim Ray from NOAA/NGS during his short visits to the laboratory. Thanks to Christiane Guerin for helping me from the beginning with bureaucracy and with all non-scientific questions, usually related to French customs.

I thank all the scientific and administrative members of the University of La Rochelle for the warm welcome in several short stays. Remote access to the computing facilities of the University of La Rochelle has been a crucial support for this work. Special thanks to Mikael Guichard for always being there to solve arcane computing problems. Marc Boisis-Delavaud's

Table of Contents

Glossary

Main acronyms

AC	Analysis Center
ARP	Antenna Reference Point
AR4	IPCC Fourth Assessment Report
AVISO	Archiving, Validation and Interpretation of Satellite Oceanographic data
BIH	Bureau International de l'Heure
CE	Center of mass of the solid Earth
CF	Center of Figure
CGPS@TG	Continuous GPS station co-located with Tide Gauge
CIP	Celestial Intermediate Pole
CM	Center of Mass of the Earth
CN	Center of Network
cpy	cycles per year
DCB	Differential Code Bias
DORIS	Doppler Orbitography and Radiopositioning Integrated by Satellite
DOY	Day Of Year
ECMWF	European Centre for Medium-Range Weather Forecasts
EOP	Earth Orientation Parameters
ERP	Earth Rotation Parameters
FFT	Fast Fourier Transform
FN	Flicker Noise model
GG	General Gauss-Markov noise model
GIA	Glacial Isostatic Adjustment
GLOSS	Global Sea Level Observing System
GM	first-order Gauss-Markov noise model
GNSS	Global Navigation Satellite Systems
GMF	Global Mapping Functions
GPS	Global Positioning System
GPT	Global Pressure and Temperature model
IAG	International Association of Geodesy
IAPSO	International Association for the Physical Sciences of the Oceans
ICRF	International Celestial Reference Frame
IDS	International DORIS Service
IERS	International Earth Rotation and Reference Systems Service
IGS	International GNSS Service
IGSr	IGS reanalysis campaign
ILRS	International Laser Ranging Service
IOC	Intergovernmental Oceanographic Commission
IPCC	Intergovernmental Panel on Climate Change
ITRF	International Terrestrial Reference Frame

IVS	International VLBI Service
LOD	Length-Of-Day
mas	milliarcsecond
mf	mapping function
MLE	Maximum Likelihood Estimator
δML	Maximum Likelihood ratio
NANU	Notice Advisory to Navstar Users
NMF	New Mapping Functions
NNR	No-Net-Rotation
NWM	Numerical Weather Model
PCO	Phase Center Offset
PCV	Phase Center Variation
PL	Power Law noise model
ppb	parts per billion
PSMSL	Permanent Service for Mean Sea Level
RLR	Revised Local Reference
RW	Random Walk noise model
SLR	Satellite Laser Ranging
SNR	Signal-to-Noise Ratio
SONEL	Système d'Observation du Niveau des Eaux Littorales
TAC	TIGA Analysis Center
TAAC	TIGA Associate Analysis Center
TDC	TIGA Data Center
TIGA	Tide Gauge Benchmark Monitoring project
TOS	TIGA Observing Station
TW	Time-dependent White noise model
ULR	University of La Rochelle
UT1	Universal Time
UTC	Universal Time Coordinated
VLBI	Very Long Baseline Interferometry
VMF	Vienna Mapping Functions
VW	Variable White noise model
WH	White Noise model
WRMS	Weighted Root Mean Squared
ZHD	Zenith Hydrostatic Delay
ZTD	Zenith Tropospheric Delay
ZWD	Zenith Wet Delay

Introduction

Tide gauges worldwide distributed have observed sea level with respect to a point fixed on Earth's crust during decades, starting in the 18th century in a few locations. These sea level observations are termed relative. Long-term relative sea level variations, providing the net sea level rise/drop rate with respect to the coast, are very useful for human communities in order to foresee necessary coastal management actions to be taken into account.

However, from a scientific point of view, what do these long-term variations represent? Thanks to several evidences (ice cores, ocean sediments, geology traces, etc.) we know today that sea level has been continuously varying over the last hundreds of thousands years, mainly due to climate fluctuations between glacial and interglacial periods or eras. Following these glacial and interglacial eras, likely triggered by astronomic cycles of solar insolation, sea level dropped and rose over more than a hundred meters as ice masses advanced and retreated over the Earth's surface, respectively. In addition to this water mass interchange, sea water volume also fluctuates due to changes of its density through temperature and salinity variations. Temperature and ice masses variations are directly related to climate change. Sea level observations are thus a major climate change proxy. Estimates of the long-term sea level variation are then very useful to constraint the sum of these climate-related contributions.

Sea level observations are currently being carried on with tide gauges and satellite altimetry missions. Being altimetry a relative incipient technique (since the seventies), only tide gauges provide a direct observation of long-term sea level variations. However, to be used as climate change proxy, sea level observations must be referred to the Earth's center of mass due to that relative sea level observations are contaminated by vertical crustal movements. Sea level observations referred to the Earth's center of mass are termed absolute. In order to transform sea level observations from relative to absolute, the vertical movements of the Earth's crust (in which tide gauges are settled) with respect to the Earth's center of mass should be then precisely known.

Sea level rise over the second half of the 20th century has been estimated by the Intergovernmental Panel on Climate Change (IPCC) to be around 1.8 mm/yr using tide gauge observations. However, this level rise estimate is, however, somewhat uncertain, resulting in an unsatisfactory closing of the sum of the sea level rise contributors over this period. One of the sources of such uncertainty is indeed the accuracy of the vertical crustal movements. These observations have been usually corrected using models for the Glacial Isostatic Adjusment (GIA). This approach has the advantage to be worldwide and easily applicable. However, tide gauge vertical movements are not only due to isostasy. There are other regional (e.g., tectonics) or local (e.g., volcanism, sedimentation, tide gauge monument instability) movements not predicted by these models. This turns this approach to be inaccurate. Improving the accuracy and confidence of these vertical movements is therefore essential to derive precise absolute sea level trends at tide gauges.

The alternative approach we are focusing here is to directly observe those vertical movements through Global Positioning System (GPS) stations co-located with tide gauges. These vertical velocities have been widely estimated with GPS for different applications. This works represents a contribution to improve the estimation such vertical crustal rates with

GPS. This dissertation is composed of three parts.

In the first part we are reviewing the scientific context: the scientific questions behind past and present-day long-term sea level rise; the natural and socioeconomic consequences of present and future sea level rise; the techniques, with their strengths and weaknesses, used so far to observe sea level. We are discussing why is not so evident to estimate the long-term global sea level rise, that is, which are the inconveniences and the uncertainties of the methodology and data used in such estimation and why the scientific community is not entirely satisfied with the ongoing results. Vertical movements at tide gauges, the core of this work, are one of the weaknesses of the sea level rise problem. In this part we are also exposing how the geodetic community has reacted to solve it, with especial emphasis on the contribution of the University of La Rochelle consortium.

In the second part we are addressing how the vertical velocity estimation methodology can be improved. We will start testing several new models to improve the GPS data processing. The effects of different antenna phase centers patterns and tropospheric refraction models will be assessed. We will also address the geometrical distribution of stations in sub-networks to optimize the GPS processing. We will improve the combination process extracting new products to be used for further quality assessment of the data processing. As part of the velocity estimation, in this part we are thoroughly analyzing the main error sources affecting velocity estimation, as offsets, velocity discontinuities and reference frame uncertainty. Finally, we will assess the velocity field precision by analyzing the type and amplitude of the noise content in time series. The methodology of the noise analysis will be also carefully reviewed.

In the third and last part the quality assessment of the obtained results will be addressed. We will evaluate how much confident our results are. The different obtained products (orbits, EOP, apparent geocenter and terrestrial frame) will be examined and compared to the high-end IGS Analysis Center products, assessing the quality of the implemented GPS data processing strategy and looking for further future improvements. The accuracy of the estimated vertical velocity field will be assessed through the comparison to the velocity solutions from the different space geodetic techniques used to create the last release of the International Terrestrial Reference Frame (ITRF), the ITRF2008. Finally, in this part we are also demonstrating the appropriateness of the estimated vertical velocities to correct relative long-term records of a selected worldwide set of tide gauges.

PART I
CONTEXT

1. Coastal sea level change and vertical land movements

In the Quaternary Period (2.6 Ma to present), Earth's climate showed oscillations between cold (glacial) periods, also known as ice ages, and warm (interglacial) periods. These climate oscillations would be due to changes of the Earth's orbital parameters (obliquity, eccentricity, precession) which induces variations of the solar energy reaching the Earth (orbital forcing) [*Le Treut et al.*, 2007]. Following the Milankovitch orbital theory [*Milankovitch*, 1941; *Imbrie and Imbrie*, 1979], ice ages were generally triggered by a minima in high-latitude North Hemisphere summer insolation, enabling winter snowfall to persist through the year and therefore accumulate to build glacial ice sheets in the North Hemisphere.

Ice ages are directly associated with global sea level change through water mass interchange between oceans and continental ice sheets. During glacial periods, land ice sheets growth results in a global sea level drop and, conversely, during interglacial periods, land ice sheets melting results in a global sea level rise. For instance, the (present-day) ice volumes of the Greenland and Antarctic ice sheets are equivalent to approximately 7 m and 57 m of sea level rise, respectively.

Over the last 740 ka, and especially over the last 430 ka, these glacial-interglacial cycles have been well documented in ice cores, ocean sediments, geomorphology traces, and coral fossil samples [*Jansen et al.*, 2007]. Following these palaeoclimatic evidences, global sea level was between 4 and 6 m higher during the previous interglacial period (125 ka) than in the 20th century. Around 116 ka started the last glacial period in response of the orbital forcing. This last ice age culminated in the Last Glacial Maximum (LGM) about 21 ka BP. At that epoch, where ice sheets covered large parts of North America and Europe, sea level was 120 m lower than present-day level [*Shackelton*, 2000; *Waelbroeck et al.*, 2002; *Peltier and Fairbanks*, 2006]. Between the LGM and the current interglacial period, known as the Holocene epoch, a deglaciation transition period caused sea level to rise rapidly to reach near present-day one. However, this sea level rise was not homogeneous over the last 20 kyr. Holocene records (e.g., coral fossils, geological and archeological sources) indicate that sea level reached present-day level around 5 kyr, being the average sea level rise over the last 2000 years likely nil (between 0 and 0.2 mm/yr) [*Peltier*, 2002; *Lambeck*, 2002]. The origin of the present-day sea level rise probably occurred as early as the 19th century [*Donnelly et al.*, 2004; *Gehrels et al.*, 2004; *Lambeck et al.*, 2004; *Jevrejeva et al.*, 2008]. This is the background in which modern sea level rise is outlined.

Present-day warming of the climate system is unequivocal from observations of increases in global average air and ocean temperatures, widespread ice and snow melting, and global sea level rise. Sea-level is thus a fundamental component to monitor the Earth's climatic system. Past and present long-term sea level estimates are very useful to validate and constrain global climate models [*Solomon et al.*, 2007]. This way, observing long-term sea level variations is essential to better understand how this system works and which the role of the other components is: atmosphere, hydrosphere (excluding oceans), cryosphere, lithosphere and biosphere.

Sea level rise causes a wide range of issues in coastal areas. Through the 20th century, sea level rise contributed to increased coastal degradation with considerable local and regional changes or impacts [*Nicholls el al.*, 2007]. For instance, sea level rise reduces the return period of floods, damages coastal areas (e.g., beaches and cliffs) and infrastructures (e.g., transportation systems and low-lying buildings) through erosion, or threatens natural

ecosystems (e.g., wetlands, salt marshes, coral reefs and deltas) and coastal land uses through saline intrusion. Sea level rise has also an important economic impact, not only due to the cost of these directly-caused issues, but also due to the cost of protecting against these issues. For instance, flooding defenses are being reviewed or newly implemented in some areas and, in developed countries, construction and transportation sectors are paying attention to accommodate anticipated sea level rise [*Nicholls el al.*, 2007]. In addition, sea level rise has a very important sociological impact, being especially critical for island nations and low-lying populated coastal areas like deltas. Population of coastal areas (i.e., up to 100 km distance and 100 m height from coastline) has been estimated up to 1.2 billion. This represents 23% of the world's population and a population density three times higher than inland areas. Sixty percent of cities with a population of more than 5 million and 75% of cities with a population of more than 10 million are located in these areas. In addition, coastal populations are expected to increase rapidly in the next decades for both developed and developing countries [*Wilbanks et al.*, 2007]. Indeed, another direct consequence of global climate change is desertification or increasing drought periods, which will induce large population displacements towards the coasts (e.g. Africa).

The Intergovernmental Panel on Climate Change (IPCC)[1], established in 1988 by the United Nations Environment Programme and the World Meteorological Organization, is a scientific organization leading the assessment of climate change. Its main goal is to review the most recent, rigorous and balanced scientific work relevant to the understanding of climate change. Since its creation, the IPCC has produced a series of Assessment Reports (1990, 1995, 2001), the last one (AR4) being released in 2007. There are, however, many scientists and organizations working on sea level rise with different points of view and, hence, results. In order to synthesize all this research work, I have chosen to use the AR4 conclusions as reference.

From the AR4, it is evident that sea level is recently rising as climate is warming. Sea level variations are driven by changes in sea water volume, which can be decomposed in two sources: changes in sea water density and mass. Changes in water density are due to thermal expansion and salinity changes. Changes in water mass are due to exchange of water between oceans and other reservoirs (e.g., mass changes of ice sheets and mountain glaciers, and land water reservoirs, changes in amount of precipitation/evaporation). However, it is still difficult to define and precisely quantify all causes of sea level rise. Independent estimations of these causes are still highly uncertain (see Section 1.2). Even with a future stabilization of global warming, sea level rise has considerable inertia due to the thermal expansion and ice melting contribution, and it will continue for decades to centuries. In addition, partial melting of terrestrial ice sheets (especially Greenland) would make sea level rise significantly larger, representing a challenge for long-term coastal planning and questioning the viability of the low-lying coastal areas in the future. Thus, to better understand climate change by quantifying these individual contributions and constraining the sum of them, it is absolutely necessary to precisely estimate sea level rise. Two techniques are, at present, capable of directly measure sea level.

1.1. Sea level observations

Two complementary geodetic techniques coexist today to directly observe sea level variations: satellite altimetry (Section 1.1.1) and tide gauges (Section 1.1.2). Other techniques

---

1   http://www.ipcc.ch

do not observe directly sea level, but provide important constraints to indirectly estimate sea level variations (see more details later in Section 1.2). These techniques are based on observations and models of sea temperature and salinity, mass variations in ice sheet and alpine glaciers, and continental water storage [e.g., *Cazenave and Nerem*, 2004; *Cazenave and Llovel*, 2010].

1.1.1. Satellite Altimetry

Satellite altimetry estimates the vertical distance from the satellite to the Earth's surface by measuring the time taken by a short pulse of microwave radiation to travel from the satellite to the Earth's surface and back to the satellite. Actually, to avoid the frequency-dependent effect of the ionospheric refraction, the altimeter uses two microwave frequencies. The best reflected pulses are obtained over the ocean surface, which is spatially homogeneous, and conforms to known statistics. Heterogeneous surfaces, with discontinuities or significant slopes, such as land surfaces, make accurate interpretation more difficult. The measured distance then represents twice the satellite height over the Earth's surface. To derive sea level, the satellite orbit has to be accurately determined relative to an arbitrary and geocentric reference surface. The satellite position is computed through precise orbit determination, combining accurate modeling of the satellite motion and tracking measurements between the satellite and observing stations on Earth. Sea level is then computed as the difference between the satellite altitude and the measured distance. To obtain the correct sea surface height, these distances must be corrected for several phenomena, including propagation delays (ionospheric and tropospheric), tidal variations (ocean, pole and solid Earth) and loading effects. In addition, calibration of the instrumental bias and drifts of the altimeters must be regularly performed to allow a combination of estimates of the different altimetry missions.

Radar altimeters measure sea level along the orbit track projected on the Earth's surface. Orbits have been optimized to cover 90% of the ocean surface, excluding the highest latitudes of polar circles where sea is usually frozen (orbit inclination of 66° for Topex/Poseidon mission). This results in a near-global uniform coverage of repeated (every 10 days for Topex/Poseidon mission) sea level measurements (Figure 1.1).

Altimetry measurements started ending the 70's with the Seasat (1978) mission and continued with the Geosat (1985-1990) and ERS-1 (1991-2000) missions. However, it was not until 1992 with the Topex/Poseidon mission (1992-2006) and its sucessors, Jason-1 (2001-) and Jason-2 (2008-) missions, that global sea level has been measured accurately. This represents less than two decades of altimetry observation. From these data, the global mean sea level rise is estimated to be about 3-3.5 mm/yr [*Beckley et al.*, 2007; *Prandi et al.*, 2009; *Cazenave and Llovel*, 2010].

Altimetry data is archived, validated, processed and distributed by several services of the space agencies operating each satellite mission in the form of geophysical data records (GDR). For instance, the Archiving, Validation and Interpretation of Satellite Oceanographic data (AVISO)[2] continually distributes quality satellite altimetry data from the Topex/Poseidon, Jason-1, ERS-1, ERS-2, and EnviSat missions. The International Altimetry Service (IAS)[3], established in 2007, is an agency-independent service aiming to identify, pool together and coordinate international altimetry resources.

---

2   http://www.aviso.oceanobs.com
3   http://ias.dgfi.badw.de
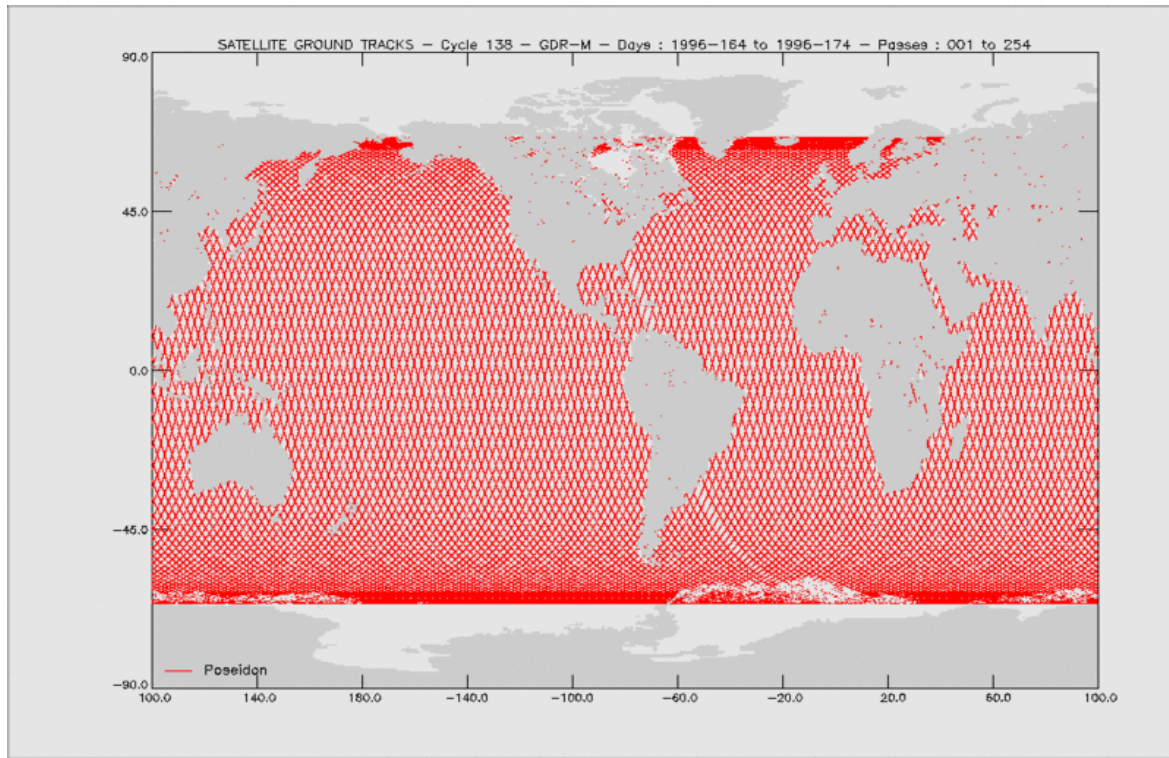
Figure 1.1. Global ocean coverage of a typical Topex/Poseidon 10-day repeat cycle. Source AVISO[2].

Tide gauges data (see next section) had previously indicated that sea level is not rising uniformly. However, the advent of satellite altimetry and its near-global coverage of the oceans made possible, for the first time, the comprehensive mapping of sea level rates variations (Figure 1.2) [*Cazenave and Llovel*, 2010]. Some regions, in particular the western Pacific, exhibit rates of sea level rise up to five times the global mean for the period 1992-2009. In other regions, as the eastern Pacific, sea level trends are negative during this period of time.

1.1.2. Tide gauges

Tide gauges measurements are based on continuously observing the vertical distance between sea surface and a nearby point fixed to the Earth's crust (local reference or benchmark) along continental coastlines, islands or shallow water platforms. This technique provides thus relative sea level observations only near the coast (see Figure 1.3). The vertical distance has been measured through time with different instrumentation as this technique has evolved: from initially a simple graduated rod attached to piers, then with a mechanized floating device in stilling wells over the 19th and most of the 20th century, and more recently with radar, sonar and barometer instrumentation.

Tide gauges have been widely used along the past 20th century mainly to measure water heights and tides at harbors. Their observations span several decades in most sites, providing a few records back to the 18th century (e.g., Amsterdam, Brest, Kronstadt, Liverpool and Stockholm). This way, tide gauges represent the only technique directly observing sea
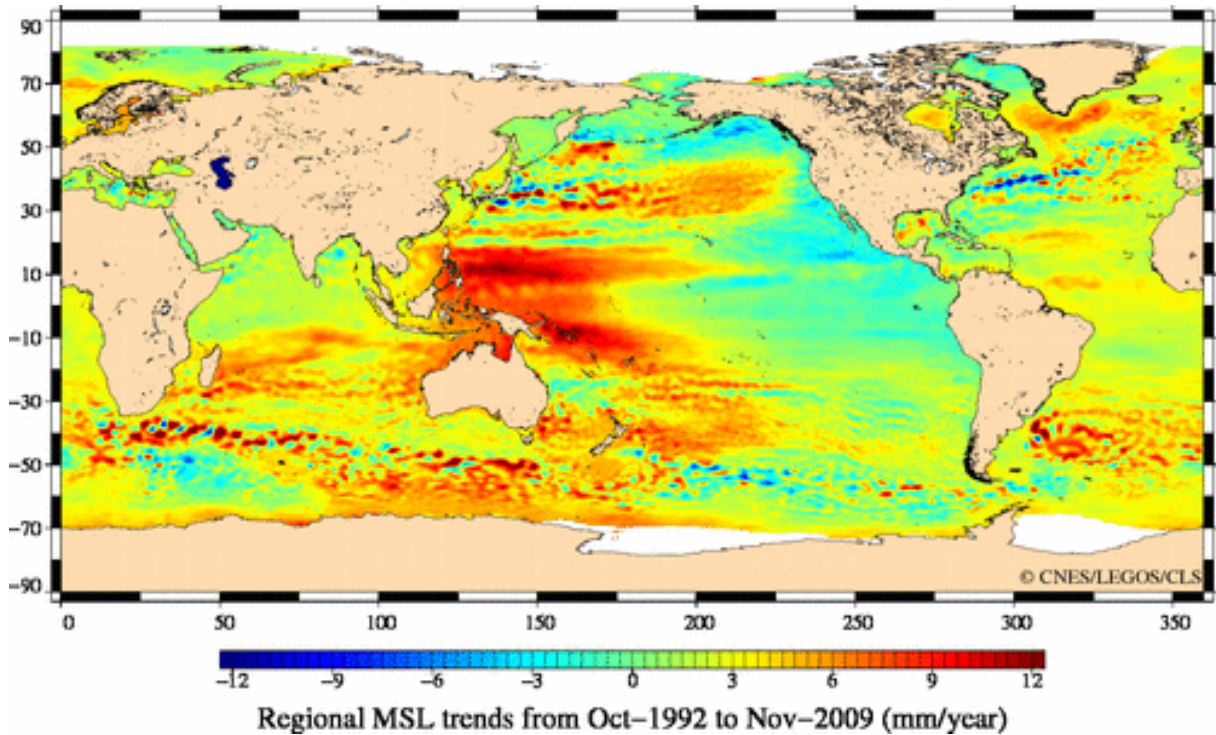
Figure 1.2. Sea level trend variability (1992-2009) from multi-mission data. Source AVISO[2].

level variations over long periods (more than a few decades).

The Permanent Service for Mean Sea Level (PSMSL)[4], established in 1933, is responsible for the collection, publication, analysis and interpretation of sea level data from tide gauges. It constitutes the largest data set with more than 2000 tide gauge records (Figure 1.3). This data base contains however a noticeable bias between the Northern and Southern Hemispheres. In addition, spatial distribution of the tide gauges was also notably sparse ending the 19th century (see Figure 1.3 b). This situation improved through the 20th century (Figure 1.3 c and d). However, only two thirds of these stations have their records reduced to a common datum, mandatory for sea level time series analysis. Through their long existence, tide gauges can be repaired, moved or upgraded. For sea level time series analysis, the local reference of the tide gauge (tide gauge benchmark) must be known to keep consistency along the record history, especially when large data gaps exist. This consistency is maintained by means of regular gauge calibration and precise leveling. These high quality controlled records are termed Revised Local Reference (RLR) set at the PSMSL.

1.2. Long-term sea level rise estimation

In view of their respective characteristics, altimetry and tide gauges are complementary techniques, in both spatial and temporal domains. While tide gauges geographic distribution is sparse (limited to shorelines mostly along populated areas), altimetry provides a regular global pattern up to 66° latitude (for Topex/Poseidon and Jason missions). However, while precise satellite altimetry has started in the 90's with ERS-1 and Topex/Poseidon missions, tide gauges usually provide records of several decades, and for a few of them over more than

---

4   http://www.pol.ac.uk/psmsl
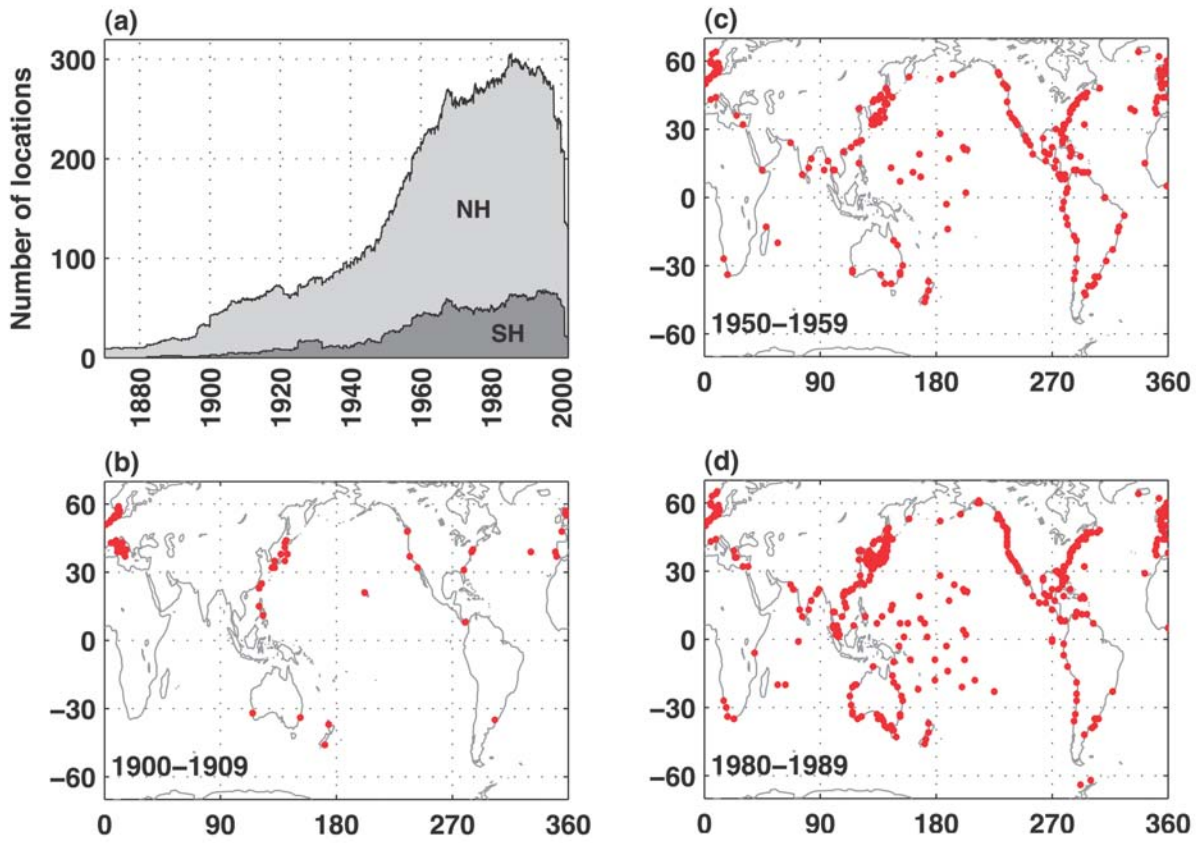
Figure 1.3. PSMSL tide gauges data set distribution over time and between hemispheres. Source AR4[1].

et al., 2004; *Church and White*, 2006; *Berge-Nguyen et al.*, 2008; *Llovel et al.*, 2009]. This method however neglects sea level variability at different time scales (e.g., thermal expansion changes), which could imply different spatial patterns too. Figure 1.4 shows the sea level estimates with tide gauge and altimetry data (both directly observations and reconstruction). The improvement in the sea level reconstruction error is due to the time increasing number of available tide gauges (see Figure 1.3). Both techniques exhibit good agreement for the common time period of the last 50 and 10 years, respectively. From these data, the AR4 concluded that sea level rose at a rate of 1.8 ± 0.5 mm/yr from 1961 to 2003 and at a rate of 3.1 ± 0.7 mm/yr from 1993 to 2003.

The higher rate consistently estimated by both techniques [*Prandi et al.*, 2009] since 1993 may reflect sea level interdecadal variability instead of a recent acceleration of sea level rise. This phenomenon, likely related to internal variability of the ocean-atmosphere system, was described by *Holgate* [2007]. Using continuous and long tide gauge records, the author found decadal sea level rise rates of up to 5.3 mm/yr or even negative trends. Due to these interdecadal sea level variations, satellite altimetry is currently unable to assess long-term sea level rise. At least, several more decades of altimetry data are needed to properly estimate long-term sea level rise. Although future sea level observations will be likely mainly based on satellite altimetry, tide gauge data constitute today the only technique available to observe long-term sea level rise [e.g., *Douglas*, 2001; *Church et al.*, 2004; *Church and White*, 2006; *Holgate*, 2007]. Therefore, this technique is still indispensable to compare past and present-day sea level estimates and detect a possible acceleration. Due also to their high temporal res-
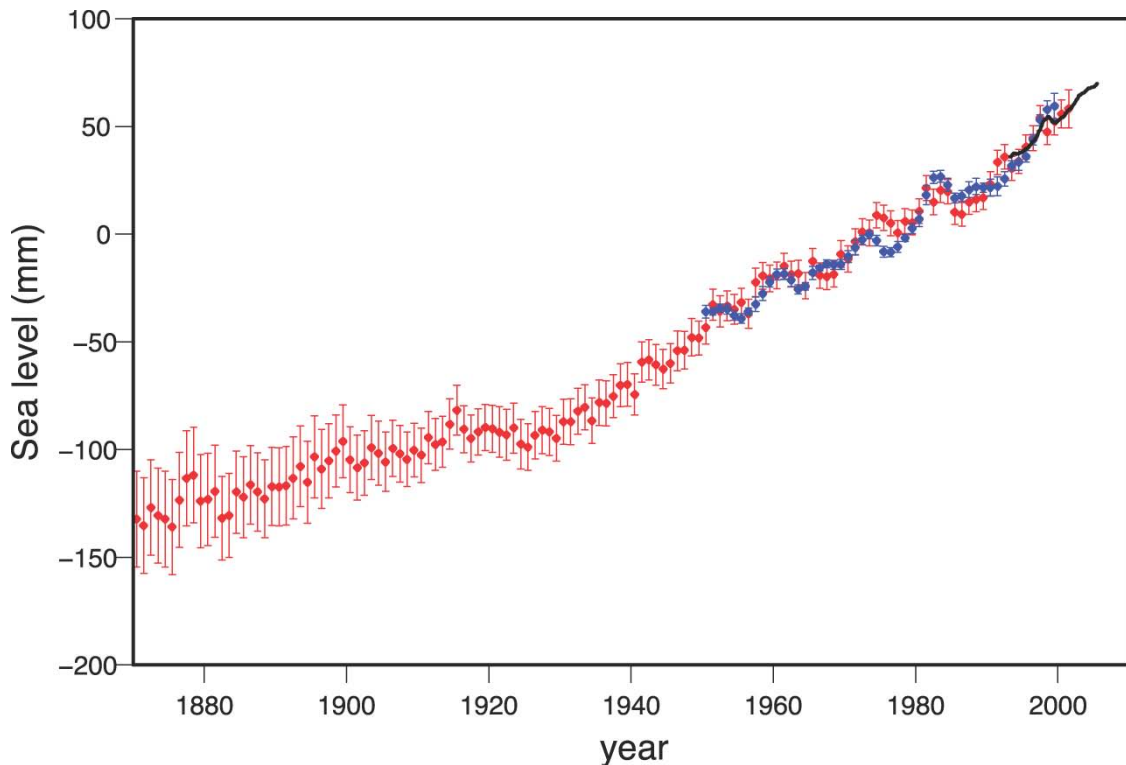
Figure 1.4. Global mean sea level estimates with satellite altimetry (black), tide gauges (blue) and sea level reconstruction (red). Source AR4.

olution, tide gauges are essential to other applications like observing storm waves or tsunamis. In addition, tide gauge observations are still necessary to calibrate satellite altimeters [*Mitchum*, 2000].

The main issue of the twentieth century sea level rise estimated from tide gauge data is however the so-called "enigma" [*Munk*, 2002], "puzzle" [*Douglas and Peltier*, 2002], or "attribution" [*Woodworth*, 2006] problem. As shown in Figure 1.5, the sum of the individual climate contributors to sea level rise differs from the tide gauge estimation by 0.7 ± 0.7 mm/yr. This is the same difference reported in the past AR3 when the enigma of 20th sea level rise was acknowledged. In other words, the observed sea level rise cannot be fully explained by the observed/modeled individual climate contributors. This difference is reduced for the 1993-2003 decade estimates, where sea level rise is mainly driven by thermal expansion (see Figure 1.5). Although both long-term sea level rise estimations (tide gauge observation and sum of climate contributors) are statistically consistent considering their large uncertainties, this situation is not satisfactory [*Woodworth*, 2006]. To improve the understanding of sea level rise and its causes, it would be desirable to reduce this discrepancy together with the estimation uncertainties.

There are obviously only two possible sources for this discrepancy: a biased estimation of the individual climate contributors and/or a biased tide gauge observation. Bias of the individual climate contributors estimation could come from a underestimated thermal expansion effect, the uncertainty of the mass change in the ice sheets and mountain glaciers or the unaccounted effect of other contributors (salinity changes, terrestrial reservoirs changes)
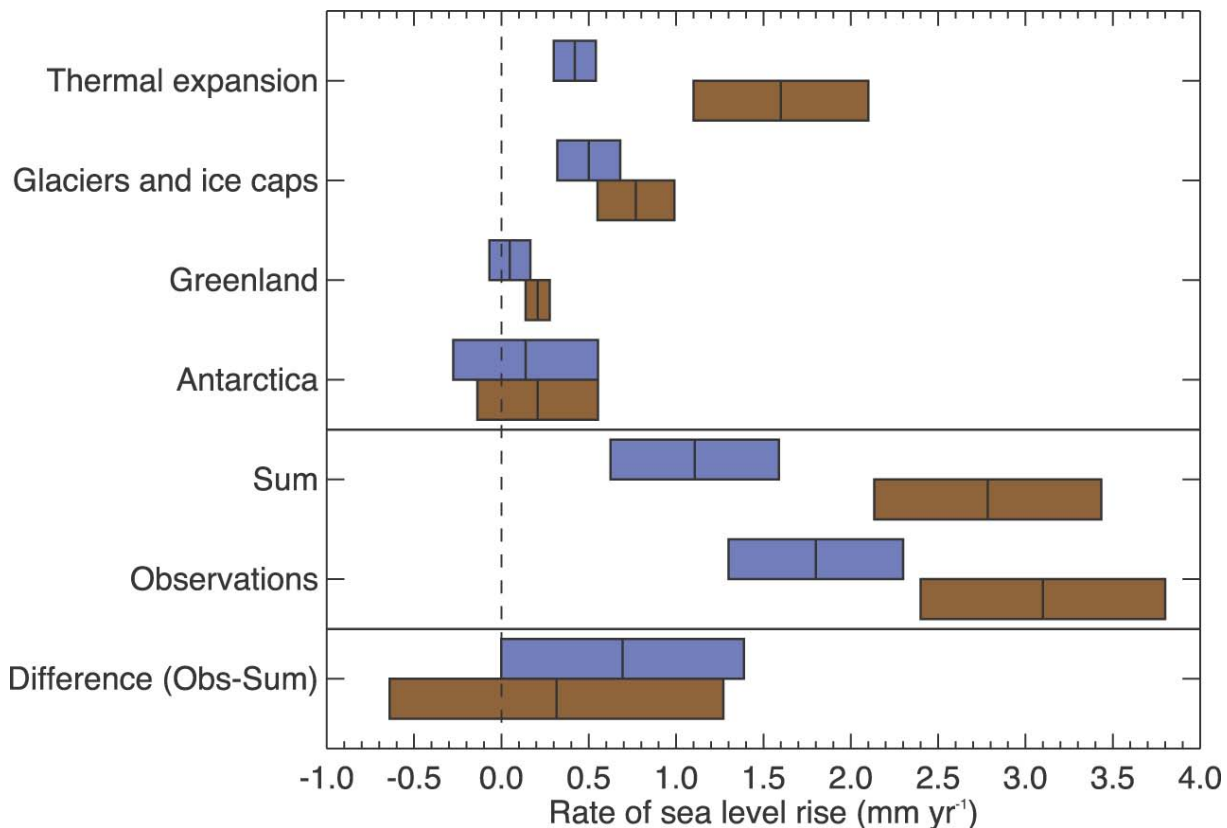
Figure 1.5. Sea level rise estimation for various individual climate contributors (top), for the sum of the climate contributors and for the directly observed estimation (middle), and the difference between them (bottom). Values are for the 1961-2003 (blue) and 1993-2003 (brown) periods. Bars are 90% error range. Source AR4.

[*Cazenave and Nerem*, 2004]. The estimations of these contributors improve throughout time as more data become available. For instance, for the 1993-2003 decade, the observed sea level rise value agrees more closely with the sum of the individual contributors than for the last half century, nearly closing the sea level budget (see Figure 1.5).

Bias of the tide gauge estimation could come from two different effects: the geographical distribution of the tide gauges and their vertical movements.

The first source of error is due to the fact that if sea level rise were spatially homogeneous, only one high quality long tide gauge record could be used to estimate global sea level rise. However, as shown in Figure 1.2, sea level trends are not homogeneous. Satellite altimetry has proven that there are regional sea level variations at decadal timescales. This effect coupled with the geographical distribution of tide gauge records (only in coastlines, mostly in North Hemisphere) could be a main issue to properly estimate global sea level rise. Some authors [e.g., *Douglas*, 2001] recommend using only very long records (60 years or more) to avoid the effects of this interdecadal variability. These long records are only available for some tens of tide gauges of the RLR set and are mainly located in Europe and North America (see Figure 1.3). The idea behind this approach is that even a limited set of poorly distributed tide gauges could filter the decadal and multi-decadal sea level variations.

In other words, the spatial variations would be less significant over very long-term records. However, tide gauge data, GIA and ocean circulation models suggest that this spatial variability could be significant over much longer timescales [*Mitrovica et al.* 2001; *Woodworth*, 2006]. This way, a low-frequency spatial-variable sea level rise sampled with a sparse data set could bias the estimation of the global sea level rise. Though some filtering is expected when the data from the different gauges are averaged, the uncertainty caused by these ocean signals on the estimated global sea level rise could still be large. This major issue is still open within the scientific community [*Cabanes et al.*, 2001; *Tamisiea et al.*, 2001; *Miller and Douglas*, 2004, 2006; *Plag*, 2006]. To provide definitive conclusions, future research will be useful to know the magnitude and the impact of the interannual, decadal, and interdecadal variability of mean sea level at the global scale.

The second source of error, and a major difficulty in estimating long-term sea level variation from tide gauges, consists in that tide gauge records are relative to the Earth's crust, which is also affected by vertical movements with respect to the Earth's center of mass. These coastal relative sea level observations are valid to analyze local impacts. However, to understand sea level rise and to evaluate the impact of sea level projections at coastal locations, vertical land movements must be determined. These vertical land movements at tide gauges represent the core of this work and are discussed in the next section.

1.3. Vertical movements at tide gauges

As already shown, sea level rise estimation from tide gauges for the second half of the 20th century is under 2 mm/yr. For shorter periods of time, satellite altimetry (in agreement with tide gauges) has shown regional sea level trends of ± 12 mm/yr. The same range of vertical rates can exist for the land upon which the gauges are situated [e.g., *Wöppelmann et al.*, 2007], mitigating or accentuating the relative sea level rise from climate contributions at the coast. Therefore, vertical rates of tide gauges must be taken into account and corrected for. Otherwise, long-term sea level trends from tide gauges will remain contaminated by this error. For instance, the large sea level rise uncertainty for the last half century, as stated in the AR4 (± 0.5 mm/yr), actually reflects the broad band of sea level rise estimates for that period. These estimates, while using the same tide gauge data set, are still different due to the methods used to correct for the vertical movements at tide gauges [*Douglas and Peltier*, 2002]. In this sense, *Mitchum* [2000] also pointed out that unknown vertical movement is one of the main errors when tide gauges are used to calibrate satellite altimeter drift.

Vertical land movements at tide gauges are a consequence of a wide range of phenomena, resulting in a similar wide range of time and spatial frequencies.

In the spatial domain, there are two kinds of vertical movements. Those who affect large regional areas and those local or specific to a tide gauge. The first kind of vertical movement mainly corresponds to the Glacial Isostatic Adjustment (GIA). This phenomenon consists in the viscoelastic response of the Earth's crust, the upper mantle, and the lower mantle to long-term ice mass variations. GIA effect decays exponentially in time since the LGM based on the Earth's viscosity, but it is still significant today [e.g., *Sella et al.*, 2007; *Khan et al.*, 2008]. For instance, large high-latitude areas (e.g. Fennoscandia, the Laurentides) currently undergo rapid uplift (up to 7-8 mm/yr). Nevertheless, GIA does not only produce crustal uplift near the centers of former ice sheets, but also subsidence in peripheral areas due to mantle mass flow to restore isostatic equilibrium. GIA is the only geodynamical process for which there are available models capable to predict vertical land movements at tide gauges

[e.g., *Tushingham et al.*, 1991; *Davis and Mitrovica*, 1996; *Milne et al.*, 2001; *Peltier*, 2001; 2004; *Paulson et al.*, 2007]. However, different GIA models predict different radial rates due to the unknown spatial and temporal variability and uncertainties on some fundamental parameters like the mantle viscosity, the lithosphere thickness and the ice sheets history since the last glacial maximum [*Argus and Peltier*, 2010].

In addition, GIA models do not take into account vertical movements related to different phenomena. There are other geophysical or human related effects that may cause significant uplift or subsidence at different time-scales. Short-term movements may be due to seismic displacements, volcanic deformations, collapse of the tide gauge support, etc. Tidal and seasonal movements are due, for instance, to atmospheric, oceanic and present-day ice mass loading. Long-term movements, assumed to be constant for the period of time for which we dispose of direct sea level observations, may be due to tectonic processes (interseismic velocities in subduction zones) [e.g., *Bergeot et al.*, 2009], continental water storage loading [e.g., *Fiedler and Conrad*, 2010], sedimentation or instability of the tide gauge support [e.g., *Schenewerk et al.*, 1999]. All these processes are generally not or incompletely modeled, and therefore not accounted for in global sea level trend studies.

Since vertical movement of tide gauges cannot be properly predictable, the rigorous approach is then to directly measure it [e.g., *Carter et al.*, 1989; *Carter*, 1994; *Neilan et al.*, 1998; *Blewitt et al.*, 2006]. Since more than a decade, two space geodetic techniques have become available to monitor vertical movements at tide gauges: the Doppler Orbitography and Radiopositioning Integrated by Satellite (DORIS) and the Global Navigation Satellite Systems (GNSS). This last technique is mainly represented by the Global Positioning System (GPS). Absolute gravity constitutes a third available and independent geodetic technique bringing some clue on vertical deformation. Between these three techniques, GPS is the most precise and easy to use.

Despite their limitations, GIA predictions are still widely used to correct vertical movements at tide gauges [e.g., *Church and White*, 2006; *Holgate*, 2007; *Douglas*, 2008; *Jevrejeva et al.*, 2008; *Llovel et al.*, 2009; *Prandi et al.*, 2009] and also satellite altimetry estimations [*Cazenave et al.*, 2008; *Ablain et al.*, 2009; *Leuliette and Miller*, 2009]. This is mostly due to its ubiquitous and easy application. Nevertheless, some recent studies using GPS velocities to correct tide gauge trends have shown very encouraging results [e.g., *Sanli and Blewitt*, 2001; *Snay et al.*, 2007; *Wöppelmann et al.*, 2007; *Mazzotti et al.*, 2008].

For tide gauges co-located with a GPS station, their estimated vertical velocity can be used to correct the long-term relative sea level record from the vertical land movement. This way, tide gauge records would contain exclusively climate-related long-term sea level variations. However, with this approach, two hypotheses must be adopted. First, we assume that vertical velocities estimated with GPS are constant over the last century. And second, we assume that the vertical velocity estimated with GPS is representative of the tide gauge support velocity.

First hypothesis is supported by the fact that for the 20th century, long period land movements affecting tide gauges (GIA and plate tectonics movements) can be considered constant at most sites. Several authors [*Woodworth*, 1990; *Gornitz and Solow*, 1991; *Douglas*, 1992; 2001] analyzed long (>60 yr) relative RLR tide gauge records and no conclusive evidence of acceleration was found. This demonstrates that vertical crustal movements, as recorded by relative long records, are likely constant and they are absorbed by a linear trend. A small but significant acceleration was found however in reconstructed global sea level back

to the 19ᵗʰ century [*Church and White*, 2006] (see red dots in Figure 1.4). Second hypothesis depends on the relative local stability between tide gauges and GPS stations [*Bevis et al.*, 2002]. If this stability is not ensured (e.g., tide gauge installed on an unstable peer), then both stations should be as close as possible to avoid any bias in the vertical movement correction applied. Conversely, if this stability is ensured (e.g., tide gauges on bedrock foundation), distance between both co-located techniques is a less critical issue. In any case, the relative stability of the co-located instruments must be periodically monitored by means of high precision leveling or by applying the dual-GPS approach [*Teferle et al.*, 2002].

The next chapter deals with how the international community has organized itself around the scientific problem of monitoring vertical movements at tide gauges with GPS. I also present the framework of my study.

2. International efforts to monitor tide gauge benchmarks

This chapter deals with the itinerary followed by the international scientific community to solve the problem of the vertical motion at tide gauges. A description of the first steps is given in Section 2.1. The international efforts ended up with the creation of the TIGA Pilot Project by the IGS (Section 2.2). The contribution of the University of La Rochelle Consortium, in which this research work is framed, is finally described in Section 2.3.

2.1. First steps

GPS satellites started to orbit the Earth around 1978, but it was not until 1983 that the system was made available for civilian use, after the tragedy of the commercial flight KAL007. Shortly after this epoch, the Commission on Mean Sea Level and Tides (CMSLT) of the International Association for the Physical Sciences of the Oceans (IAPSO) and the Global Sea Level Observing System (GLOSS) expressed the need for unifying the vertical tide gauge references in a common global reference system and for monitoring their vertical land movements to compare tide gauge and satellite altimetry techniques (Seasat and Geosat missions, see Section 1.1.1). This way, in 1988 the CMSLT organized a meeting between tide gauge and geodesy experts at the Woods Hole Oceanographic Institution, in USA. One of the main conclusions of this first meeting was that tide gauge benchmarks should be connected to the International Terrestrial Reference Frame (ITRF), realized at that epoch with Very Long Interferometry Baseline (VLBI) and Satellite Laser Ranging (SLR) techniques. The link between those fundamental stations and tide gauges should be realized through iterative GPS campaigns [*Carter et al.*, 1989]. With this new geodetic technique, setting up an easily-to-access and global reference system at tide gauges became achievable, even before the Navstar constellation was completed. This way, tide gauge benchmarks would have geocentric coordinates which should be stored at the PSMSL along with the sea level data.

From its beginning, the GPS system has been continuously evolving, for both the satellite constellation and the receivers, which become gradually cheaper and reliable. Since 1990 the number of permanent GPS stations increased very quickly. In 1993, the Navstar constellation reached its final configuration of 24 satellites and then the Initial Operational Capability of the system was declared. Also in this year, the International Association of Geodesy (IAG) recognized the International GPS Service (IGS, today International GNSS Service), which began its routine operations on January 1994. Since its inception, IGS plays a decisive role in promoting and developing the GPS technique through its models, products and structure. At the same time, a follow-up meeting of the tide gauge and geodesy communities, also supported by the IAPSO, took place at the Institute of Oceanographic Sciences, in Godalming, UK. A report on the started recommendations from the last meeting was made in which first results of the SELF, EUROGAUGE and other national projects were shown [e.g., *Ashkenazi et al.*, 1994; *Zerbini et al.*, 1996; *Becker et al.*, 2002]. The main conclusion of this meeting was that, following IGS procedures, continuous GPS stations should be installed at about 100 tide gauges world-wide to form a core network of a global absolute sea level monitoring system [*Carter*, 1994].

In 1997, at the Jet Propulsion Laboratory (USA), an interdisciplinary workshop on this topic was jointly organized by the IGS and the PSMSL together with the 5th Session of the Intergovernmental Oceanographic Commission (IOC) GLOSS Group of Experts (GE). This

workshop was dedicated on how the GPS and tide gauge techniques can be applied together to study long-term absolute sea level variations and to calibrate the satellite altimeters drift. In 1994 the first permanent GPS stations started operating near tide gauges. However, GPS campaigns were still the main approach for monitoring tide gauges. In this workshop, the IGS was encouraged to include some additional stations co-located with tide gauges into its global GPS network and to produce vertical velocity estimates in an annual basis [*Neilan et al.*, 1998][1]. Since this workshop, the number of permanent GPS stations at tide gauges increased quickly replacing campaign-mode observations.

In 1999, a fourth meeting took place in Toulouse together with the 6th GLOSS GE meeting. In this meeting a Joint Working Group[2] on "How to operate GPS stations at tide gauges" (CGPS@TG) was created between IAG, IAPSO, IGS, PSMSL and GLOSS. The sea level community aimed at estimating the vertical position at tide gauges with an accuracy of 1 cm (for satellite altimeter calibration) and the corresponding vertical rates with accuracy better than 1 mm/yr (for long-term sea level studies), within a well-defined geocentric reference frame. Within such a challenging goal, the task of the Working Group was to provide standards of instrumentation, installation and operational procedures for GPS stations at tide gauges [*Bevis et al.*, 2002].

Although recommendations from the CGPS@TG Working Group are mainly focused on the practical aspects of managing CGPS@TG stations, it was also recommended to address the GPS data processing issues. For instance, existing GPS solutions showed significant discrepancies within the height time series. The need for an IGS Pilot Project on this topic was raised in 2001 at the 7th GLOSS GE meeting in Hawaii. This project would be dedicated to bring the expertise of the IGS community to develop an optimal GPS data processing strategy taking advantage of the existing IGS infrastructure to precisely estimate vertical positions and velocities at tide gauges. Thus, in 2001, at the 16th IGS Governing Board meeting in Nice, the Tide Gauge Benchmark Monitoring (TIGA) Pilot Project was established by the IGS. The objectives and structure of this project are described in the next section.

2.2. The TIGA Pilot Project

The GPS Tide Gauge Benchmark Monitoring (TIGA)[3] is a pilot project of the IGS for establishing a service to analyze GPS data from stations at or near tide gauges on a continuous basis (CGPS@TG). My research work lies within the framework of this project.

The primary goal of TIGA is to provide homogeneous height position and vertical velocities of the CGPS@TG stations. This implied, from the early stage of the project, the reprocessing of a significant part of the IGS data. Other objectives of the TIGA project are:

– To establish and expand a global CGPS@TG network oriented towards long term sea level variation and satellite altimeter calibration studies. TIGA promotes and disseminates the technical recommendations from the CGPS@TG Working Group for the scientific implementation of GPS-equipped tide gauge systems.

– To contribute to the IGS realization and densification of a global terrestrial reference frame.

---

1 Proceedings available at http://igscb.jpl.nasa.gov/igscb/resource/pubs/psms.pdf
2 http://www.soest.hawaii.edu/cgps_tg/
3 http://adsc.gfz-potsdam.de/tiga/index_TIGA.html

The products of the pilot project contribute to climate change studies and other oceanographic activities by correcting vertical land movements at tide gauges. These corrections facilitate the distinction between absolute and relative sea level records, and they will reduce the calibration errors of satellite altimeters.

To reach these objectives, TIGA implemented a structure based on four main components:

- TIGA Observing Stations (TOS) (Section 2.2.1).
- TIGA Data Centers (TDC) (Section 2.2.2).
- TIGA Analysis Centers (TAC) (Section 2.2.3).
- TIGA Associate Analysis Centers (TAAC) (Section 2.2.4).

2.2.1. TIGA Observing Stations (TOS)

Observing stations included in the project consist of GPS stations co-located at or near tide gauge stations fulfilling some additional and special requirements. In order to assess the long-term stability of the co-location with an accuracy of better than 1 mm/yr, all tide gauge benchmarks and the GPS station marker should be leveled on a routine basis. However, these regular leveling observations are often neglected, especially if the co-location distance is more than 1 km. Therefore, only leveled CGPS@TG stations are retained in TIGA. Stations not belonging to the IGS network are also included, provided that they satisfy the guidelines of official IGS sites[4]. For instance, one of the IGS requirements is the free access to the data. On the contrary, IGS data latency requirements were set much more flexible (460 days) within TIGA as the project is focused on long term signals. Latency is less mandatory than data availability at the processing stage. In addition to those IGS and leveling requirements, at least monthly mean sea level values of the tide gauge should be provided to the PSMSL.

In 1999 a survey was carried out by Wöppelmann and others to identify the existing permanent GPS stations located within approximately 10 km from a tide gauge. In a progress report of this survey presented at the 7th GLOSS GE in 2001, an action item was agreed to update this survey at regular intervals, being the last one released in 2007[5]. From this progress report the survey is permanently updated on the Internet[6]. In this survey, 285 worldwide CGPS@TG stations were identified (see Figure 2.1), following a constant increment since 1999. From these stations, 131 are co-located with tide gauges committed to GLOSS (red squares in Figure 2.1), i.e. meaningful tide gauges for the oceanographic community.

However, only 77% of the CGPS@TG stations were identified as freely providing data on the Internet. Taking into account all the above-mentioned constraints, Figure 2.2 shows the global distribution of the TOS network. At this moment, 107 stations are committed to TIGA, among them 52 are GLOSS tide gauges.

2.2.2. TIGA Data Centers (TDC)

Data Centers are required to retrieve, store and make freely available the GPS data of the TOS network. For the tide gauge data, the TDC are not committed to store or provide these data but are supposed to establish links to official tide gauge data centers (e.g., PSMSL).

---

4   http://igscb.jpl.nasa.gov/network/guidelines/guidelines.html
5   Available in http://www.sonel.org/stations/cgps/surv_update.html
6   http://www.sonel.org/-CGPS-TG-Survey-.html
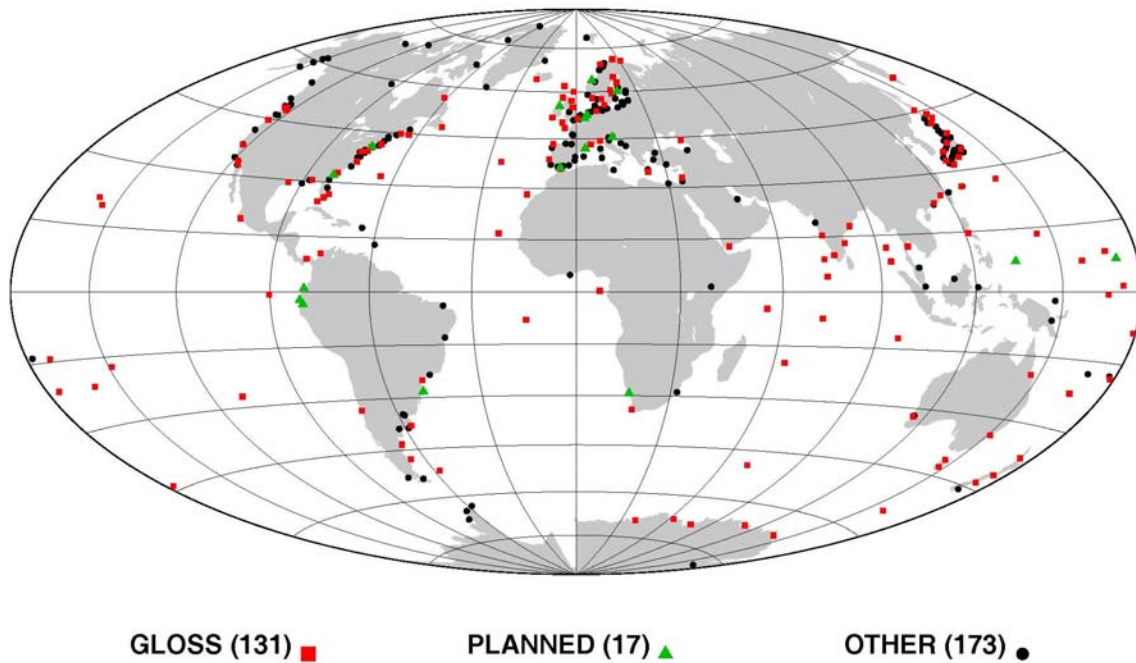
Figure 2.1. Worldwide distribution of CGPS@TG stations. Source CGPS@TG survey[4].
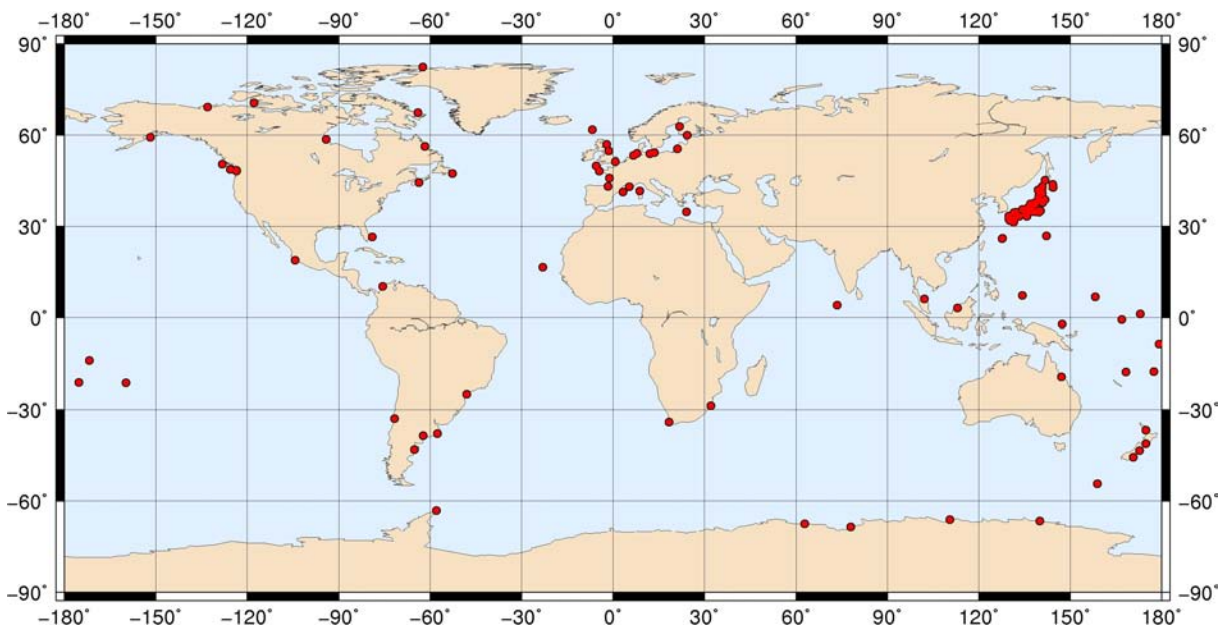
Figure 2.2. TIGA Observing Station network.

There is only one TDC: the University of La Rochelle (ULR), in France. The ULR TDC[7] was set up in 2001 to support the scientific community working on the CGPS@TG topic, especially in the frame of the TIGA pilot project. This data center is a component of the French national sea level observation infrastructure (SONEL), which is constituted by a

7   ftp.sonel.org

national component (French tide gauge data) and an international component (CGPS@TG data). In addition, ULR TDC also provides the ULR coordinate and velocity solutions estimated at the ULR TIGA Analysis Center (see Section 2.3), and expects to expand this facility to the other TAC solutions and hopefully the combined TIGA solution, once a TAAC becomes operational (see Section 2.4).

2.2.3. TIGA Analysis Centers (TAC)

TIGA Analysis Centers are in charge of processing the TOS network following the IERS Conventions[8] with special emphasis on the vertical component. In addition to TOS, TAC include in their processing networks a subset of IGS reference stations to realize a common reference frame. They can also include other non-TOS or non-IGS stations to achieve a homogeneous spatial network.

A second main objective of TAC is to study the vertical accuracy of the GPS coordinates and rates, and to provide advice on their improvement. This way, every time a new modeling advance or a new improved reference frame are available, TAC should perform a new reprocessing of all the available GPS data of the TOS network.

At this moment there are six centers contributing to the project (Figure 2.3):

- GeoScience Australia (AUT), Australia.

- Consortium of the University of Canberra, the University of Tasmania and the Australian National University (CTA), Australia.

- IAG EUREF sub-commission (ETG), Germany.

- Deutsches Geodätisches ForschungsInstitut (DGFI), Germany.

- GeoForschungsZentrum Potsdam (GFZ), Germany.

- Consortium of the University of La Rochelle (ULR), France (see Section 2.3).
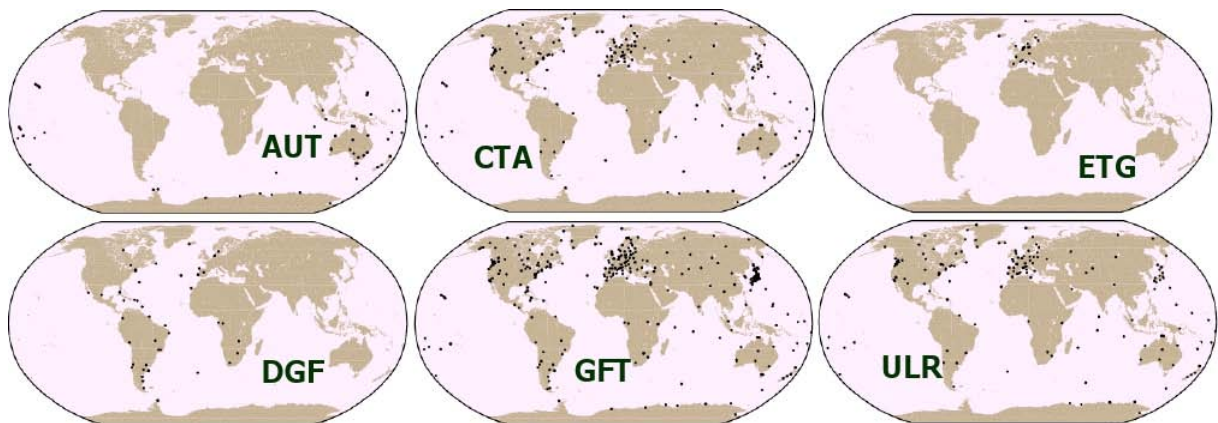
Figure 2.3. Processing networks of the TIGA Analysis Centers.

Among these TAC, only GFZ and ULR have processed global networks from the very beginning of TIGA. Later on, CTA also moved on a global tracking network. The other three

---

8   http://www.iers.org/IERS/EN/DataProducts/Conventions/conventions.html

TAC process a regional network. These regional network solutions must be combined with the global solutions (in a weekly solution basis) in order to assess the realization of a common reference frame [*Schöne et al.*, 2009]. *Legrand et al.* [2010a; 2010b] (see Annex D) compared both regional and global network approaches and evidenced some bias in the reference frame realization when using the regional approach.

2.2.4. TIGA Associate Analysis Centers (TAAC)

TIGA Associate Analysis Centers are required in order to combine the individual weekly solutions of the TAC. However no TAAC is operational to date. Thus, most of scientific results published are based on the individual TAC solutions [e.g., *Tregoning et al.*, 2004; *Tregoning and van Dam*, 2005; *Ge et al.*, 2005; *Schoene*, 2006; *Sanchez and Krügel* 2006; *Wöppelmann et al.*, 2007; 2009; *Zhang et al.*, 2007; *Bouin and Wöppelmann*, 2010]. Being ULR TAC the first global solution to be published. Only *Schöne et al.* [2009] used a preliminary TIGA combined solution for the reconstruction of sea level anomalies using GPS-corrected tide gauges and altimetry data. In that preliminary TIGA combined solution, only ULR provided a global solution necessary for the combination of regional TAC solutions. Future steps of TIGA project will be directed towards a full combination of the TAC individual solutions [*Schöne et al.*, 2009].

2.3. The University of La Rochelle TIGA Analysis Center

The ULR TAC activities started in October 2002 as a consortium between the Earth Sciences laboratory (CLDG, for *Centre Littoral de Géophysique*) of the University of La Rochelle and the geodetic laboratory (LAREG, for Laboratoire de Recherche en Géodesie) of the French national mapping agency (IGN, for *Institut Géographique National*).

ULR TAC objective since its inception was to reprocess, as much as possible, all the available GPS data of the CGPS@TG stations, not only those stations committed to TIGA. The aim was to set up the infrastructure anticipating future stations availability. The reprocessing of the data improves the long-term stability of the reference frame and allows including lately delivered ULR TDC data.

In general GPS processing at ULR TAC is based on double-differenced ionosphere-free phases used to estimate station positions, orbits, Earth Orientation Parameters and zenith tropospheric delays among other parameters. The following scientific software are used at the ULR TAC:

– GAMIT/Globk package [*Herring et al.*, 2006a; 2006b], used for processing GPS data, and

– CATREF [*Altamimi et al.*, 2007], used for combination of GPS coordinate solutions, reference frame definition and velocity estimation.

Since its creation in 2002, the ULR TAC has continuously evolved, improving the GPS processing strategy and densifying the global tracking network. This led to a series of ULR solutions, termed from ULR1 to ULR4 (this work).

The first GPS network reprocessed at ULR TAC (ULR1 solution) was composed of about 140 stations, among which 120 were CGPS@TG stations [*Wöppelmann et al.*, 2004; 2008]. ULR1 solution contained data from 1997 to 2003. Computing facilities used at that time consisted in a Linux Pentium III with 750 MB of RAM. With that infrastructure,

processing a day of data took almost 24 hours. This represented an unacceptable situation to fulfill the objective of reprocessing backwards the entire GPS data set and even to repeat the process when improved models or new processing strategies were implemented. In 2003, the situation improved with the setting up of a temporary pool of 7 to 9 computers, although 7 of them were used only at night because they were being friendly shared with other ULR laboratories.

In 2006, ULR1 solution became obsolete due to the advent of the absolute phase center model for the GPS antennae (see Section 3.1). Following IGS recommendations, a new reprocessing (ULR2 solution) started; it took almost one year to process 10 years of data (from 1997 to 2006.9). The tracking network was upgraded up to 225 stations, among which 160 were CGPS@TG. The resulting vertical velocities of the preliminary ULR2 solution where exploited to correct relevant tide gauges records world-wide distributed [*Wöppelmann et al.*, 2007b]. This study showed a reduced dispersion of the GPS-corrected sea-level trends with respect to GIA corrections. This indicates that GPS data analysis can provide useful information to separate land motion from oceanic processes recorded by tide gauges.

Velocities of both ULR1 and ULR2 solutions were estimated in the ITRF2000 reference frame. In October 2006, the ITRF2005 reference frame was released [IGS electronic mail message 5432, 2006]. Therefore, weekly coordinate solutions from ULR2 solution were aligned to the new reference frame and a new long-term solution was estimated, resulting in the ULR3 solution. Although this did not correspond to a change in the GPS processing strategy or the network size, the significant effect of the frame change on the estimated velocities entailed a new solution. The corresponding results were published by *Wöppelmann et al.* [2009] (see Annex D). The ULR3 solution was the only global TAC solution (processed with the absolute antenna model) available in the first (preliminary) TIGA combined solution [*Schöne et al.*, 2009]. Therefore, the ULR TAC contribution to TIGA was indispensable to tie together all the regional solutions [*Schoëne et al.*, 2009].

The beginning of my research work in 2007 coincides with the completion of the ULR3 solution. My work has dealt with the methodological study to improve the procedures of the ULR TAC, which has recently culminated in the last ULR solution, called ULR4. A complete description of the GPS processing strategies of ULR3 and ULR4 solutions is provided in Annex A. ULR4 processing strategy is also summarized by *Santamaría-Gómez et al.* [in press] (see Annex B). Since that moment, the consortium of the University of La Rochelle is formed by the LIENSs laboratory of the University of La Rochelle and CNRS (UMR 6250), the Spanish IGN and the LAREG laboratory of the French IGN and GRGS.

In 2008, almost at the midpoint of my research work, the ULR computing facilities were considerably upgraded by the acquisition of a computer cluster composed of 128 processing cores. This new facility allowed us to reduce the time needed to process 10 years of data of a global network of about 200 stations from almost one year to less than a month. This significant time reduction let me perform global long-term solutions with different processing strategies, opening then the way to a great experimentation capability. Such a computing upgrade can be noticed, for instance, in the different extent of the processing tests we performed to define the new processing strategy (see Chapter 3). Specifically, thanks to this computing capability and also in the frame of my thesis work, ULR TAC participated in the first reprocessing campaign of the IGS[9] with its ULR4 solution. This contribution was very useful to compare for the first time the ULR TAC performance with respect to the high-

---

9   http://acc.igs.org/reprocess.html

end IGS Analysis Centers solutions. Also at the beginning of 2009, the ULR TAC contributed to the IGS combined solution used to realize the next ITRF2008. Unfortunately, ULR4 was not completed at the ITRF2008 deadline, so the ULR3 solution was submitted to the IGS. Finally, the ULR4 solution contributed to the IAG Working Group on Regional Dense Velocity Fields[10] as the unique global velocity field solution useful to link together all the regional solutions in a common reference frame [*Bruyninx et al.*, in press, see Annex D].

---

10 http://www.epncb.oma.be/IAG/index.php

PART II
METHODOLOGY

3. GPS processing strategy definition

In order to reach the state-of-art GPS processing, all the processing parameters used for the ULR3 solution were carefully reviewed and updated if necessary.

Sections 3.1 to 3.3 describe the three main tests carried out to define the new GPS data processing strategy. The impact of the different antenna calibration models, the impact of the different tropospheric delay models and the impact of the geometric distribution of the sub-networks were tested. These three tests were not carried out with the same processing capabilities. The impact of the different antenna calibration models and the tropospheric delay models were done with a single CPU. On the contrary, the impact of the geometric distribution of the sub-networks was done with the new cluster (see Section 2.3). This explains the different amounts of data used to perform the tests. Section 3.4 describes other changes implemented in the final processing strategy. These changes correspond to the evolution of some models already tested and validated and recommended by others and therefore they were not tested here. Finally, section 3.5 gives a summary of the changes implemented in the data processing strategy of the new solution and their impact on vertical velocities.

All other parameters and models not described in this section remain the same as for the ULR3 solution strategy. Appendix A contains a summary of the complete GPS processing strategy used in both the ULR3 and ULR4 solutions.

3.1 Testing the antenna modeling impact

3.1.1. Introduction and objective

GPS measurements represent the range, expressed as code pseudodistances and phase differences, between the instantaneous radio-electrical centers of the transmitter antenna on board the satellite and the tracking antenna on Earth's surface. This radio-electrical center, called phase center, differs from the antenna reference point (ARP) for which satellite-station ranges are considered. For satellites, the ARP is defined as the center of masses, for which the coordinates are given following the equations of motion of satellites. For tracking stations, the ARP depends on the antenna model but it is usually located at the bottom of the antenna. Orbits (time varying satellite positions) are estimated for the satellite ARP. Similarly, the tracking station positions are estimated for the station ARP (rigorously for the station marker, fixed with the station monument; the known three-dimensional distance between station marker and antenna ARP is called antenna eccentricity). Range observations, between phase centers of satellites and tracking antennas, must then be converted to ARP ranges prior to any estimation (Figure 3.1). Otherwise, the station vertical component will be heavily affected.

The phase center location of the transmitting/tracking antenna depends on the radio signal frequency. In addition, the radiation phase pattern does not constitute a perfect hemispherical front [*Elósegui et al.*, 1995; *Schmid and Rothacher*, 2003]. Thus, the phase center location for a satellite/station pair depends on the direction of the transmitted/received radio signal. The mean location of all these phase centers for a given antenna is known as mean phase center and its three-dimensional vector to the ARP is known as phase center offset (PCO). The azimuth and elevation dependent phase center locations from the mean phase center are known as phase center variations (PCV) (Figure 3.2). This way, the antenna
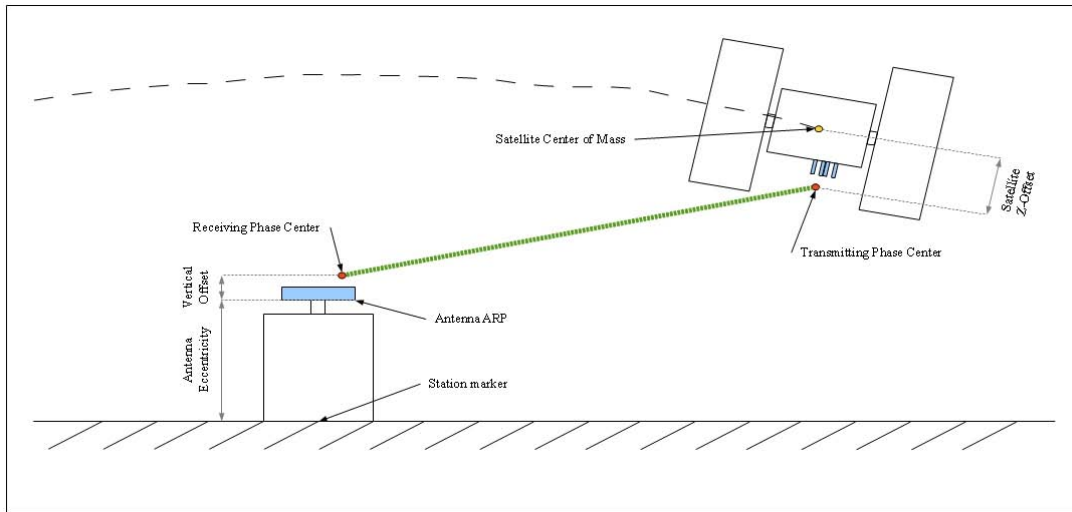
Figure 3.1. Schema of measured ranges and phase center corrections for stations and satellites.

phase center correction is arbitrarily partitioned into two terms (PCO and PCV) which must be used in a consistent manner [*Schmid et al.*, 2007]. To do this, both quantities, PCO and PCV, must be accurately estimated and reported in a so-called antenna calibration model.
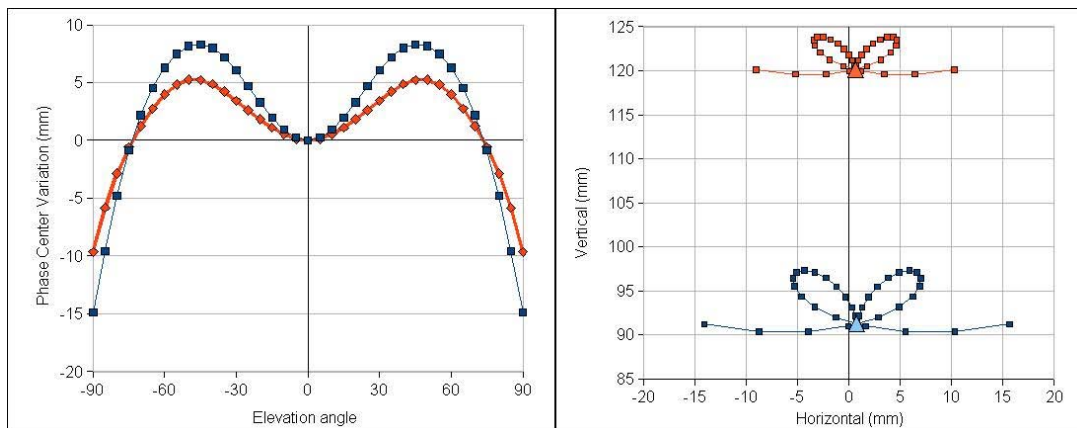
Figure 3.2. Left: Elevation-dependent PCV values of the AOA D/M_T antenna model for the L1 (blue) and L2 (red) GPS signals (negative elevation angles correspond to the symmetric part of the antenna). Right: Complete L1 and L2 tracking antenna phase pattern (PCO with triangles and PCV with squares) for the same antenna model but seen from the antenna side with an azimuth of 0°. Values are extracted from the igs05_1515.atx antenna calibration model.

From 30 June 1996, the official IGS antenna calibration model, known as relative model (hereafter RPCV), was available and applied in the state-of-the-art GPS analysis [IGS electronic mail message 5189, 2005]. In this model, using a short-baseline field calibration approach, PCO and elevation-dependent PCV corrections for all IGS common models of

tracking antennas were estimated with respect to a reference antenna (the Allen Osborne Associates Dorne Margolin Model T). For the reference antenna, the PCO values were estimated and the PCV values were considered to be zero [*Mader*, 1999]. In order to avoid ground multipath noise, these phase antenna corrections were estimated with an elevation cutoff angle of 10°. The precision of these phase corrections is estimated in 1-2 mm by comparing different calibration sources [*Rothacher and Mader*, 2003]. For satellite antennas, block-type PCO values were estimated from theoretical analysis and the PCV values were not estimated, thus assuming a perfect hemispherical phase radiation front [*Cardellach et al.*, 2007].

Earlier studies [*Zhu et al.*, 2003] showed that 4 to 6% (depending on the elevation cut-off angle) of the averaged error of the estimated satellite PCO values would translate directly into a station height bias. Thus, assuming an average satellite PCO error of 1 m [*Schmid et al.*, 2005], this would introduce a global change of ~5 cm in the station heights, which is equivalent to a terrestrial frame scale change of ~8 ppb. Other studies [*Zhang et al.*, 2004] showed that the impact of the satellite PCO error is not constant due to the evolution of the GPS constellation (new satellites and new satellite blocks). That is, since the averaged satellite PCO error depends on the satellites accounted for, a changing constellation will result in a changing averaged PCO error. Thus, the change of the averaged satellite PCO error with time also introduces a global time-dependent change of the estimated station heights correlated with the constellation evolution. This represents an artificial frame scale drift of about 1 ppb/yr during the year 2000, or equivalently, a global vertical velocity change of 6.5 mm/yr at the Equator. Additional studies [*Ge et al.*, 2005] confirmed this relationship between the averaged satellite PCO error and the frame scale and scale drift bias and recommended to estimate satellite-specific PCO values for obtaining the highest accurate products.

In November 2006, the IGS switched to a new antenna calibration model, known as absolute model (hereafter APCV) [IGS electronic mail messages 5149 and 5189, 2005; 5447 and 5455, 2006]. In this model, the PCO and azimuth- and elevation-dependent PCV of a subset of tracking antennas (including the antenna used as reference in the RPCV model) were estimated down to an elevation angle of 0° for both GPS signals by means of a rotating robotic system. The precision of this calibration method is estimated in 1 mm by comparison with the relative calibration values [*Rothacher and Mader*, 2003]. For the rest of the tracking antennas, the RPCV model (PCO and PCV values) was transformed to the APCV model using the absolute calibration values of the reference antenna. There are however some tracking stations with unknown antenna plus radome combinations which remain uncalibrated in both models. For instance, in the ULR4 network, using the absolute calibration file corresponding to the GPS week 1515 (January 2009), 61% of the antenna models (antenna with radome combination) have absolute calibration, 16% have relative calibration converted to absolute and 23% have no calibration. For these uncalibrated stations, the calibration values of the antenna model without radome (whatever absolute or converted values) are used instead of using null values. These numbers of the ULR4 network agree with those of the IGS network, according to the IGS Antenna Working Group [*Schmid et al.*, 2009].

Using these new absolute phase pattern values for receivers, the satellite-dependent Z-PCO and block-nadir-dependent PCV values (both only for the ionosphere-free linear combination observable) were estimated as new parameters in a dedicated GPS processing [*Schmid and Rothacher*, 2003]. Due to high correlation between satellite PCO and PCV, the PCO values were estimated in such a way that the PCV values are minimized over the whole range of the satellite nadir angle (0°-14°). Block-dependent X- and Y-PCO values were not

estimated but extracted from the nominal manufacturer's information, therefore horizontal-dependent PCV were not estimated either. The satellite phase patterns adopted in the new APCV model were estimated through the combination of two independent reprocessed solutions of more than 10 years of GPS data [*Schmid et al.*, 2007]. These newly estimated Z-PCO parameters are, along with the receiver antenna phase pattern, clock bias and tropospheric delay parameters, highly correlated with the estimated station heights, that is, the scale of the terrestrial frame [*Zhu et al.*, 2003]. Thus, to unambiguously estimate them, the ITRF2000 scale was held fixed through the coordinates of the IGS reference frame stations (IGb00 station set). IGb00 station coordinates are the IGS frame realization of the official (at that time) ITRF2000 reference frame. IGb00 scale and scale drift were defined to be consistent with ITRF2000 by frame alignment [IGS electronic mail message 4666 and 4748, 2003]. This absolute antenna calibration process makes then the GPS terrestrial frame scale dependent on the ITRF2000 scale definition.

The objective of our test was to estimate the impact of using the APCV model rather than the RPCV model on the vertical station positions. Although the APCV model was already used in the ULR3 solution, the impact of this model on station positions was not assessed yet by the ULR analysis center.

3.1.2. Data and results

A global test network was devised by selecting 42 well distributed IGS reference frame stations (IGS05 station set) [IGS electronic mail message 5456, 2006]. We processed one week of data per month for the year 2006. We used GAMIT software version 10.32 with the same processing strategy (see ULR3 processing strategy in Appendix A) except for the APCV and RPCV models respectively.

For both solutions, the respective 84 daily position solutions were accumulated into a unique solution. Then, a 7-parameter transformation was estimated between the APCV solution and the RPCV solution used as reference (Table 3.1, rotations are not shown because they are not significant).

Table 3.1. Translations and scale transformation parameters between APCV and RPCV solutions in 2006.0 epoch.

TX (mm)	TY (mm)	TZ (mm)	Scale (ppb)
0.1±0.5	-2.2±0.5	-4.8±0.5	2.0±0.1

The scale bias estimated between both solutions for January 2006 is consistent with other results on APCV/RPCV comparisons [*Ge et al.*, 2005; *Ferland*, 2006; *Schmid et al.*, 2007]. This scale change represents a global change of station heights of ~13 mm at the Equator, whereas station velocities remain unchanged. The unique effect on vertical rates is the relative drift of translations and scale parameters. In the one hand, translation drifts would be partially mapped into vertical velocity biases depending on station location. On the other hand, a scale drift will be entirely mapped into a global vertical velocity bias [e.g., *Wöppelmann et al. 2009*, see Annex D]. This test was unfortunately too short to confidently estimate the parameter drifts. For the same reason, station velocities were also not confidently

estimated. However, as both the global and local (see later in text) biases agree with results from long-term reprocessed solutions, we think that the same transformation parameters drifts found in those solutions would be also found in our test. The scale drift was estimated to 0.19 ppb/yr (difference between relative and absolute solutions with respect to IGb00 in *Schmid et al.* [2007]), representing a global vertical velocity bias of ~2 mm/yr at the Equator. It is worth noting that applying this scale drift with the scale bias also found by these authors (0.95 ppb in 2000.0), will result in a scale bias consistent with our results.

Once the global differences were removed (transformation parameters applied), the WRMS of the station coordinate differences in the local coordinate system were extracted (Table 3.2). This table shows that even after removing the global height difference (represented by the translation and scale parameters), remaining local (station-dependent) height differences between both solutions are noticeable. These differences reach up to ±15 mm (Figures 3.3 and 3.4), in agreement with the same order of differences found in a long-term reprocessed solution with more than 10 years of data [*Schmid et al.*, 2007]. These significant local differences mean that the global translation and scale parameters do not fully absorb the station position differences obtained using both models.

Table 3.2. WRMS between APCV and RPCV solutions.

WRMS E (mm)	WRMS N (mm)	WRMS U (mm)	WRMS 3D (mm)
1.7	2.8	6.9	4.4
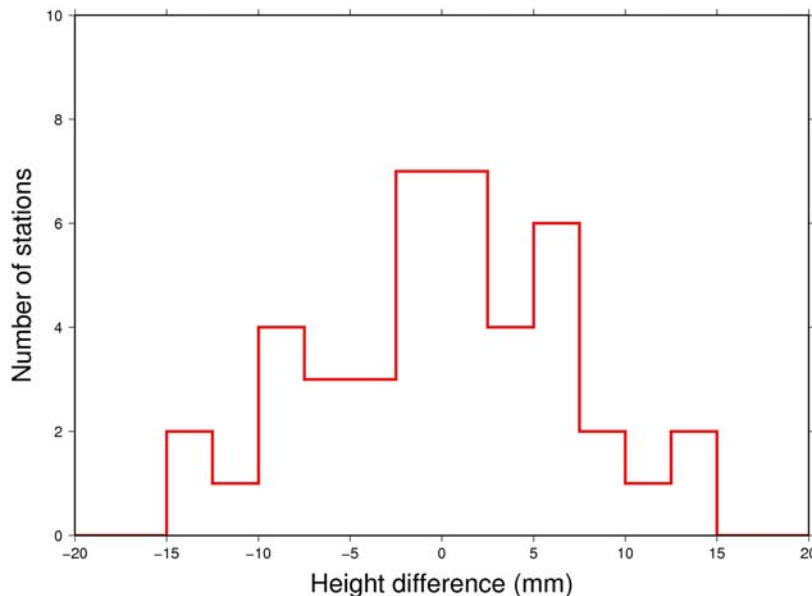
Figure 3.3. Histogram of height differences between APCV and RPCV solutions.
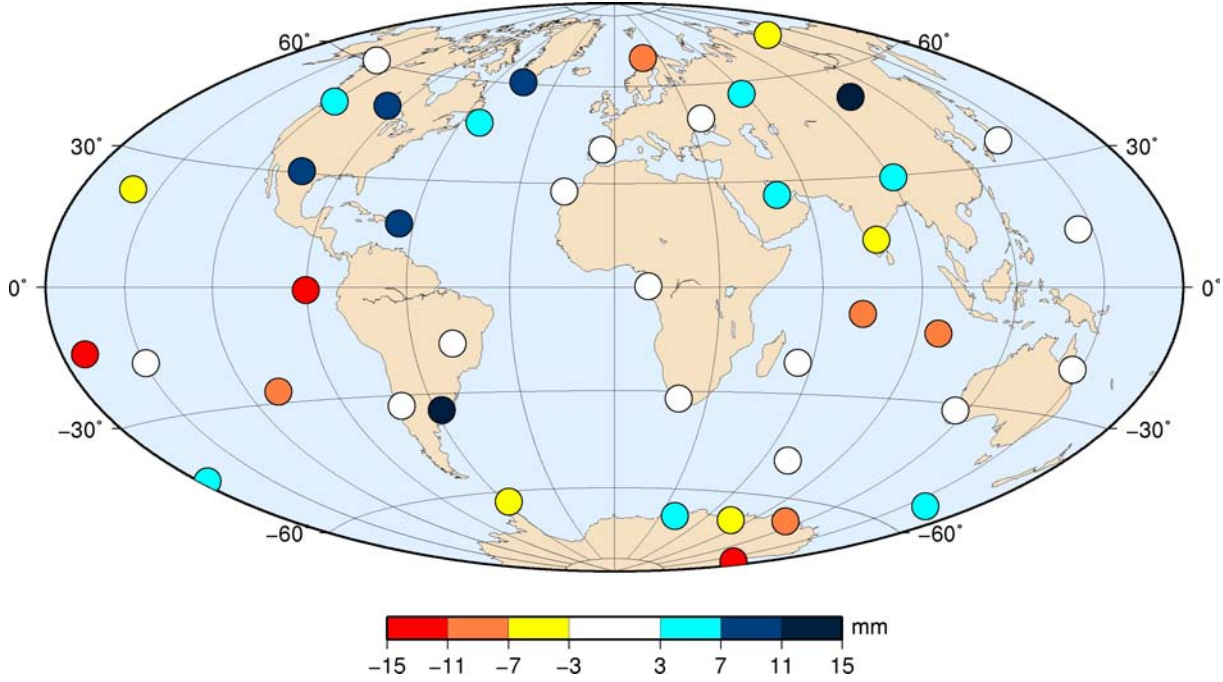
Figure 3.4. Map of local height differences between APCV and RPCV solutions.

The range error induced by an error on the satellite PCO has a large constant term and a small elevation angle-dependent term. This error is approximated by the following expression [*Zhu et al.*, 2003]:

$$\Delta \rho = \Delta \zeta \cdot \cos \theta \,, \tag{1}$$

where $\Delta\rho$ is the range error, $\Delta\zeta$ is the satellite PCO error and θ is the nadir angle from the satellite to the station. This satellite nadir angle (to the station) is directly related to the station elevation angle of the satellite, ε, by the following expression [*Rothacher and Mader*, 2003]:

$$\sin(\theta) = \frac{R}{r} \cdot \sin(\varepsilon) \,, \tag{2}$$

where R is the Earth's radius and r is the geocentric distance of the satellite. Replacing Eq. 2 into Eq. 1 and using the values of R and r, this expression leads to [*Cardellach et al.*, 2007]:

$$\Delta \rho = \Delta \zeta \sqrt{0.94 + 0.06 \cdot \sin^2 \varepsilon} \,, \tag{3}$$

This expression represents the large constant and the small elevation-dependent error terms.

This means that, for a satellite not located at the station zenith, the impact of the PCO error is slightly reduced. The constant part of the range error is mainly absorbed by the clock bias estimation and, to a lesser extent, by a frame scale change. However, the elevation-dependent part of the error depends on satellite geometry, and thus, it is station-dependent.

The local differences found in our study might be related to this station-dependent effect of the satellite PCO error through the satellite geometry. Satellite geometry depends, on the one hand, on station local masks (limiting minimum elevation angle) and, on the other hand, on station latitude (limiting maximum elevation angle). Differences in satellite geometry among sites could then introduce vertical error differences at the several mm level producing a spatial pattern that cannot be removed by a global transformation parameter. This spatial pattern is related to the number of satellites at zenith, where the impact of the PCO error is larger. The number of satellites at zenith is larger for mid-latitude regions (due to the orbit inclination of 55°) than at the Equator and very much larger than the Polar regions (where the number of satellites at zenith is equal to zero). Sorting the station height differences of Figure 3.4 by latitude, the spatial pattern is then recognized (Figure 3.5).
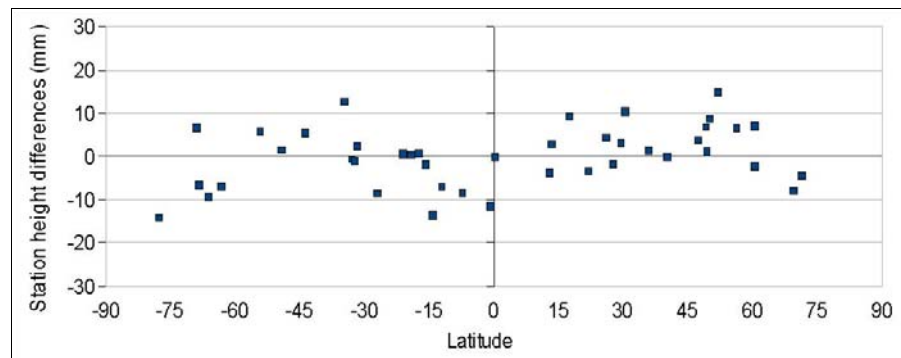
Figure 3.5. Local station height differences between APCV and RPCV
solutions sorted by latitude.

Moreover, as the averaged satellite PCO error is not constant in time, neither the resulting station elevation-dependent error. Thus, the time evolution of the averaged satellite PCO error could also introduce local errors in estimated vertical velocities, which cannot be accounted for with the estimation of a global transformation drift either. Simulations carried out by *Cardellach et al.* [2007] showed that, for GPS observations with a minimum elevation angle of 15º, these local errors are estimated to be ±17 mm for station heights (consistent with the results of our test) and ±0.7 mm/yr for station vertical velocities.

Therefore, since the complete (global plus local) station coordinate and velocity differences between solutions using both models are not completely removed when the global differences are accounted for (e.g. by aligning the solution to an external frame), it is mandatory to use the best up-to-date model of the antenna phase corrections. Otherwise, significant local bias will remain in station heights and vertical rates.

It is worth to mention here that the ITRF2005 was computed using the IGS weekly GPS solutions until end 2005, so those GPS solutions were estimated using the RPCV model. Once that the IGS contribution was aligned in origin and scale to the SLR and VLBI contributions of the ITRF2005 respectively, the local station coordinate errors using the

RPCV model were transferred to the resulting reference frame. That is, they were not removed in the frame alignment. Later, along with the outcome of the first APCV model in 2006, the IGS carried out a test campaign to assess the station-by-station coordinate differences resulting of the change from the RPCV model to the APCV model. The estimated station-dependent differences were then applied as corrections to the IGS reference frame station positions belonging to the ITRF2005. These estimated corrections were larger in the vertical component than in the horizontal ones, up to 15 mm [IGS electronic mail message 5447, 2006]), in agreement with our test. The new corrected IGS05 reference frame was then re-aligned to the current ITRF2005 realization in order to keep the consistency of the frames. Nevertheless, the station height coordinates of both frames are not exactly the same due to the application of the station-dependent APCV/RPCV corrections to the IGS05 [*Ferland and Piraszewski*, 2009; IGS electronic mail message 5447, 2006].

       To show the differences of these two realizations of the reference frame, our APCV and RPCV solutions were aligned to the ITRF2005 and IGS05 frames respectively using the same set of reference stations. Table 3.3 shows the WRMS of the station coordinates differences between each of our solutions (APCV and RPCV) and each reference frame (ITRF2005 and IGS05). APCV solution fits slightly better to IGS05 than to ITRF2005 reference frame with an improvement of 14% in the vertical component. RPCV solution fits better to ITRF2005 than to IGS05 reference frame with an improvement of 46% in the vertical component. This comparison confirms that the IGS05 reference frame realization should be used for aligning GPS solutions estimated with the APCV model instead of the ITRF2005 coordinates.

Table 3.3. WRMS of station coordinate differences between ARPC/RPCV solutions and ITRF2005/IGS05 reference frames.

	WRMS E (mm)	WRMS N (mm)	WRMS U (mm)	WRMS 3D (mm)
APCV-ITRF2005	1.9	1.9	5.8	3.7
APCV-IGS05	1.3	2.0	5.1	3.3
RPCV-ITRF2005	1.5	1.5	5.2	3.2
RPCV-IGS05	1.4	1.9	7.6	4.6

3.2. Tropospheric modeling test

3.2.1. Introduction and objective

       GPS microwave signals (1.5 and 1.2 GHz for L1 and L2, respectively) traversing the troposphere are affected by electromagnetic refraction, that is, their velocity and direction of propagation is changed. Both effects represent an observed phase delay or an equivalent increment of the range measurement. Since the troposphere behaves as a non-dispersive

electrically-neutral medium for these electromagnetic signals, it is not possible to remove the tropospheric refraction effects with a combination of the two GPS frequencies, as it is partially done with the ionospheric refraction. Then, to correct the GPS measurements for this refraction, the tropospheric delay must be modeled or estimated.

The tropospheric delay for both GPS frequencies depends mainly on the troposphere refractivity along the signal path. The refractivity (N), also known as refractive index (n), at any point of the troposphere is defined by the following equation [*MacMillan*, 1995]:

$$N = (n-1) \times 10^6 = \frac{77.6}{P_d} + \frac{64.8 \cdot P_v}{T} + \frac{3.776 \times 10^5 \cdot P_v}{T^2}, \tag{4}$$

where P_d is the atmospheric pressure in hPa, P_v is the water vapor pressure in hPa and T is the temperature in K. The tropospheric delay (TD) of any observation is given by the integral of the refractivity over the path length through the troposphere (s) [*Chen and Herring*, 1997]:

$$TD = \int_s N(s)\,ds. \tag{5}$$

Equation 5 requires to known the refractivity at any point of the signal path, which is actually not possible since the refractivity itself changes the signal path [*Davies et al.*, 1985]. Therefore, a model of the structure of the atmosphere has to be used. Within these models, the signal path length (ds) is approximated by the cosecant of the elevation angle of the observation. This represents a minimum delay at the zenith and an increasing delay with lower elevation angles.

Following this model, the tropospheric delay at an elevation angle (e) can be represented by the combination of the Zenith Tropospheric Delay (ZTD) and a coefficient, called mapping function (mf), which relates the tropospheric delay at the elevation angle with the tropospheric delay at the zenith:

$$TD(e) = ZTD \cdot mf(e). \tag{6}$$

Thus, assuming an azimuthally symmetric troposphere, the mapping function constitutes the model that describes the elevation dependence of the tropospheric refractivity. All mapping functions commonly used in GPS processing describe this atmospheric refractivity dependence by means of the continued fraction form in *sin(e)* suggested by *Marini* [1972]:

$$mf(e) = \cfrac{1}{\sin(e) + \cfrac{a}{\sin(e) + \cfrac{b}{\sin(e) + \cfrac{c}{\dots}}}}, \tag{7}$$

where the parameters *a, b, c* … are estimated by fitting this function to external data of atmospheric temperature, pressure and water vapor pressure profiles. The deviation of such a model from atmospheric ray traces was estimated to be 0.3% and an error of less than 0.1% is obtained by neglecting the fourth parameter (*d*) [*Niell*, 1996]. These profiles can be obtained from standard atmospheres, radiosonde data or numerical weather models (NWM), the latter being preferred due to their higher spatial and temporal resolution.

In addition, the ZTD may be partitioned in two components, one corresponding to the contribution of the hydrostatic equilibrium part of the troposphere and the other to the water vapor content effect. Both components affect the GPS microwaves propagation, while optical waves (e.g. satellite laser ranging) are affected mainly by the hydrostatic part. Thus, the tropospheric delay of Equation 6 is given by the sum of these hydrostatic (H) and wet contributions (W):

$$TD(e) = ZHD \cdot mf_h(e) + ZWD \cdot mf_w(e) \ , \tag{8}$$

where different mapping functions are defined for the hydrostatic (mf_h) and the wet (mf_w) parts due to the different spatial distribution of the refractivity for both components.

The ZHD represents globally 90% of the total ZTD, typically a range bias of 2.3 m at sea level [*Niell*, 1996]. It can be precisely obtained from surface atmospheric pressure and station location (latitude and height) following the equation of *Saastamoinen* [1972] given by *Davis et al.*, [1985]:

$$ZHD = 0.0022768 \frac{p}{(1 - 0.00266 \cdot \cos(2\varphi) - 0.28 \cdot 10^{-6} \cdot h)} , \tag{9}$$

where *p* is pressure in hPa, *φ* is station latitude and *h* is station altitude in m. *Davis et al.* [1985] discussed about the uncertainty of this expression and concluded that the uncertainty of the constant term is very small, usually 0.5 µm/hPa, under hydrostatic equilibrium conditions, being the influence of station latitude and altitude negligible. This represents a maximum error of ~0.5 mm at sea level (~1000 hPa). The uncertainty could reach up to 20 µm/hPa (~20 mm at sea level) in extreme weather conditions like thunderstorms or heavy turbulences. This error in the a priori ZHD value can be translated into a station height error of between 1 and 4 mm, depending on the data processing strategy (see later in text). These non-hydrostatic conditions, although unavoidable, can be prevented by using co-located continuous gravity observations.

The remaining 10% of the total ZTD corresponds to the ZWD, that is, ~0.2 m at sea level, reaching extreme values of 0.3 m at mid-latitudes and 0.4 m in the tropics [*Niell*, 1996]. Despite these relatively small values, the ZWD cannot be however directly estimated nor precisely modeled. This is due to the fast variability of the water vapor concentration and its heterogeneous distribution. Thus, for high precision GPS applications this variable part of the ZTD must be estimated within the GPS data processing. Assuming an a priori precise knowledge of the ZHD and the mapping function values, the residual ZTD is adjusted in the GPS data processing as being composed only by the contribution of the wet part.

Finally, to complete Equation 8, the deviations from the hypothetical azimuthally symmetry of the mapping functions can also be partly taken into account within the GPS data processing by estimating horizontal refractivity gradient vectors. A gradient can be seen as resulting from a tilted atmosphere, that is, it represents the horizontal direction of the maximum tropospheric delay difference of lowest observations [*Chen and Herring*, 1997]. Several studies [*MacMillan*, 1995; *Chen and Herring*, 1997; *Bar-Server et al.*, 1998], using VLBI and GPS data, showed the benefits of estimating atmospheric horizontal gradients. They concluded that adding this parameter to the processing leads to both an improvement in the precision (by means of a reduction of the repeatability of 15-20%) and in the accuracy (by comparison of independent techniques like radiometry and ray tracing) of the solution. Thus, Equation 8 can be rewritten as:

$$TD(e,a) = ZHD \cdot mf(e)_h + ZWD \cdot mf(e)_w + (G_N \cdot \cos(a) + G_E \cdot \sin(a)) \cdot mf_g(e), \qquad (10)$$

where a is the station azimuth of the signal measured east from north, G_N/G_E are respectively the north and east components of the gradient vector and mf_g is the gradient mapping function. This Equation 10 corresponds to the parameterization of the tropospheric delay recommended by the IERS Conventions[1] [*McCarthy and Petit*, 2004].

As the ZTD/ZWD estimation depends on the a priori ZHD value used, this parameter must be accurately known. Therefore, following Eq. 9, this requires an accurate knowledge of the atmospheric pressure at the station height. From this equation, an error of 1 hPa represents an error of ~2 mm in the ZHD. Moreover, the separation of the hydrostatic and wet mapping functions increases at low elevations. This difference between both mapping functions reaches 5% at an elevation angle of 5° (for the New Mapping Function, [*Tregoning and Herring*, 2006]). This way, any error of the atmospheric pressure leads to a ZHD error that will be mapped with the wrong mapping function (mf_w) for low observations. Due to the different mapping functions, the ZHD error will not be absorbed by the ZWD estimation, resulting in a bias which propagates mainly in the station height. Furthermore, this error will be amplified for stations located at higher latitudes, where low observations are predominant due to the GPS constellation geometry. For example, for a site located in the Antarctic region (DAV1) 24% of the observations are below 15° of elevation angle [*Tregoning and Herring*, 2006].

This error source, also called mapping function separation error, reveals the direct relationship between lower observations and biased heights. For a specific pressure error, lower observations represent a larger mapping function separation and then a larger height bias. Several authors [*Niell et al.*, 2001; *Boehm et al.*, 2006a; *Kouba*, 2009] have computed a linear relationship to describe the amount of the mapping function separation error that is transferred to a station height bias. This relationship, so-called "rule of thumb", varies between 1/5 and 1/20 depending on the different elevation cutoff angle and elevation-dependent weighting applied. Inversely, this error implies that, to keep a small height bias, decreasing the elevation cutoff angle requires a higher precision on the a priori pressure data. Thus, for an elevation cutoff angle of 10° and a maximum height bias of 1 mm, the pressure uncertainty must be of the order of ~10 hPa [*Kouba*, 2009]. To keep the same height bias (1 mm), this uncertainty must be improved down to ~4 hPa if using a cutoff angle of 5°. These accuracies are only possible with local pressure measurements or with a state-of-art NWM.

---

1   http://tai.bipm.org/iers/convupdt/convupdt.html

Furthermore, mapping function values are also an a priori critical known model. For low elevation angles, where mapping function values are larger, an error of 0.01% on the hydrostatic mapping function or an error of 0.1% on the wet mapping function can lead to a height error of 1 mm. (depending on the rule of thumb used, here we used 1/20 found by *Kouba* [2009]). Thus, mapping functions as accurate as possible are also mandatory for precise GPS processing.

Earlier publications [*Boehm and Schuh*, 2004] showed the improvement resulting by using the Vienna Mapping Functions (VMF) [*Boehm and Schuh*, 2004] and the Isobaric Mapping Functions (IMF) [*Niell*, 2001], both based on the reanalyzed meteorological data of the European Centre for Medium-Range Weather Forecasts (ECMWF), versus the empirical New Mapping Functions (NMF) [*Niell*, 1996], based on averaged atmospheric profiles of radiosonde data. For VMF, the parameters of Eq. 9 were rigorously estimated for each station by direct ray-tracing through pressure levels of the ECMWF NWM. Nevertheless, NMF has been broadly used in GPS analysis due to its easy implementation. To use NMF, only station height, station latitude and day of the year are required as input parameters.

In 2006 two new mapping functions were published: the Vienna Mapping Function 1 (VMF1) [*Boehm et al.*, 2006a] and the Global Mapping Function (GMF) [*Boehm et al.*, 2006b]. VMF1, like VMF, is based on ray-tracing through refractivity profiles of the ECMWF NWM. The hydrostatic VMF1 is an improved version of the hydrostatic VMF which includes a day-of-year dependence, asymmetry with respect to the Equator and the geometric bending effect. Wet mapping functions are the same for VMF1 and VMF. The VMF1 mapping function has shown to provide the best up to date results [*Niell*, 2006, *Boehm et al.*, 2007; *Tesmer et al.*, 2007]. However, it was initially only available in the form of IGS site-dependent values and not for the whole period of GPS observations. To overcome these limitations, GMF was also published. Like NMF, GMF is also an empirical mapping function. It is based on spherical harmonic coefficients up to degree and order 9 fitted to annual variations of the VMF1 values, thus keeping consistency between both mapping functions. Therefore, unlike NMF, GMF is also based on NWM data. It is also an easy to use mapping function which does not need any external data. It requires only the day of the year and station location (latitude, longitude and height). This allowed the possibility to use GMF where and when VMF1 values were not available or even extrapolate the values for periods where no NWM analysis existed yet (e.g. real time applications).

More recently, VMF1 products were made available[2] in the form of yearly gridded files back to 1992 from where values could be extracted by interpolation [*Kouba*, 2007]. These VMF1 grids contain the first parameter of the fraction form (Eq. 7) for both the hydrostatic (a_h) and wet (a_w) mapping functions and also the ZHD value at a mean ellipsoidal height. VMF1 grids supply these data with a time resolution of 6 hours and a space resolution of 2° x 2.5°. The b and c parameters of the fraction form (representing a constant value and a seasonal plus latitudinal dependence respectively) are also used to estimate the mapping function values, but they are not contained in the grids as they can be calculated from empirical equations. The difference between the ZHD values extracted from the VMF1 grids and computed from local pressure measurements (Eq. 9) are estimated to be below 10 mm, which corresponds to a pressure precision of 5 hPa [*Kouba*, 2009].

For the GMF, the mapping function coefficients are computed analytically with the harmonic coefficients. The a priori ZHD values must be computed with external values of

---

2 http://www.hg.tuwien.ac.at/~ecmwf1

atmospheric pressure and Eq. 9. The best way to obtain surface atmospheric pressure is to directly measure it at the GPS station height. When this data is not available, it is recommended to extract it from the Global Pressure and Temperature (GPT) model [*Boehm et al.,* 2007b]. This model is also based on a spherical harmonic expansion of degree and order 9 fitted to annual variations estimated with 3 years of the ECMWF NWM reanalysis. The maximum RMS of the GPT model residuals is estimated to be 20 hPa over the Antarctic region [*Boehm et al.,* 2006c; 2007b]. This is related to the larger pressure variations of this region, which are not accounted for in the modeled annual variation. Nevertheless, the GPT model shows to perform better than a standard sea-level pressure model approach, like the Hopfield model [*Hopfield,* 1969] (implemented in GAMIT software) or the Berg model [*Berg,* 1948] (implemented in the Bernese software) [*Tregoning and Herring,* 2006; *Boehm et al.,* 2006c, *Boehm et al.,* 2008].

The objective of our test was to compare and to quantify the differences between station positions/velocities obtained using VMF1 and GMF+GPT models. Both mapping functions are ECMWF-based and both are recommended by the IGS for the reprocessing campaign and also in the updated version of the IERS Conventions. GMF was used in the ULR3 solution for practical reasons: VMF1 external products were not available for the whole period at the beginning of the last reanalysis.

3.2.2. Data and results

The same test network and the same data span and sampling as those used for the antenna phase center model test (see Section 3.1.2) were used here. This data set was processed twice with the same processing strategy but using either the VMF1 grids (VMF1 solution) or the GMF+GPT models (GMF solution), respectively.

More processing time is expected for the VMF1 solution than for the GMF solution since some tropospheric parameters are extracted from additional external products (grid files) instead of being analytically computed. Furthermore, the phase corrections are more sophisticated (tropospheric parameters are extracted 5 times a day instead of being computed once a day respectively). With the test network of 42 stations, the average daily processing time for the 84 daily solutions was 34% longer for VMF1 solution than GMF solution (52 min vs. 39 min averaged time). This time difference is not significant on the short time span used in this test. However, for a reprocessing of more than 10 years of data and using the ULR4 network, the time difference represents approximately 4.4 months of additional processing time. For such solutions it is desirable to benefit from a high-performance processing facility like the upgrade carried out at the ULR analysis center (see Section 2.3).

As for the antenna calibration model test, the 84 daily solutions obtained were combined into a one-year solution. A 7-parameter transformation was then estimated between both combined solutions. All estimated transformation parameters (not shown) are below the mm level, indicating that both strategies realize the same terrestrial frame. The residuals of the station coordinates and their WRMS are shown (Table 3.4, Figures 3.6, 3.7 and 3.8). Not surprisingly, local height differences are larger than horizontal ones, which will not be further considered in the discussion.

Table 3.4. WRMS between VMF1 and GMF solutions.

WRMS E (mm)	WRMS N (mm)	WRMS U (mm)	WRMS 3D (mm)
0.2	0.1	0.7	0.4
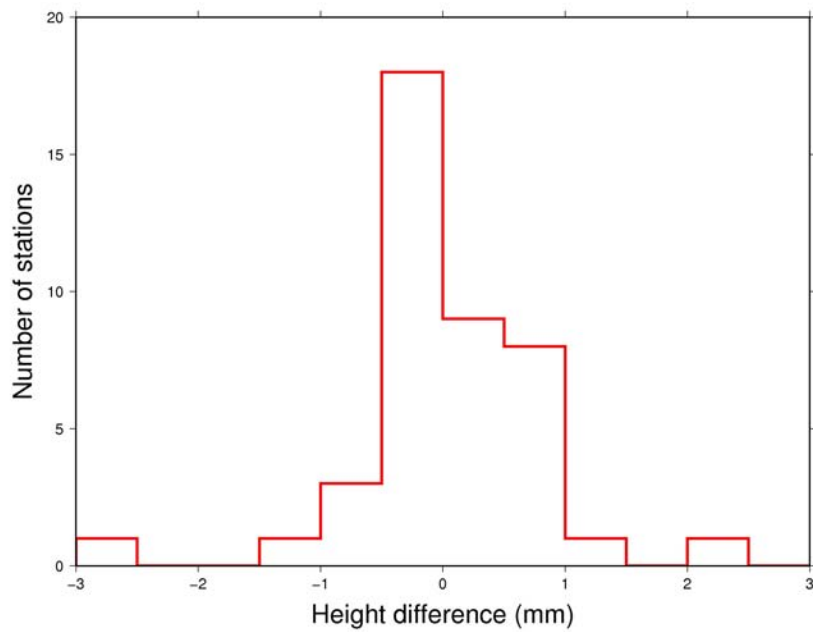
Figure 3.6. Histogram of station height differences between VMF1 and GMF solutions.
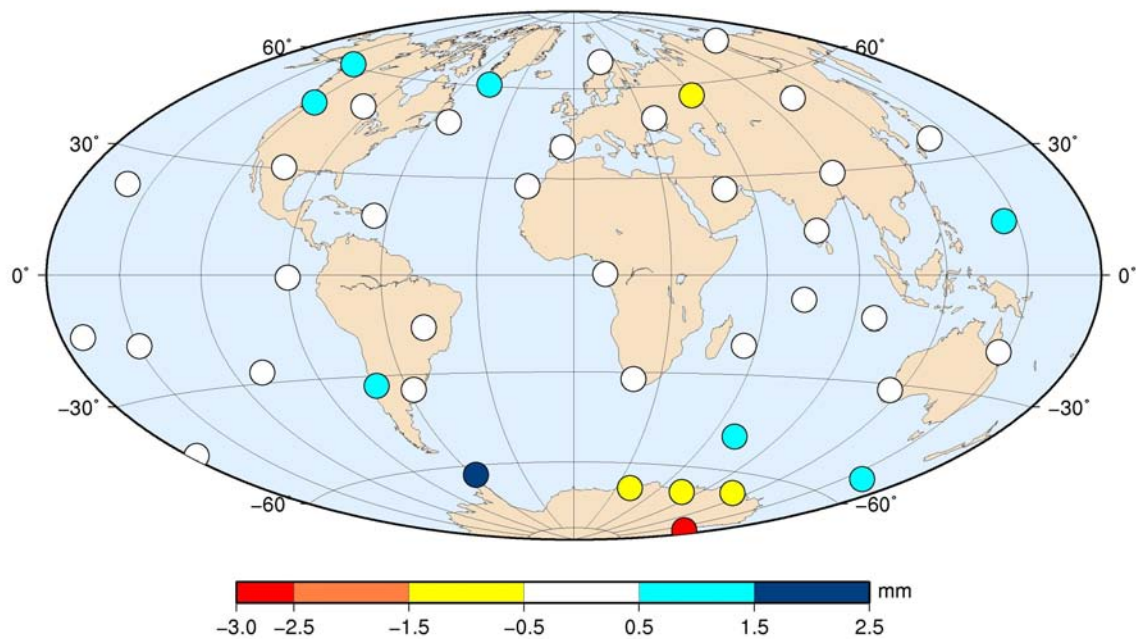
Figure 3.7. Map of station height differences between VMF1 and GMF solutions.
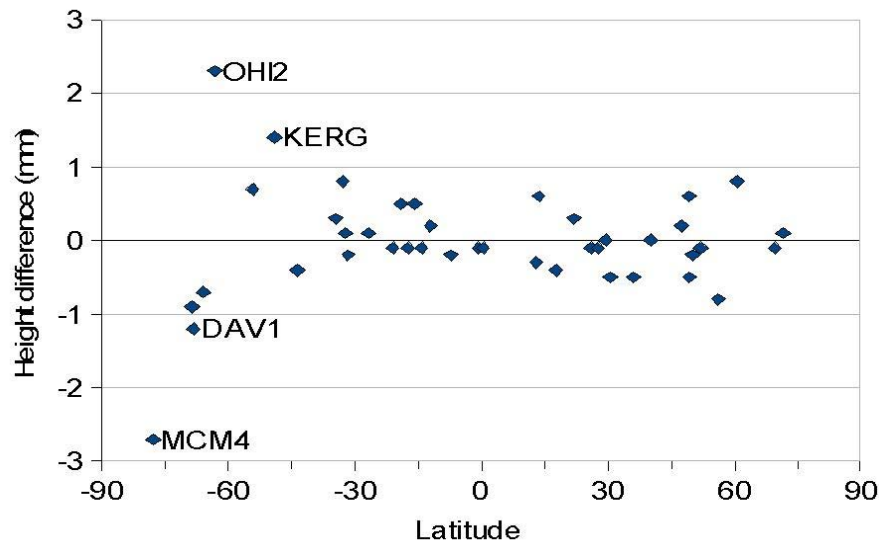
Figure 3.8. Station height differences between VMF1 and GMF
solutions ordered by latitude.

Height differences are below 1 mm for low- to mid-latitude stations. Differences grow towards the Poles. They are higher than 1 mm only in the Antarctic region, reaching almost 3 mm in OHI2 and MCM4 stations. About 64% of analyzed stations have a residual smaller than 0.5 mm showing the overall good agreement between both solutions. These height residuals include the effects of both a priori ZHD errors and the differences between VMF1/GMF hydrostatic and wet mapping function values. As in the antenna calibration model test, the data span of this test was too short to confidently estimate the impact on vertical velocities.

Earlier publications [*Tregoning and Herring*, 2006] showed that the increased height errors for the southernmost regions are related to the error in the atmospheric pressure values used to estimate the ZHD. Using the GPT model and a standard pressure model, they found a spatial correlation between the station height errors and pressure errors. More recent publications found similar results. *Kouba* [2009], analyzing 11 stations in 2005 with the Precise Point Positioning technique, also found a height bias of 2 mm for the MCM4 station between using VMF1 grids and GMF+GPT models. The author argues that this could correspond to a regional (Antarctic) limitation of the GPT model such as an inadequate resolution of the harmonic approximation. *Steigenberger et al.* [2009], using GMF and VMF1 models with a 12-year reprocessed solution and a denser network, found similar results for these height differences. They also estimated vertical velocity differences between both solutions to be below 0.2 mm/yr. In addition, they found that VMF1 mapping function performs slightly better than GMF mapping function, with an improved height repeatability of 2%. These authors relate some of the larger height residuals to the low precision of the station height extrapolation either when extracting the ZHD values from the VMF1 grids or within the GPT model. They noted that a station height bias of 6.4 mm could result from an extrapolation error between the heights of the VMF1 grid nodes and the MKEA station (altitude 3 km).

Within GAMIT software the procedure to extract the ZHD value at the station height

from the VMF1 grids is done as follows. The ZHD values are extracted for the four nodes of the VMF1 grid surrounding the station location. These ZHD values correspond to the ellipsoidal height of each grid node. All of them are then corrected to the station height. To do that, the atmospheric pressure is calculated from the GPT model at both the node altitude and the station altitude. For each node, a new ZHD is then calculated at both heights using Eq. 9. This is in fact the procedure followed in the GMF solution to obtain the ZHD values (see section 3.2.1, hereinafter GPT extracted ZHD values). The difference between both newly calculated ZHD values gives the ZHD height correction. By applying this height correction to the four ZHD values extracted from the grid, we have four ZHD values at the station height. Finally, the ZHD value for the station is interpolated between these four values.

This procedure implies that the differences of ZHD values between VMF1 grids and GPT model (used in GMF solution), for the same epoch and the same location, are always the same whatever the height considered. Certainly, this procedure is resumed in the following expression:

$$\Delta ZHD_{VMF1-GPT}^{GPS} = ZHD_{VMF1}^{GPS} - ZHD_{GPT}^{GPS} = ZHD_{VMF1}^{GRID} + \underbrace{\left(ZHD_{GPT}^{GPS} - ZHD_{GPT}^{GRID}\right)}_{ZHD\ height\ correction} - ZHD_{GPT}^{GPS}\ , \quad (11)$$

where ZHD_i^j is the ZHD value from the i model at the j altitude. Simplifying this expression leads to:

$$\Delta ZHD_{VMF1-GPT}^{GPS} = ZHD_{VMF1}^{GRID} - ZHD_{GPT}^{GRID}. \quad (12)$$

Thus, the ZHD difference at the GPS station height is the same as at the VMF1 grid node height. However, atmospheric pressure values extracted from the GPT model need also a height correction. These values are calculated at the sea level altitude (exactly at the geoid surface) and they are then height-corrected using the following expression, which indeed corresponds to the Berg standard pressure model [*Boehm et al.*, 2007a]:

$$p = p_0 \cdot \left(1 - 0.0000226H\right)^{5.225}, \quad (13)$$

where p is atmospheric pressure in hPa at the orthometric altitude H in m and p_0 is the atmospheric pressure at sea level in hPa. As usually orthometric heights are unknown, ellipsoidal heights are used and corrected using geoid undulations from the EGM96 model [*Lemoine et al.*, 1998]. Including this height correction into expression 12 results in:

$$\Delta ZHD_{VMF1-GPT}^{GPS} = ZHD_{VMF1}^{GRID} - \left(ZHD_{GPT}^{GEOID} + \delta ZHD_{GPT}^{GRID}\right) \quad (14)$$

Equation 14 does not just show that the difference of ZHD is constant, but it also shows that this difference depends on the VMF1 grid height (expressed in the orthometric system). Assuming that the VMF1 pressure errors can be neglected since they are four times smaller than GPT pressure errors, the ZHD differences between VMF1 and GMF solutions result then from errors on the GPT extracted ZHD values (also assuming the error of Equation 9 insignificant) and errors of the GPT height correction (Eq. 13). For instance, the ellipsoidal heights of the four VMF1 grid nodes surrounding the station MCM4 vary between -49 m and 718 m. This height correction might be the main source of error for the southernmost latitudes since it assumes a pressure gradient independent of temperature and temperature lapse rate [*Boehm et al.*, 2007b; *Boehm et al.*, 2008]. So errors in the height correction of the GPT model might then explain the height differences in Antarctic region between VMF1 and GMF solutions found in our test. This hypothesis is supported by *Kouba* [2009] results, where 70% of the height difference in MCM4 by using VMF1 and GMF+GPT models comes from the different ZHD value, not from the different mapping functions. For this region, it would be preferred to use pressure values directly observed at the station height to estimate the ZHD rather than using the GPT model or the VMF1 grids. We performed some test using station meteorological data in RINEX format, but they were finally given up due to frequent problems with uncalibrated meteorological sensors (for instance relative humidity exceeding 100%) and file format errors which reduced the available meteorological data and required constant intervention of the processing.

Daily repeatability of VMF1 and GMF solutions with respect to their combined solutions are similar, the difference being smaller than 0.1 mm. However, in a station-by-station basis, the mean repeatability of VMF1 solutions is higher than those of GMF solutions by 0.17 mm. If we exclude the Antarctic stations (namely OHI2, SYOG, DAV1, CAS1 and MCM4), the mean repeatability difference falls to 0.07 mm. However, the mean repeatability difference for these five Antarctic stations is 0.94 mm. This unexpectedly poor repeatability for the VMF1 solution is in fact related to the above mentioned errors of the GPT model (pressure values and height correction) for the Antarctic region, as explained in the text below.

Kouba [2009] also found that VMF1 solutions have a worse repeatability than GMF+GPT solutions by 0.14 mm. He related this to the fact that VMF1 solutions does not account for atmospheric loading correction, whereas GMF+GPT solutions partially account for this correction. *Steigenberger et al.* [2009] found a mean repeatability improvement of ~0.2 mm using VMF1 instead of GMF mapping functions, using only one source of ZHD (GPT or VMF1). However, they also found better repeatability by 0.26 mm with the VMF1 mapping function when extracting the ZHD values from GPT model instead of VMF1 grids. They concluded that using GPT-derived ZHD partially compensates the atmospheric loading effect on station heights. Since atmospheric loading is inversely proportional to the ZHD, any ZHD error will modify the vertical displacements related to atmospheric loading, compensating them [*Tregoning and Herring*, 2006]. This results in a better global repeatability (~0.2 mm) for solutions using ZHD values from the GPT model than those of the VMF1 grids. Therefore, using VMF1, the atmospheric loading signals are entirely revealed, allowing to properly remove them at the observation level or in a post-processing step. If atmospheric loading corrections are taken into account, then VMF1 solutions perform better than GMF+GPT solutions, confirming the partial compensation of GPT model [*Kouba*, 2009; *Steigenberger et al.*, 2009; *Tregoning and Watson*, 2009].

Latest studies [*Tregoning and Watson*, 2009] corroborated this finding and extended the comparison between GMF+GPT and VMF1 solutions to the power spectra analysis. The

authors showed that differences between solutions obtained using VMF1-extracted and GPT-derived ZHD contain significant correlated noise (higher power for low frequencies). Despite GMF and GPT models are based on an annual fit to VMF1 and ECWMF models respectively, the authors also showed that there is remaining power at the annual period. Comparing solutions using VMF1 and GMF mapping functions, they also showed correlated noise between them with power three times larger. Both issues point to the better high-frequency time resolution of the VMF1 grids. They assert that the solution improvement is then more significant when changing from GMF to VMF1 mapping functions, than changing from GPT-derived to VMF1-extracted ZHD. They also agreed with previous publications that using VMF1 and applying atmospheric loading corrections (in post-processing or at the observation level) significantly reduces the amplitude of correlated noise content.

Even with the limitations of our test, we showed overall small station height differences, which are consistent with recent published results. These height differences are larger in Antarctic region likely due to the deficient GPT and GPT height corrected pressure values. VMF1 products (ZHD and mapping functions) provide the most accurate results and are now available anywhere and anytime between 1992 to the present time, and even for near real-time applications such as ultra rapid IGS products [*Boehm et al.*, 2008b]. Therefore, we decided to change the tropospheric delay modeling from the previous GMF approach to the VMF1 grids in the next processing (ULR4).

3.3 Sub-network distribution

3.3.1. Introduction and objective

GPS processing time increases roughly proportionally to the square of the number of stations [*Blewitt et al.*, 1993]. Thus, to process a network of 90 stations takes approximately 10 times longer than a network of 30 stations. To overcome this computational burden the so-called cluster analysis technique is commonly used. This way, the whole network is split into several sub-networks, processed independently and then combined into an unique daily solution.

Within the past ULR solutions (ULR1 to ULR3, see Section 2.3), the stations were manually assigned to a specific sub-network under visual (subjective) considerations to achieve an even global distribution. The stations were distributed in five global sub-networks once and for all (hereinafter static sub-networks approach). Using this approach, the stations included in each static sub-network were always the same, whether or not their data were available for a specific day. Thus, when several stations were missing, the station distribution within the sub-networks was not homogeneous anymore and the number of sub-networks used was larger than necessary. This led to longer baselines and probably to regionalized sub-networks. That is, since missing stations for a day are rather random, it could be possible (we did not check that) that a sub-network would end with the available stations concentrated in North America and Europe, where they are numerous. This effect was especially noticeable for the early years of each reprocessing due to the limited number of available stations (Figure 3.9). For example, for the ULR4 network, the number of daily processed stations between 1996 and 2009 varies between a minimum of 53 and a maximum of 239. Maintaining the static sub-network approach means to distribute 53 stations in five sub-networks, resulting in ~10 stations per sub-network. Obviously, this is not the best approach. For that reason, past ULR solutions did not include data earlier than 1997. Moreover, since static sub-networks

were initially distributed with ~50 stations per sub-network, this hardly constrained the network evolution between successive ULR solutions. That is, adding or removing stations implied to redistribute the list of stations in new static sub-networks.
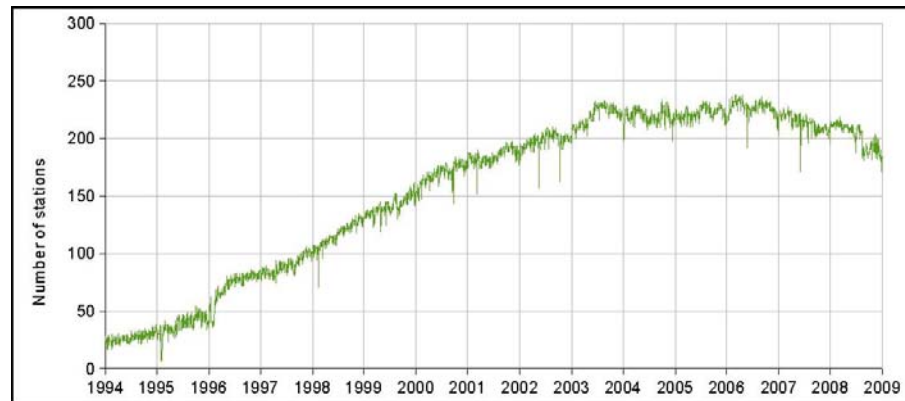
Figure 3.9. Number of daily stations in the ULR4 solution network.

In order to combine the static sub-network solutions into a daily solution, the IGS reference frame stations were used. Applying minimal constraints in all the transformation parameters with respect to these IGS coordinates, all sub-network solutions were aligned and combined simultaneously (see Chapter 4). That is, it was not necessary to include common stations between the sub-networks. However, as a drawback, the minimal number of IGS reference stations and their global distribution within a sub-network, requested for frame alignment, was not always assured, especially for the early years of the processing.

The ambiguity resolution process is more efficient on shorter baselines. Thus, improving the sub-network geometry should result in shorter baselines, which helps to resolve the ambiguities and then improves the solution. Also, with global well-distributed sub-networks, the estimation of global parameters like Earth Orientation Parameters and orbital parameters should be improved. We therefore decided to implement a new geometry-based approach to efficiently distribute the stations in the sub-networks. To assess the quality of the sub-network distribution and to validate the different methods tested, we chose three geometric parameters to analyze:

- the distance between the sub-network centroid and the coordinate system origin (centroid distance),
- the baseline length dispersion, and
- the coordinates dispersion along the three coordinate axes (XYZ).

ITRF2005 positions, or approximate when unavailable, are taken as the station coordinates. Thus, the considered coordinate system origin is actually the ITRF2005 origin. With these three parameters, the three conditions defined to reach the best sub-network distribution are:

- minimum centroid distance,
- minimum baseline dispersion, and

    – maximum coordinate dispersion.

All these three criteria are complementary, and the best value in all of them will ensure the best distribution to be reached. Starting with the first condition, a small centroid distance should indicate a good global coverage. For instance, if the stations of the sub-network were regularly and perfectly distributed over the Earth's surface, the centroid distance will be zero. This is in fact not possible, but a smaller centroid distance should indicate a better global coverage. However, a sub-network composed by two or more regionalized groups of stations with an inadequate global geometry (for instance, a sub-network composed by two regional groups of stations concentrated in Europe and Australia) could also lead to a centroid distance quite small. To avoid this we use the second condition. Geometrically well distributed sub-networks should have minimum baseline distance dispersion, that is, the baselines between neighbor stations should be equally in length. Note that even for the above example of a perfectly regular global distribution, the baseline dispersion (estimated here between all stations of the sub-network) will not be zero but minimum. This way, the problem with two or more regionalized sub-networks is solved because they will show larger baseline dispersion. However, this condition does not ensure a global coverage either as only one small regional sub-network (EUREF network for instance) will lead to a small baseline dispersion too. To avoid this, we need the third and last condition. A globally well-distributed sub-network should have a maximum dispersion of the stations along the three-coordinate axes. This station dispersion is estimated by the coordinate dispersion along each coordinate axis. However, there could be different sub-networks with the same three-axes dispersion and different centroid distances. To avoid this and to choose the best distribution, we need again the first condition.

The selected approach is called dynamic sub-networks approach because it is based on the optimal distribution of stations whose data are actually available for each day. Thus, the number of sub-networks and the stations they include is changing daily. Each dynamic sub-network is limited to a maximum of 50 stations. We consider this number as a good trade-off between processing time and sub-network density needed to estimate global parameters [e.g., *Blewitt et al.*, 1993].

Before the station distribution process itself, a group of common stations is selected every day to be used as a backbone for the sub-network combination (see Chapter 4).

Theoretically, three common stations should be sufficient to ensure the reference frame consistency between different sub-network solutions. However, to improve the datum consistency between solutions and to avoid the possible irregularities of the different solutions, six globally well-distributed IGS reference stations are selected as the common subset. IGS reference stations with less than 12h of observation are not considered. From the remaining reference stations, the northernmost and southernmost stations are always retained. The other four stations are selected as follows. In an iterative process, all baseline lengths are computed and one of the stations showing the shortest baseline is removed. From the two stations of the shortest baseline, the closest to the other stations (having the smaller isolation value, see following explanation) is removed. Thus, the four stations retained are usually located near the Equator, where the isolation is larger. These six common and daily-variable stations are then assigned to all the sub-networks.

The station distribution procedure is performed now as follows. For a given station and dynamic sub-network (which is already composed of at least the six common stations), we define the station isolation as the weighted sum of the distances to the nearest three

stations (see Eq. 15). For each station to distribute (red dot in Figure 3.10), we estimate this isolation within each candidate sub-network (blue boxes in Figure 3.10) and we assign the station to the sub-network in which this isolation value is larger. Once the station has been assigned to a sub-network, this sub-network is updated and the next station is analyzed. This iterative procedure is equivalent to populate successively the deserted areas of the sub-networks with the available stations.

$$Isolation = 3 \cdot d_1 + 2 \cdot d_2 + d_3 \quad . \qquad (15)$$
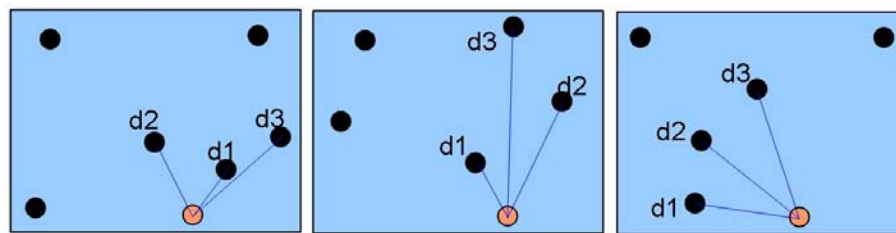
Figure 3.10. Dynamic station distribution scheme.

The weights used in Eq. 15 were determined empirically. These weights were necessary in order to improve the geometry distribution in order to favor the areas more isolated. That is, to favor when the nearest station (d_1) is the farthest one of the candidate sub-networks. For instance, in the example of Figure 3.10, without weighting, the isolation value would lead to assign the station to the second sub-network; by applying the empirical weights, the station is assigned to the third sub-network, which looks geometrically better-distributed. The benefit of these weights was confirmed by the analysis of the aforementioned three geometrical conditions. Following this procedure, stations for a day in 1997 where distributed twice, with and without applying the empirical weights. For each sub-network, the centroid, the baseline dispersion (standard deviation) and the mean coordinates dispersion (mean value of the standard deviations of the three coordinates) were estimated (Table 3.5). Mean values for each approach show that the empirical weights slightly improved the geometric quality of the sub-network distribution. That is, the sub-network centroid is closer to origin, the baseline dispersion is smaller and the mean coordinate dispersion is larger. Although the station distribution is better using weights, for this day, the global available network is not globally equilibrated, 75% of the stations being in the North Hemisphere. This explains the large value found for the distance between the ITRF2005 origin and the network centroid, which should be located between North America and Europe (see for instance Figure 3.13).

With the dynamic approach, all daily available stations are distributed in the strictly necessary number of sub-networks, ensuring geometrically optimal and dense sub-networks. So it is expected to improve the ambiguities resolution, and therefore the quality of the processing, with respect to the static sub-networks. The objective of the test was to compare the performance of the processing between using the static or the dynamic sub-network distribution approaches.

Table 3.5. Baseline dispersion, centroid distance to origin and mean coordinate dispersion for

station distribution with and without empirical weights. The mean values for each approach are also shown. Values in km.

	Sub-network	Stations	Baseline	Origin	Axes
With weights	1	38	3462	1974	3025
	2	38	3352	2312	3652
	3	37	3526	2597	3701
	Mean		3446	2294	3459
Without weights	1	38	3461	2104	3015
	2	38	3384	2077	3654
	3	37	3510	2733	3694
	Mean		3451	2304	3454

3.3.2. Data and results

To compare both approaches, a network of 225 stations was daily distributed in static and dynamic sub-networks and then processed with the same parameters for nine years of data, between January 1997 and December 2006.

As a comparison of both distribution approaches, Figure 3.11 shows the number of sub-networks obtained from the static and dynamic distributions. The number of dynamic sub-networks varies according to the evolution of the tracking network (see Figure 3.9). Figure 3.12 show the five static sub-networks and Figure 3.13 the two sub-networks resulting from the dynamic approach for DOY 336 of 1997. As expected, static sub-networks are excessively sparse, with only 18 to 25 stations per sub-network. On the contrary, both dynamic sub-networks contain 48 stations globally well-distributed, as far as the daily available stations permit this.
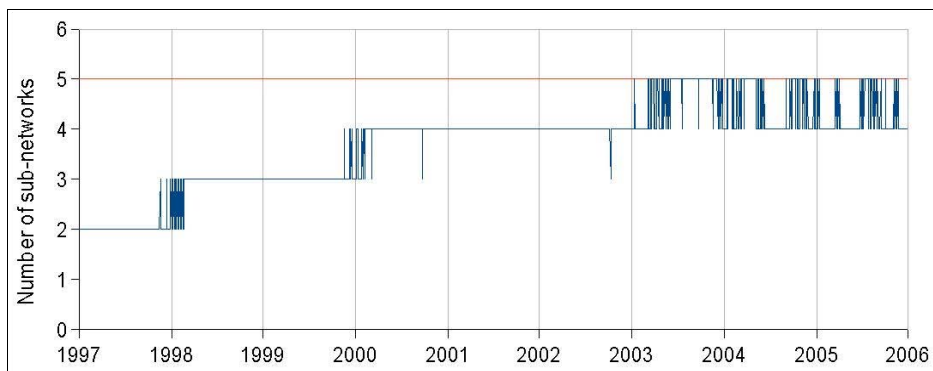
Figure 3.11. Number of static (red) and dynamic (blue) daily sub-networks.
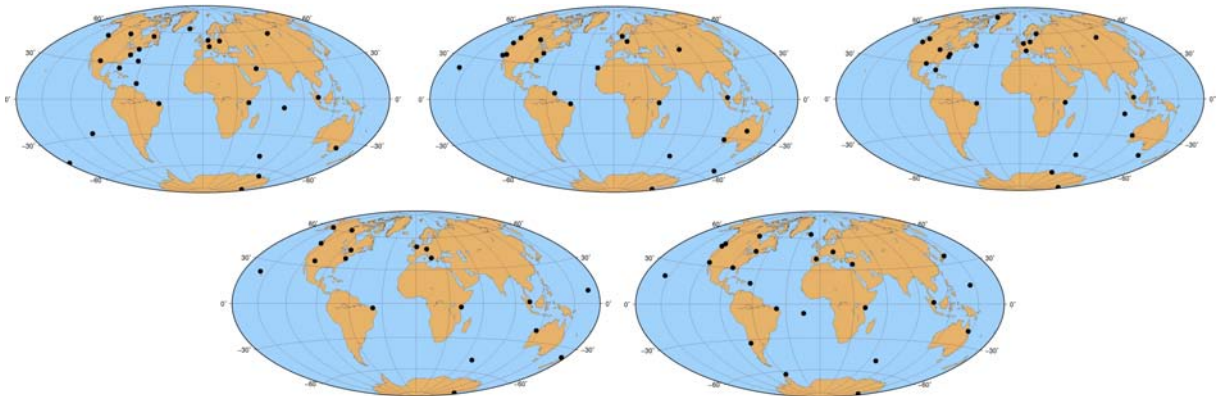
Figure 3.12. Static sub-networks in DOY 336 of 1997.
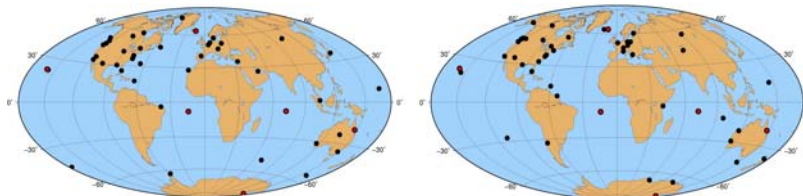
Figure 3.13. Dynamic sub-networks in DOY 336 of 1997. Red
stars represent the six common stations.

The main advantage of the new geometrical distribution is the improvement of the ambiguity resolution. Figure 3.14 shows the percentage of daily resolved ambiguities for the static and dynamic approaches and the difference between them for the nine years period. The number of stations (Figure 3.9) and the difference of resolved ambiguities percentage (green line in Figure 3.14) are highly anti-correlated (correlation coefficient of -0.91), confirming that most of the improvement comes from the new optimally distributed and denser dynamic sub-networks (Figure 3.15). Thus, as the network becomes sparser, using the dynamic distribution rather than the static one leads to an increase of up to 20% of the resolved ambiguities in 1997. After the year 2000, the improvement of the resolved ambiguities percentage becomes smaller and constant. This would indicate that the static sub-networks after year 2000 are not far from optimal distribution (there is only one less sub-network, see Figure 3.11).

The offset of about 10% detected in both approaches at the end of year 2000 is related to the use of the differential code bias (DCB) corrections estimated at the CODE IGS Analysis Center[3] [IGS electronic mail message 2827, 2000; 3160, 2001]. At the beginning of the test, these corrections were only available for post-2000 period (the first corrected day was December 26, 1999). Also, the offset of about 10-15% detected in both approaches at the beginning of 1997 is related to the temporal deactivation of the encryption of the P code, known as anti-spoofing (GPS Operational Advisory[4] 280.OA1, 1997).

---

3   ftp://ftp.unibe.ch/aiub/CODE/

4   http://www.navcen.uscg.gov/archives/GPS/opsadvisories
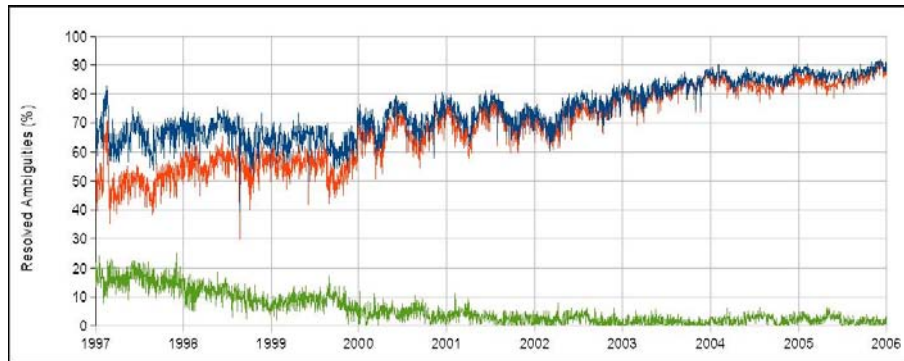
Figure 3.14. Percentage of resolved ambiguities for static (red line)
and dynamic (blue line) sub-networks. Green line represents the
difference between both.
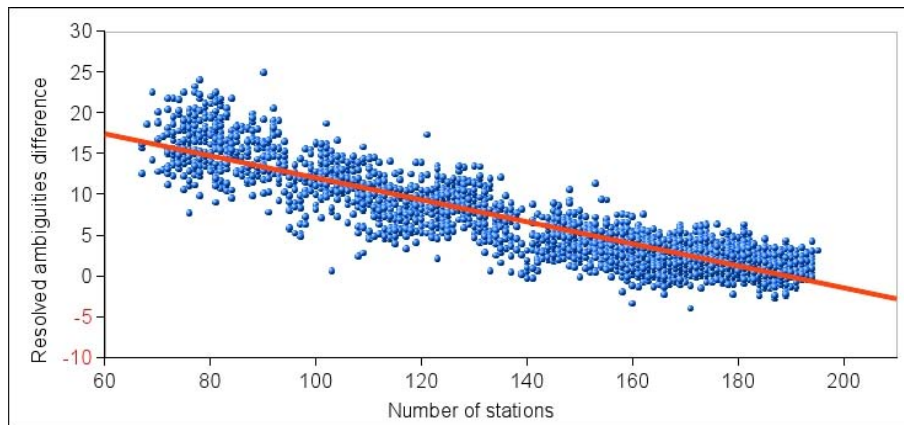
Figure 3.15. Relationship between the number of stations and the
difference of resolved ambiguities percentage between the static and
dynamic distribution approaches.

For both station distribution strategies, daily solutions were combined into weekly solutions and these weekly solutions where further combined into a long-term solution (see Chapter 4). The stations with more than 2.5 years of data were extracted for each solution (see Section 5.2). Then a 14-parameter transformation was estimated between the extracted stations of both solutions (Table 3.6). Some small differences (1-2 mm) were found for the origin definition. However, none of the estimated transformation parameters rates were significantly different from zero, indicating that there is no global velocity bias between both strategies. The post-fit WRMS of the station coordinates and velocities differences are shown in Table 3.7. Vertical position differences are larger than horizontal ones, exceeding the mm level. Maximum differences of station positions between both solutions reach 3 mm and 6 mm in horizontal and vertical components respectively (Figure 3.16). For velocities, maximum differences reach 1 mm/yr and 2 mm/yr for horizontal and vertical components respectively. About 97% of the vertical velocity differences are below 1 mm/yr and 81% are below 0.5 mm/yr (Figure 3.17).

Table 3.6. Transformation parameters between the dynamic and the static long-term solutions.

TX (mm) (mm/yr)	TY (mm) (mm/yr)	TZ (mm) (mm/yr)	Scale (ppb) (ppb/yr)
2.1±0.1	-0.2±0.1	0.7±0.1	0.00±0.00
0.2±0.1	-0.1±0.1	0.2±0.1	0.00±0.00

Table 3.7. WRMS of position and velocity differences between the dynamic and the static long-term solutions.

	WRMS E	WRMS N	WRMS U	WRMS 3D
Positions (mm)	0.6	0.7	1.5	1.1
Velocities (mm/yr)	0.2	0.2	0.4	0.3
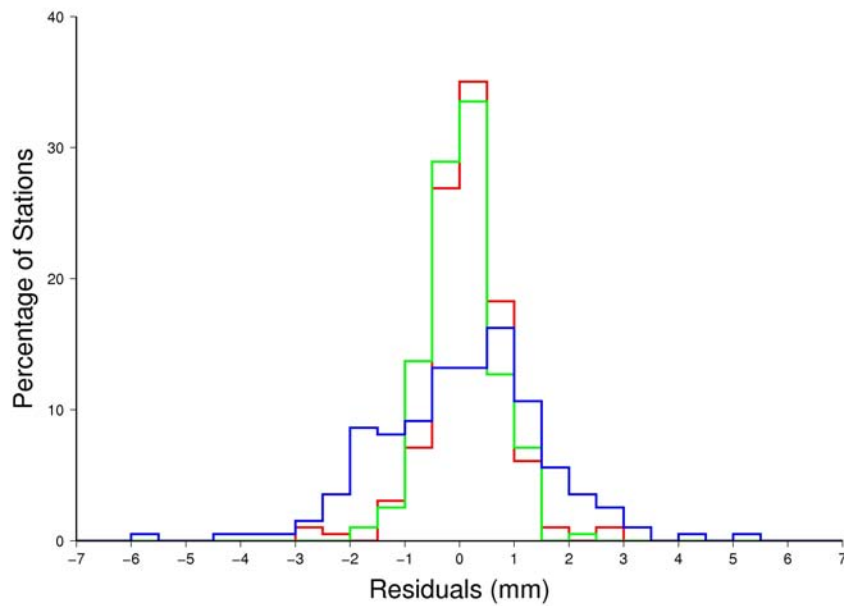
Figure 3.16. Histogram of station position differences between dynamic and static solutions for East (red), North (green) and Up (blue) components.

Horizontal and vertical repeatability of the weekly solutions with respect to the combined solution were extracted (Figure 3.18). As expected, the horizontal and the vertical weekly repeatability are worse in the early years for the static solution. On the contrary, in the
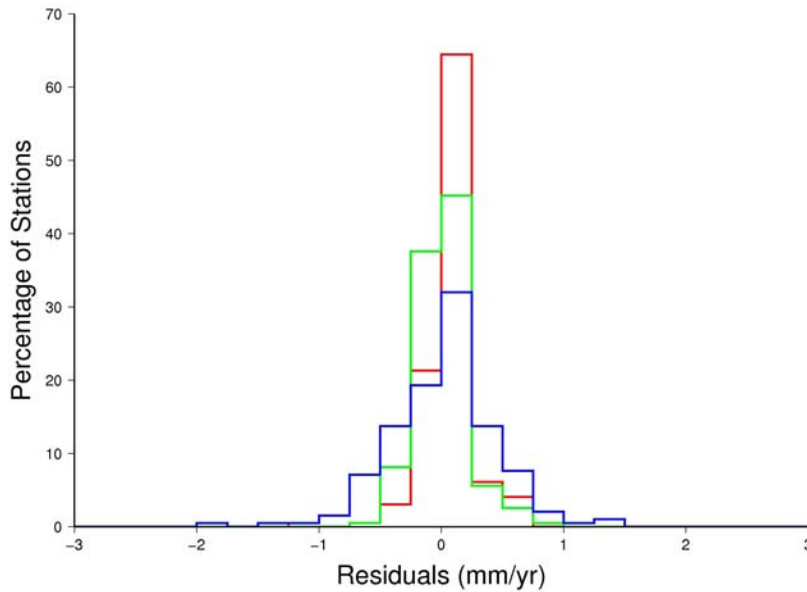
Figure 3.17. Histogram of station velocity differences between
dynamic and static solutions for East (red), North (green) and Up
(blue) components.

latest years, the horizontal and vertical repeatability for both solutions are similar. This corresponds to the evolution of the tracking network and the improvement of the station distribution in the early years. Analyzing the repeatability in a station-by-station basis, using the dynamic sub-networks improves the mean repeatability by 0.14 mm and 0.21 mm for horizontal and vertical components respectively.
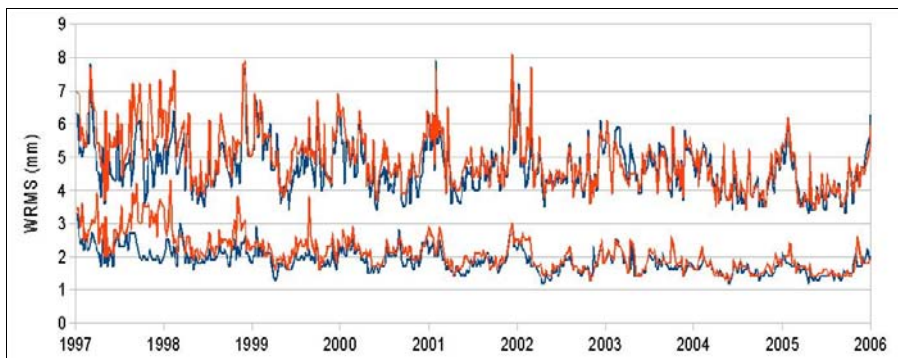
Figure 3.18. Horizontal (lower line) and vertical (upper line)
repeatability of static (red) and dynamic (blue) solutions.

To estimate the impact of the network distribution approach on the orbit estimation, dynamic and static daily estimated orbits were compared using a 7-parameter transformation. Figure 3.19 shows the daily 1D RMS (average of RMS of each component) estimated after

the transformation. The RMS of the differences between dynamic and static daily estimated orbits is between 1 and 2.5 cm. The 1D RMS was also extracted when comparing static and dynamic orbits to the IGS final orbits (Figure 3.20). Both curves (Figures 3.19 and 3.20) are well correlated with the difference of the resolved ambiguities percentage, showing the impact of an increased number of observations in the GPS processing.
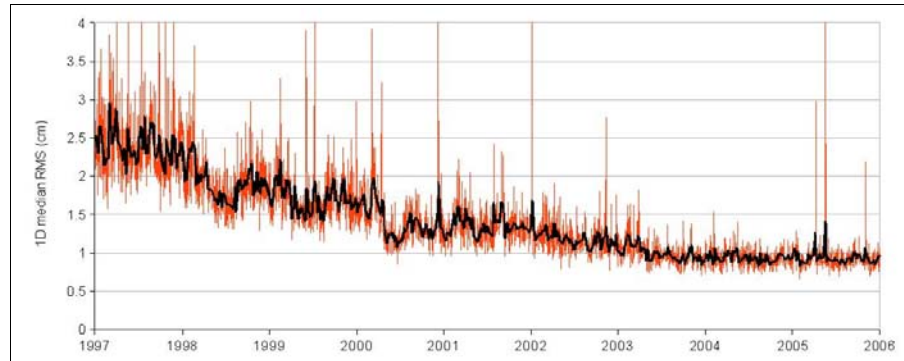
Figure 3.19. Daily (red) and 7-day smoothed (black) 1D median RMS
between dynamic and static estimated orbits.
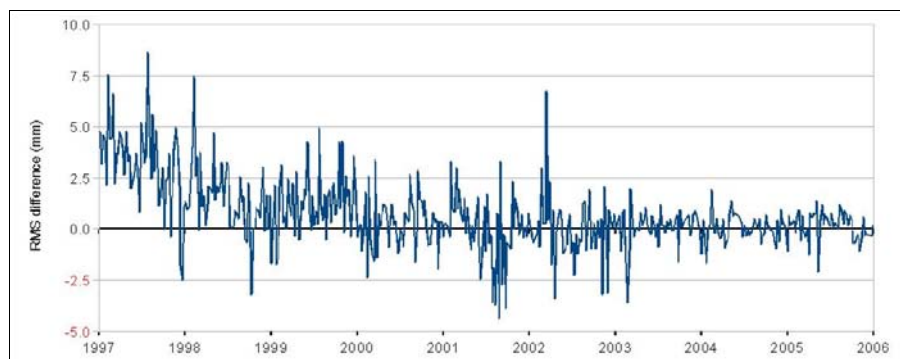
Figure 3.20. 7-day smoothed 1D RMS difference between dynamic
and static estimated orbits compared to IGS final orbits. Values are
RMS_dynamic subtracted from RMS_static.

Using a geometrically-optimal dense sub-network distribution based on available data clearly improves the quality of the estimated parameters through the increase of the percentage of resolved ambiguities. Moreover, the dynamic distribution makes the processing more flexible since adding or rejecting station of the network at any time is straightforward. Finally, the data processing of earlier years is more robust which allows us to lengthen the time series backwards accordingly, overcoming the 1997 limit of precedent ULR solutions.

3.4 Other changes

Apart from tropospheric mapping functions and sub-network distribution, a few other parameterization changes were implemented in ULR4 solution with respect to ULR3 solution. Their individual impacts on the quality of the solution were not directly examined due to its a

priori expected small impact or due to a clear external recommendation from the IGS or IERS services. The following changes were implemented:

- Ocean tide loading model changed from CSR4.0 [*Eanes and Bettadpur*, 1995] to FES2004 [*Lyard et al.*, 2006]. The main improvement of this model is its reduced errors of ocean tides and its 4 times improved spatial resolution, from 0.5º to 0.125º. This model is recommended by the updated version of the IERS Conventions[1].

- A priori station ZHD was changed from estimation using together the Hopfield standard pressure model and Eq. 8 to directly extraction from VMF1 grids. Several authors (see section 3.2.1) showed the drawbacks of using such a simple pressure model. ZHD extracted from VMF1 grids is recommended by the updated version of the IERS Conventions as valuable backup information when local pressure measurements are not available.

- IAU 1980 nutation theory was changed into the new IAU 2000, following the IAU 2000 Resolution B1.6 (IERS Conventions).

- Erroneous tight constrains on a priori EOP values for ULR3 solution were corrected to loose constraints. For the ULR3 solution these constraints were set to 0.001 arcsec (~3 cm) for Wobble, 0.0005 arcsec/day (~1.5 cm/day) for Wobble rate. For ULR4 solution, a meter-level constraint was applied to be consistent with the station a priori constraints. Those wrong tight constraints on EOP might be the cause of a noticeable bias for the North component of ULR3 solution with respect to other IGS AC reprocessed solutions [Jim Ray, personal communication].

- A refined preprocessing of the observation RINEX files was implemented. For ULR3 solution small RINEX files were directly rejected as they were expected to have some kind of error during its recording. This simple procedure was improved in ULR4 solution by the inclusion of a quality check of all the input RINEX files using TEQC software [*Estey and Meertens*, 1999]. Thus, only those RINEX files passing the quality check (mainly file format) and having more than five hours of observation were used in the subsequent GPS processing.

- The observation sampling rate for parameter estimation was changed from 5 to 3 minutes. Due to the enhanced performance of the processing facilities, it was decided to take into account a higher amount of phase data. This will result in smaller formal errors of daily solutions, whereas the values themselves must be almost exactly the same [Thomas Herring, personal communication]. Sampling rates of the current IGS Analysis Centers are between 30 s and 5 min, being 3 min the mean value.

3.5. Summary

The new ULR4 solution was processed by using the absolute antenna calibration model (already used in ULR3 solution actually), the VMF1 grids (for the a priori hydrostatic delay at zenith and for the mapping functions) and a new dynamic sub-network distribution approach.

The impact on station vertical velocities using the relative antenna calibration instead of the absolute one are mainly driven by the satellite PCO errors and it is composed of a

global bias plus station-dependent or local errors. The global bias represents a vertical velocity change of 2 mm/yr. However, it can be absorbed with a terrestrial frame scale drift parameter, for instance by alignment of the solution to an external reference frame. The remaining local errors follow a spatial latitude-dependent pattern and can reach up to ± 0.7 mm/yr. These local errors represent a network distortion which is not absorbed by any transformation parameter. Thus, it is mandatory to use the absolute antenna calibration model to estimate reliable long-term vertical velocities.

The impact of the tropospheric delay modeling using the simple GMF mapping function with the a priori ZHD calculated from the GPT model instead of the more preciseVMF1 grids consist of global vertical velocity differences up to ±0.2 mm/yr. Furthermore, a noticeable reduction of the time correlated noise is expected. This should allow us to reduce the uncertainties of the estimated velocities. No spatial pattern was found for these differences but worse results were found in the Antarctic region. This is due to a wrong extrapolation of atmospheric pressure with altitude which leads to station height errors of several millimeters. Unfortunately, the same pressure extrapolation model is used for both approaches (GMF and VMF1 solutions). Therefore, it is expected that some station height errors remain at those latitudes. In addition, it is also expected that the local variability of atmospheric conditions (pressure and temperature) at different time scales could result in time-dependent extrapolation errors. Its impact on vertical velocities in this region is unknown. Further studies using meteorological observations taken at the station heights are needed to clarify this.

Results of both comparisons (antenna phase center correction and tropospheric model) were given by *Santamaría et al.* [2008a] (see Annex D).

Finally, the stations are distributed following a better geometry-based approach which improves the data processing in the early years. The impact on vertical velocities of this new distribution, specially conceived for the new solution, is estimated in a station-dependent term of ±0.4 mm/yr. No global velocity bias was found by applying the new dynamic sub-networks approach. These results were given by *Santamaría et al.* [2008b; 2009a] (see Annex D).

All of these changes lead to a state-of-art GPS processing strategy comparable to those used by the IGS Analysis Centers. The summary of the complete strategy used for ULR4 can be found in Annex A and also in *Santamaría-Gómez et al.* (in press, see Annex D). To assess the quality of the ULR4 solution, the products resulting from the implementation of this strategy are compared to those of the IGS Analysis Centers through our contribution to the IGS reanalysis campaign[5] (see Chapter 7).

---

5   http://acc.igs.org/reprocess.html

4. Combination and products

The processing strategy defined in Chapter 3 was used to process all the available GPS data from 1996 to 2009 with the GAMIT software. A detailed description of the processed network is done in Chapter 8. As output of this processing, we obtain the daily sub-network solutions. These solutions are made up of a group of estimated parameters including station positions, Earth Orientation Parameters (EOP), ZTD, atmospheric horizontal gradients, orbital parameters and station/satellite clocks bias among others as well as their covariance matrix. These parameters (especially station positions, EOP and orbital parameters) are expressed in a fiducial-free or loose sense [*Heflin et al.*, 1992]. That is, they are expressed in an unknown frame defined at the given a priori constraint level (see later in text). This fiducial-free approach is preferred to the use of fiducial sites to realize the terrestrial reference frame because the estimated polyhedron is geometrically self-consistent.

As mentioned in Section 3.3, the sub-network solutions for a day must be combined to rebuild the daily solution of the whole network. Thus, these combined solutions contain the daily positions of the whole station network. In order to estimate the station velocities, it is necessary to properly stack the station positions creating a long-term combined solution. This long-term combined solution is composed of the station positions, expressed in a reference epoch, their velocities and the covariance matrix. However, due to the large amount of daily solutions usually managed in a reprocessed solution (e.g. ~4750 for ULR4 solution), it is a common practice to first combine these daily solutions into weekly solutions. Thus, this intermediate weekly combination reduces by a factor 7 the number of solutions to deal with for velocity estimation. Furthermore, it removes the high frequency information of the station displacements while it still preserves all the linear and non-linear information of station displacements for longer periods (from a couple of weeks on, following the Nyquist-Shannon sampling theorem).

This Chapter 4 is dedicated to the daily and weekly combinations, that is, the intermediate steps between GPS data processing and station velocity estimation. The long-term combination of weekly solutions for velocity estimation, the so-called stacking, will be considered in the next Chapter 5. Section 4.1 describes the combination procedure of the past ULR3 solution. Section 4.2 describes the new combination procedure implemented in the ULR4 solution. Section 4.3 compares both ULR3 and ULR4 combination approaches and finally, a summary is given in section 4.4.

4.1. ULR3 combination procedure

For ULR3 solution, daily and weekly combinations were performed with the Combination and Analysis of Terrestrial Reference Frame (CATREF) software [*Altamimi et al.*, 2002; 2007] (see Figure 4.1).

CATREF software was built to combine coordinate sets (station positions and velocities) and EOP by means of a classic weighted least squares adjustment. The general model used in this software to combine several frames is the transformation of Bursa-Wolf [*Boucher*, 1979], also known as 7-parameter Helmert's transformation:

$$X_s = T + \lambda \cdot P \cdot X \ , \tag{1}$$
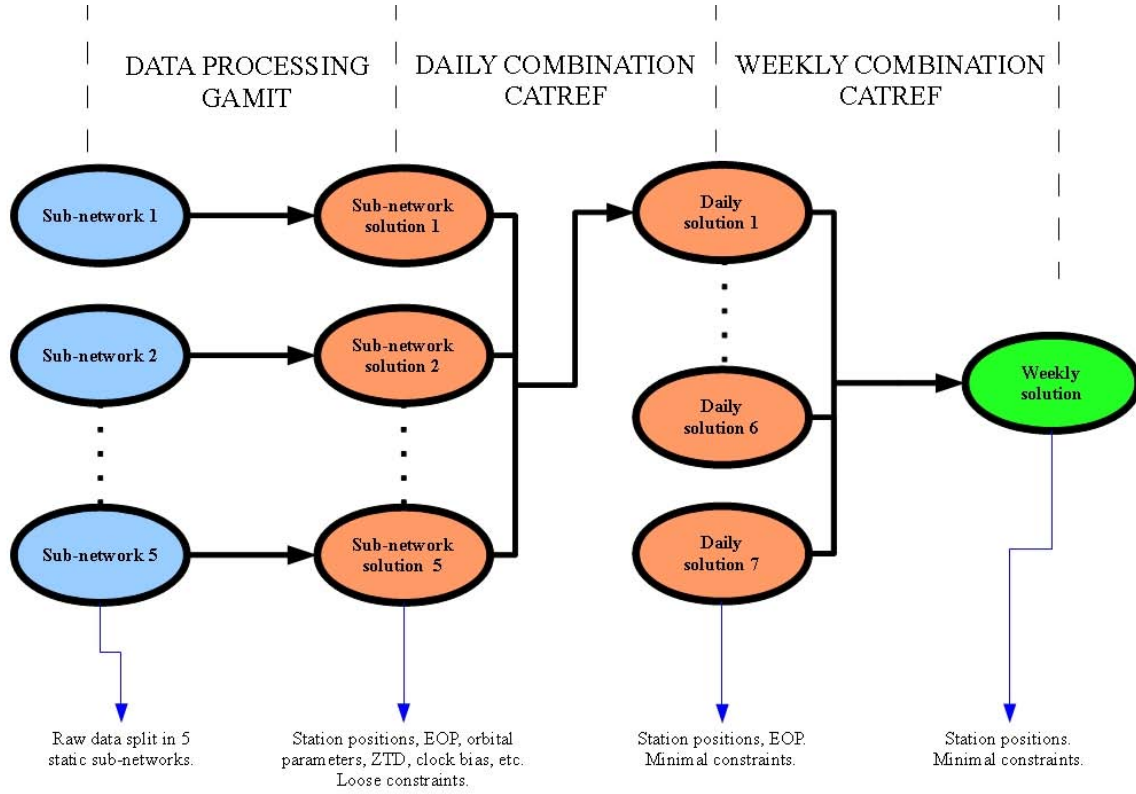
Figure 4.1. Scheme of combination procedure for ULR3 solution.

where X_s are the input solutions, X is the combined output solution, T, λ and P represent the three translations, scale factor and three rotations respectively of the combined frame with respect to each input solution frame:

$$
X_s = \begin{pmatrix} x_s^i \\ y_s^i \\ z_s^i \end{pmatrix} \quad X = \begin{pmatrix} x^i \\ y^i \\ z^i \end{pmatrix} \quad T = \begin{pmatrix} T_x \\ T_y \\ T_z \end{pmatrix} \quad \lambda = (1+D) \quad P = (I+R) \quad R = \begin{pmatrix} 0 & -R_z & R_y \\ R_z & 0 & -R_x \\ -R_y & R_x & 0 \end{pmatrix}. \quad (2)
$$

Substituting Eqs. 2 into Eq. 1 and linearizing the combination model (due to that space geodetic techniques scale and orientation differences are at the 10^{-5} level), it can be written as:

$$
\begin{pmatrix} x_s^i \\ y_s^i \\ z_s^i \end{pmatrix} = \begin{pmatrix} x^i \\ y^i \\ z^i \end{pmatrix} + (t_s^i - t_0) \cdot \begin{pmatrix} \dot{x}^i \\ \dot{y}^i \\ \dot{z}^i \end{pmatrix} + \begin{pmatrix} T_x \\ T_y \\ T_z \end{pmatrix}_k + D_k \cdot \begin{pmatrix} x^i \\ y^i \\ z^i \end{pmatrix} + R_k \cdot \begin{pmatrix} x^i \\ y^i \\ z^i \end{pmatrix} + (t_s^i - t_k) \cdot \left[\begin{pmatrix} \dot{T}_x \\ \dot{T}_y \\ \dot{T}_z \end{pmatrix}_k + \dot{D}_k \begin{pmatrix} x^i \\ y^i \\ z^i \end{pmatrix} + \dot{R}_k \begin{pmatrix} x^i \\ y^i \\ z^i \end{pmatrix} \right], \quad (3)
$$

where superscript i represents each station, subscript s represents each input solution, t

represents time epoch, t_0 the reference time epoch and subscript k represents the time epoch of the transformation parameters. To handle the EOP combination, the following equations are added to the combination model of Eq. 3:

$$
\begin{aligned}
x_s^p &= x^p + R_y & \dot{x}_s^p &= \dot{x}^p + \dot{R}_y \\
y_s^p &= y^p + R_x & \dot{y}_s^p &= \dot{y}^p + \dot{R}_x \\
UT_s &= UT - \frac{1}{f} \cdot R_z & LOD_s &= LOD + \frac{\Lambda_0}{f} \cdot \dot{R}_z
\end{aligned}
\tag{4}
$$

The combination model represented by Eq. 3 provides, for each station i, the combined coordinates at the reference epoch $(x^i,\ y^i,\ z^i)$ and their estimated velocities $\left(\dot{x}^i, \dot{y}^i \text{ and } \dot{z}^i\right)$. However, there is no velocity estimation in the combination of sub-network solutions since they always refer to the same epoch $(t_s^i = t_0)$. Furthermore, in the combination of daily solutions we do not estimate velocities either. The resulting weekly station velocities are supposed to be equal to zero due to the short time span. That is, we assume that the daily variation of station positions within a week is mainly due to random errors rather than to tectonic movement. Thus, we apply a tight constraint (0.1 mm/yr) to the a priori weekly velocities which are equal to zero. The transformation parameter rates are not estimated for combining sub-network, daily nor weekly solutions either. They are only estimated when combining long term solutions velocity estimation. For such a combination, we can derive a equation similar to Eq. 3 to estimate station combined velocities (by differentiating Eq. 3 with respect to time). Thus the combination model of Eq. 3 is simplified to:

$$
\begin{pmatrix} x_s^i \\ y_s^i \\ z_s^i \end{pmatrix} = \begin{pmatrix} x^i \\ y^i \\ z^i \end{pmatrix} + \begin{pmatrix} T_x \\ T_y \\ T_z \end{pmatrix}_k + D_k \cdot \begin{pmatrix} x^i \\ y^i \\ z^i \end{pmatrix} + R_k \cdot \begin{pmatrix} x^i \\ y^i \\ z^i \end{pmatrix}.
\tag{5a}
$$

or in matrix notation to:

$$
X_s = X + T_k + D_k \cdot X + R_k \cdot X.
\tag{5b}
$$

Eq. 5b can be further simplified as:

$$
X_s = X + A\theta,
\tag{6}
$$

where:

$$A = \begin{pmatrix} 1 & 0 & 0 & x_0^i & 0 & z_0^i & -y_0^i \\ 0 & 1 & 0 & y_0^i & -z_0^i & 0 & x_0^i \\ 0 & 0 & 1 & z_0^i & y_0^i & -x_0^i & 0 \end{pmatrix} \qquad \theta = \begin{pmatrix} T_x & T_y & T_z & D & R_x & R_y & R_z \end{pmatrix}^T .$$

Since the unknown parameters (X and θ) are small, they are linearized around their a priori values with:

$$X = X_0 + \delta X \qquad \theta = \theta_0 + \delta \theta \tag{7}$$

Setting the a priori transformation parameters equal to zero ($\theta_0 = 0$), the observation equation system is then defined as:

$$X_s = \begin{pmatrix} 1 & A \end{pmatrix} \begin{pmatrix} \delta X \\ \theta \end{pmatrix} . \tag{8}$$

However, the normal equation system built with the Eq. 8 is singular, meaning that the input unconstrained solutions (X_s) do not suffice to define all the estimated parameters (δX and θ). There is a rank deficiency corresponding to the definition of the combined frame (origin, scale and orientation). These parameters are defined through their correspondent transformation parameters (three translations for the origin, scale and three rotations for the orientation) and their rates if applicable. This way, the frame definition is always a relative quantity.

In order to define the combined frame, it is necessary to add to the normal equation system some additional condition equations. These condition equations, called minimal constraints in the CATREF software, are applied on the frame parameters and not over the station coordinates, preserving then the quality of the observations without introducing any distortion of the terrestrial frame. Thus, these constraints involve the cancellation of the transformation parameters between an external reference frame and the output combined frame. Solving for θ in Eq. 8, the minimal constraint equation is defined by:

$$\theta = \left(A^T A \right)^{-1} A^T \left(X_R - X \right) = 0, \tag{9}$$

where X_R are the coordinates of a selected group of stations of the reference frame, the so-called datum. This way, the combined frame definition is imposed by the reference frame. The rank deficiency is overcome and the inversion of the solution is ensured [*Altamimi et al.*, 2007].

Following this approach, all loose constrained sub-network solutions of ULR3 were combined into daily and later into weekly solutions (Figure 4.1). For both combinations, minimal constraints over all the transformation parameters were applied with respect to the

ITRF2005 coordinates of the IGS05 stations included in the solutions. This way there is no need to process common stations in all the sub-networks. In the subsequent stacking of the weekly solutions, the estimated transformation parameters were estimated at the mm level, demonstrating a correct frame alignment [*Wöppelman et al.*, 2009].

However, combining sub-network and daily solutions this way has two drawbacks. First, the intrinsic physical information of the GPS technique about the geocenter motion is not available in the weekly solutions. This is due to the fact that before the weekly combination, the sub-network and daily solutions were constrained to ITRF2005 reference frame through the minimal constraints. Second, the estimated daily orbits are not available from the combination of the sub-networks either. These two by-products, geocenter motion and orbits, are designated as new insights to compare and to verify the quality and performance of the new ULR4 solution with respect to other high-end GPS solutions (i.e. in the frame of the IGS reanalysis campaign). Therefore, a new combination approach was implemented for the ULR4 solution.

4.2. ULR4 combination procedure

All the satellite-based geodetic techniques (GPS, SLR and DORIS), known as dynamical techniques, are sensitive to the Earth's center of mass. Certainly, the computed orbits are defined with respect to this center by fixing to zero the degree-1 coefficients of the spherical harmonic expansion of the gravity field. This way, tracking GPS stations fixed to the Earth's crust are sensitive to the motion of the Earth's center of mass, caused by mass redistribution in the whole Earth (interior and surface), through the displacements observed on the satellite constellation (see more details in Section 7.2.2). On the contrary, space-geodetic techniques (satellite techniques and VLBI) are not sensitive to the frame orientation. The frame orientation is an unobservable parameter and then it is defined by convention through specific constraints. For instance, the orientation of the successive ITRS realization frames are defined to be consistent with the orientation defined by the Bureau International de l'Heure at epoch 1984.0 [*McCarthy and Petit*, 2004]. The time evolution of the orientation is defined with a No-Net-Rotation (NNR) condition with respect to an absolute plate motion model as the NNR-NUVEL-1A [*DeMets et al.*, 1994]. Finally, all space-geodetic techniques are sensitive to the frame scale. However, for the GPS technique in particular, the frame scale is not an independent parameter since it was fixed to the ITRF2000 scale in order to determine precisely the PCO bias of the satellite antennas (see Section 3.1.2). Thus, the only frame parameter which preserves a physical meaning for the GPS technique is the geocenter motion. Therefore, in a rigorous sense, only the constraints applied over the frame orientation are true "minimal" constraints. No external constraints should be needed in the GPS origin and scale definition because they are respectively intrinsically and externally defined.

Then, using the minimal (i.e. external) constraints equations over the 7 transformation parameters does not allow to preserve the information about the geocenter motion of the GPS technique. To cope with this limitation and to preserve the intrinsic physical frame parameters of the space-geodetic techniques, for instance the geocenter motion for GPS or the scale for VLBI, it is necessary to add to the normal equation system of CATREF some different condition equations substituting the minimal constraints. These conditions are known as internal constraints since they avoid the use of any external frame to define the combined frame.

By fitting a linear regression to the transformation parameters (θ) of the combined

frame with respect to the input solutions we get:

$$P_k = P_0 + (t_k - t_0) \cdot \dot{P} \, , \tag{10}$$

where P_k is any of the transformation parameter of θ at epoch t_k, P_0 is the transformation parameter value at epoch t_0 and $\dot{P}$ is the transformation parameter rate; the internal constraint conditions are defined as:

$$P_0 = 0 \qquad \dot{P} = 0 \tag{11}$$

Representing Eq. 10 in a least squares equation system leads to:

$$\begin{pmatrix} K & \Sigma (t_k - t_0) \\ \Sigma (t_k - t_0) & \Sigma (t_k - t_0)^2 \end{pmatrix} \begin{pmatrix} P_0 \\ \dot{P} \end{pmatrix} = \begin{pmatrix} \Sigma P_k \\ \Sigma (t_k - t_0) \cdot P_k \end{pmatrix} . \tag{12}$$

Applying then Eqs. 11 into Eq. 12 results in:

$$\Sigma P_k = 0 \qquad \Sigma (t_k - t_0) \cdot P_k = 0 . \tag{13}$$

Eq. 13 represents the internal constraint conditions to add to the observation equation system of Eq. 8. These internal constraints are then defined in such a way that the sum of the transformation parameters is equal to zero. That is, the estimated transformation parameters of each sub-network/daily solution frame represent the deviation from a "mean" frame. The combined frame is then defined to be this mean frame. This way, the estimated transformation parameters of the input solutions using internal constraints are the same as those estimated with minimum constrains but detrended (without a trend and centered on zero). This implies that the residual station positions (with respect to the combined solution) are the same using both constraints, but not the frame of the combined solution. That is, the internal consistency of the combined frame is insensitive to its definition. The advantage of this is that we can analyze the non-linear station movements (e.g. periodic signals or apparent geocenter variations) without taking care on which reference frame are expressed the combined station positions and velocities. As with the minimal constraints, the internal constraints overcome the rank deficiency and let to invert the solution. More details about the internal constraints can be found in *Altamimi et al.* [2007].

It is also worth to note that we can mix up minimum and internal constraints in the same combination by adding to the model of Eq. 8 the corresponding Eq. 9 and 13 for different transformation parameters. For instance, when combining sub-networks or daily GPS solutions, we can apply internal constraints to translation and scale parameters to preserve their intrinsic information and minimal constraints to the rotation parameters, to use

an externally defined orientation.

However, to apply internal constraints while combining sub-network solutions using CATREF leads to a weak combination as the only common parameters between the sub-network solutions are the positions of the six common stations (see comparison in next Section 4.3). Note that with the ULR3 combination procedure all available IGS05 stations were used to combine the sub-networks through the minimal constraints. In addition, the estimated daily orbits are still unavailable since CATREF software only deals with terrestrial frames, that is, station positions, velocities and EOP. Both limitations are overcome if sub-network orbital parameters are also combined and extracted. Therefore, the use of the Globk software [*Herring et al.*, 2006b] was investigated.

Globk is a Kalman filter [*Kalman*, 1960] analysis software built to combine solutions resulting from the processing of space-geodetic data, specially GPS and VLBI solutions. The Kalman filter is an estimation method based on parameters whose values change during the estimation procedure. Globk combines the loose constrained estimates (e.g. resulting from GAMIT) of station coordinates and velocities, earth-rotation parameters and orbital parameters. As with CATREF, Globk can be used to perform daily/weekly combinations and to stack solutions for velocity estimation. The main differences of Globk with respect to CATREF are:

- Globk allows us to combine orbital parameters,

- any estimated parameter can be represented as a stochastic process rather than being deterministic, and

- input and output Globk solutions are always loose solutions. The frame definition for the output (combined) solution is an optional and independent step.

The estimation process within the Kalman filter is carried out sequentially. First, given the a priori values of the parameters and their covariance matrix (a priori constraints), the parameters are estimated at epoch t with the observations of epoch t. The linearized combination model which relates the input observations with the output estimated parameters at epoch t is as follows:

$$Y_t = A_t X_t^t + V_t, \tag{14}$$

where Y_t are the differences between the observations and their theoretical values calculated from the a priori values of the parameters to be estimated, X_t^t are the adjustments to the a priori values of the estimated parameters, A_t is the matrix of partial derivatives and V_t are the residuals representing the measurement noise. The subscript represents the epoch of the values and the superscript the epoch of the last data used for the estimation. Second, the estimated parameters and their covariance matrix (C_t^t) are predicted for the next data epoch ($t+1$):

$$X_{t+1}^t = S_t X_t^t$$
$$C_{t+1}^t = S_t C_t^t S_t^T + W_t \tag{15}$$

where S_t is the state transition matrix relating the estimated parameters at different epochs and W_t is the stochastic nature of the estimated parameters. V_t and W_t are assumed to be uncorrelated. Thirdly, by adding the observations at epoch $t+1$ to the model, the predicted parameters and their covariance matrix at epoch $t+1$ are updated using the filter gain function (K):

$$X_{t+1}^{t+1} = X_{t+1}^t + K\left(Y_{t+1} - A_{t+1} X_{t+1}^t\right)$$
$$C_{t+1}^{t+1} = C_{t+1}^t - K A_{t+1} C_{t+1}^t \tag{16}$$
$$K = C_{t+1}^t A_{t+1}^T \left(V_{t+1} + A_{t+1} C_{t+1}^t A_{t+1}^T\right)^{-1}$$

This procedure is called forward running filter [*Herring et al.*, 1990] and its phases, prediction and update, are applied sequentially with all the available data. If an observation is not available for any epoch, the update phase is skipped to the next available data epoch, thus performing multiple prediction steps. In the same way, if multiple independent observations are available at the same epoch, then multiple update steps will be performed. Thus, to start the filter, for each parameter to be estimated within Globk, it is necessary to provide its a priori values and some level of constraint. These constraints have the form of one sigma uncertainties of the a priori values used for the combination. The level of these constraints defines whether the parameter will be loosely constrained, tightly constrained of fixed to its a priori value. In addition, if the parameter is considered to follow a stochastic process, its a priori constraint is loosened over time. However, if the estimated parameters are treated as deterministic, the gain function (Eq. 16) is reduced in such a way that the Kalman filter becomes similar to a weighted least squares estimation.

For the new ULR4 solution, loose sub-network solutions are combined into daily solutions using Globk (Figure 4.2). The parameters used to combine the sub-networks are the estimated orbital parameters, the estimated EOP (except UT1 which is fixed to its a priori value), the estimated positions of the six common stations (see Section 3.3) and also their estimated daily mean ZTD. All the a priori values for the combination are extracted from one of the input solutions. All a priori constraints are set to 10 m or equivalent (~300 mas for EOP). Since there is no different epoch between the solutions, no parameter is considered to be stochastic. Daily solutions are constrained in rotation with respect to the reference frame. In Globk, these constraints are called generalized constraints, and are similar to the minimal constraints of CATREF as they minimize the departure from the a priori coordinates of a selected set of stations (datum, see next Section 5.3) while estimating the transformation parameters of the frame. From these daily constrained solutions the ULR orbits are extracted. Then, using CATREF, the daily solutions are combined into weekly solutions. Minimal constraints with respect to ITRF2005 are applied to rotations and internal constraints to translations and scale parameters respectively. This way, geocenter motion information is kept in the weekly solutions. ULR4 products, consisting in weekly station positions (containing apparent geocenter motion) and daily orbits and EOP, resulting from this combination procedure were submitted to the IGS in the frame of the reanalysis campaign (see Chapter 7).

Although the IGS05 coordinates should be used as reference frame to align and define the combined frame (see Section 3.1), the ITRF2005 coordinates were used instead for the frame orientation of daily/weekly solutions as in the case of the ULR3 solution. This was due
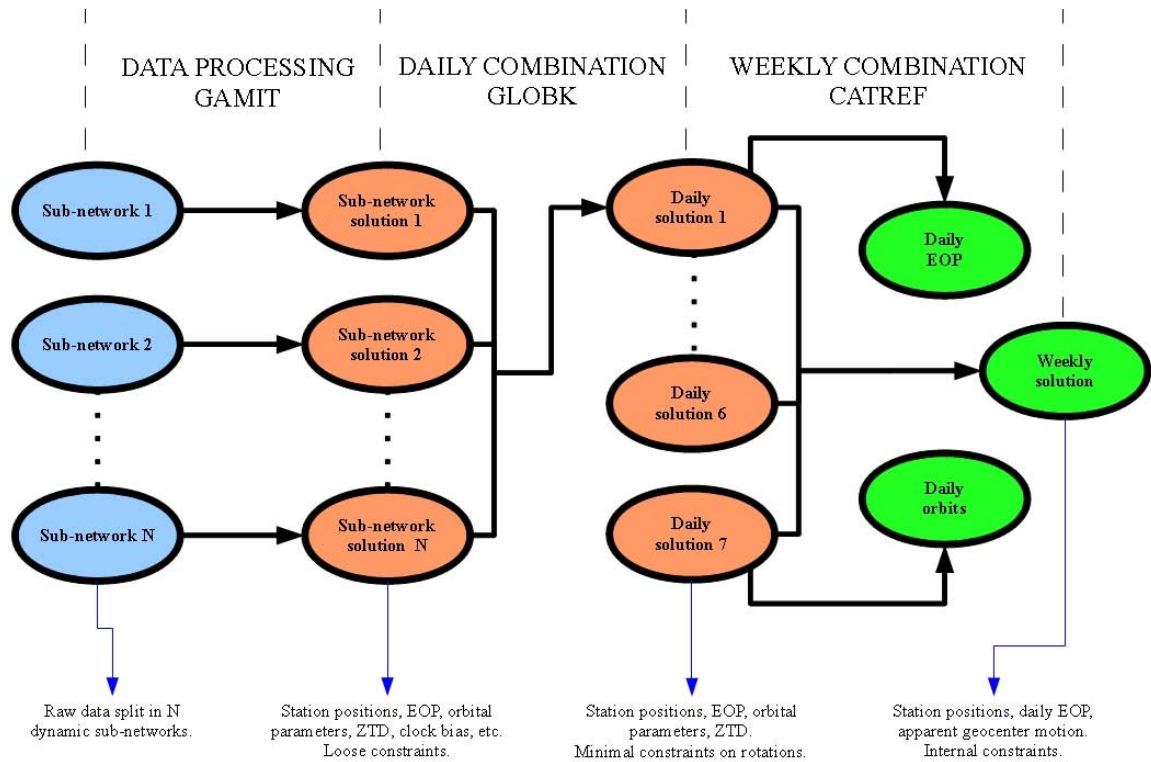
Figure 4.2. Scheme of the first combination procedure for ULR4 solution.

to the fact that the original IGS05 reference frame only contained the latest estimation of the station positions of the ITRF2005 (corrected for the antenna calibration model change, see section 3.1.2). For each station of the ITRF2005, different coordinates are available within specific and defined epochs due to permanent station position changes, known as position offsets. These different coordinates are termed as the solution number (soln) of the stations (see more details in next Section 5.1). Thus, using only the latest ITRF2005 estimates (soln) in the IGS05 to align 15 years of weekly solutions would lead to a large number of reference stations aligned to the wrong reference coordinates (and thus rejected) for the early years of the processing. Nevertheless, the effect of choosing IGS05 rather than ITRF2005 coordinates for the frame orientation is assumed to be small [*Kass et al.*, 2009] as estimated horizontal coordinate differences are at the mm level (see Section 3.1.2).

Once the products were submitted and due to feedback from the IGS reanalysis, the combination procedure was changed to improve the internal consistency of the extracted ULR4 products. In this new combination procedure loose daily solutions are combined into weekly solutions also using Globk (see Figure 4.3). For this weekly combination only station positions and EOP are considered. Orbit parameters are not estimated in weekly but daily arcs. Constraints to the a priori values are also set to 10 m or equivalent. Pole motion, pole rate and length of day are considered to vary stochastically with amplitude of 365 mas^2/yr, which is equivalent to a sigma increment of 1 mas between daily estimations. The loose weekly combined solutions are then constrained and aligned (rotation only) to the ITRF2005 frame. In the alignment, all IGS05 stations are used a priori and then some stations are rejected in a iterative process. This procedure is made in two steps [*Herring et al.*, 2006b]. First, before frame alignment, stations with a height uncertainty larger than three times the

difference between the median and the minimum height uncertainty are rejected. However, the station is finally retained if the height uncertainty is not larger than 15 mm from the median uncertainty. Only height uncertainty values are used since, before the frame definition, the horizontal uncertainties will be larger than usual [*Herring et al.*, 2006b]. The frame alignment is then performed and the post-fit residuals analyzed. Second, any station having a normalized position residual higher than 4 is also rejected and the procedure iterated. These values for the datum selection are applied based on the Globk software recommendations [*Herring et al.*, 2006b]. Once the weekly combination is performed and aligned, the resulting constrained weekly station positions and daily EOP are extracted. Using these station positions and EOP as new fixed a priori values, a second daily combination (with the original loose sub-network solutions) is performed to re-estimate the daily orbit parameters. This way, the weekly station coordinates and the daily orbits and EOP products are fully consistent. This is the recommended combination procedure for the IGS Analysis Centers [*Kouba et al.*, 1998].
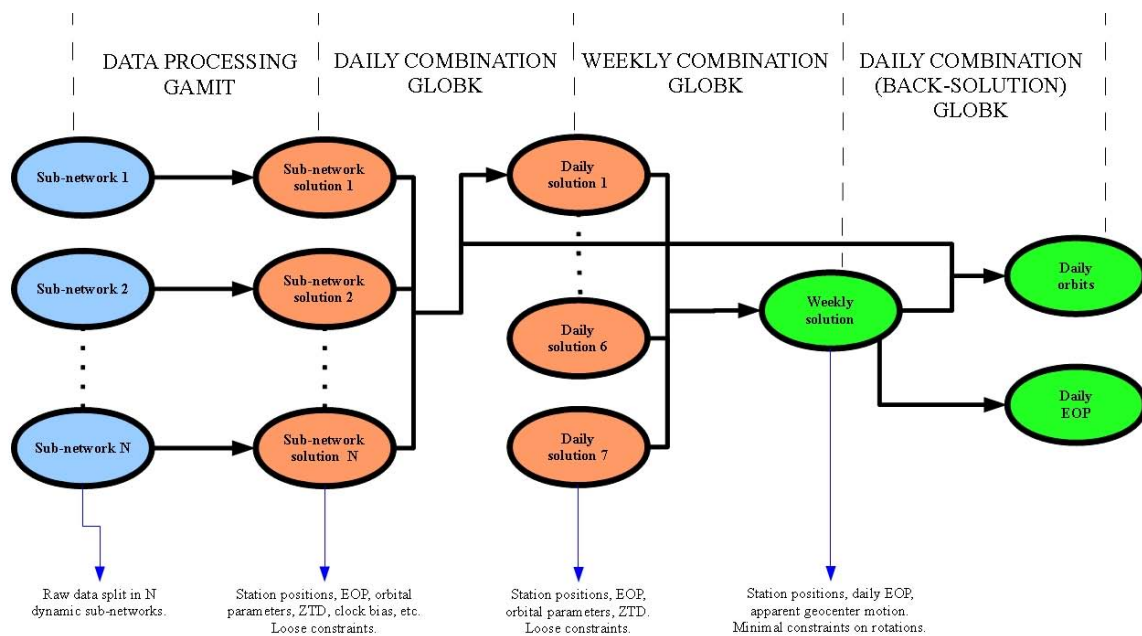
Figure 4.3. Scheme of the last combination procedure for ULR4 solution.

Both issues, the reference frame used for the daily/weekly frame orientation and the consistency of weekly station coordinates and daily orbits/EOP, might explain the large rotation values found for ULR4 orbits with respect to the combined IGS reanalyzed orbits (see more details in Section 7.4). However, the weekly station coordinate estimates were not affected by these issues as is shown in next section.

4.3. Comparison between ULR3 and ULR4 combination procedures

A test was carried out to assess the new daily and weekly combination procedure of the ULR4 soltion. The dynamic sub-networks in 2008 were combined into daily/weekly solutions using four different approaches:

- CATREF_min: is the combination procedure of the ULR3 solution using CATREF with minimal constraints as described in Figure 4.1 (without geocenter and orbits).

- CATREF_int: combination using CATREF with internal constraints (without orbits).

- Globk_igs: is the combination procedure of the ULR4 solution using Globk as described in Figure 4.2. Products of this combination were submitted to the IGS reanalysis campaign.

- Globk_back: is the final combination procedure of the ULR4 solution using Globk as described in Figure 4.3.

The resulting weekly solutions of each approach were stacked with CATREF into a one-year solution using internal constraints. The repeatability of the weekly residuals with respect to the stacked solution of each approach was analyzed (Figure 4.4). It is confirmed that applying internal constraints in CATREF to combine the sub-network solutions with only six stations in common is the worst approach, especially in the horizontal component (CATREF_int combination, green line). Figure 4.4 also shows that CATREF_min (red line) and Globk_igs (black line) perform equally, even with different constraints applied in CATREF for both combinations (minimal and internal, respectively). Comparing Globk_igs to Globk_back (blue line) combinations, they look to perform similarly, with a slightly higher repeatability for Globk_back (mean difference is 0.3 mm for both horizontal and vertical components).
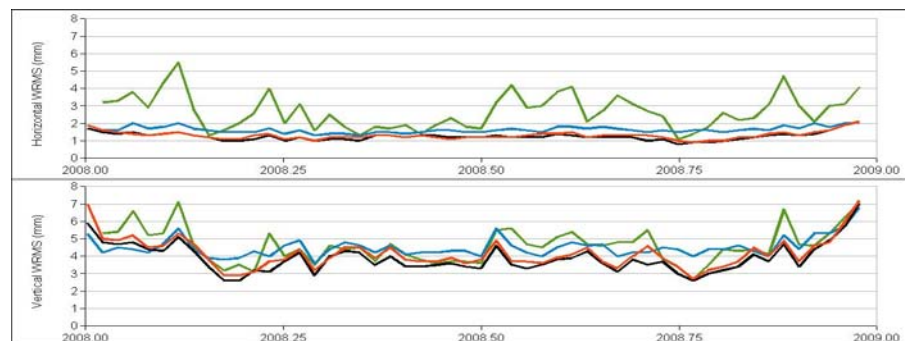
Figure 4.4. Horizontal (top) and vertical (bottom) WRMS of weekly solutions for CATREF_min (red), CATREF_int (green), Globk_igs (black) and Globk_back (blue) combination approaches.

In addition, time series of the weekly translations with respect to the respective stacked solution (Figure 4.5) show that, unlike the CATREF_min procedure (used in ULR3 solution), the Globk_back procedure (used in ULR4 solution) preserves the apparent geocenter information. Seasonal variations are clearly seen in Figure 4.5. See Section 7.2.2 for further details on these estimates.

From both stacked solutions, a subset of 156 stations with at least 90% of weekly solutions available in 2008 was extracted to be compared. The transformation parameters between both solutions (Table 4.1) are not equal to zero. These transformation parameters represent the mean differences, for the year 2008, between the frame definition of the ITRF2005 (CATERF_min combination) and the internal constrained solution (Globk_back
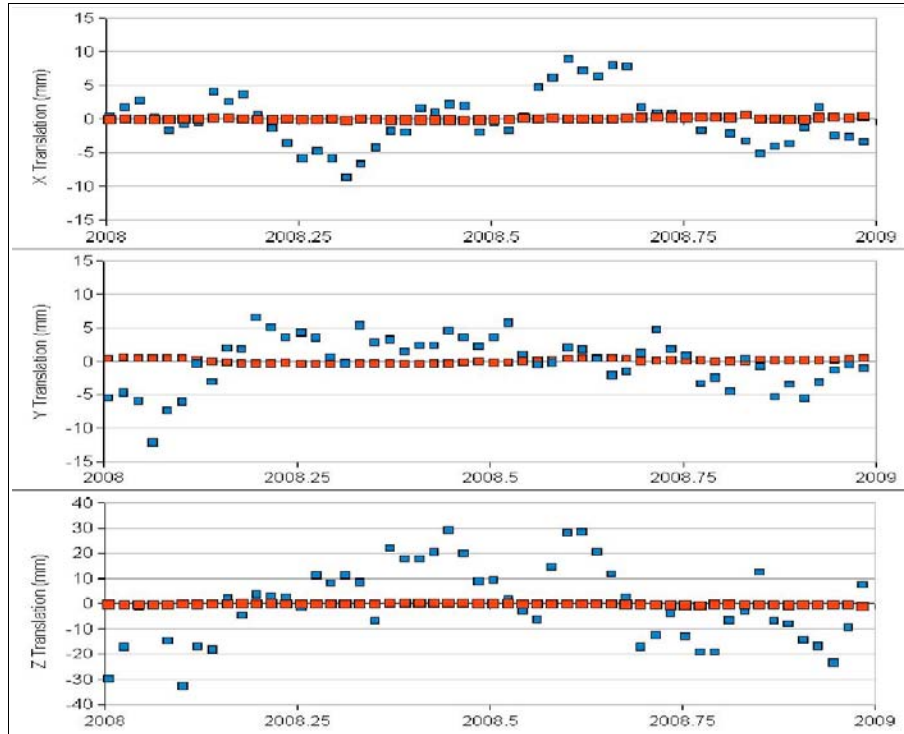
Figure 4.5. Translation values between weekly solutions and the
stacked solution for CATREF_min (red) and Globk_back (blue)
combination procedures.

combination). This is due to the fact that weekly solutions of CATREF_min are already minimally constrained to the ITRF2005 (and does the stacked solution). These values would be close to zero if the stacking of the Globk_back weekly solutions had been minimally constrained to the ITRF2005. The large transformation parameter rates observed might be due to the short time of the test and the presence of seasonal signals in the transformation parameters (Figure 4.5). Also, although the weekly solutions of both CATREF_min and Globk_back are constrained in rotations to the ITRF2005, there is a noticeable rotation of ~3 mm around the Y axis between both stacked solutions. The rotations around X and Z axes are ~0.3 and ~1 mm respectively. This might be related to the different number of stations used to align the frame rotation of the weekly solutions (Figure 4.6). In the CATREF_min combination, all available IGS05 stations are used to minimally constraint the frame rotation, whereas in the Globk_back combination, as already mentioned, there is an iterative procedure to select the stations to be used in the frame orientation definition.

Table 4.1. Transformation parameters between CATREF_min and Globk stacked solutions.

TX (mm) (mm/yr)	TY (mm) (mm/yr)	TZ (mm) (mm/yr)	Scale (ppb) (ppb/yr)	RX (mas) (mas/yr)	RY (mas) (mas/yr)	RZ (mas) (mas/yr)
-3.5±0.0	2.2±0.0	7.7±0.0	0.31±0.01	0.01±0.00	0.10±0.00	-0.03±0.00
-3.0±0.0	-3.6±0.0	-17.2±0.0	0.37±0.01	0.05±0.00	0.01±0.00	0.01±0.00
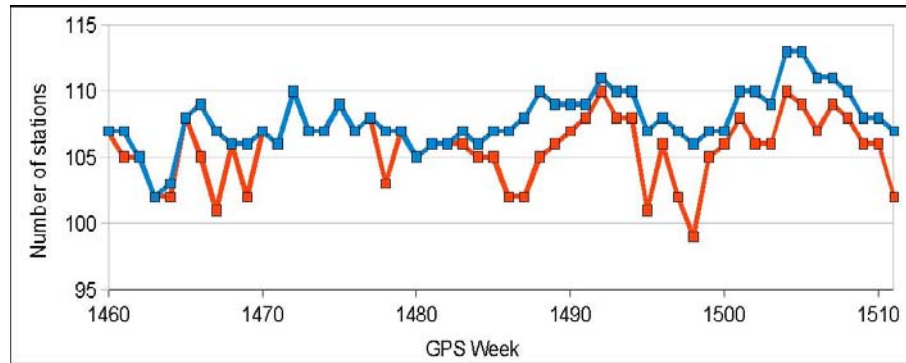
Figure 4.6. Number of IGS05 stations used to define the weekly frame rotation in CATREF_min (red) and Globk_back combinations (blue).

The post-fit (transformation parameters removed) residual differences between both solutions have a weighted RMS below the mm level (Table 4.2). This demonstrates that both combination strategies are interchangeable to obtain weekly solutions of station positions. However, using the ULR4 combination procedure gives two new products, namely the orbits and the geocenter motion. These new products will be used to complement the quality assessment of the ULR4 solution (see Chapter 7).

Table 4.2. WRMS of the station position differences between CATREF_min and Globk_back stacked solutions.

WRMS E (mm)	WRMS N (mm)	WRMS U (mm)	WRMS 3D (mm)
0.2	0.1	0.5	0.3

4.4 Summary

The new ULR4 combination procedure has proven to perform with the same quality as the old ULR3 procedure. In addition, we have for the first time a combined estimation of the orbital parameters and information of the apparent geocenter motion in the weekly solutions. Preliminary results of this new combination procedure were presented in *Santamaría et al.* [2009b]. Both new products, together with the terrestrial frame (station coordinates) and EOP, will be compared to the IGS Analysis Centers products in the frame of the IGS reanalysis campaign (Chapter 7). Although station coordinates and velocities are not affected by the internal consistency of all the extracted ULR4 products, this is a key issue for a proper IGS combination. Lessons learned from the ULR participation in the IGS reanalysis campaign will help to improve this point in the future.

5. Vertical velocity field estimation

Once all the weekly station positions are available for the whole period (1994-2009), they are stacked into station position time series using CATREF software following the combination model described in Chapter 4 (Section 4.1, Eq. 3). From these time series, the station positions at a reference epoch and their corresponding constant velocities are estimated for each component (east, north, up).

In this chapter only vertical velocities will be considered, though all discussions here presented could be extended to the horizontal components. To obtain reliable velocities, all the offsets, discontinuities, and outliers present in the time series must be removed before the velocity estimation (Section 5.1). The non-linear station motions are accessible through the time series of the post-fit position residuals. From these residuals, seasonal signals are estimated and removed in order to avoid biased velocities for shorter time series (Section 5.2). In addition, to properly express the estimated velocities in a conventional reference frame, minimal constraints are applied over the reference station set, or datum. This datum must be then carefully selected (Section 5.3). Finally, a summary of the velocity field estimation process is given (Section 5.4).

5.1. Offsets, discontinuities and outliers

Station velocities are estimated through a linear regression adjustment in a position time series. A critical matter in velocity estimation, and maybe the largest source of error, is then the presence of offsets, discontinuities and outliers in the position time series.

5.1.1. Offsets

An offset in a time series represents a sudden and permanent station position change. They can arise from crustal displacements (e.g., earthquakes), from station-related displacements (i.e., no crustal displacement) or even from apparent station-related displacements (i.e., no station displacement at all) through changes in the estimated station position. Sources of these station-related position changes are varied. Mainly, they are related to a:

−   Station monument movement. All GPS stations are tied to Earth's crust through their monumentation (pillar, rod, building, peer, etc). Any movement of these structures will induce a non-crustal-related station displacement.

−   Station equipment change. An antenna change can result in a change of the ARP position with respect to the station marker (antenna eccentricity change). A radome change can result in a change of the PCO position with respect to the ARP. Even a receiver, firmware or other hardware (wires) change might cause an offset in the estimated station position time series.

−   Local observation conditions change. If the station surroundings change (ground or near objects), it can cause signal multipath or local elevation mask changes which could induce an offset in the estimated station position time series.

−   Station metadata error. An erroneous change in the station information (e.g., the antenna model or the antenna eccentricity values) used in the data processing results in

an estimated position change.

  – Data modelization change. Any model change (e.g., tropospheric delay, antenna phase variation pattern) in the data processing directly affects the estimated station position, and then could introduce an offset in the position time series.

  – Reference frame change. Estimated station positions are tied to a reference frame. Any change in the definition of the reference frame (origin, scale and orientation) will cause an offset in the estimated station position time series.

The last two kinds of offsets are not considered here because they are inherently removed in a reprocessed solution. In such solutions the same processing strategy (modelization) and the same frame definition are applied for the whole data set.

In addition, despite all these different offset sources, not all identified offsets have a known source and some of them must be flagged as resulting from an unknown source due usually to missing information in the station changes log (equipment or environment). For instance, for the ULR4 solution, 51% of the identified offsets result from equipment changes, 16% result from earthquakes, 7% result from other documented sources (antenna malfunction, monument instability, etc) and 26% from unknown source. All these offsets, although likely interesting for some geophysical (e.g., earthquakes) or technical (e.g., antennae) studies, have a detrimental effect on velocity estimation and, therefore, they must be removed.

Whenever an offset is detected, the time series is split in two different pieces of data for which there is an independent estimation of the station position and velocity (piecewise linear model). Thus, position time series are composed of $n+1$ solutions, where n is the number of offsets. Each of these pieced solutions is called soln (for solution number). The offset amplitude is estimated as the difference of the station position of each soln, propagated to the offset epoch using each soln velocity. Then, to remove the offset, all positions after the offset epoch are corrected of this difference. The station velocities of the different soln are usually constrained to be the same, in a least-squares sense with an a priori standard deviation of 0.01 mm/yr, unless a velocity discontinuity is assumed (see next Section 5.1.2).

Not accounting for the offsets in a time series could lead to an error of the estimated velocity up to several mm/yr depending on the offset amplitude, time series length and offset position in the time series (or inversely, the length of the resulting soln). The worst case is when a large offset is located in the middle of a short time series. For instance, Figure 5.1 shows the detrended residual time series for HNPT and HOFN stations. HNPT station has an offset of ~60 mm resulting in a velocity bias of 1.8 ± 0.1 mm/yr (difference of the estimated velocity with and without removing the offset), whereas HOFN station has a smaller offset of ~47 mm but a much larger velocity bias of 6.0 ± 0.1 mm/yr. This is because the offset in HOFN time series is more centered and its time series is slightly shorter. Both examples also give the amplitude of the velocity bias that may result from a large offset. In these examples, both offsets are due to an antenna change.

Fortunately, these large offsets, with known or unknown source, can easily be detected and removed by a simple visual inspection of the residual time series. Certainly, from Fig 5.1, both offset epochs can be easily estimated with a time resolution of a week. However, smaller offsets (amplitude of some mm) masked in the time series noise are much more difficult to detect. These unnoticed offsets still represent a bias of the estimated rates and they also introduce a time-correlated noise signature close to random walk [Williams, 2003a] (see Chapter 6 for more details about noise). To highlight this fact, Figure 5.2 shows the residual
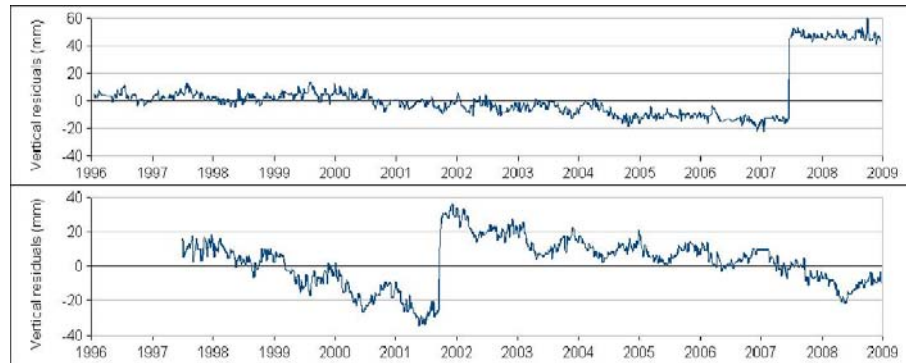
Figure 5.1. HNPT (top) and HOFN (bottom) residual vertical time
series without removing the offsets.

vertical time series for HYDE station. In this time series, two offsets at the end of 2004 (Sumatra 9.1 earthquake) and 2007 (antenna change) were easily detected in the horizontal components by visual inspection. In the vertical component however, they could remain undetectable in a visual inspection of the raw time series (red line). The amplitude of both offsets in the vertical component was estimated to 3.7 ± 0.9 mm and 4.3 ± 0.9 mm, respectively. The amplitude of the annual signal was estimated to 6.4 ± 0.3 mm and the weekly vertical residual repeatability (WRMS), annual signal removed, is estimated to 3.5 mm. This way, although both offsets are significant (with respect to their formal uncertainties), they are masked by the scattering of the residual time series. The vertical rate difference between both time series, with and without removing the offsets, is estimated to 1.5 ± 0.4 mm/yr. This example shows the significant magnitude of the velocity bias introduced by two offsets, with the same sign, undetectable in the vertical component alone. On the contrary, if both offsets had opposite signs, the velocity bias would fall to ~0.2 mm/yr.
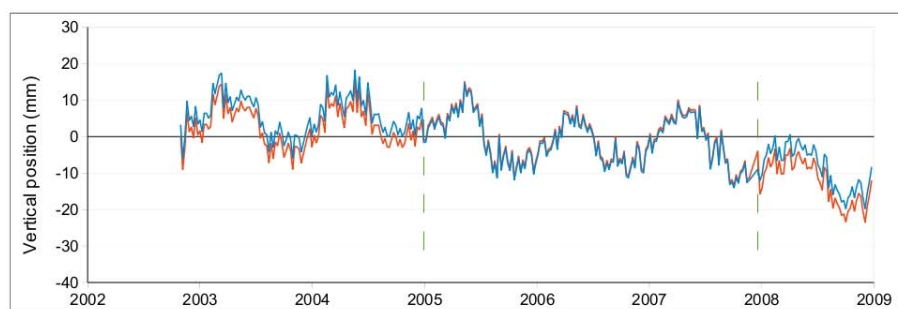
Figure 5.2. HYDE vertical position time series with offsets (red) and
without offsets (blue). Values are with respect to mean station
position. Green dashed lines represent the offset epochs.

To test the robustness of the offset estimation process and its effect on estimated rates, an inexistent offset was flagged to be estimated with CATREF in the middle of 2006 for the HYDE vertical time series (Figure 5.2). The estimated offset amplitude was not significant (1.3 ± 0.9 mm) and the new estimated velocity for this time series had a difference of 0.1 mm/yr, which is not significant even at the formal uncertainty level. This would indicate that

there is little harm to introduce an offset wherever in the time series and then estimate the station velocity by constraining the different soln. However, time series having a large number of offsets (some of them being not significant) could also lead to a biased velocity if the resulting constrained soln are not sufficiently long. This effect is emphasized in the presence of periodic signals in the time series. For instance, a not significant offset can actually be estimated as being significant due to seasonal signals (see next Section 6.2). In addition, as the soln are shortened by the inclusion of offsets, the formal uncertainty of the station velocity will be artificially increased. However, this effect may be insignificant if the velocity uncertainties are estimated by taking into account the correlated noise content in time series (see Chapter 6). For instance, unaccounted small offsets have little or no impact on the rate uncertainty if the time series are heavily correlated (e.g., random walk noise) [*Williams*, 2003a]. Therefore, it is necessary to remove all the significant offsets from the time series, but velocities estimated from time series with a large number of offsets (or inversely, very shortened soln) should be taken with caution (see Section 8.1).

5.1.2. Velocity discontinuities

As described in the precedent section, the estimated velocities of each soln are constrained to estimate a unique station velocity. However, if the time series is assumed to contain a velocity discontinuity, then the velocities of both affected soln are left unconstrained. Since stations affected by a velocity discontinuity have no unique long-term velocity (one per soln), they are useless for this study and will not be further considered (see Section 8.1). Fortunately, this kind of discontinuity is not very common (less than 2% of the stations of ULR4 solution are suspected to have one). They can result from tectonics (e.g. pre or post seismic deformation) or any local event affecting the station monumentation or its basement. A velocity discontinuity does not necessarily correspond to an offset in station position. For instance, Figure 5.3 shows the vertical position residuals for MANA station. In this time series, the Managua 7.0 earthquake in the middle of 2004 likely caused a velocity change in the station. This velocity discontinuity was also pointed out in the preliminary ITRF2008 analysis [Xavier Collilieux, personal communication]. In order to properly detect them, it is crucial to have time series as long as possible because a velocity change could also be confused with long-term non-linear station movement. For instance, Figure 5.4 shows the vertical position residuals for THU3 station. This time series has a continuous "banana" shape where no point is susceptible to separate a significant velocity change. In such a cases, it becomes more uncertain, even impossible, to identify the source of the velocity change and the epoch of change. In such a case, the poor performance of the functional model fitted (linear trend) causes a long-term systematic residual pattern (banana-shaped). This systematic residual pattern will be absorbed by the stochastic model, increasing therefore the velocity uncertainty (see Chapter 6).

5.1.3. Detecting offsets and velocity discontinuities in ULR4

Although an automated process to remove the offsets and the velocity discontinuities would be highly desirable, for the moment no algorithm has proved to perform perfectly and this task must be carried out by visual examination of the time series. *Williams* [2003a] tested a change detection algorithm based on the estimation of the offset epoch by maximizing the difference of the soln mean positions. This algorithm shows to work adequately for normalized offsets (offset amplitude divided by its uncertainty) larger than 4 and located near the middle of the time series (elsewhere the normalized offset must be larger to be correctly
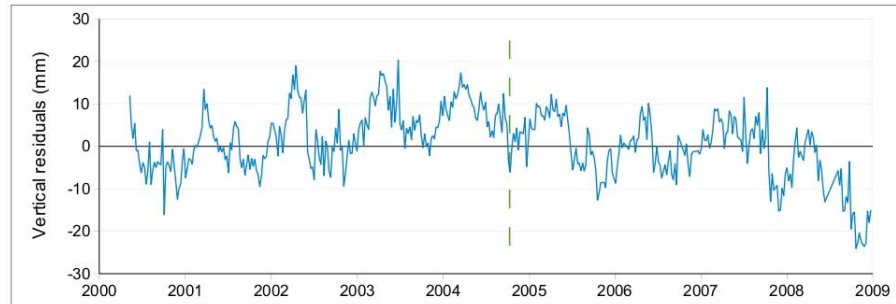
Figure 5.3. MANA vertical residual time series. Green dashed line represents the velocity discontinuity epoch.
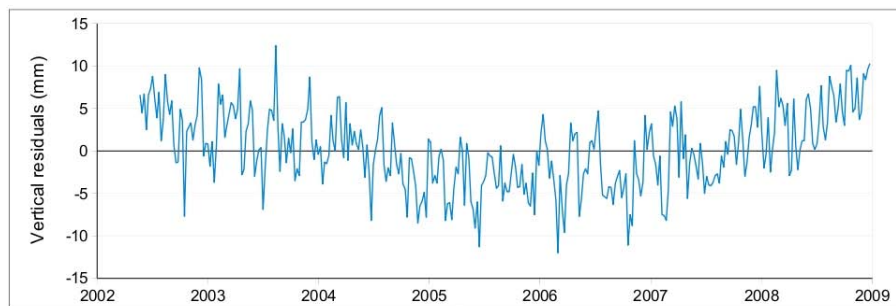
Figure 5.4. THU3 vertical residual time series.

detected). However, these large offsets are likely already easily detected by visual inspection. For smaller and visually unnoticed offsets, the probability to detect the correct epoch decreases with the normalized amplitude. Thus, for small normalized offsets (down to a value of 0.5), the author shows that although the offset can be detected, any of the time series epoch have a chance to be wrongly identified as the offset epoch. Thus, this solution is not optimal since a wrong estimated offset epoch can also introduce a bias in the estimated station velocity. This author discusses that there are several algorithms to detect offsets, based on different techniques, but none of them is completely optimal. The main problems found within such algorithms are that there are usually several offsets in a time series (whose number must be a priori defined for some algorithms), that there are also unaccounted seasonal signals and that data in time series are in general assumed as time-uncorrelated.

Therefore, ULR4 residual position time series were visually examined to detect the offset epochs. To make this task easier it is necessary to use external information like station site logs and earthquake databases (e.g., the USGS earthquake database[1]). The official discontinuities list of the ITRF2005 reference frame solution was used as reference. The time series were then completed for the stations not contained in the ITRF2005 and for the more recent period of data used. Also, as commented above, some offsets might be introduced by the station information used in the GPS processing. In order to avoid this kind of offsets in future reprocessed solutions, for all the detected offsets, the information used in the data processing was checked against the information contained in the station status logs and corrected if necessary. Therefore, the discontinuity set used in the ULR4 solution are different

---

1   http://earthquake.usgs.gov

to those used in the ITRF2005 reference frame. This has some implications when choosing the group of stations (group of soln in fact) for defining the reference frame of the solution (see next Section 5.3).

All the detected offsets (flagged to be estimated) in the ULR4 solution were verified and retained if they were significant (normalized amplitude larger than 3). Large offsets can propagate into near stations causing spurious offsets their time series. Therefore, the offset detection and elimination was done iteratively for all time series from larger to smaller offset amplitudes. The quality of the offset detection and its significance depends mainly on the offset amplitude itself but also on the noise amplitude of the time series. Thus, reducing the time series noise by improving the GPS processing can also indirectly improve the velocity estimation as ambiguous and hidden offsets become more certain.

5.1.4. Outliers

Once all the offsets and the velocity discontinuities have been removed, aberrant or deviant points in time series, known as outliers, must also be removed. An outlier is defined as an input observation which is noticeably away from the ensemble of similar input observations (large residual) and which has a relative large weight (small incertitude) to bias the estimated parameter. Compared to an offset event, an outlier represents a sudden, but not permanent, station position change.

Outliers are related to specific physical events happening on the station equipment or its surroundings, isolated modelization errors, etc. Since CATREF fits the station position time series with a linear deformation model (constant velocity), points with large residuals can also result if offsets, non-linear signals (e.g., seasonal) or high noise amplitude are present in the time series. That is, since the model does not fit optimally the observations, the post-fit residuals do not have a zero expectation value (i.e., a bias or a systematic error in the model). The largest residuals could be then wrongly identified as outliers by a threshold-based detection algorithm. Thus, to consider a residual position as an outlier, it must be first compared to its complete residual time series.

For the ULR4 solution, the residual time series of the three components were visually examined to remove the outliers. Like offsets, outliers can also propagate into time series of near stations. Therefore, they were removed in an iterative process, from larger to smaller residual amplitude. As a general criterion, outliers were removed if their amplitudes were larger than 2 cm for residuals and 4 for normalized residuals.

5.2. Seasonal signals

The frequency spectrum of GPS vertical time series is clearly dominated by annual and semiannual periods, which are called seasonal signals. These periodicities were reported since earlier GPS results [e.g., *Van Dam et al.*, 1994]. These seasonal signals can represent true Earth-crust related motion unmodeled in the GPS data processing due to atmospheric [e.g., *Tregoning and Van Dam*, 2005] and hydrological loading [e.g., *Van Dam et al.*, 2001]; they can also represent non Earth-crust related station motions resulting from monument and bedrock thermal expansion [e.g., *Yan et al.*, 2009]; and they can even represent not real station movement at all resulting from spurious aliased signals from data processing mismodeling, that is, solid Earth tides [e.g., *Watson et al.*, 2006], ocean loading [e.g., *Van Dam et al.*, 2007; *Vergnolle et al.*, 2008], tropospheric delay [e.g., *Tregoning and Watson*, 2009], antenna phase

corrections [e.g., *Cardellach et al.*, 2007], orbital effects [e.g., *Dong et al.*, 2002] and antenna near-field multipath [e.g., *King and Watson*, 2010].

Figure 5.5 shows the percentage of significant periodicities in the ULR4 vertical time series. For the detection method used see Section 6.3.1. Neglecting low-frequency (<1 cpy) signals, seasonal signals are present in ~70% of vertical time series. Analyzing the amplitude of these significant signals (Figure 5.6), it is clear that annual and semiannual periodic signals have the largest amplitude.
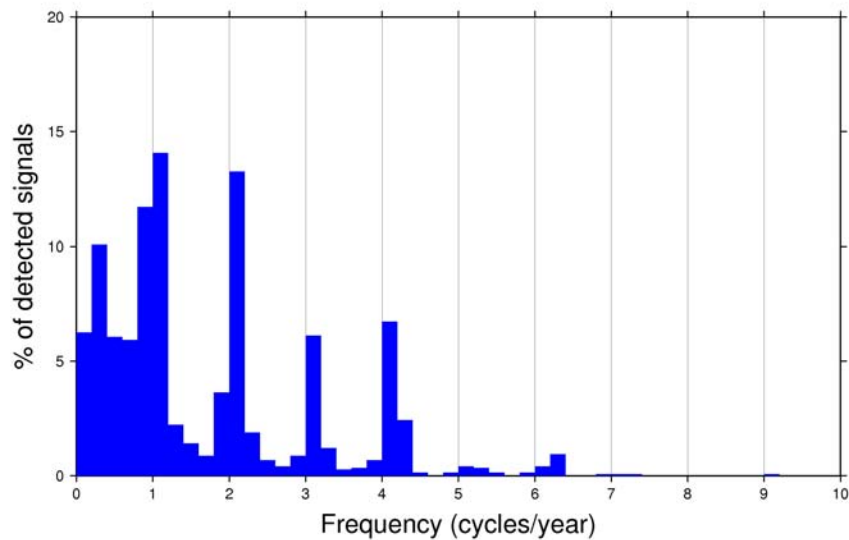
Figure 5.5. Histogram of significant signals in ULR4 vertical residual time series
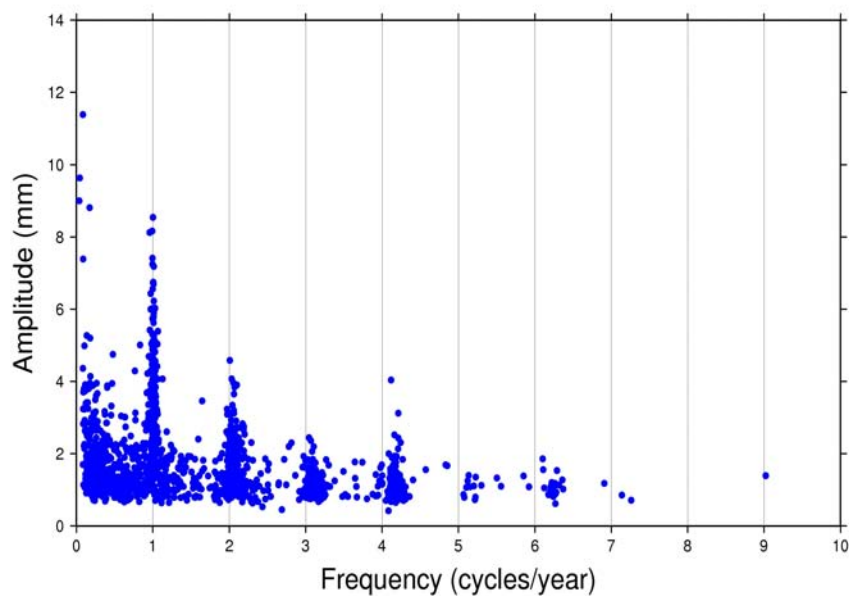
Figure 5.6. Amplitudes of significant detected signals in ULR4 vertical residual time series.

These seasonal signals, like offsets (see Section 5.1.1), can lead to derived geophysical research, but they represent a nuisance and a source of noise for velocity estimation. Seasonal signals can bias the estimated velocity if they are not taken into account, especially for time series shorter than 4.5 years of data [*Blewitt and Lavallée*, 2000]. Therefore, annual and semiannual signals should be estimated/removed from time series together with station rates. Adding these parameters (amplitude and phase) to the combination model (see Section 4.1) will increase the formal velocity uncertainty for shorter time series, but this should not be necessarily a drawback as realistic uncertainties are estimated later (see Chapter 6). Nevertheless, even after removing these signals, velocities estimated for time series shorter than 2.5 years of data are not fully reliable due to the correlation between the estimated periodic parameters and trends [*Blewitt and Lavallée*, 2002]. Therefore, estimated velocities for time series shorter than 2.5 years should be discarded (see Section 8.1).

With CATREF software it is not possible to estimate seasonal signals and trends at the same time. Therefore, we removed the effect of these seasonal signals in a two-step procedure. First, once all time series are free of offsets and outliers, amplitudes and phases for annual and semiannual signals were fitted by weighted least squares using the detrended residual time series. Mean vertical amplitudes of 3.00 ± 0.09 mm was found for the annual and 1.18 ± 0.04 mm for the semiannual periods (see Figure 5.6). Second, the stacking procedure is back-solved using the information of the estimated seasonal signals to remove their effect from the estimated velocities. However, since trends and seasonal parameters are not estimated at the same time, this procedure to remove the seasonal signals effect on trends is not fully optimal.

A test was carried out to quantify the impact of the seasonal periods on velocity estimation. Estimated station positions and velocities of the stacked ULR4 solution were compared with and without removing the annual and semiannual signals following the procedure described earlier. Only stations with more than 2.5 years of data were used in the comparison. Table 5.1 shows the weighted RMS of the station position and velocity differences between both solutions. As expected, differences are higher in the vertical component (for both position and velocity) due to the larger amplitude of the vertical seasonal signals. This table shows that the effect of seasonal signals on position and velocity estimates is significant.

Table 5.1. WRMS between solutions with and without annual signal.

	WRMS E	WRMS N	WRMS U	WRMS 3D
Positions (mm)	0.4	0.3	1.3	0.8
Velocities (mm/yr)	0.1	0.1	0.3	0.2

Focusing on vertical velocities, Figure 5.7 shows the differences in the station vertical velocities as a function of time series span. Since both stacked solutions were aligned to the ITRF2005 (see next Section 5.3), there is no systematic velocity bias between both solutions. The time series are split in series shorter and longer than 4.5 years following *Blewitt and Lavallée* [2002]. The RMS of the vertical velocity differences for shorter and longer time series are 0.39 mm/yr and 0.16 mm/yr, respectively. This confirms that the effect of seasonal signals is more important in shorter time series, as stated by *Blewitt and Lavallée* [2002].

Nevertheless, there are also some stations (shown in red in Figure 5.7) with longer time series for which there are large velocity differences. Thus, HYDE and ALEX stations with little more than 6 years of data have a difference of 1.9 mm/yr (the largest one) and 0.6 mm/yr respectively; PIMO and KUNM stations with about 10 years of data have a difference of 0.5 mm/yr and 0.8 mm/yr, respectively; and even stations with almost 13 years of data like DGAR and TSKB have a noticeable difference of 0.4 mm/yr and 0.3 mm/yr, respectively. Moreover, differences are not significantly reduced at integer-plus-half years with respect to integer years as stated by *Blewitt and Lavallée* [2002]. Both issues might point to the effect of spatial correlation between stations and to the non-rigorous procedure used to remove the seasonal signals influence on the estimated velocities. In fact, estimated offset amplitudes are coupled with seasonal signals. That is, the estimated offset amplitudes are not the same once the seasonal signals are removed and, as stated in Section 5.1.1, offset amplitude is one of the main sources for a velocity bias. For instance, by removing the annual (6.4 mm amplitude) and semiannual (0.9 mm amplitude) signals in HYDE station, its two detected offsets (see section 5.1.1) are now estimated for the vertical component to -2.3 ± 0.6 mm and 0.8 ± 0.6 mm, respectively (offset amplitudes with seasonal signals were of 3.7 ± 0.9 mm and 4.3 ± 0.9 mm, respectively). This large change in the estimated offset amplitudes results in a large velocity difference for this station. Therefore, in the presence of offsets, it is mandatory to take into account the effect of seasonal signals on estimated velocities even for long time series. Note that these seasonal signals were not taken into account in the ULR3 solution. Our test also shows that a consistent procedure to estimate offsets, seasonal signals and trends, while rigorously stacking the position time series, is desirable to improve the consistency of the estimated velocities. Unfortunately, this procedure is not available at this moment within the CATREF software, but may be in a near future [Xavier Collilieux, personal communication].
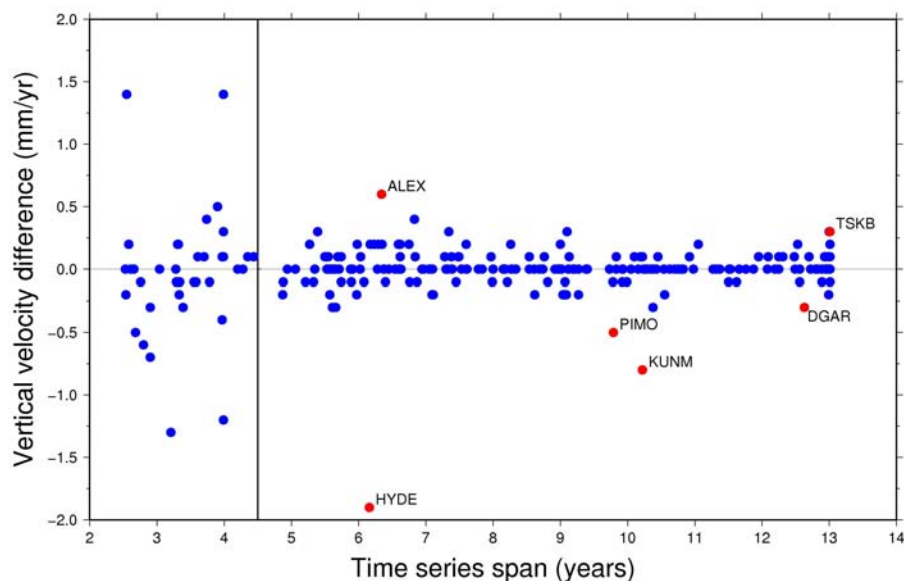
Figure 5.7. Vertical velocity differences with and without seasonal signals.

5.3. Datum selection

In order to realize a solution as consistent as possible with the ITRF2005 reference frame, the stations used to align both solutions must be carefully selected. This set of stations is also called "datum". Thus, the stations belonging to the datum should satisfy five conditions:

−   to be as many as possible, this way individual station errors are mitigated,

−   to be as globally well-distributed as possible, fundamental to estimate the transformation parameters with confidence,

−   to have as much data as possible, to assure the alignment consistency through all the processed data,

−   to have the minimum discontinuities as possible, to assure confident estimated velocities, and

−   to have the smallest deviations as possible with respect to the frame to be realized, to avoid ULR4 or ITRF2005 estimation errors to affect the frame alignment.

As a priori datum were chosen all the IGS05 stations for which weekly solutions are available for at least 80% of the whole reprocessed period, that is, at least 540 weekly solutions. This way, 71 stations were selected. Since ULR4 and ITRF2005 discontinuities applied are not the same (see discussion in Section 5.1.3), for each of the datum stations, we used only one soln (one estimated position and velocity) to align ULR4 to ITRF2005. This way, using only one position estimate per station, the alignment is more consistent than if all ULR4 and ITRF2005 soln with different validity periods (offset epochs) were used. The soln extracted for each station was the soln for which the longest common period between the ULR4 and ITRF2005 solns was available.

Then, stations with known or suspected velocity discontinuities were rejected. WES2, NYAL, MAC1 and REYK were rejected at this point, WES2 and NYAL were rejected because they have a velocity discontinuity in the ITRF2005 and MAC1 and REYK were rejected because they have one in the ULR4 solution. Therefore, 67 IGS05 stations were finally retained.

Two sets of coordinates with these 67 stations were extracted from IGS05 and ITRF2005 and compared. Besides some transformation parameter between both sets reaching the mm level, any transformation parameter rate was statistically different from zero. Thus, the alignment of the velocity field is expected not to be affected by choosing IGS05 or ITRF2005 coordinates. IGS05 coordinates were used instead of the ITRF2005 ones due to the corrected vertical coordinates resulting from the change of the antenna phase pattern model (see Section 3.1.2).

Then, a set of coordinates for these 67 stations was extracted from ULR4 solution and compared to the IGS05 coordinates. In an iterative process, the station with the largest position or velocity residual with respect to IGS05 was rejected from the datum. Thresholds applied were 5 mm and 10 mm for horizontal and vertical positions respectively and 1.5 mm/yr and 2 mm/yr for horizontal and vertical velocities respectively. There is a trade-off between keeping as many stations as possible and selecting only the best stations to realize the reference frame. These thresholds were chosen to keep a reasonable number of stations globally well-distributed. Up to 8 stations exceeding any of these thresholds were rejected

(IISC, JOZE, WUHN, WHIT, PERT, CEDU, TRO1 and MALI). The final datum retained for the alignment of the ULR4 solution is then made up of 59 stations. By rejecting these 8 stations from the initial datum (equivalent to 12% of the stations), the global distribution of sites is not heavily affected. In both cases, only 28% and 30% of the stations are located in the Southern Hemisphere, respectively.

The position and velocity residual histograms by component are shown in Figures 5.8 and 5.9. Vertical residuals, for both positions and velocities, are the largest ones. These local inconsistencies (not absorbed by the translation and scale parameters and their rates) between the combined solution and the reference frame probably result from the different discontinuities applied in both solutions. Also the large vertical position residuals may result from the procedure used to correct the phase center pattern model change in the IGS05 coordinates (a posteriori corrections, see Section 3.1.2). Residual velocities of ULR4 solution will be further analyzed in Chapter 8.
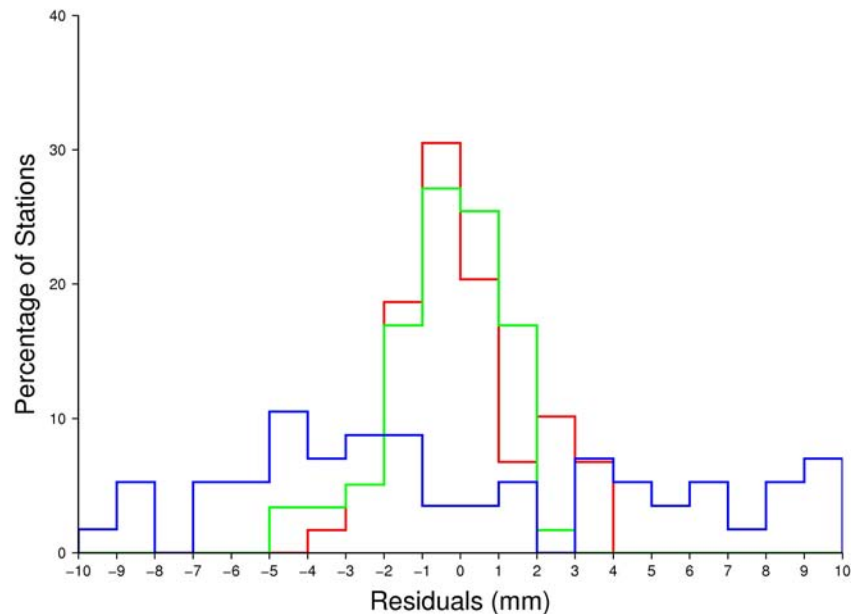
Figure 5.8. East (red), North (green) and Up (blue) position residuals of datum stations.

In order to quantify the impact of the selected datum stations on the realization of the reference frame a test was carried out. The solution aligned with the datum formed by the initially selected 67 stations was compared to the solution aligned with the final datum of 59 stations. Their misalignment (14-parameters transformation) is shown in Table 5.2. Even if this misalignment is small, it is significantly different from zero for translations and scale. The transformation parameter rates are much less affected being not significantly different from zero. Therefore, although ULR4 station coordinates are slightly different depending on the selected datum, ULR4 station velocities do not change significantly with the datum. This assures a consistent frame alignment of the velocity field.
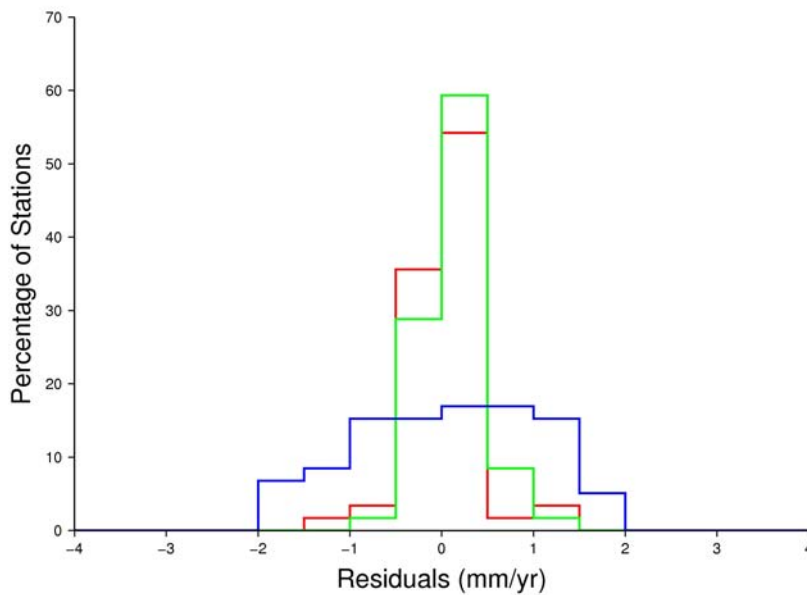
Figure 5.9. East (red), North (green) and Up (blue) velocity residuals
of datum stations.

Table 5.2. Transformation parameters between 59 and 67 datum stations.

TX (mm) (mm/yr)	TY (mm) (mm/yr)	TZ (mm) (mm/yr)	Scale (ppb) (ppb/yr)
0.5±0.1	-0.2±0.1	0.6±0.1	-0.05±0.01
-0.1±0.1	0.1±0.1	-0.1±0.1	0.00±0.01

The geographic distribution of the 59 datum stations is shown in Figure 5.10. It is expected, and very desirable, that as the GPS time series are becoming longer, the number and distribution of the datum stations will improve in future ULR solutions.

5.4. Summary

780 weekly solutions (spanning from January 1994 to December 2008) were rigorously stacked using the combination model of CATREF software (see Section 4.1). With this model, station position at a reference epoch and constant velocities for all the stations were adjusted. Also, offsets were iteratively flagged and their amplitude was estimated at the same time within the stacking procedure. Only significant offsets were finally accounted for in the stacking. Once all the discontinuities were removed, the time series were further inspected to remove the outliers.

The effect of seasonal signals on velocity estimates was analyzed. This effect was found to be small (RMS of 0.1-0.2 mm/yr) for long times series, in agreement with *Blewitt and Lavallée* [2002]. However, due to the presence of offsets in some time series, seasonal signals can introduce large velocity bias even in long time series. Removing or not seasonal
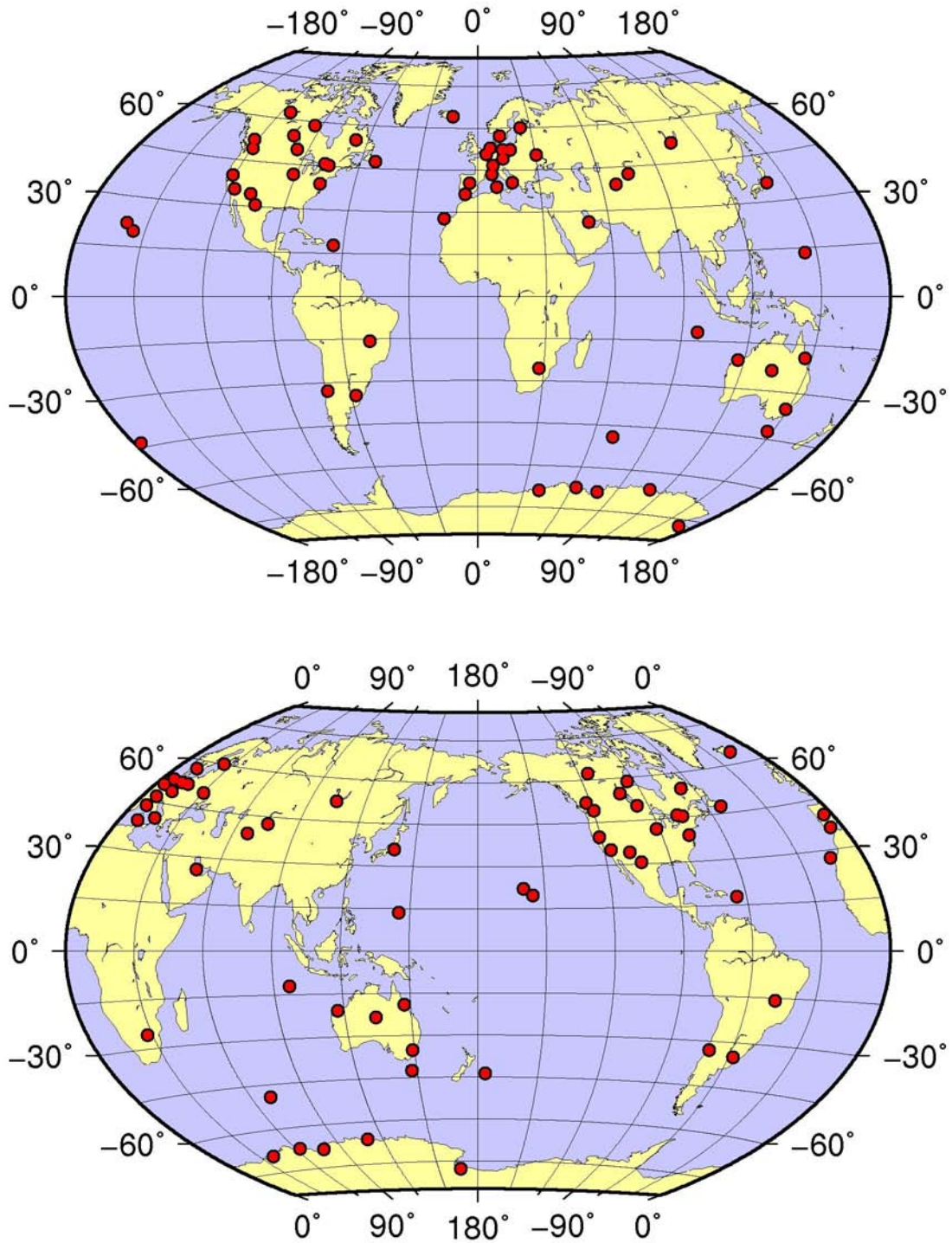
Figure 5.10. ULR4 datum distribution.

signals while removing offsets can change the estimated offset amplitude, and then, the estimated velocity. Therefore, we consider that seasonal signals must be removed even for long time series. Using the station detrended cleaned post-fit residual time series, annual and semiannual sinusoid were adjusted to each station coordinate component. These values were then reintroduced in the stacking procedure to remove the effects of these seasonal signals

from the velocity estimation. To improve the consistency of the estimated velocity field, both offset amplitudes and seasonal signals should be estimated/removed at the same time. This procedure is not available at this moment.

Finally, the estimated velocity field was aligned to the ITRF2005 through minimal constraints over a datum comprised of 59 IGS reference frame stations. These stations were carefully selected based on duration and quality. Choosing IGS05 or ITRF2005 coordinates did not result in a change of the velocity field, however IGS05 coordinates were used to keep consistency with the absolute antenna phase model used in the data processing. Also, a different datum including early rejected stations did not result in significant velocity field differences. This indicates a robust frame alignment of the ULR4 velocity field.

6. Vertical velocity field uncertainty

Once the station velocities are estimated, their realistic uncertainties must be computed. In order to extract the adequate geophysical information and conclusions from geodetic Earth-crust displacements, we need accurate estimates of both rates and their uncertainties. Otherwise, an erroneous interpretation could be derived from an incomplete displacements information.

In this chapter, we start with the description of noise and its influence on the estimated velocity uncertainties (Section 6.1). The noise estimation method and the main stochastic processes used in noise analysis are described (Section 6.2). Then the data and the procedure used in the noise analysis are described together with several procedural issues and their impact on the noise analysis (Section 6.3). Then, in order to estimate a reliable velocity uncertainty, several noise models are tested to choose the one that best describes our data (Section 6.4). In addition to the analysis of the internal precision of time series (noise in post-fit residuals), the effect of the datum accuracy used to align the velocity field to a reference frame is also taken into account (Section 6.5). Finally, a summary of the velocity field uncertainty is given (Section 6.6).

6.1. Noise effect on velocity uncertainties

A physical variable, like residual station position, is estimated at a set of times t_i, resulting in a discrete time series of data $X(t_i)$ (where $i = 1, 2, ..., N$). This time series is assumed to be composed by the sum of parameters of interest (X^S), like trends or periodic signals, and observational errors (X^R) [*Scargle*, 1982] given by:

$$X_{t_i} = X^S_{t_i} + X^R_{t_i} \ .$$

(1)

The sum of the errors is usually called background or floor noise and is characterized by stochastic properties such as its variance, distribution, and spectral density. Following this equation, the estimated parameters from the time series depend on the background noise level. This noise is usually assumed to be random, that is, $X^R_{t_i}$ is assumed to be statistically independent of $X^R_{t_{i+j}}$, where $j = 1, 2, ..., N-i$. However, reliable velocity estimates and their uncertainties must take into account the type and the amplitude of the time-correlated noise content in the time series. It is important to take into account both parameters, the noise amplitude and its type (degree of correlation or background noise power spectrum), since both affect the estimate of the velocities and their uncertainties.

Following is a demonstration of the impact of the time-correlated noise in the velocity uncertainty. We simplify the velocity estimation model of CATREF (see Section 4.1) into a typical linear regression fit of the time series (neglecting the estimation of frame transformation parameters) following *Zhang et al.* [1997]:

$$x_i = x_0 + r \cdot t_i$$

(2)

where x_i is the position at epoch i, x_0 is the intercept, r is the constant time series rate and t_i is the time difference between x_0 and x_i. Eq. 2 can be transformed into the following weighted least-squares system:

$$y = \binom{x_0}{r} = \left[A^T C_x^{-1} A \right]^{-1} A^T C_x^{-1} X, \tag{3}$$

where y is the vector of the estimated parameters (x_0 and r), A is the partial derivative matrix, C_x is the data covariance matrix and X is the vector of residual positions. The covariance matrix of the estimated parameters is as follows:

$$C_y = \begin{pmatrix} \sigma_{x_0}^2 & \sigma_{x_0 r} \\ \sigma_{x_0 r} & \sigma_r^2 \end{pmatrix} = \left(A_t C_x^{-1} A \right)^{-1}. \tag{4}$$

Thus, to determine the velocities (r) and their uncertainties (σ_r), some estimate of the data covariance matrix (C_x) is needed. By estimating velocities using CATREF, and generally with all least squares-based algorithms, the station position from one epoch to another in the time series are assumed to be independent, making the covariance matrix diagonal:

$$C_x^{-1} = \begin{pmatrix} \dfrac{1}{\sigma_{x_1}^2} & 0 & \cdots \\ 0 & \dfrac{1}{\sigma_{x_2}^2} & \cdots \\ \vdots & \vdots & \ddots \end{pmatrix}. \tag{5}$$

Then substituting Eq. 5 into Eq. 4 leads to:

$$C_y^{-1} = \begin{pmatrix} \Sigma \dfrac{1}{\sigma_{x_i}^2} & \Sigma \dfrac{t_i}{\sigma_{x_i}^2} \\ \Sigma \dfrac{t_i}{\sigma_{x_i}^2} & \Sigma \dfrac{t_i^2}{\sigma_{x_i}^2} \end{pmatrix}. \tag{6}$$

Assuming that input data uncertainty is constant, that is:

$$a = \sigma_{x_i}, \quad C_x^{-1} \simeq a^{-2} \cdot I, \tag{7}$$

where *a* represents the mean uncorrelated amplitude, or equivalently, the time series scatter, and *I* is the identity matrix, then:

$$\varSigma \frac{1}{\sigma_{x_i}^2}=a^{-2}\cdot N \qquad \varSigma \frac{t_i}{\sigma_{x_i}^2}=a^{-2}\cdot \varSigma t_i \qquad . \tag{8}$$

Substituting Eq. 8 into 6 leads to:

$$C_y^{-1}=a^{-2}\cdot \begin{pmatrix} N & \varSigma t_i \\ \varSigma t_i & \varSigma t_i^2 \end{pmatrix} \tag{9}$$

where N is the number of points. Now we assume that N is a large number and that the sampling rate ($\varDelta T$) is constant (equally spaced data), that is, $T=(N-1)\cdot \varDelta T$, where T is the time data span. Then, inverting Eq. 9 and simplifying the rate uncertainty equation leads to [*Zhang et al.*, 1997; *Williams*, 2003b; *Bos et al.*, 2008]:

$$\sigma_r^2 \simeq \frac{12\cdot a^2}{N\cdot T^2} \simeq \frac{12\cdot a^2}{\varDelta T^2\cdot (N^3-N)} . \tag{10}$$

Following Eq. 10, when uncorrelated noise is assumed, the formal velocity uncertainties are proportional to the uncorrelated noise amplitude and inversely proportional to the number of points and the time series length. This way, by incrementing the sampling interval or the observation time span, the uncertainty of the estimated velocity is considerably reduced.

Since large time periods of observation are needed to estimate unbiased velocities (see Section 5.2), this leads to a very small formal uncertainty. However, long periods of observation might contain position estimates that are no more time independent as more error sources with different temporal behavior will be introduced [*Zhang et al.*, 1997]. Moreover, the error sources can also change with time, for instance due to ageing equipment [*Mao et al.*, 1999]. Thus, the noise spectrum can turn to be frequency-dependent resulting in time-correlated noise content. Early publications detected this time-correlated noise in several geodetic data sets including GPS data [*Wyatt*, 1982; 1989; *Langbein and Johnson*, 1997; *Zhang et al.*, 1997]. Nevertheless, this time correlation may be not noticed in the residual time series unless it reaches large amplitudes [*Johnson and Agnew*, 1995]. The sources of the time-correlated processes are very varied. They include mismodeling of tidal/non-tidal displacements, orbit mismodeling, antenna phase center mismodeling, multipath effects, instrumental effects, satellite constellation evolution and monument instability (for instance soil and rock desiccation weathering, rainfall-induced soil swelling, freeze-thaw cycles, water withdrawal or landslides). Note that monument instability effects are related to the GPS

monument structure and its anchoring media (soil, bedrock, etc). For deeper crustal deformation, correlated noise larger than those considered here can be found [*Wyatt et al.*, 1988]. Therefore, assuming that time series are formed by time-independent positions leads to extremely reduced or optimistic formal uncertainties. The factor of optimism was estimated to be up to one order of magnitude for a global GPS network [*Mao et al.*, 1999].

If we assume that time series contains time-dependent positions, for example by supposing that GPS monuments move as if they were under the influence of small random forces following an integrated white noise model (that is, a random walk model, see next Section 6.2 for a description of the noise models), then the covariance matrix of the observations takes the following form [*Zhang et al.*, 1997]:

$$C_x = b^2 \cdot \Delta T \cdot \begin{vmatrix} 1 & 1 & 1 & \cdots & 1 \\ 1 & 2 & 2 & \cdots & 2 \\ 1 & 2 & 3 & \cdots & 3 \\ \vdots & \vdots & \vdots & \ddots & \vdots \\ 1 & 2 & 3 & \cdots & N \end{vmatrix}, \tag{11}$$

being b the amplitude of the random walk noise. Inverting Eq. 11 and substituting into Eq. 4 leads to:

$$C_y^{-1} = \frac{b^{-2}}{\Delta T} \cdot \begin{pmatrix} 1 & t_1 \\ t_1 & c_{22} \end{pmatrix}$$
$$c_{22} = t_N^2 + 2 \sum_{i=1}^{N-1} t_i^2 - 2 \sum_{i=1}^{N-1} (t_i \cdot t_{i+1}) \tag{12}$$

Inverting Eq. 12, the formal uncertainty of the estimated velocities is now given by [*Zhang et al.*, 1997; *Williams*, 2003b; *Bos et al.*, 2008]:

$$\sigma_r^2 \simeq \frac{b^2}{T} = \frac{b^2}{\Delta T(N-1)} \quad . \tag{13}$$

Eq. 13 shows that, in the presence of heavily correlated time series, the rate uncertainties are significantly augmented with respect to the rate uncertainties from uncorrelated time series. In this case, the addition of more (correlated) positions by extending the observation span, even keeping a similar time series scatter (RMS), barely reduces the rate uncertainty. Moreover, changing the sampling interval and keeping the observation span constant does not affect the estimated uncertainties at all. This would indicate that there is no practical interest (from a rate uncertainty point of view) of using permanent stations with respect to campaign observations when time series contain random walk noise [*Zhang et al.*, 1997]. However, continuous observations of permanent stations are very helpful to locate offsets which severely affect velocity estimations (see Section 5.1.1).

These two examples (white noise and random walk) represent the two extremes of time-correlation noise. They prove that CATREF software, and by extension all least squared-based algorithms assuming uncorrelated time series, provides velocity uncertainties that are not optimal since some level of correlated noise is expected. Therefore, in order to properly quantify the uncertainties and then to infer a proper interpretation of the estimated velocities, the stochastic properties of the time series noise must be taken into account, rather than considering the time series noise having a random nature.

6.2. Noise analysis methodology

6.2.1. Maximum likelihood estimator technique

We use the maximum likelihood estimator (MLE) of the Create and Analyze Time Series (CATS) software [*Williams*, 2008] to address the nature and the amount of time-correlated noise in the residual time series (trends, offsets and outliers removed, see Section 5.1). The nature and amplitude of the correlated noise is given by the estimated parameters of the data covariance following a given noise model. Most common noise models are described in section 6.2.2. This technique has shown to perform better than the classical spectral analysis, improving the precision and the sensibility to the time-correlated noise content [*Langbein and Johnson*, 1997; *Mao et al.*, 1999].

Given a residual sample of n data $X=(x_1, x_2, ..., x_n)$ following a normal distribution, the probability of observing the x_i point is given by the density probability function:

$$f(x) = \frac{1}{\sigma\sqrt{2\pi}} \exp\left(-\frac{1}{2}\left(\frac{x}{\sigma}\right)^2\right) \qquad (14)$$

and the probability of observing the whole data sample is given by the joint Gaussian probability density function:

$$f(x) = \frac{1}{2\pi^{\frac{n}{2}}|C|^{\frac{1}{2}}} \exp\left(-\frac{1}{2}X^T C^{-1} X\right) \quad . \qquad (15)$$

Then, to analyze the noise content of the given sample, the parameters of the data covariance matrix are adjusted by maximizing Eq. 15, that is [*Langbein and Johnson*, 1997]:

$$lik(N,C) = \frac{1}{2\pi^{\frac{n}{2}}|C|^{\frac{1}{2}}} \exp\left(-\frac{1}{2}X^T C^{-1} X\right) \quad , \qquad (16)$$

or by taking the natural logarithm:

$$MLE = \ln[lik(N,C)] = -\frac{1}{2}\left[\ln|C| + X^T C^{-1} X + n\ln(2\pi)\right]. \tag{17}$$

To find the maximum probability, a downhill simplex algorithm is used [*Press et al.*, 1992]. Hence, the MLE method estimates the noise model parameters (*N*) of the data covariance (*C*) that maximizes the logarithm of the joint probability density function. This is similar to estimate the data covariance matrix that most likely caused the observed data to occur [*Papoulis and Pillai*, 2002]. The parameters of the covariance matrix to be estimated actually can be composed of a linear combination of different stochastic noise models [*Langbein and Johnson*, 1997]:

$$C = \sum_i \sigma_i Q_i, \tag{18}$$

where *i* represents each stochastic model, Q_i the unit covariance matrix and σ_i the noise amplitude. The stochastic process driving the noise type (with its corresponding covariance matrix *Q*) must be previously defined. For instance, the matrix *C* for the uncorrelated white noise and for the random walk noise models are given by Eqs. 7 and 11 respectively. The amplitude of the noise model is then estimated through the MLE analysis. More details about several noise models are given in section 6.2.2. The unit covariance matrix used in the noise analysis is then the key factor of the MLE technique since it conditions the degree of coherence (likelihood) between the noise model and the input data and thus, the significance of the estimated model parameters [*Langbein*, 2004].

Finally, once the data covariance matrix is known, the realistic velocity uncertainties can be estimated following Eq. 4. In order to avoid the computing effort of inverting several times the data covariance matrix, if the time-correlated noise properties (noise type and amplitude) are already estimated or given externally, an easy-to-use analytical expression exists to approximate the velocity uncertainty with a precision of 5% (Eq. 25 in *Williams*, [2003b]).

6.2.2. Noise models

Geophysical phenomena, monitored for instance using GPS observations, are usually described by a one-dimensional frequency-dependent stochastic process known as power law process and given by [*Agnew*, 1992]:

$$P(f) = P_0 f^k, \tag{19}$$

where *f* is temporal frequency, *k* is the spectral index, which defines the frequency dependence of the process, and P_0 is a normalizing constant given by [*Langbein*, 2004]:

$$P_0 = \frac{2\,(2\,\pi)^k\,\sigma^2}{f_S^{\,1+\frac{k}{2}}} \quad , \tag{20}$$

where σ represents the power law noise amplitude and f_s the sampling frequency.

Following Eq. 19, for a spectral index $k = 0$, there is no dependence on frequency, thus all frequencies contains the same power in the process (blue line in Figure 6.1). By semblance with the optical spectrum, these uncorrelated processes are called white noise processes. Conversely, for a $k \neq 0$, power is not equally distributed within the spectrum and then time-correlated noise exists. Following the same naming principle, they are called colored noise processes. Most geophysical phenomena have spectral indices $k \leq 0$, showing that there is more relative power at low frequencies resulting in a so-called reddish spectrum. Specific stochastic models with integer spectral index are named flicker or pink noise for $k = -1$ (pink line in Figure 6.1) and random walk, Brownian or red noise for $k = -2$ (red line in Figure 6.1).
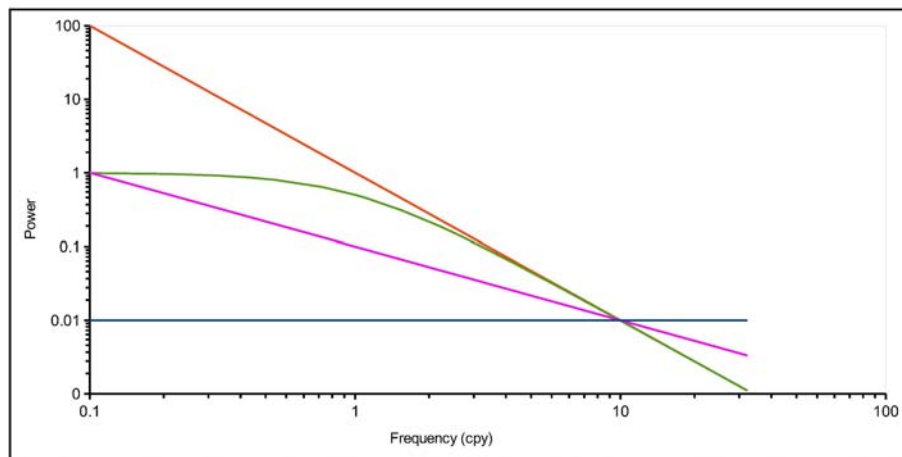
Figure 6.1. log-log plot of the relative power spectrum density of white noise (blue), flicker noise (pink), random walk (red) and Gauss-Markov (green) stochastic models.

Furthermore, different error sources and geophysical effects can lead to different power law noise processes mixed in the same time series (see Eq. 18). Thus, noise in time series are usually not fully described by only one integer colored noise model. A combination of different white and integer colored noise models can then be used to describe the temporal correlation in the data [*Williams*, 2003b], for instance, using both flicker and random walk noise models. Another option might be to directly estimate an extra parameter for the spectral index in the noise analysis, that is, to use a non-integer colored noise model.

Langbein [2004] stated that the noise models applied for GPS data (in regional networks) might be more complex than the commonly used power law process. Another stochastic method used to describe the time-correlated nature of geodetic observations is the Gauss-Markov process [*Gelb*, 1994]. This process also likely describes the spectra found in some geophysical loading models [*Ray et al.*, 2008]. The power spectral density of the generalized Gauss-Markov process is given by [*Langbein*, 2004]:

$$P(f) = \frac{P_0}{f^n + \beta^n} \quad , \tag{21}$$

where β is the transition or crossover frequency and $n=-k$. The crossover frequency represents the point where the spectrum of low and high frequencies cross each other. Thus, for lower frequencies, this process is frequency-independent (flat spectrum or $k = 0$) and for the higher frequencies, the process is consistent with a power law process (green line in Figure 6.1) [*Langbein*, 2004]. Therefore, if $\beta = 0$, this process becomes similar to a power law process of spectral index k. The First-order Gauss-Markov process [*Gelb*, 1994] is a special case of the generalized Gauss-Markov process where $k = -2$ [*Langbein*, 2004].

As described in the previous section 6.2.1., MLE indicates the degree of coherence between the data and an underlying stochastic noise model. Thus, in order to assess which stochastic model better describes the data, the maximum likelihood ratio (δML) between the noise models is analyzed. This ratio actually represents the difference of the MLE values since a logarithm is estimated (see Eq. 17). This way, the model showing the highest MLE value is signaled as the best stochastic model to describe the data.

Several authors have discussed the appropriateness of the δML metric to assess model significance [*Langbein and Johnson*, 1997; *Mao et al.*, 1999; *Calais*, 1999; *Williams*, 2004; *Langbein*, 2004; 2008; *Beavan*, 2005; *Williams and Willis*, 2006]. The main issue to retain is that the δML between two different stochastic models can be used as a decision parameter provided that the difference in the number of estimated parameters (degree of freedom) for each model is taken into account. Thus, *Williams and Willis* [2006] performed several Monte Carlo tests which led to a value of δML between 2.9 and 3.1 for one degree of freedom difference and 4.7 for a two degree of freedom difference. *Langbein* [2004] proposed a value of δML equal to 2.6 per degree of freedom difference.

To obtain a proper δML threshold value for all the stochastic models used here, we used the Equations 7 to 9 of *Williams* [2003b] to create 1000 synthetic time series of 10 years of data (average span of ULR4 solution time series). 500 synthetic time series were created following a flicker noise and 500 more following random walk noise, both with a unit noise amplitude (1 mm yr$^{-1/4}$ and 1 mm yr$^{-1/2}$, respectively). The synthetic time series were then analyzed using flicker, random walk, power law, Gauss-Markov and First-order Gauss-Markov noise models. Tables 6.1 and 6.2 show the mean values of the estimated noise parameters (spectral index, noise amplitude and crossover frequency) for both groups of synthetic time series. Spectral indices are well determined for all noise models tested, with an insignificant deviation of about 2%. Noise amplitudes of both flicker and random walk noise models have a precision of between 1% and 2% respectively. These values represent actually the precision of the MLE technique. This precision is also reached with the power law noise model. However, the noise amplitudes for both the Gauss-Markov and the First-order Gauss-Markov models are larger, with a mean error between 3.3% and 4% respectively. Moreover, the estimated crossover frequency for these two models, even if it is small (between 0.1 and 0.2 cpy), departs significantly from zero. For instance, the scatter of the estimated crossover frequency for the Gauss-Markov model is large (RMS of 0.23 cpy), ranging from nearly 0 to 1.28 cpy. Considering that the noise source is constant, the scatter of the crossover frequency of the Gauss-Markov model would indicate a problem of fit [*Williams and Willis*, 2006].

Table 6.1. Mean noise parameters for the flicker, power law and Gauss-Markov noise models using synthetic data following a flicker noise model of amplitude 1 mm $yr^{-1/4}$. Parameters with no uncertainties are held fixed (not estimated).

	Synthetic	Flicker	Power Law	Gauss-Markov
Spectral Index	-1	-1	-0.982 ± 0.007 (1.8 %)	-1.022 ± 0.009 (2.2%)
Noise Amplitude	1	1.007 ± 0.003 (0.7%)	0.980 ± 0.008 (2.0%)	1.033 ± 0.009 (3.3%)
Crossover Frequency	0	0	0	0.214 ± 0.023 cpy

Table 6.2. Mean noise parameters for the random walk, power law, First-order Gauss-Markov and Gauss-Markov noise models using synthetic data following a random walk noise model of amplitude 1 mm $yr^{-1/2}$. Parameters with no uncertainties are held fixed (not estimated).

	Synthetic	Random Walk	Power Law	First-order Gauss-Markov	Gauss-Markov
Spectral Index	-2	-2	-1.979 ± 0.007 (2.1%)	-2	-2.021 ± 0.007 (2.1%)
Noise Amplitude	1	1.025 ± 0.003 (2.5%)	0.998 ± 0.008 (0.2%)	1.040 ± 0.003 (4.0%)	1.038 ± 0.009 (3.8%)
Crossover Frequency	0	0	0	0.112 ± 0.009 cpy	0.121 ± 0.010 cpy

Results of Tables 6.1 and 6.2 show that the noise values estimated using the power law process model are closer to truth than those of the Gauss-Markov process. Then, the MLE values were extracted for each synthetic time series and each noise model. Comparing the estimated MLE values, the Gauss-Markov processes obtain however a higher MLE value for the 87% of the synthetic time series. This is related to the larger number of degrees of freedom of the Gauss-Markov process as it adjusts an extra parameter (crossover frequency) with respect to power law and two with respect to flicker or random walk noise models (spectral index and crossover frequency). *Langbein* [2004] obtains the same results when comparing random walk and First-order Gauss-Markov noise models using synthetic time series created following a random walk noise model. From Eqs. 19 and 21 and also from Fig. 6.1, the differences between the power law and the Gauss-Markov processes are located at low frequencies. Therefore, longer time series are probably necessary to discriminate the more complex model from the simpler one [*Beavan*, 2005]. However, using the same synthetic time series but 20- and 40-year long, still about 80% of the time series show a preference for the Gauss-Markov process. The estimated mean crossover frequency with such longer time series is very small in both cases (about 0.1 and 0.05 cpy respectively), which practically turns the Gauss-Markov process into a power law process, even though the MLE value points towards the first one. The δML values at the 95th percentile found between the different models tested (see Table 6.3) are consistent with the above-mentioned values found in the literature. These 95th percentile values will be used in section 6.4 as threshold to assess

the model significance. This way, if the *δML* found between two models is larger than the correspondent value in Table 6.3, then the more complex model (left) if preferred over the simple one (right).

Table 6.3. ML ratio between different noise models tested with synthetic data. DoF stands for the difference of degrees of freedom.

	DoF	95% *δML*
PL vs. FN/RW	1	2.2
GM vs. RW	1	4.3
GG vs. FN/RW	2	5.2
GM vs. PL	0	3.4
GG vs. PL	1	4
GG vs. GM	1	2.3

6.3. Noise analysis procedure

As described in Section 6.1, signals and background noise are directly related. This way, to estimate reliable quantities of the background correlated noise content, all the significant periodic signals in time series must be taken into account in CATS (Section 6.3.1). Then, although CATS can also estimate several linear parameters like offsets and trends, this task is already performed with CATREF and it will not be considered here. Thus, velocity uncertainties are estimated with CATS using the post-fit residual time series resulting from CATREF. However, note that estimated velocities actually take into account the spatial correlation and the velocity constraints applied between different soln and between collocated stations. By analyzing residual time series in a station by station basis with CATS, we neglect both effects. The impact of these effects is addressed in Section 6.3.2. In addition, using detrended time series in CATS could lead also to a biased estimation of noise content to low values (Section 6.3.3). Finally, the effect of the time series span and data epoch on the noise analysis is also addressed (Section 6.3.4).

6.3.1. Periodic signals

As commented in Section 6.1, the estimated parameters characterizing the time series background noise are sensitive to superimposed periodic signals present in time series [*Mao et al.*, 1999; *Beavan*, 2005; *Williams and Willis*, 2006; *Amiri-Simkooei et al.*, 2007]. Thus, before carrying out the MLE analysis, in order to avoid biased estimates of correlated noise, it is necessary to remove any significant predictable (periodic) signal from the time series. For instance, neglecting seasonal signals could lead to biased power law estimates to higher values [*Blewitt and Lavallée*, 2002]. However, note that seasonal signals were already removed in the velocity estimation with CATREF (Section 5.2). To verify the existence of remaining periodicities we used the power spectral technique to examine the residual time series in the frequency domain. The Lomb-Scargle redefined periodogram [*Press et al.*, 1992] was used. This method is based on a non-linear least squares fit of sinusoids to the available

data. Tested with evenly spaced data, this method provides the same probability distribution than the FFT method, and furthermore, it provides reliable results with uneven spaced data [*Scargle*, 1982].

Using this method, the periodogram for each residual vertical time series of ULR4 solution was estimated. Then, frequency-averaged values were estimated by stacking all the time series spectra. The stacked periodogram for the vertical component is shown in Figure 6.2. In this figure up to 5 peaks are clearly observed standing out the background noise near 1, 2, 3, 4 and 6 cycles yr^{-1} (cpy) respectively. However, these peaks are not harmonics of the 1 cpy frequency, but harmonics of a different fundamental frequency. *Ray et al.* [2008], using the 6th harmonic, estimated this fundamental frequency to be about 1.04 ± 0.1 cpy (or a period of 351.2 ± 2.8 days). These periodicities were not found in other space geodetic techniques (VLBI and SLR) nor geophysical fluid loading models (atmospheric, non-tidal ocean and continental water) [*Ray et al.*, 2008]. That is, they are not expected to be real station movement, constituting then a GPS systematic error. The authors stated that the source of this systematic error is likely related to the GPS «draconitic» year period, that is, the revolution period of the GPS constellation in inertial space with respect to the Sun. The mapping of this effect into position time series may be driven by orbit mismodeling or by station-dependent multipath errors [*Ray et al.*, 2008]. This systematic periodic error should be modeled in the data processing (functional model) or, if not possible, as is currently the case, it must be removed before the noise analysis. Otherwise it will be captured by the stochastic model when noise content is analyzed.
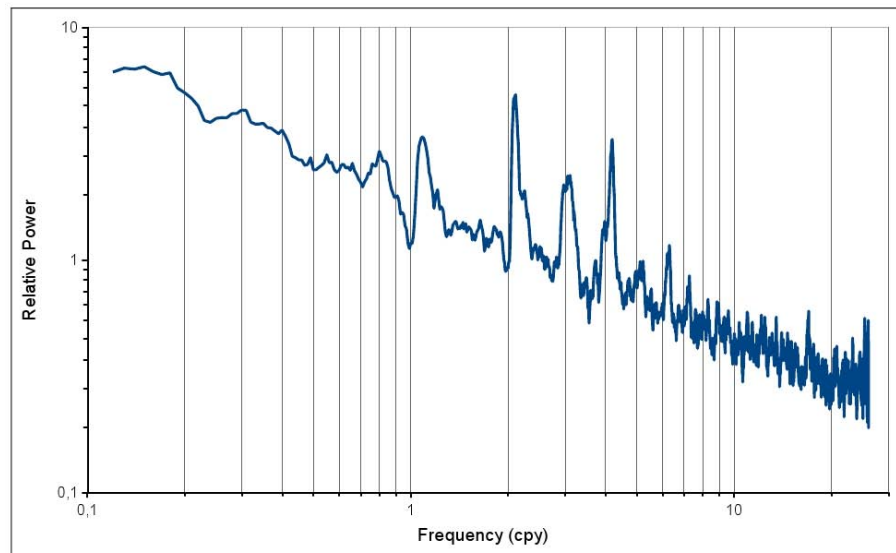
Figure 6.2. Log-log plot of the stacked periodogram for the residual vertical time series of the ULR4 solution.

In order to properly identify and remove these harmonics before running the noise analysis, we use the Frequency Analysis Mapping on Unusual Sampling (FAMOUS) software [*Mignard*, 2005; *Collilieux et al.*, 2007]. This tool uses a non-linear least squares fit to uneven data to detect the most powerful spectral line. Then, this signal is removed from the data and the least squares fit is iterated to estimate the next spectral line. This way, a maximum of 10 signals were estimated for each vertical time series assuming a white background noise. In

order to keep the low frequencies, which drive the main effect of time correlation content on velocity uncertainties, only significant frequencies higher than the annual frequency were retained. The significance criterion is based on the signal-to-noise ratio (SNR) as follows:

$$SNR = \frac{P_{signal}}{P_{noise}} \qquad (22)$$

that is, the power ratio between the signal, or meaningful information, and the background noise at the signal's frequency once the signal is removed. The higher the ratio, the less obtrusive the background noise is and then the more significant the signal is. Therefore, the signal significance is then dependent on the assumed background noise, which in turn, we want to estimate later with CATS. Thus, using a white background noise, low frequency signals may be flagged as significant when they actually correspond to correlated background noise. The rigorous approach to estimate the significance of detected frequency signals is then to use a realistic background noise, for instance a flicker noise. Here, we devised a simpler approach based on a frequency-dependent SNR threshold to assign significance of detected signals. Assuming that background noise is dominated by a flicker noise (with a frequency spectrum that falls off steadily into the higher frequencies), lower frequencies require a higher SNR to assume that detected signals are significant over the colored background noise.

Using a white background noise (approximately corresponding with the data variance) and a SNR threshold of 4, the SNR of all detected signals was extracted (Figure 6.3). A non-linear regression equation $\left(y = ax^b\right)$ (linear in the log-log plot of Fig. 6.3) was fitted to the SNR data to be used as SNR threshold. This approach yielded a SNR threshold between four for higher frequencies and six for near-annual frequencies. The resulting significant signals (Figure 6.4) clearly show to be centered on the above-mentioned draconitic harmonic periods. Also significant signals were found at the highest frequencies (~24.76 cpy or a period of ~14.75 days). These signals are likely due to aliasing effects of mismodeled ocean tide periods [*Penna et al.*, 2007].

It is also appreciable in Figures 6.2 to 6.4 that, due to this 1.04 cpy signal, even after removing the seasonal signals (annual and semi-annual), remaining power is still noticeable near these bands. Some authors have already shown this effect [*Amiri-Simkooei et al.*, 2007; *Ray et al.*, 2008; *Collilieux*, 2008]. This remaining power could also result from neglecting possible time-varying amplitudes of seasonal signals [*Bennett*, 2008]. If they are not taken into account, these near-seasonal signals could bias the velocity estimation (see Section 5.2). Nevertheless, the mean amplitude of these remaining signals is small enough to generally not significantly affect the velocity estimation. Mean amplitudes of these signals are shown in Table 6.4. However, maximum values of these harmonics reach 4 mm for KODK in the 1.04 cpy and for ALRT in the fourth harmonic. While the fourth harmonic of ALRT station (clearly seen in Figure 6.5), is expected to not bias the velocity estimation due to its high frequency, we cannot pretend the same for KODK station. Nevertheless, from results of Section 5.2, we estimated that similar annual amplitudes (4 mm) and time series span (6 years) result in a velocity bias of the order of 0.2 mm/yr. In conclusion, the impact of these harmonics on velocity estimation can be neglected.
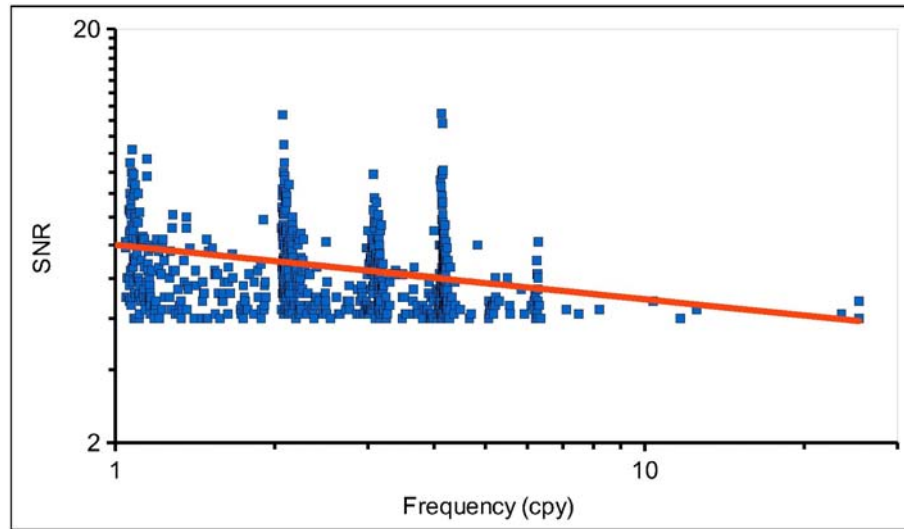
Figure 6.3. Log-log plot of the Signal-to-Noise Ratio (SNR) over 4 for all the significant periodic signals detected using a white background noise. A linear function (red) was fitted to the data to be used as SNR threshold.
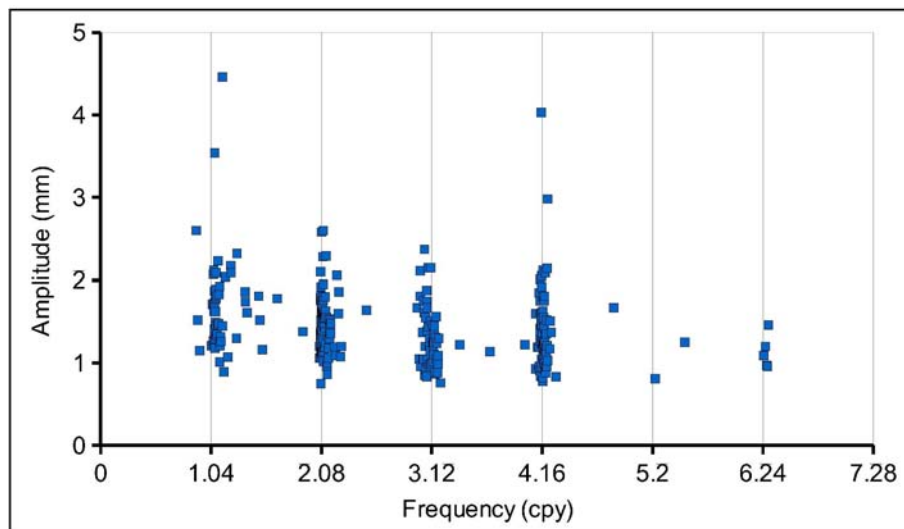
Figure 6.4. Significant periodic signals using a frequency-dependent SNR threshold. Only the first seven harmonics of the 1.04 cpy frequency are shown.

Figure and Table 6.4 also show that the estimated frequencies for the first three harmonics are a little scattered, specially the first one. In addition, there are some significant signals that are apparently not related to these harmonics. Both effects might result from the aliasing effect of unmodeled or mis-modeled periodic loading, which could be station-dependent since they are function of the relative position of stations and satellites [*Stewart et al.*, 2005; *Penna et al.*, 2007]. Another station-dependent effect is multipath, which actually could be one of the reasons for the existence of the draconitic period in position time series [*King and Watson*, 2010]. In addition, the GPS draconitic orbital period varies for each satellite and also over time [*Choi et al.*, 2004], so its effect on time series might not be purely harmonic.

Table 6.4. Mean frequency and scatter (in cpy) and mean and maximum amplitudes (in mm) of the significant GPS draconitic harmonics detected in residual time series of ULR4 solution.

Draconitic harmonic	Mean Frequency	Scatter Frequency	Mean Amplitude	Maximum Amplitude
1	1.09	0.10	1.7	4.5
2	2.10	0.05	1.5	2.6
3	3.10	0.07	1.3	2.4
4	4.17	0.04	1.4	4.0
6	6.27	0.02	1.1	1.5
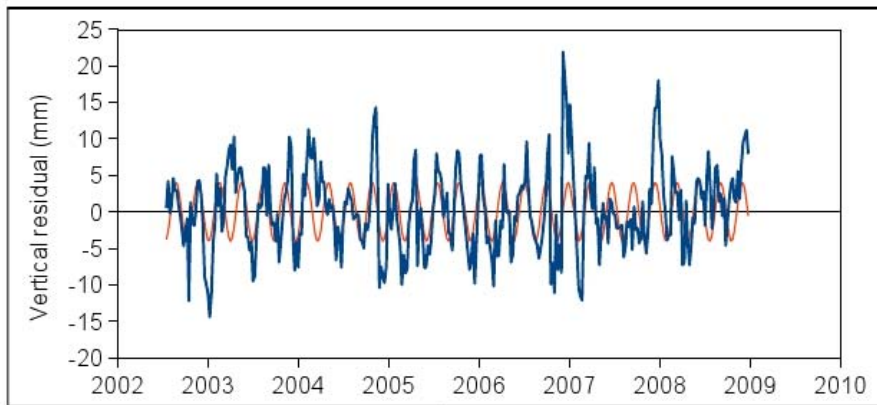
Figure 6.5. ALRT vertical residual time series (blue) and the 4th draconitic harmonic (red).

In the noise analysis of the last ULR3 solution, seasonal signals and only the fixed harmonics of the 1.04 cpy signal were removed from all time series. Following this procedure means that, for some stations, removing a fixed frequency of 1.04 cpy and their harmonics might not remove nearby significant signals, and then possibly yielding a biased noise analysis. For instance, as it has been demonstrated, significant signals remain near 1.04 cpy after removing the annual signal. Therefore, a new approach was tested to account for these hidden periodicities in time series. Instead of removing a central draconitic harmonic, as done with ULR3 solution, the detected significant periodic signals of Fig. 6.4 were removed in station-by-station basis. With this procedure, all station-dependent significant peaks at mid to high frequencies were properly filtered out while preserving the background noise to be estimated with CATS. For instance, Figure 6.6 shows four power spectra for the NRIL station corresponding to the raw time series (no periods removed) and to the time series with different periodic signals removed (seasonal, seasonal plus fixed draconitic and seasonal plus station-specific). The raw spectra (black line in Fig. 6.6) contains all the periodicities, notably a prominent annual signal. When seasonal signals are removed (blue line in Fig. 6.6) the remaining peaks correspond mainly to the draconitic periods already shown in Fig. 6.4. However, by removing these fixed draconitic periods (red line in Fig. 6.6), as it was done for ULR3 solution, there is remaining and significant power near 1 and 3 cpy frequencies. Using the new approach, these signals are also filtered out (green line in Fig. 6.6). This new approach to remove periodic signals was used in the noise analysis of ULR4 solution.
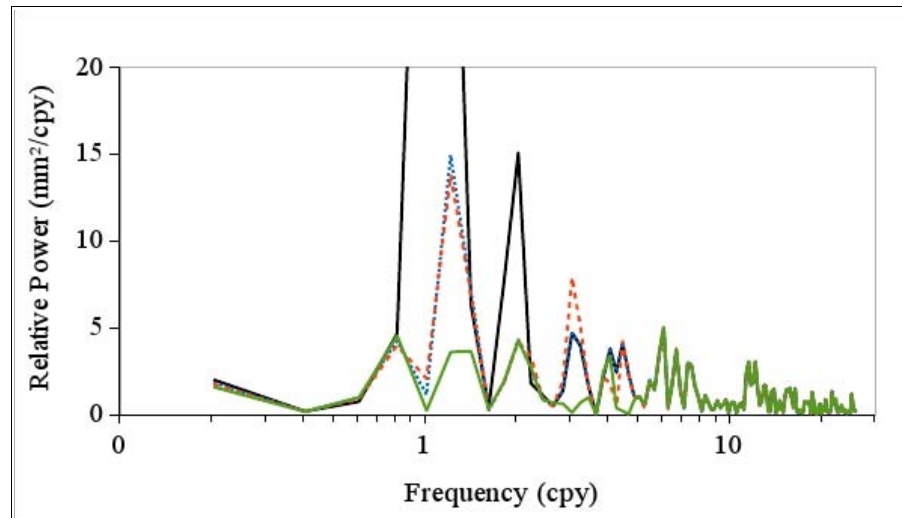
Figure 6.6. Vertical power spectrum for NRIL station with raw time series (black), time series without seasonal signals (blue), without seasonal plus fixed harmonics (red) and without seasonal plus station-specific signals (green). X-axis in logarithmic scale.

6.3.2. Spatial and temporal correlated time series

As commented starting this chapter, the procedure followed to compute the vertical velocity field is to use CATREF to estimate vertical velocities in a well-defined reference frame and then to use the post-fit residuals to estimate velocity uncertainties with CATS. However, by following this procedure two problems become obvious. First, an incomplete or simplified data covariance matrix is used in CATREF. Since the estimated parameters depend on this covariance matrix (see Eq. 3), this simplification could result in a significant estimated velocity difference. Nevertheless, this difference is assumed to be smaller than the velocity uncertainty [*Williams*, 2003b]. Second, using CATS to estimate velocity uncertainties might not be a fully optimal procedure either since spatial correlation is neglected, whereas it is not with CATREF. This second problem was briefly discussed by *Williams et al.* [2004] where several solutions were formulated. The authors argued that, even being an approximation, velocities can be estimated with a least square processing taking into account spatial correlation and then each velocity uncertainty can be treated separately, in a station by station basis, taking into account temporal correlation. However, as far as we know, this has not been demonstrated.

Therefore, we carried out a study to validate the procedure of using CATREF and CATS together to estimate the velocity field. This study has a twin purpose. It will help us to assess the effect of a complete data covariance matrix on estimated velocities and also the effect of neglecting spatial correlation in CATS when estimating the velocity uncertainties. The Kalman filter technique implemented in the Globk software (see Section 4.2) was used to estimate velocities taking into account both time and spatial correlated time series, that is, using the full covariance matrix for the input weekly data. These velocities and their uncertainties were then compared to those obtained using the current procedure, that is, to those obtained with CATREF and CATS, respectively. The preferred model used to describe

the time correlation of GPS time series is commonly a flicker noise plus white noise model [*Zhang et al.*, 1997; *Mao et al.*, 1999; *Calais*, 1999; *Williams et al.*, 2004; *Amiri-Simkooei et al.*, 2007]. Nevertheless, the Kalman filter needs the time correlation process to be parameterized with a finite number of terms, which is unfeasible with this kind of noise model [*Langbein*, 2008]. Thus, within Globk only a random walk noise model can be used to describe the time correlation of position time series. Consequently, velocity uncertainties were also estimated in CATS by fitting a random walk process to the data. This represents a limitation in our study since random walk is not actually the best suited model to describe the type and amount of time correlated noise. We make use of the hypothesis that this comparison can be extended to different stochastic models like the power law process in general. Nevertheless, although a random walk noise model provides pessimistic velocity uncertainties, a combination of white noise plus random walk noise model still represents the GPS data covariance better than the optimistic white noise model (see next Section 6.4).

Noise content of the residual time series resulting from the stacking with CATREF (see Chapter 5) was analyzed with CATS using a random walk plus white noise model (CC solution). Annual and semiannual signals and six harmonics of the GPS draconitic period (1.04 cycles yr^{-1}) were removed before the adjustment. This information (periodic signals and random walk amplitudes for each station) was extracted to be used as a priori information in the Kalman filter. The information obtained from the stacking with CATREF (discontinuities, outliers and soln constraints) was also applied in the stacking with Globk. Then, the same weekly solutions used with CATREF were stacked into two new long-term solutions using Globk:

− considering time-uncorrelated time series (GWH solution hereafter), and

− considering a random walk model to describe time correlation of time series, that is, considering station positions as a stochastic parameter (GRW solution hereafter).

The GWH solution was done to assess that both softwares (CATREF and Globk) yield a similar solution using the same stochastic model (only white noise). Since CC and GWH solutions have not used the same datum to align the combined solution to the ITRF2005 (see frame alignment with Globk in Section 4.2), a 14-parameter transformation was estimated between them and then the vertical velocity differences were extracted. Thus, 88% of the resulting vertical velocity differences were below 0.2 mm/yr being the maximum difference 0.6 mm/yr. However, none of these differences exceeded the 1 sigma level, showing a good coherence between both solutions, in agreement with *Collilieux* [2004].

Once the GWH solution was validated, the CC solution was compared to the GRW solution. First, vertical velocity uncertainties of both solutions were compared. Figure 6.7 compares the station vertical velocity uncertainties between GRW and CC solutions, both of them using a random walk noise model. There is a very good agreement between both estimations being the mean value of the uncertainty differences of 0.06 mm/yr with a RMS of 0.07 mm/yr, and being 83% of differences smaller than 0.1 mm/yr. This test shows that the impact of spatial correlation on velocity uncertainty is not significant. To further show the effect of spatial correlation on the estimated parameters (station positions and velocities), the correlation was computed from the covariance matrices of the GWH and GRW combined solutions (Figure 6.8). To reduce the computation load, a reduced covariance matrix was used (only collocated multi-technique sites were used, see more details in Section 8.3). From Fig. 6.8 it is obvious that by considering time correlation through a random walk noise model, the spatial correlation is actually masked and station positions and velocities can be considered to

be uncorrelated between them. Conversely, the spatial correlation is noticeable when a simple white noise model is used to represent time series noise. We thus verify that CATS can be used to estimate realistic velocity uncertainties neglecting spatial correlation.
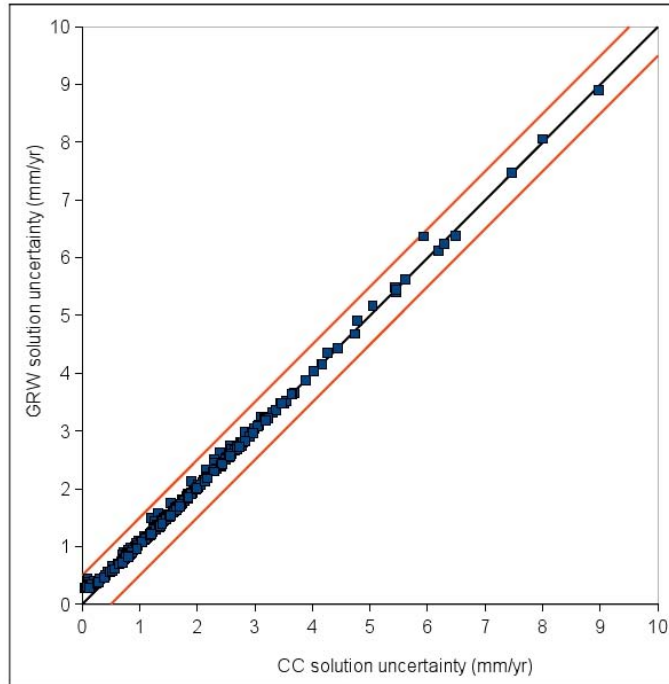
Figure 6.7. Comparison of vertical velocity
uncertainties between CATS (CC solution) and
Globk using a random walk model (GRW solution).
Red lines represent differences of ±1 mm/yr.
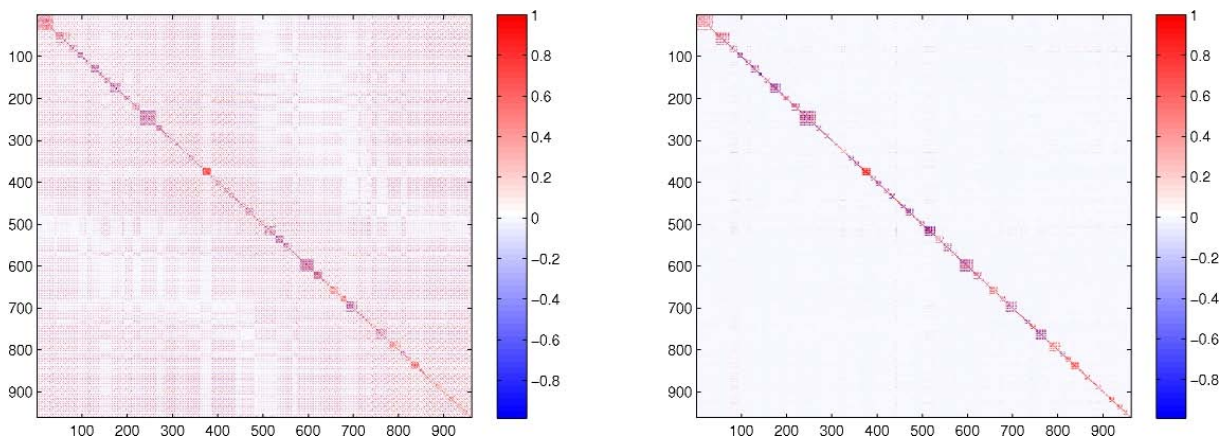
Figure 6.8. Representation of the spatial correlation between stations positions and velocities through the covariance matrices of GWH solution (left) and GRW solution (right). Colored squares in the diagonal represent the different station soln and the constrained stations in the same site.

Second, after applying a 14-parameter transformation between the CC and GRW solutions, the vertical velocities of both solutions were compared (Figure 6.9). The weighted RMS of the velocity differences was 0.6 mm/yr. Each velocity difference was then examined and compared with its uncertainty and only for 3% of stations the ratio reached the two-sigma level, for the rest they remained at the one-sigma level. This shows that taking into account time-correlated noise when estimating velocities may result in a different value for the estimated velocity, but this value is coherent within its correspondent increased uncertainty. Figure 6.10 shows the histogram of the vertical velocity differences. 82% of the velocity differences between CC and GRW solutions are below 1 mm/yr, and 63% are below 0.5 mm/yr, being the maximum difference of 6 mm/yr for CAS1 station (Figure 6.9). This station has in fact the largest amplitude of the random walk noise model used in the GRW solution, resulting thus in the largest velocity difference.
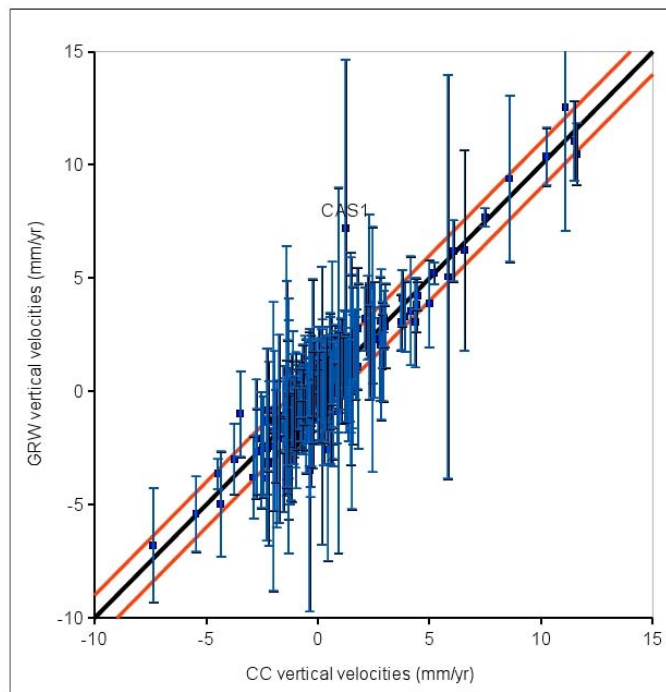
Figure 6.9. Comparison of vertical velocities
between CC and GRW solutions. Red lines represent
differences of ±1 mm/yr.

The fact that different velocity values are obtained with different covariance matrices is a proof that time series contain trends that result from geophysical movement but also from the correlated noise content itself. Both trend sources unfortunately cannot be split up [*Williams et al.*, 2004]. For example, as shown by *Johnson and Agnew* [1995], synthetic data leads to different estimated trends depending on their correlated noise content. This explains the velocity differences found between CC and GRW solutions due to the different covariance matrix used. Nevertheless, as it has been demonstrated, these velocity differences lie between the velocity uncertainty itself whenever time-correlated noise is taken into account. Certainly, the increased or realistic velocity uncertainties are actually due to this effect. This effect support even more the fact that estimated velocities must be enclosed by realistic uncertainties, otherwise they will appear to be significantly biased.
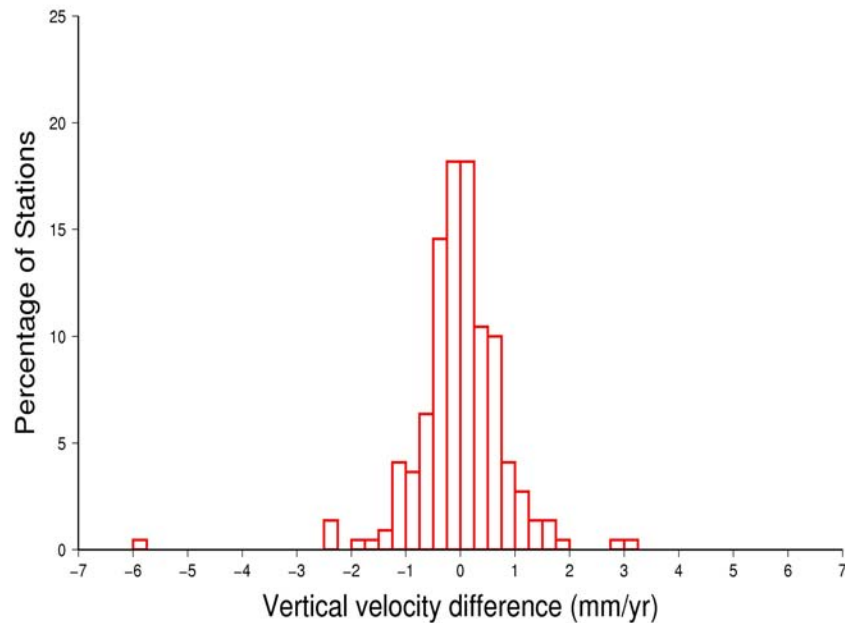
Figure 6.10. Histogram of vertical velocity differences between CC
and GRW solutions.

The test presented here shows that using both CATREF and CATS software together to obtain the velocity field is an adequate procedure. First, velocity uncertainties are not biased by neglecting spatial correlation. Thus, formal velocity uncertainties estimated with CATREF can be substituted by those estimated with CATS. Second, estimated velocities with CATREF are not biased when temporal correlation is taken into account, since their differences are smaller than their realistic uncertainties.

6.3.3 Time-correlated noise trends

As it has been shown in the previous study, time-correlated noise content also contributes to the time series trends. Thus, by removing trends in CATREF, the noise analysis using residual time series could also be biased low as some amount of the correlated noise is captured when the trend was estimated by CATREF. *Langbein and Johnson*, [1997] carried out some simulations with the MLE technique showing to be accurate and sensitive to correlated noise content. However, when time series trends were removed, the author showed that MLE technique provides slightly biased noise estimates towards lower values of about 15%.

To examine this effect, we carried out a test with the synthetic time series of Section 6.2.2. The 500 synthetic time series following a flicker noise model were twice analyzed with CATS by adjusting the spectral index of a power law noise model with and without removing the trend (No-trend and Trend analyses, respectively). Results of both analyses were compared between them and also with respect to truth. Note that since data covariance matrix is scaled by noise amplitude (Eq. 18), the same results can be obtained with different flicker noise amplitudes by multiplying the estimated noise amplitudes and velocity uncertainties (for instance see Eqs. 10 and 13) by a different amplitude. Table 6.5 shows the comparison of the

estimated noise amplitude and spectral index when time series trends were removed (No-Trend solution), or not (Trend solution) and also with respect to truth (Real solution). The mean effect of removing the time series trend prior to analyze the noise content (1%) is not significant (RMS of 1%) and is below the mean MLE precision level (2%). Maximum noise amplitude and type (spectral index) differences were estimated to be about 7% lower when trend was removed. However, these maximum differences between Trend and No-Trend solutions are smaller than between Trend and Real solutions. Thus, in conclusion, residual time series from the stacking with CATREF can be fairly used in the noise analysis with CATS.

Table 6.5. Differences of noise amplitude and spectral index of synthetic time series when trends are removed (No-trend) or not (Trend). Comparison with real values is also shown.

	Noise amplitude (Truth = 1)		Spectral Index (Truth = -1)	
	Trend vs No-Trend	Trend vs Real	Trend vs No-Trend	Trend vs Real
Max.	0.07 (7%)	0.16 (16%)	0.00 (0%)	0.21 (21%)
Min.	0.00 (0%)	-0.21 (21%)	-0.07 (7%)	-0.12 (12%)
Mean	0.01 (1%)	-0.02 (2%)	-0.01 (1%)	0.02 (2%)
RMS	0.01 (1%)	0.08 (8%)	-0.01 (1%)	0.08 (8%)

In addition, note that since the synthetic time series were created without trend, the estimated trend values come entirely from the effect of the correlated noise content. The mean value of the 500 estimated trends is 0.02 mm/yr with a scatter (RMS) of 0.12 mm/yr. As expected, this scatter corresponds to the predicted velocity uncertainty (Eq. 25 in *Williams*, [2003b]) for these time series, that is, the uncertainty of the zero-value trends due to the correlated noise. This way, the realistic uncertainties account for the correlated-noise trend which is not a real trend and that is included within the estimated time series trend.

6.3.4 Time series span and data epoch effects

Noise analyses of global GPS solutions are useful to get deeper inside into noise sources of the GPS technique. For instance, analyzing if correlated noise content is constant or time-dependent can provide relevant information about its sources. Here, we analyzed the effect of different time series lengths using synthetic and real data. In addition, we made use of real data to assess different data epoch effects on estimated noise parameters.

Mao et al. [1999], using synthetic data following a power law plus white noise model, stated that spectral indices can be estimated reliably with spectral analysis for time series longer than 2 years. Conversely, for shorter time series the estimation of the spectral index is not guaranteed, specially if the time series trend is removed. This would largely suit us since only time series larger than 2.5 years are retained in our velocity field (see Section 5.2). However, as stated by *Williams et al.* [2004], the estimated index using spectral analysis appeared to be biased even for for time series of 15 years in length. These authors, using synthetic daily time series of different lengths and different noise amplitudes, showed that the spectral index bias depends on the ratio of the noise amplitudes (colored/white) and the length of the time series. That is, if the colored noise dominates over the white noise, the spectral

index bias is negligible even for shorter time series, provided that time series length is at least longer than the crossover period. At this crossover period, the amplitudes of the white and colored noise models are the same. In addition, as longer time series are more sensitive to low frequency time-correlated noise, they will show a smaller spectral index bias.

We used 54 residual time series of the ULR4 solution spanning more than 12 years and with more than 95% of available data. This way possible biases resulting from data gaps are minimized. Each of these time series was windowed with a decreasing rate of 1 year, from 12 to 2 years of data. Different periods of the same data span were analyzed separately, from the newer data (group A) to the oldest (group B, C, D, E or F). Table 6.6 resumes the 28 different groups of times series analyzed. Each group of 54 time series corresponds to a different time series length or to a different data epoch. Data of Table 7.6 is also shown in Figure 6.11. The analyzed groups are named 12, 11a, 11b, 10a, ….. , 2d, 2e and 2f.

Table 6.6. Summary of time series groups analyzed. Time series are distributed into 11 groups of different time series lengths (left) and in up to 6 groups of different periods of data (up).

Span \ Period	A	B	C	D	E	F
12	1997-2009	-	-	-	-	-
11	1998-2009	1997-2008	-	-	-	-
10	1999-2009	1997-2007	-	-	-	-
9	2000-2009	1997-2006	-	-	-	-
8	2001-2009	1997-2005	-	-	-	-
7	2002-2009	1997-2004	-	-	-	-
6	2003-2009	1997-2003	-	-	-	-
5	2004-2009	1997-2002	-	-	-	-
4	2005-2009	2001-2005	1997-2001	-	-	-
3	2006-2009	2003-2006	2000-2003	1997-2000	-	-
2	2007-2009	2005-2007	2003-2005	2001-2003	1999-2001	1997-1999

A white plus power-law noise model was fitted to each time series and then the median estimated noise parameters (power law noise amplitude and spectral index) were extracted by group. Then, 500 synthetic time series with 12 year length were created using the median spectral index and the median white and correlated noise amplitude values obtained for the solution 12 using real data. This synthetic time series were windowed and analyzed following the same scheme that for the real data.

The first noticeable result of this noise analysis is that as real data time series become shorter it was more difficult to solve the colored noise parameters, in agreement with *Mao et al.* [1999] results, whereas for synthetic data the relative loss of solutions is almost insignificant (Figure 6.12). This is specially noticeable for some of the 2-year groups of real data, where less than 50% of the time series converged to a solution. Nevertheless, the large number of time series analyzed is still suitable to estimate statistical properties of the noise
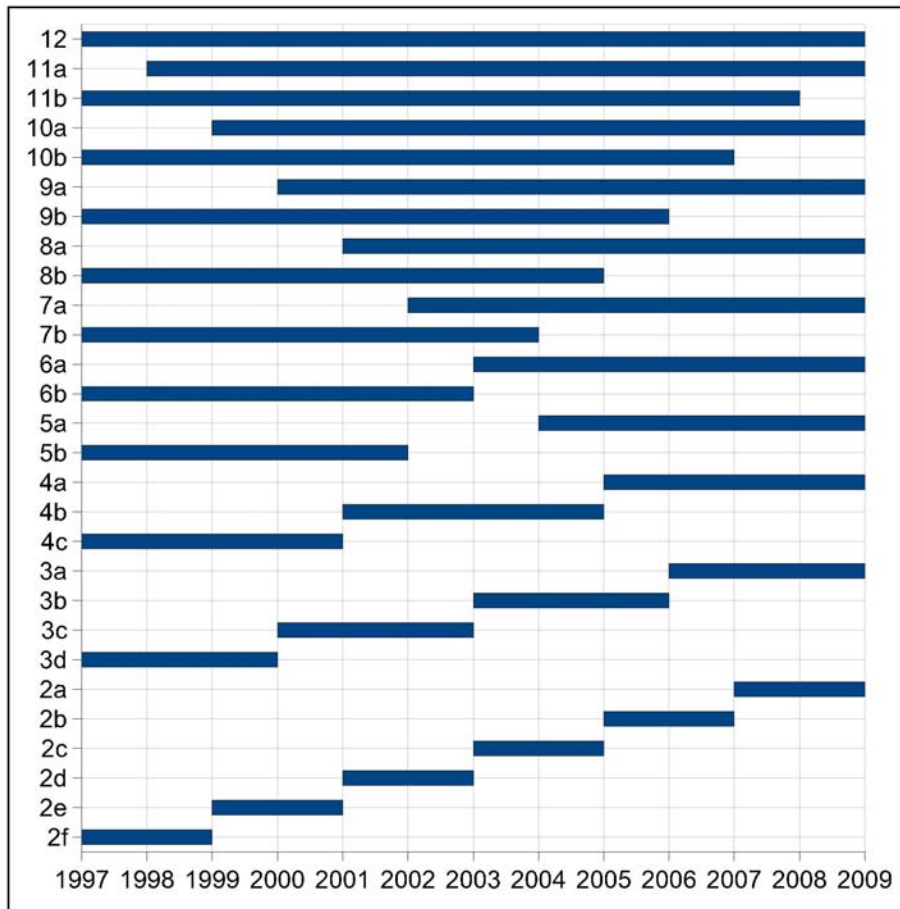
Figure 6.11. Summary of time series groups analyzed.
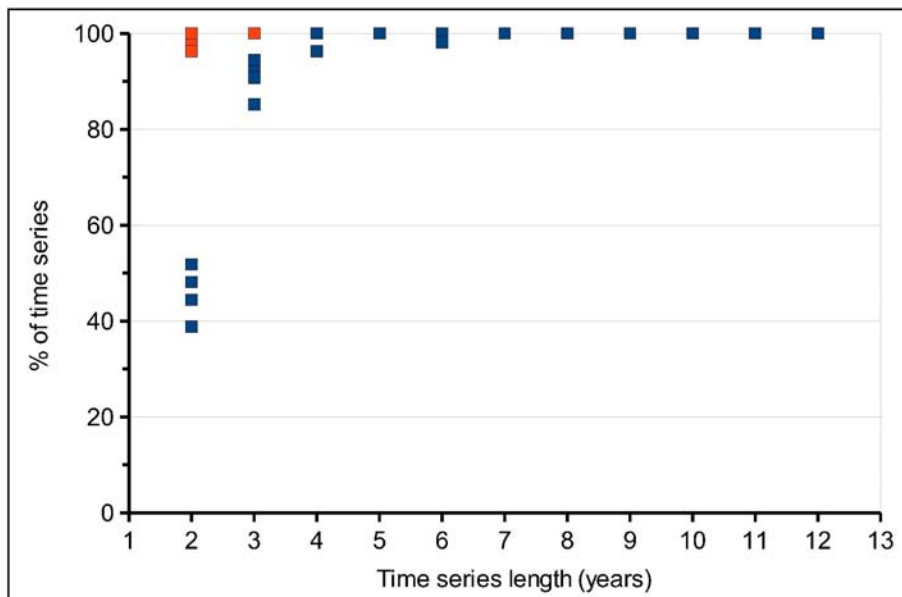
Figure 6.12. Percentage of solutions obtained with respect to time
series length using real data (blue) and synthetic data (red).

content of each group of real time series. The loss of solutions for real data is due to the fact that shorter time series are mostly dominated by the white noise and by the fact that by removing the station velocities, some of the correlated noise is also removed (see previous Section 6.3.3). Conversely, for the synthetic time series, the factor between correlated and white noise is always the same, as it was defined from the noise results of solution 12 using real data. Thus, since for shorter synthetic time series the correlated noise still dominates over the white noise amplitude, they are easily solved, in agreement with the *Williams et al.* [2004] test.

Figures 6.13 and 6.14 show the median spectral index, that is, the noise type, and the median power law noise amplitude of each analyzed group of real and synthetic time series of Table 6.6.
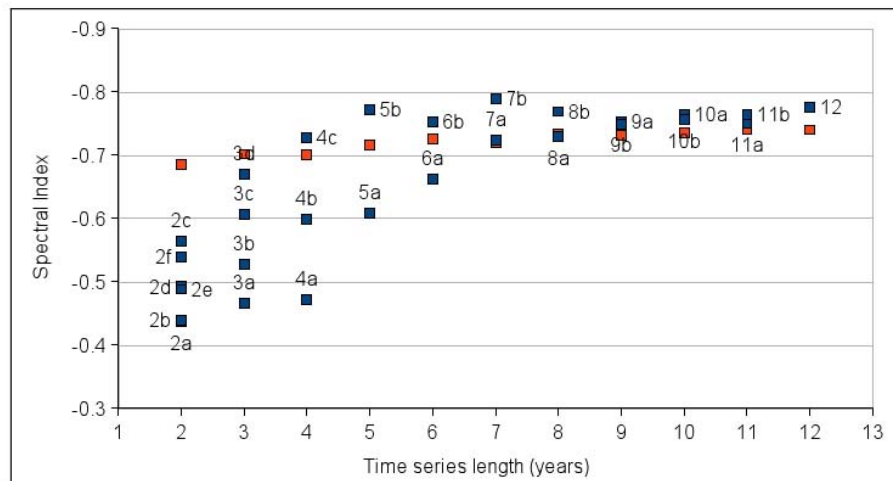
Figure 6.13. Median spectral index for each group of real (blue) and synthetic (red) time series with respect to time series length.
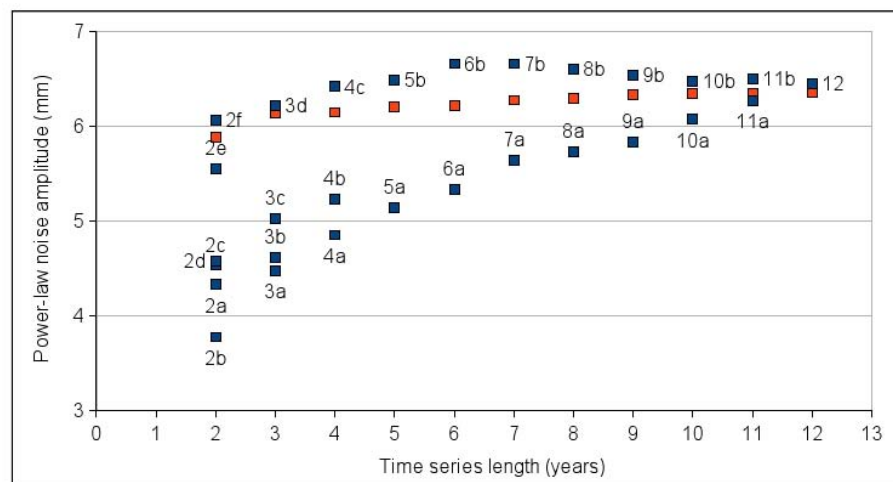
Figure 6.14. Median power law noise amplitude for each group of real (blue) and synthetic (red) time series with respect to time series length.

Regarding the spectral index (Fig. 6.13) of the synthetic data, where the nature of the noise does not change with time, it shows that the spectral index is not significantly biased using different time series lengths. This proves the quality of the MLE estimator and the independence of results from time series span when the noise characteristics are constant. However, regarding the real data, the picture is different. In this case, shorter time series result in a higher (mean value of different groups of the same length) spectral index or, in other words, in a lower correlation. This indicates either that as time series get longer then time correlated noise increases or that longer time series are more sensitive to correlated noise content. Moreover, given a time series length, older data clearly results in a smaller (farther to zero) spectral index. That is, older data contains noise more correlated than newer data. This way, it is remarkable that by using only 3, 4 or 5 years of the oldest data (solutions 3d, 4c and 5b), the noise type is similar to that obtained using the synthetic data, and therefore, similar to that using the complete 12 years of real data. Conversely by using the 3 or 4 years of the newest data, the noise type estimated is less correlated. This would indicate that longer time series are very influenced by the noise type of the oldest data and that by adding new and less correlated data, the estimated noise type does not change significantly.

This hypothesis is also confirmed regarding the amplitude of the power law noise (Fig. 6.14). In this case the separation between older and newer data is more striking as the good agreement between synthetic data and older real data. In this case, even with time series of only 2 or 3 years of older data, the noise amplitude is similar to that found for the whole 12 years data. In addition, regarding solutions of 2, 3 and 4 years it seems that solutions that used data before years 2000-2001 (2e, 2f, 3d and 4c solutions) are noisier than the rest of solutions of the same length. This grouping of older and newer solutions was not noticed in the spectral index. However, it is indirectly there. Certainly, we can see in Fig. 6.13 how the spectral index of older and newer solutions begin to diverge at the 8-year solutions, where the newer solution (8a) is the first one that does not use data before year 2001. This would indicate that a major modelization improvement occurred at that epoch.

Since spectral index and noise amplitude depend on data epoch, it is clear that the noise source of this variation cannot be monument noise. This would involve that an important change of the environmental conditions (specially climatological ones) of all the stations had occurred, which is unrealistic. This remark supports the idea that correlated noise in current global GPS solutions is mainly produced by the data processing itself which is improved over time and not by monument noise. We state that even when performing a reprocessing, the quality of the solution would not be homogeneous. Inhomogeneities within the reprocessing might come, for instance, from the evolving quality and quantity of stations in the tracking network, the evolving constellation, the orbital parameters estimation (through the time increasing number of stations), the tropospheric model (a priori pressure or mapping function values changing with improved ECMWF analyses), differential second-order ionospheric effects (through the solar 11-year cycle). The inhomogeneity is also noticeable in the increased percentage of resolved ambiguities over time, from ~50% in 1996 (~70% in 1997) to ~95% in 2009 (Fig. 6.15) which indirectly could also be an additional reason for smaller correlated noise for newer data. For instance, *Tregoning and Watson* [2009] and *King and Watson* [2010] have recently shown that fixing ambiguities reduce the magnitude of power law noise and propagated spurious signals. Due to the dynamic sub-networks applied (see Section 3.3), the increased percentage of solved ambiguities is not related to the increased number of stations in our tracking network (see Figure 3.9). The number of processed stations per sub-network remains nearly constant for the whole period and the
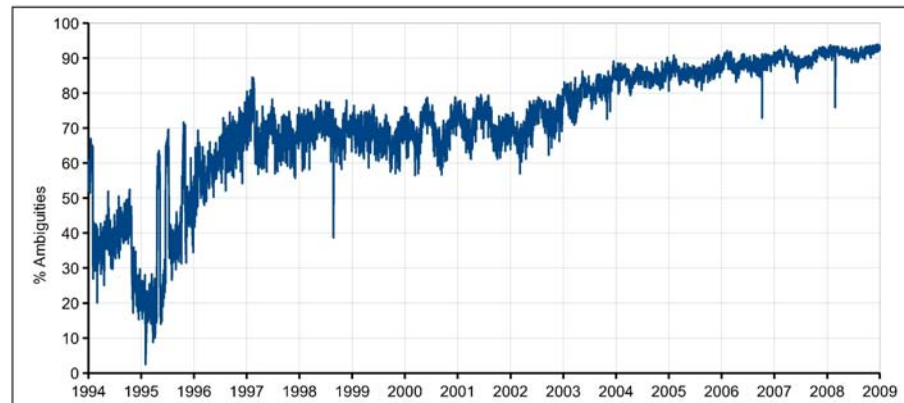
Figure 6.15. Percentage of resolved ambiguities of ULR4 solution.

increased number of stations is absorbed by the increased number of dynamic sub-networks (see Figure 3.11). The increased number of resolved ambiguities must be then related to other sources, as improved receivers quality. In this sense, *King and Watson* [2010] also showed that constellation evolution represents a clear driver for time-correlated noise content in GPS position time series.

From Figures 6.13 and 6.14 the most interesting outcome of our study is that noise content depends on time series length but mainly on time series epoch. Furthermore, it is expected that this dependency will be larger if a non-reprocessed solution is concerned. A derived conclusion is that noise content comparisons between different solutions and different regions should take into account the respective time series length and data epoch included, specially if non-reprocessed solutions are concerned. For instance, *Mao et al.* [1999] studied a global distribution of sites to assess regional differences in noise. *Williams et al.* [2004] compared noise content of different global and regional networks of different time series lengths (from 2 to 11 years) and different data epochs (from 1991 to 2003). *Langbein* [2008], using recent data with a median span of 6.5 years from 1996 onwards, compared noise results to *Williams et al.* [2004] ones within the same regional network (mean data span for *Williams et al.* [2004] network was 3.2 years between 1991 and 2003). His results showed a reduced correlated noise amplitude, in agreement with our results. *Beavan* [2005] used data from a regional network with time series lengths between 2 and 4 years from 2000 to 2004.5. He also compared his noise analysis (resulting from shorter and newer data) to those performed by *Williams et al.*, [2004] (longer and older data) and concluded that his results were only slightly noisier. This led him to conclude that common concrete pillars monuments perform similar to expensive deep braced monuments. However, none of these studies did take into account the fact observed here, that is, noise parameters are time-dependent. Therefore, those noise comparisons were incomplete, involving that their derived conclusions might not be right.

Following is the example of another possible erroneous conclusion. The spectral index for all the residual time series of ULR4 solution was estimated with CATS following a power law plus white noise model. Figure 6.16 shows the geographical distribution of the estimated spectral index. One noticeable aspect is that Japanese stations appear to have a whiter spectral index than other regions. Similarly, European stations seem to have a spectral index between white and flicker. Both aspects could be assumed to result from regional correlation of noise. However a closer inspection reveals that most of the Japanese stations used in ULR4 solution

were installed at the same epoch (2003) and have similar time series lengths (6 years). Thus, all the ULR4 time series were limited (windowed) to the period 2003-2009 and the noise analysis repeated. The geographical distribution of the new estimated spectral index is shown in Figure 6.17. It is clear that now Europe turns to have in general a whiter noise in agreement with Japan and that a regional noise signature is difficult to detect.
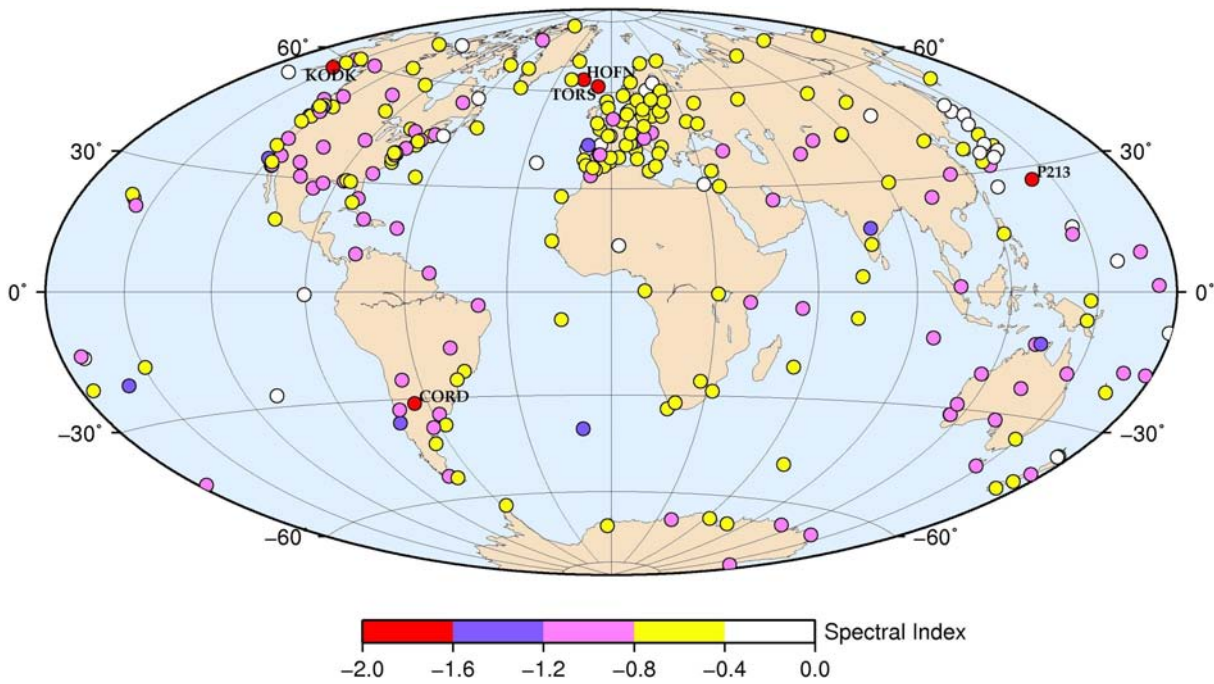
Figure 6.16. Spectral index of ULR4 station network (1996-2009).
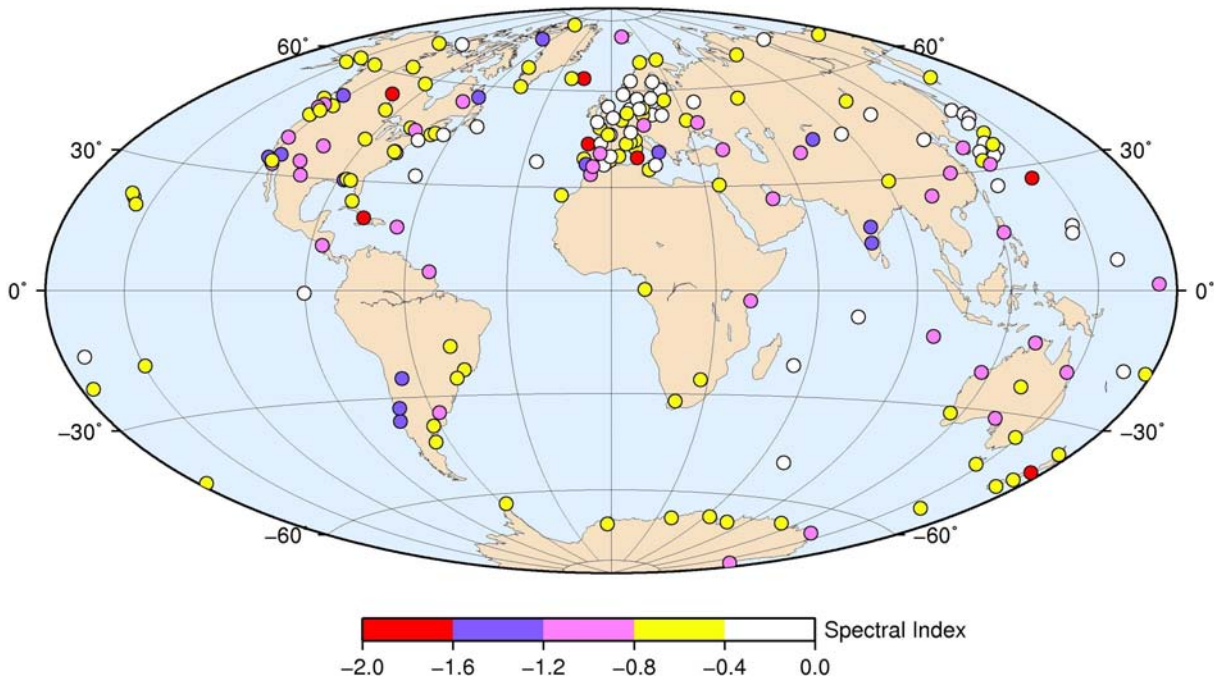
Figure 6.17. Spectral index of ULR4 station network (2003-2009).

We demonstrated that older data is noisier than recent ones and that noise level with 12 years is similar to that of 4-5 years of the oldest data. However, time series length is still a key parameter to reduce the estimated velocity uncertainties, although not as fundamental as if noise content was exclusively white (see Eq. 10). Figure 6.18 shows the median velocity uncertainty for each time series group of Table 6.6. It shows a reduction of the velocity uncertainty with time series lengths following a *1/T* relationship, where *T* is time series length, corresponding to a flicker noise [*Mao et al.*, 1999] (note that the noise model used in the analysis was a general power law process). Regarding exclusively older (red line in Fig. 6.18) and recent data (green line in Fig. 6.18), the relationships estimated are:

$$\sigma_r^{older} = 3.38\, T^{-1.10}$$
$$\sigma_r^{newer} = 1.79\, T^{-0.96}.$$

(23)

being expressed in mm/yr and *T* in years.Figure 6.18 also shows the uncertainty prediction given by equation 25 of *Williams* [2003b] (blue line). This prediction closely matches the uncertainty estimated using older data, representing then an upper bound (conservative) prediction.
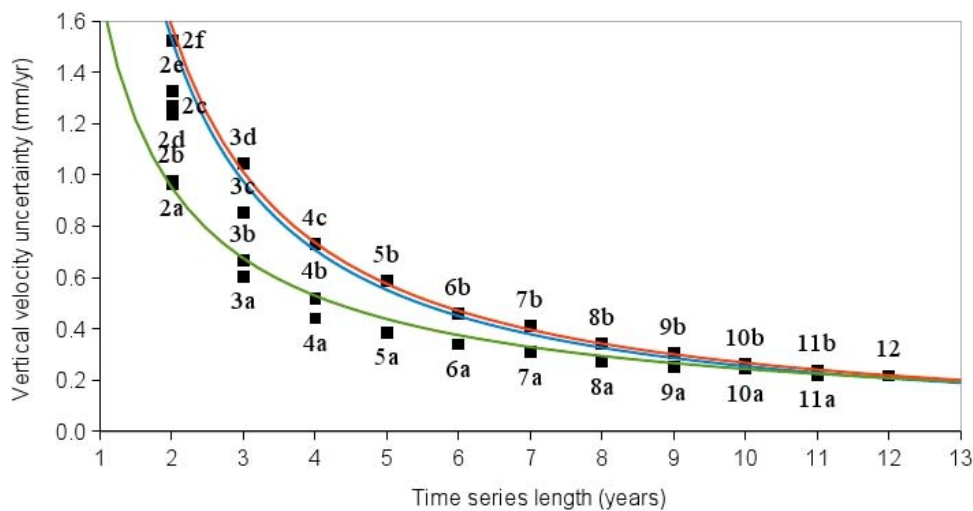
Figure 6.18. Median vertical velocity uncertainty for each group of time series with respect to time series length. Fitted curves represent the relationship between data span and mean velocity uncertainty for older (red) and newer (green) data.

Equation 23 and Figure 6.18 show that, for instance, to reach a mean velocity uncertainty of 0.45 mm/yr, 4 years of newer data (4a) are needed against 6 years of older data (6b). To see more clearly the uncertainty decay with respect to data epoch, the velocity uncertainties of different data epochs for solutions of 2, 3, 4, 5 and 6 years were extracted (Figure 6.19). This figure shows that the uncertainty reduction with data epoch is more noticeable for shorter time series.
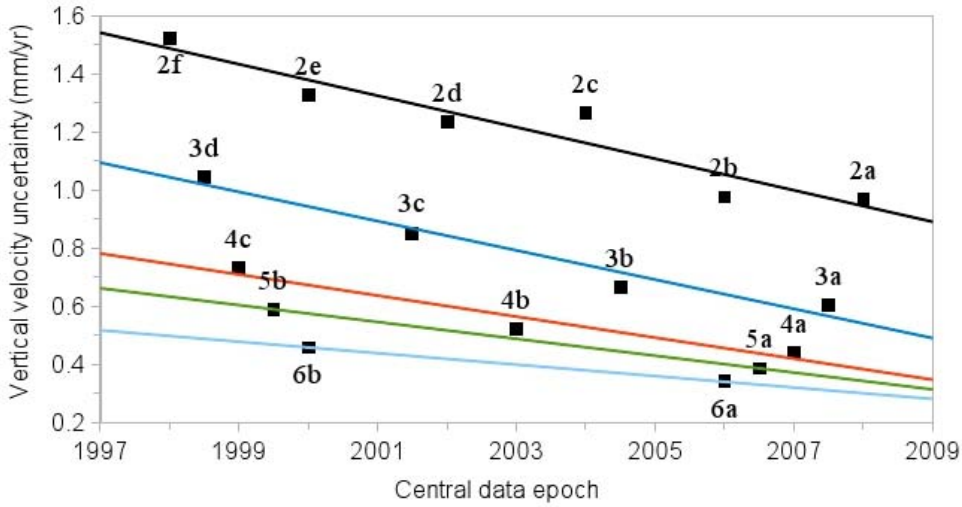
Figure 6.19. Median vertical velocity uncertainty for time series length of 2 (black), 3 (blue) and 4 (red), 5 (green) and 6 (cyan) years with respect to data epoch.

Therefore, to properly account for the colored noise dependency on data epoch, the known data covariance matrix used in noise analyses should take the following form:

$$C = a(t)\,I + b_{k(t)}\,\boldsymbol{Q}_{k(t)}(t) \quad , \tag{24}$$

where C is the data covariance matrix, a(t) is the time-dependent white noise amplitude, I is the identity matrix, $b_{k(t)}(t)$ is the time-dependent colored noise amplitude of the time-dependent spectral index k and Q_k is the noise model covariance matrix. Note that a(t) was already implemented in the noise analysis carried out in this study (see next Section 6.4).

6.4. Stochastic noise model selection

Using the MLE technique with CATS software (Section 6.2) and removing periodic signals in a station-by-station basis (Section 6.3.1) several noise models were tested to describe all the vertical post-fit residual time series of the ULR4 solution. By combining several white noise and colored noise components, up to 27 different stochastic models were considered (Table 6.7). This range of stochastic models is larger than that used in recent noise analysis of global GPS solutions [*Williams et al.*, 2004; *Amiri-Simkooei et al.*, 2007] and also larger than for the noise analysis of the latest ULR3 solution [*Wöpelmann et al.*, 2009].

Thus, the models tested to adjust the data were: WH, VW, TW, FN, RW, WH+FN, WH+RW, VW+FN, VW+RW, FN+RW, PL, GM, WH+PL, WH+GM, VW+PL, VW+GM, TW+FN, TW+RW, WH+FN+RW, VW+FN+RW, GG, WH+GG, VW+GG, TW+PL, TW+GM, TW+FN+RW and TW+GG.

The WH model represents a mean value of the white noise content of the time series (see Eq. 7). As opposed to this basic model, the VW model uses the weekly formal errors of the residual time series (Eq. 5) and solves for a scale covariance parameter. The TW model, in

Table 6.7. Components of stochastic models used to estimate the realistic rates uncertainty. The number of each component represents the number of estimated parameters.

WHITE NOISE MODEL	COLORED NOISE MODEL
White noise (WH) - 1	Flicker noise (FN) - 1
Variable white noise (VW) - 1	Random walk (RW) - 1
Time-dependent variable white noise (TW) - 2	Flicker noise + Random walk (FN+RW) - 2
	Power-law (PL) - 2
	First-order Gauss-Markov (GM) - 2
	Generalized Gauss-Markov (GG) - 3

addition to the constant term of the WH model, fits an exponential decay term which represents a time-dependent amplitude of the white noise over a finite time span [*Williams and Willis*, 2006].

The number associated with each noise components in Table 6.7 represents the number of parameters that are adjusted for each component. Thus, for example, for a WH+PL noise model there will be three parameter to adjust, that is, white noise mean amplitude, power law noise amplitude and spectral index.

As described in Section 6.2.2, the δML value between different models is used to select the best model. Thus, for each station and each model tested, the MLE value was extracted. Figure 6.20 shows the mean δML value of each model with respect to the RW model, which is the model that provides the smallest MLE value. Table 6.8 contains the same values of Figure 6.20 but distributed by noise component.
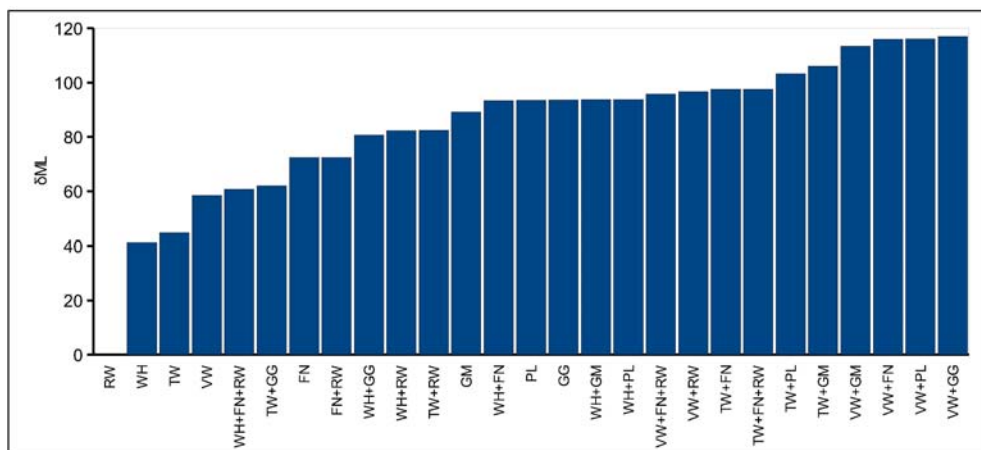
Figure 6.20. ML ratio of each stochastic model with respect to RW model (RW MLE value subtracted from all models). Stochastic models are sorted by increasing ML ratio value, thus, higher ratio represents a better model.

Table 6.8. ML ratio of each stochastic model with respect to RW model (RW MLE value subtracted from all models). Stochastic models are grouped by nature (white or colored). Last column and row (in blue) represents the mean value of each noise component. The best models are shown in bold.

	FN	RW	FN+RW	PL	GM	GG	
	72.4	0	72.4	93.5	89.2	93.6	
WH	41.3	93.4	82.3	60.7	93.8	93.8	93.6	79.9
VW	58.5	**116.0**	96.7	95.7	**116.1**	**113.4**	**117.0**	101.9
TW	44.8	97.6	82.4	97.6	103.3	106.1	62.0	84.8
	94.9	65.4	81.6	101.7	100.6	91.6	

By examining results of Table 6.8 by noise component (blue values) we can assess the following general conclusions:

a) regarding the white noise models:

− any combination of colored noise with VW is significantly superior to the other types of white noise combinations tested. When using a WH noise model, CATS software often finds a zero white noise amplitude, in agreement with *Beavan* [2005] findings. Conversely with VW model there is always some level of (scaled) white noise amplitude, which might improve the MLE analysis. However, these differences between WH and VW models did not translate into significant differences in the estimated velocity uncertainties.

− the TW model does not perform significantly better than a simple WH model, contrary to the results found for Doppler Orbitography and Radiopositioning Integrated by Satellite (DORIS) data [*Williams and Willis*, 2006]. This means that, in general, there is no appreciable decay of white noise in GPS data. Only for 2-3% of the time series, a TW was significantly detected.

b) regarding the colored noise models:

− as expected, the RW model is the worst choice to describe the data. The data are better described by any of the white noise models used, VW, TW and WH, in this order. Note, however, that any combination of any white noise model plus RW is significantly superior to the white noise only model, supporting the assumption made in the Globk test of Section 6.3.2.

− the mean value of the PL model is significantly superior to the other colored noise models. This is due to an important loss of performance for the TW+GG model, where only 86% of the time series were successfully solved (for the other models it was between 98% and 100%). This is probably due to the large number of parameters to solve (5) for the TW+GG model;

− with respect to the integer noise models (FN, RW, FN+RW and GM), FN model is clearly superior to RW model. Thus, RW noise, found with different geodetic measurements and related to monument instability, is not clearly found in our results, in agreement with other global GPS solutions [*Williams et al.*, 2004]. For these global solutions, this could be due to the shortness of time series or to the dominance of the

other noise types, like FN, which could mask the RW noise. This is corroborated by the performance of the FN+RW model, in agreement with *Langbein* [2008] findings. For those time series with an estimated spectral index between -1 and -2, the δML value between PL and FN+RW is not significant. This would indicate that, although RW noise may exist, it is masked under FN noise and it only would appear when FN is taken into account through regional noise filtering, assuming that RW is station-dependent, or by using a FN+RW noise model. Finally, GM and FN models perform similarly, due to that GM tends to mimic FN noise for the middle frequencies [*Langbein*, 2008].

Comparing each noise model individually we can derive the following conclusions:

− the WH+FN, WH+PL and PL models, all of them tested for the ULR3 solution [*Wöppelmann et al.*, 2009], perform equally from a point of view of the δML criterium. However, the WH+PL model, used in ULR3 solution, is clearly not the best model to describe ULR4 data in terms of the MLE value;

− the VW+RW model is unexpectedly superior to all of the noise models tested with WH component. For instance, it is significantly superior to the WH+PL or WH+FN models;

− from Table 6.8 and Figure 6.20, we can exclude all models except VW+GG, VW+PL, VW+GM and VW+FN.

Using the δML values at the 95th percentile of Table 6.3 as threshold to assess model significance, we found that they all are larger than the δML values found between the best four models. This means that, regarding the δML metric, the FN, PL, GM and GG noise models can be muddled up and no decision can be taken to select the best model. A different criterion must then be used to select the noise model. Thus, if velocity uncertainties between this four retained models were similar there would be no issue to arbitrary select one of them. However, this is not the case. Figure 6.21 represents the estimated velocity uncertainties of the ULR4 solution estimated using the four models with the highest MLE value. Vertical velocity uncertainties of VW+FN, VW+GM and VW+GG models are plotted against the VW+PL model. This way, points located on the right of the red line indicate that the represented model in the y-axis is more optimistic than the VW+PL model. From this figure it is clear that both Gauss-Markov models (GG and GM) show more optimistic results (smaller uncertainty) with respect to the PL model. The uncertainty values provided by the Gauss-Markov noise models appear to be unrealistically small for some stations. The same conclusions were obtained with baseline rates observed with the two-color electromagnetic distance meter (EDM) technique [*Langbein*, 2004] and with station velocity uncertainties observed with DORIS technique [*Williams and Willis*, 2006]. For these optimistic uncertainties (a 2-3 factor smaller than PL uncertainties), the estimated crossover frequency of the Gauss-Markov processes war remarkably large, with a median crossover period of 2.3 months (median crossover period was 5.5 months and 1.5 years for the whole VW+GM and VW+GG models, respectively). Therefore, since the true uncertainties are unknown, we chose to be conservative and to take the stochastic model that provides the least optimistic uncertainties. Thus, both Gauss-Markov models (GG and GM) were discarded.

Comparing VW+FN and VW+PL models in Fig. 6.21, the differences are much more varied, which would represent the station-by-station deviation of the fixed spectral index from the FN model. The fact that uncertainty differences are centered near zero (mean uncertainty

difference is 0.02 ± 0.01 mm/yr) shows that, in general, the power law noise model is driven by a flicker nature. Figure 6.22 represents the histograms of the spectral index, the correlated noise amplitude and the velocity uncertainty estimated with the VW+PL noise model. We can see that the spectral index of the PL is close to the spectral index corresponding to a flicker noise (mean value of -0.88 ± 0.05). The dispersion of the spectral index (RMS of 0.27) results in the uncertainty dispersion already shown between VW+FN and VW+PL (Fig. 6.21). Therefore, to properly account for the individual spectral index of each time series the VW+PL model is preferred to the VW+FN. Thus, the selected noise model for the ULR4 solution is VW+PL. The mean correlated noise amplitudes estimated using both VW+PL and VW+FN models are 5.8 ± 0.1 mm and 6.0 ± 0.1 mm, respectively, showing again a general good agreement between them. The vertical velocity uncertainty estimated using the selected noise model ranges between 0.1 to 2.4 mm/yr with a mean value of 0.39 ± 0.02 mm/yr (median value of 0.31 mm/yr).
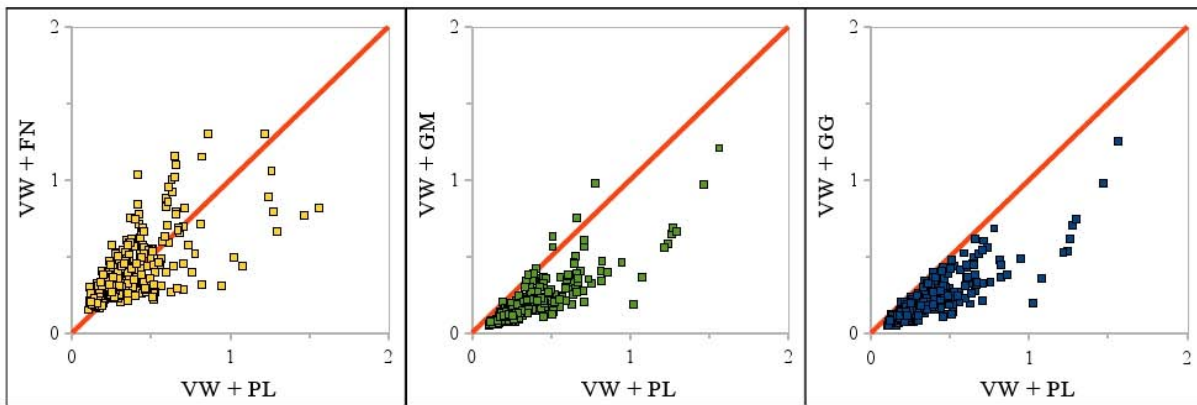
Figure 6.21. Comparison of vertical velocity uncertainties (in mm/yr) between VW+PL model and VW+FN, VW+GM and VW+GG models respectively.
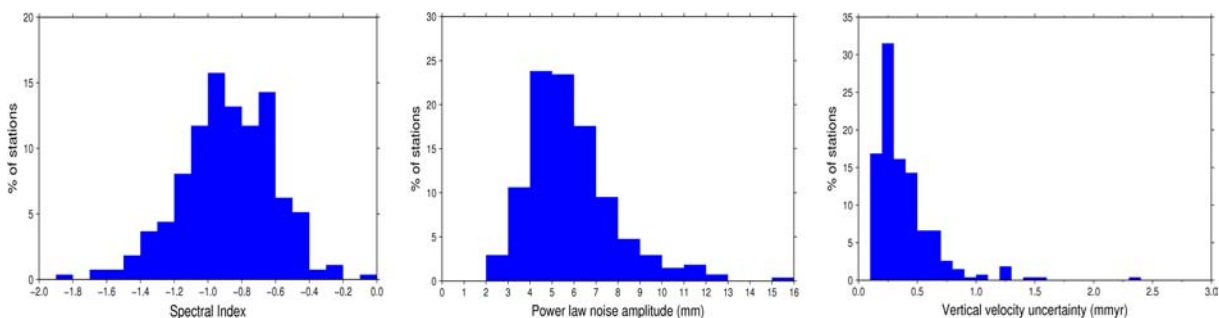
Figure 6.22. Histograms of spectral index, power law noise amplitude and velocity uncertainty of ULR4 vertical velocity field following a VW+PL noise model.

However, although the selected VW+PL model describes the GPS data used here in a general way, it is also possible that not all the time series follow this noise model. Thus, some stations affected by specific error sources or differentiated geophysical effects can contain a noise type that is not well described by the preferred VW+PL model [*Langbein*, 2004]. Then, to estimate the most reliable velocity uncertainty in a station-by-station basis, the *δML* value was estimated between all the tested models. GM and GG noise models were rejected if their

estimated crossover frequency exceeded the semiannual period (about 10% of the stations). Taking the null hypothesis of a white noise model, the δML value was compared with FN and RW noise models and if significant the null hypothesis was changed for the FN or RW model. This comparison was carried out successively towards more complicated colored noise models: from FN and RW to PL and FN+RW, then to GM and finally to GG. For each comparison, if the δML value of each individual time series did not exceed the threshold of Table 6.3 then the null hypothesis was not rejected, otherwise the null hypothesis was rejected and the preferred model for this station was changed. Following this procedure, Table 6.9 shows a summary of the percentage of stations retained for each colored noise model component. The estimated ULR4 velocities and their correspondent uncertainties issued from the station-dependent best noise model can be found in Annex B. ULR4 vertical velocity uncertainties range from 0.1 to 3.3 mm/yr with a median value of 0.34 mm/yr. This uncertainty represents a factor of degradation between 4 and 5 if no time-correlated noise is assumed. Table 6.9 also shows that the main colored noise type is flicker noise, followed by a general power law. This way, reprocessing the GPS data with a homogeneous strategy did not depose flicker noise as the dominant type of correlated noise content for a global GPS solution.

Table 6.9. Percentage of stations described by each colored noise model component. White refers to both white noise models (WH, VW and TW) for which no colored content was found.

Noise model	Number of stations
FN	71%
PL	24%
GM	2%
RW	2%
FN+RW	1%
GG	0%

6.5. Reference frame uncertainty

Precedent sections of this chapter were dedicated to the velocity uncertainty resulting from the time-correlated noise content of post-fit residual time series. Thus the velocity uncertainty estimated in previous sections is considered to be an internal precision estimation. However, estimated velocities must be expressed in a well-defined frame to be useful. Therefore, velocity uncertainties also depend on the realized frame, that is, they depend on the datum accuracy of the reference frame. Since residual time series are independent of the reference frame in which velocities are estimated (see Section 4.2), the velocity uncertainty resulting from the reference frame uncertainty is assumed to be independent from the internal uncertainty (or precision) resulting from noise content of post-fit residual time series. Therefore a complete evaluation of the vertical velocity field uncertainty should contain the effect of both terms added quadratically.

The GPS technique is sensitive to Earth's center of mass (see Section 7.2), and then to

the frame origin definition. However, due to some systematic errors, the temporal behavior of the geocenter as seen by GPS technique is not sufficiently adequate to be used for origin frame definition [*Altamimi et al.*, 2007]. Therefore, we were forced to choose an external frame to express the velocity field. The reference frame used is the ITRF2005 through its realization by the IGS (see Section 5.3). The ITRF represents the absolute long-term reference frame, that is, the most accurate realization of the terrestrial frame origin, scale, orientation and their time derivatives [*Ray et al.*, 2004]. However, as this realization is computed from space geodetic observations it is not free of errors and uncertainties. A scale rate error of the ITRF2005 would propagate entirely to the vertical velocities, whereas an origin rate error would propagate to the vertical velocities depending on the station location [*Collilieux and Wöppelmann*, 2010] following:

$$\sigma_{v_i}^2 = \begin{pmatrix} 1 & G(\varphi_i, \lambda_i) \end{pmatrix} \Sigma_{\dot{S}, \dot{T}} \begin{pmatrix} 1 & G(\varphi_i, \lambda_i) \end{pmatrix}^T = \sigma_{\dot{S}}^2 + G^2(\varphi_i, \lambda_i) \cdot \sigma_{\dot{T}}^2$$

$$\Sigma_{\dot{S}, \dot{T}} = \begin{pmatrix} \sigma_{\dot{S}}^2 & 0 \\ 0 & \sigma_{\dot{T}}^2 \end{pmatrix} \qquad \sigma_{\dot{T}}^2 = \begin{pmatrix} \sigma_{\dot{T}_x}^2 & 0 & 0 \\ 0 & \sigma_{\dot{T}_y}^2 & 0 \\ 0 & 0 & \sigma_{\dot{T}_z}^2 \end{pmatrix} \qquad (25)$$

$$G(\varphi_i, \lambda_i) = \begin{pmatrix} \cos\varphi_i \cos\lambda_i & \cos\varphi_i \sin\lambda_i & \sin\varphi_i \end{pmatrix},$$

where σ_{v_i} is the velocity uncertainty of station i, $\sigma_{\dot{S}}$ is the frame scale rate uncertainty, $\sigma_{\dot{T}}$ is the frame origin rate uncertainty (given by its three Cartesian components) and G is a function of the station location being φ_i and λ_i the station latitude and longitude respectively.

The uncertainty of the reference frame is difficult to estimate since this would imply to know the truth. There is nothing approaching the quality of the ITRF definition, except maybe an older realization of the reference frame. This is why the accuracy of the reference frame is estimated in terms of the level of consistency between different ITRF realizations [*Altamimi et al.*, 2008]. Another approach is to compare the performance of the geodetic techniques submitted to compute the ITRF realization. The ITRF2005 scale definition uncertainty was assessed in *Altamimi et al.*, [2007] by comparing the consistency of the VLBI and SLR scales with respect to the ITRF2000 scale and also by comparing the SLR and the VLBI scales between them in the ITRF2005 combination. Both comparisons yielded a conservative accuracy of 0.1 ppb/yr (~0.6 mm/yr). For the case of the ITRF2005 origin, which is defined exclusively using the SLR technique, a comparison between ITRF2000 and ITRF2005 origin definitions was the only possible approach. This comparison showed a relative drift along the Z component of 1.8 mm/yr [*Altamimi et al.*, 2007]. This drift is likely due to the poor geometry of the SLR network and its change over time. It is also related to the ITRF2000 datum precision. For the Equatorial components there is no significant drift between ITRF2005 and ITRF2000. Thus Eq. 25 simplifies to:

$$\sigma_{v_i}^2 = \sigma_{\dot{S}}^2 + \sigma_{\dot{T}Z}^2 \cdot \sin^2\varphi_i. \qquad (26)$$

Following Eq. 26, and assuming that the estimated uncertainty of the long-term scale

(0.6 mm/yr) and the Z component of the origin (1.8 mm/yr) are uncorrelated, this leads to a velocity uncertainty that varies from 0.6 mm/yr at the Equator to 1.9 mm/yr at the Poles. These values show that the reference frame uncertainty is currently one of the most limiting factors for vertical velocity estimates.

6.6. Summary

Through this chapter we have improved and assessed the methodology for a proper background noise analysis. Specifically we removed the station-dependent significant signals that can contaminate the estimated noise parameters. We also verified that using together CATREF and CATS for estimating the velocity field and its uncertainty respectively is an adequate procedure. Using this procedure, we found significant time-correlated noise content in residual vertical time series of the ULR4 solution. We asserted that the best model that describes this noise is a combination of variable white noise, given by the formal sigmas of the input weekly solutions, and power law noise. This noise process is mainly driven by a flicker noise nature. The median amplitude of the correlated noise is 5.8 mm/yr$^{1/4}$ and the median spectral index is -0.88. These values result in a median uncertainty of the vertical velocity field of 0.34 mm/yr, which represents a factor of degradation between 4 and 5 if no time correlated noise is assumed.

It is worth noting that noise properties of time series, and hence their rate uncertainty, clearly depends on time series length and data epoch. This way longer time series and older data exhibit larger correlated noise. This effect should be taken into account when comparing noise, or velocity uncertainties, between different solutions. Further tests and research will be carried out to determine the noise sources of this effect.

Finally, it was observed that uncertainty of the reference frame secular definition, in which is based the estimated velocity field, constitutes at the present one of the largest sources of velocity error.

PART III
RESULTS

7. ULR4 products

This chapter deals with the quality check of the main products derived from the GPS data analysis and combination (Chapters 3 and 4). These products are the frame transformation parameters (Section 7.1), the station coordinates (Section 7.2), the Earth orientation parameters (Section 7.3), and the orbital parameters (Section 7.4). The chapter ends with a summary of the quality assessment of these products (Section 7.5). The vertical velocity field is addressed in a dedicated chapter (next Chapter 8) as it represents the main purpose of this study (Section 1.1).

Throughout this chapter, the quality check is mainly based on the comparison with respect to results from the IGS Analysis Centers (AC) and other analysis centers contributing to the IGS reanalysis campaign (IGSr hereinafter). Within the IGSr, the different ULR4 products were called UL1. The combined reprocessed IGS products are termed IG1. Some of the graphics displayed here were published on the IGS Analysis Center Coordinator website[1,2] and by the IGS Reference Frame Coordinator[3] [IGS electronic message 6136, 2010].

7.1. Frame transformation parameters

In order to estimate the station positions (the terrestrial frame, see next Section 7.2) and velocities (see Chapter 8), each weekly solution was transformed to a common terrestrial frame. This common frame is defined to be consistent with a given terrestrial reference frame in which the estimates of the geodetic parameters (e.g., site velocities) will be expressed. Thus, analyzing the quality and the temporal behavior of the estimated transformation parameters is a fundamental procedure to validate our results. As described in Chapter 4, frame transformations are usually carried out using a similarity transformation comprised of a scale (Section 7.1.1), three translations (Section 7.1.2) and three rotations (Section 7.1.3). The estimated transformation parameters between two frames are deeply dependent on the set of stations used to estimate them.

Transformation parameters of the ULR4 solution were estimated and analyzed in three different ways. First, to estimate the ULR4 velocity field, weekly solutions were transformed into the ITRF2005 and then rigorously stacked by applying minimal constraints (see Chapter 5). All the stations contained in each weekly solution were used to estimate the transformation parameters. Time series of these estimated weekly transformation parameters are helpful to analyze their non-linear variations, especially annual signals.

Second, the transformation parameter rates (secular terrestrial frame definition), which are directly related to the estimated velocity field, were also analyzed. Weekly solutions were stacked as before but using internal constrains to define the combined solution, rather than using a reference frame (see Chapter 4). Then, a 14-parameter transformation (7 parameters plus their rates) was estimated between this long-term solution and the ITRF2005. This way, the estimated transformation parameter rate uncertainties take into account the level of disagreement between ULR4 and ITRF2005 velocities. This approach is then more rigorous than fitting a linear regression to the early estimated weekly transformation parameters, where the station velocities and their formal uncertainties were not considered in the weekly frame

---

transformation.

Third, in the frame of the IGSr, all contributing weekly solutions were transformed into a common frame and then combined by the IGS Reference Frame Coordinator. The transformation parameters between the contributing IGSr solutions were estimated using the IGS reference frame station network (IGS05 stations) as processed by each AC. Even if this network is not homogeneously distributed (see green dots in Figure 8.1 for IGS05 stations in the ULR4 solution), it is rather similar in most solutions participating to the IGSr (Figure 7.1). Thus, the transformation parameters comparison between ULR4 and those solutions can provide us important clues of the relative ULR4 performance.
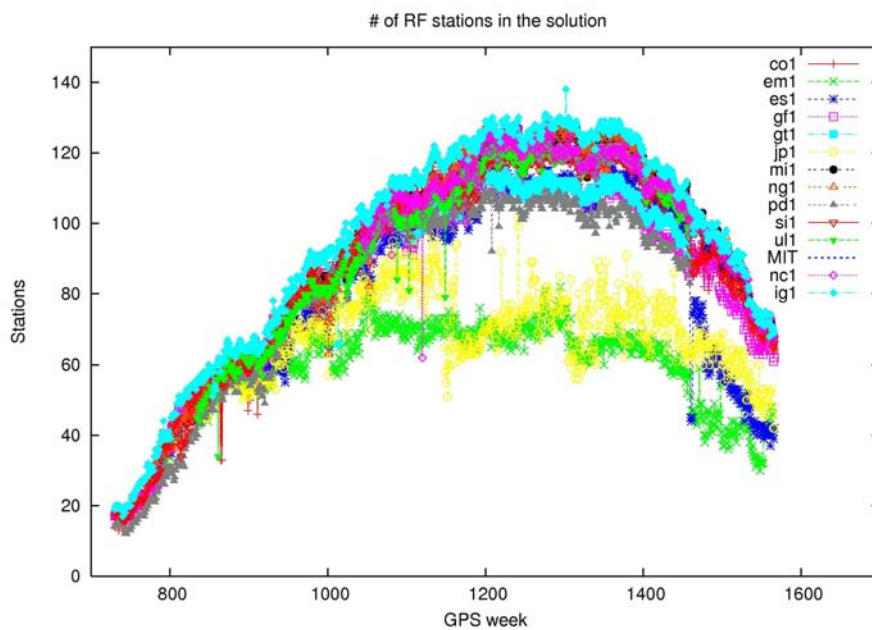
Figure 7.1. Number of IGS reference frame stations (IGS05) analyzed
by solution contributing to the IGSr[3].

7.1.1. Scale

The scale parameter represents the dimensionless relative unit ratio between two terrestrial frames. Within the GPS technique, the terrestrial frame scale is defined by three constants: the gravitational coefficient of the geopotential model used to estimate the orbits, the speed of light and the selected time scale. This way, the GPS technique, through the estimated distance between stations and satellites, defines theoretically its own frame scale. However, as it was discussed in Section 3.1.2, the GPS frame scale is not an independent parameter since ITRF scale was held fixed to estimate the phase center offsets of satellite antennae. Using these satellite antenna phase centers in the GPS data processing, the ITRF scale was transferred to the GPS fiducial-free network scale. If no other scale factor variation is introduced elsewhere in the data processing, for instance by not modeling or mismodeling some phenomena, then there is no theoretical reason that a scale factor needs to be estimated when transforming between fiducial-free weekly solutions and a secular reference frame.

Figure 7.2 shows the estimated scale parameter between each weekly ULR4 solution

and ITRF2005. The mean (0.03 ± 0.06 ppb) and rate (0.00 ± 0.06 ppb) values are not significantly different from zero, showing that there is no long-term deviation in the defined terrestrial frame scale. A clear annual variation with an amplitude of 1.8 ± 0.1 mm (~0.3 ppb at the Equator) is nevertheless noticed. The same order of annual amplitude was observed in other GPS results [e.g., *Lavallée et al.*, 2006]. In addition, a similar annual variation was found between all weekly solutions contributing to the IGSr (Figure 7.3, bottom).
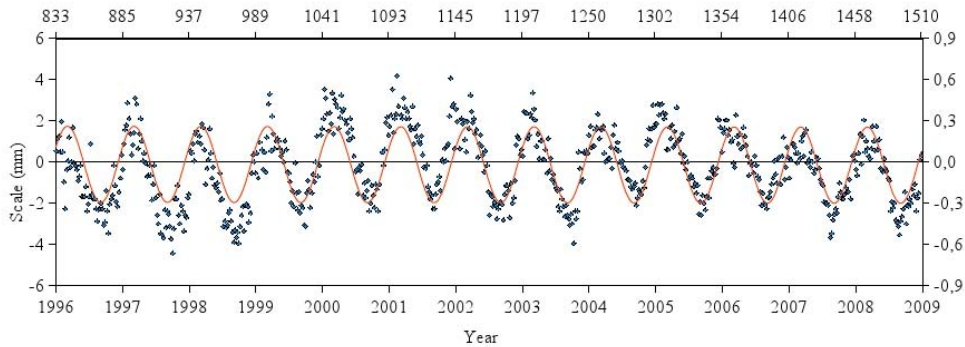
Figure 7.2. Weekly estimated scale frame parameter between ULR4 and ITRF2005. Red line represents the fitted annual signal.
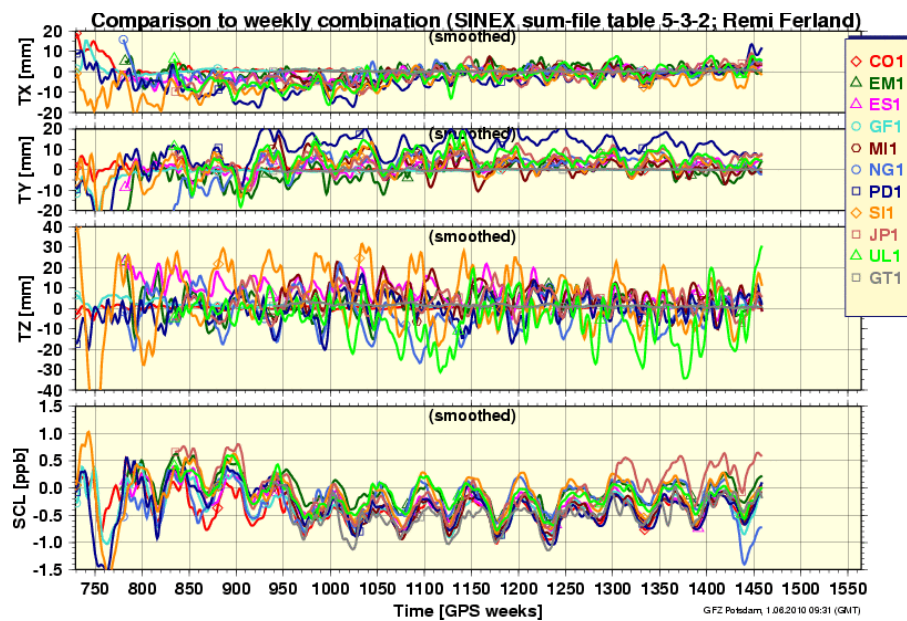
Figure 7.3. Translation and scale parameters between different IGSr weekly solutions and IGS long-term reference. ULR4 solution is represented by a light green line[2].

This non-linear scale variation is considered to be mainly due to the aliasing of surface loadings into frame transformation parameters, since no systematic annual variation of the terrestrial radius is expected. *Tregoning and Van Dam* [2005] already stated that any network, even those simulated with an homogeneous distribution across all land surfaces, cause aliasing of the Earth's crust deformation into the translation parameters and, more

significantly, into the scale factor. These authors showed that estimating a scale factor parameter in the transformation degrades the accuracy of the terrestrial frame results if unmodeled surface deformations are present in the fiducial-free network polyhedron. Also, the geographical distribution of the stations used to estimate the transformation parameters is less critical when the scale is not estimated. This effect also corrupts the geocenter translation estimates [*Lavallée et al.*, 2006] and introduces errors in the station position time series, and in particular, in the height component [*Tregoning and Van Dam*, 2005]. The most rigorous approach to prevent the site coordinates and geocenter estimates from being corrupted by surface loading effects is obviously to properly model these station displacements in the data processing. In practice, this is not yet realizable due to the inaccuracy of the available loading models. An alternative solution is then to not estimate a scale factor when transforming weekly ULR4 solutions into ITRF2005. This approach is valid since we did not find discontinuities nor long-term variations in the realized terrestrial scale (see Figure 7.2).

The mean impact of the scale parameter on the estimated translations (geocenter motion, see next section) is small (RMS of 0.4 mm), the maximum differences being 1.2 mm for Z-translation. Therefore, the 1.8 mm of the estimated scale seasonal variation should be mainly mapped into the station residual time series. To corroborate this, the weekly solutions were stacked without estimating the scale parameter. Then, for all stations, the annual signal on the vertical component was compared with and without the scale parameter estimated. Figure 7.4 shows these differences in the station annual amplitudes of the vertical component. The amplitude differences have a null mean (0.1 ± 0.1 mm) and a RMS of 1.2 mm, being the maximum difference of ± 2.3 mm. Differences in the station annual phases (not shown) are small, with a RMS of 30 deg. An increased amplitude (reddish dots) means that the station had a positive contribution to the scale parameter. From this figure, we can see that mainly European stations actually drive the estimated global scale parameter due to their relative dense network coupled with regional loading phenomena.
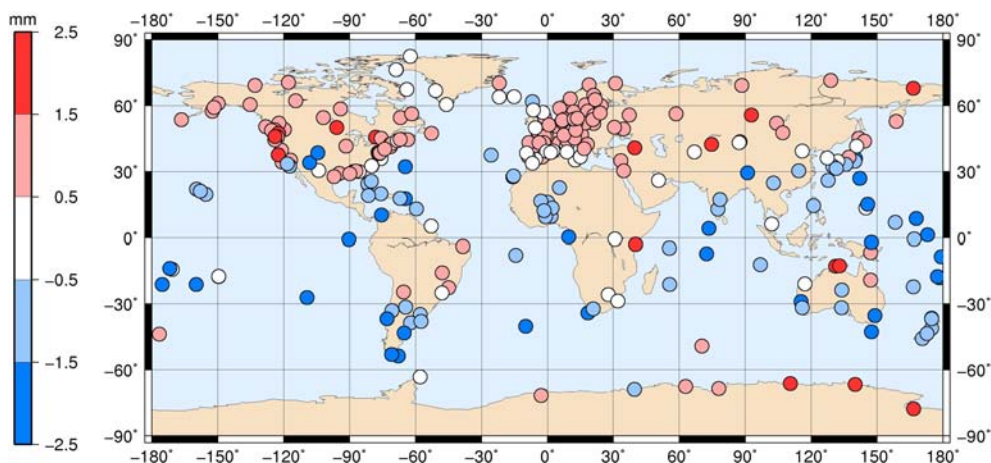
Figure 7.4. Annual signal amplitude differences in station heights when scale frame parameter is not estimated in the stacking of the weekly solutions.

7.1.2. Apparent geocenter motion

Before defining apparent geocenter motion, we define here the geocenter as the center of mass of the whole Earth system (CM hereinafter). This includes both the solid Earth mass and the surface fluids mass (atmosphere, oceans, continental water, ice sheets, etc). The physical principle behind this definition is the cancellation of the whole Earth's relative mass momentum. Satellite orbits are estimated about this quasi-instantaneous (daily or larger integrations) dynamically defined origin by fixing to zero the degree-one coefficients of the geopotential model.

All tracking stations from the space geodetic techniques used today to realize the terrestrial frame (i.e., VLBI, SLR, DORIS and GPS stations) are located on the Earth's surface. The Earth's surface realizes a different center called center of surface figure (CF). The CF frame is then defined geometrically as the center of a uniform and infinitely dense array of points covering the Earth's loading-deformed surface. The surface fluids, also located on the solid Earth's surface, move independently of the solid Earth's crust causing surface loading. Therefore, due to the displacement and redistribution of mass (oceans, atmosphere, but also Earth's internal mass) and to the loading deformation of the Earth's crust, the CM and CF centers will not generally coincide. That is, a change in the center of mass of the surface loads induces a detectable translation of the solid Earth, dragging stations fixed on the crust (CF), relative to the center of satellite orbits (CM). As we early defined CM as the geocenter, this is similar (changing the direction) to say that the coordinate frame attached to the Earth's center of mass (CM) moves relative to the coordinate frame of the Earth's crust (CF). This relative displacement (CM with respect to CF) is what we define here as geocenter motion. This way, dynamic space geodetic techniques, such as SLR, DORIS and GPS, realizing the CM, are sensible to this geocenter motion when fiducial-free coordinate solutions are transformed in a way that there is no-net translation with respect to some previously established secular frame, like an ITRF realization.

In practice, however, space geodetic stations are a discrete sample of the emerged Earth's surface only. Thus, CF, being inaccessible, is approximated by the barycenter or the center of the tracking network (CN). The position of CN is then highly dependent on the tracking network and it should be close to CF through averaging over a sufficiently dense global distribution of stations, which usually presents no problem in the case of GPS. This dependency on the tracking network implies, however, that when fiducial-free coordinate solutions are aligned to the secular reference frame, the CN drifts linearly following the time evolution of the secular frame (ITRF velocities) [*Collilieux et al.*, 2009]. This drift tends to separate CN and CF centers. Therefore, by using detrended translation time series, the effect of the kinematic model applied (ITRF2005 velocities) is removed. Neglecting the inaccessible constant between CF and CN, the estimated translation variations, which represent CM-CN detrended geocenter motion, are close to CM-CF geocenter variations [*Collilieux et al.*, 2009]. Geocenter motion is then realized here as the time-variable three-dimensional translation variations (translation rates removed) of the fiducial-free GPS network with respect to the ITRF2005 secular origin. It is worth noting that these variations are independent of the reference frame used. That is, the same geocenter variations (CM-CN, or practically CM-CF) will be obtained if internal constraints were applied in the stacking of weekly solutions, that is, using a GPS-derived secular frame origin.

However, estimating geocenter motion this way (called the "network shift approach" by *Dong et al.* [2003]) has generally produced values with large variations that appear to be

quite sensitive to analysis procedures and are probably dominated by unmodeled noise sources [*Dong et al.*, 2003; *Lavallée et al.*, 2006]. This method is also very sensitive to the distribution and size of the tracking network [*Lavallée et al.*, 2006]. This way, due to the approximation between CF and CN, and to the systematic errors associated to any geodetic measurement, observed geocenter motion from these space geodetic techniques is usually termed "apparent". For instance, while the internal geometry of a fiducial-free GPS network can be very precise, the external (frame-defined) solution is typically an order of magnitude less precise due to the sensitivity of the frame translation (apparent geocenter motion) to mismodeling of the estimated orbits. Major error sources include the gravitational effects of time-variable spherical harmonics of degrees greater than one and the mismodeling of non-gravitational forces. Since the GPS satellites move in high-Earth orbits, they are relatively insensitive to errors of the gravity field model, particularly for relatively short data arcs of a few days or less [*Vigue et al.*, 1992]. The effect of the remaining complex non-gravitational dynamics however limits the proper realization of the CM with GPS.

Here we are not interested in estimating reliable apparent geocenter motion but rather in comparing the ULR4 apparent geocenter estimates to other high-end quality GPS estimates using the same network shift approach with a similar IGS05 reference network. To estimate a more reliable apparent geocenter motion other methods should be applied, like the estimation of degree-1 deformation [*Dong et al.*, 2003], the combination of network shift and degree-1 deformation methods [*Lavallée et al.*, 2006], or the combination of precise SLR and well-distributed GPS estimates [*Collilieux et al.*, 2009].

Figure 7.5 shows the estimated translations between ULR4 weekly fiducial-free CM solutions and the ITRF2005. An annual signal was fitted to each translation component. Their amplitudes and phases are shown in Table 7.1. Z-translation (TZ) shows larger variations than the equatorial components (note the different scale for TZ in Figure 7.5). Comparing the translation annual signal values with those estimated from SLR data [*Collilieux et al.*, 2009], we observe a good coherence for the equatorial amplitudes (X and Y) and a 3-4 times larger TZ amplitude for ULR4. Note that due to the larger TZ variations, the TZ amplitude uncertainty is four times higher than for equatorial components. These larger geocenter variations in TZ were already pointed out to not reflect actual geocenter motion, but some GPS-specific systematic errors. These errors include the solar radiation pressure effects on estimated orbits [*Vigue et al.*, 1992; *Dong et al.*, 2003; *Blewitt*, 2003], high-order ionospheric effects [*Hernández-Pajares et al.*, 2007; *Petrie et al.*, 2010], ambiguity resolution errors [*Lavallée et al.*, 2006], tidal aliasing effects of loading signals [*Penna et al.*, 2007] like the hydrological continental cycle loading effects [*Chen et al.*, 1999], and the inhomogeneous distribution of stations between northern and southern hemispheres [*Vigue et al.*, 1992; *Lavallée et al.*, 2006].

Table 7.1. Annual amplitude and phase in apparent geocenter motion. Signal is defined as $A \cos(2\pi(t-t_0) - \varphi)$, being t_0 1st January. SLR results extracted from *Collilieux et al.* [2009].

	ULR4		SLR	
	Amplitude (mm)	Phase (deg)	Amplitude (mm)	Phase (deg)
TX	2.5 ± 0.2	186.2 ± 4.9	2.7 ± 0.3	45 ± 6
TY	4.1 ± 0.2	237.2 ± 3.2	3.8 ± 0.2	327 ± 4
TZ	10.4 ± 0.8	187.5 ± 4.2	3.6 ± 0.4	4 ± 7
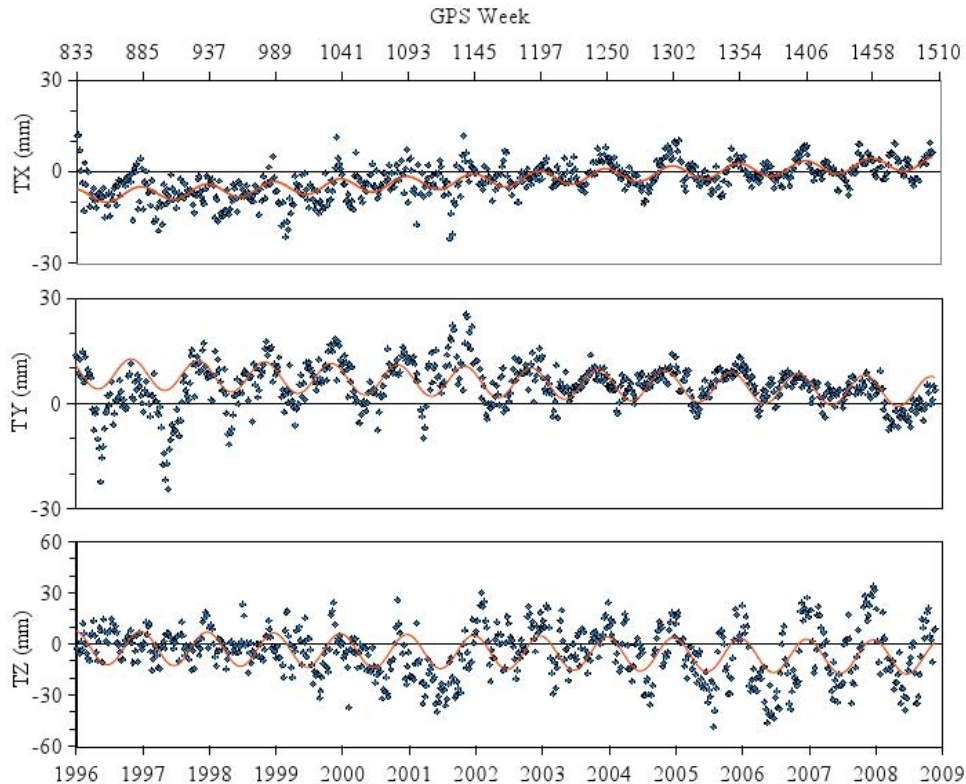
Figure 7.5. Translation time series between weekly ULR4 solutions and
ITRF2005. An annual signal (red line) was fitted to each time series.

The translation rates were estimated through a 14-parameter transformation with respect to the ITRF2005. The resulting values, 0.8 ± 0.3 mm/yr, 0.0 ± 0.3 mm/yr, and -0.5 ± 0.3 mm/yr, respectively for TX, TY and TZ, are not significant at a 3-sigma level. This demonstrates the consistency of the secular origin definition between ULR4 solution and ITRF2005.

The estimated translations between the contributing IGSr weekly solutions and the long-term IG1 solution were already shown in Figure 7.3. As seen from this figure, ULR4 apparent geocenter variation estimates are consistent with the other AC estimates. However, larger variations in TZ were obtained for some ULR4 weekly solutions. In addition, time series of ULR4 TZ would exhibit a discontinuity ending 2001 (GPS week ~1150). TZ variations for both periods, before and after the discontinuity, follow a similar unexplained pattern, from small variations at the beginning to larger variations at the end. *Vigue et al.* [1992], using early GPS data, also found an unexplained discontinuity in their GPS-derived TZ estimates. Since almost the same IGS05 network has been used for all reprocessed solutions, this pattern may be explained by differences in the data processing strategy. Among the contributions of larger TZ variations enumerated earlier, only the solar radiation pressure parameterization in orbit determination (see Section 7.4) seems to be different between the contributing IGSr reprocessed solutions. Although we are not certain of the level of fixed ambiguities in the other reprocessed solutions, we exclude this source since, for ULR4 solution, this parameter improves with time (see Figure 6.15). Constraints on the a priori orbits used within the data processing (see more details in Section 7.4) could also be a source of larger TZ variations through correlation between terrestrial and orbital TZ time series.

7.1.3. Rotation

As seen in previous sections, in a fiducial-free GPS polyhedron, frame scale and origin are self-defined parameters. Frame orientation is, however, ill-conditioned by observations. This issue extends to all space geodetic techniques, so their combination does not define any frame orientation either. This way, frame orientation is defined externally by convention. For fiducial-free GPS solutions, orientation is defined through a no-net-rotation (NNR) condition with respect to an external reference frame, such as the ITRF. As discussed in Section 4.2, the orientation of the successive ITRF frames are defined to be consistent through a NNR condition with respect to the orientation defined by the Bureau International de l'Heure (BIH) at epoch 1984.0 [*McCarthy and Petit*, 2004]. The time evolution of the ITRF orientation is defined with a NNR condition with respect to the absolute plate motion model NNR-NUVEL-1A [*DeMets et al.*, 1994].

Figure 7.6 shows the estimated ULR4 weekly frame rotation parameters with respect to ITRF2005. RMS of these rotations is 2.5 mm, 2.8 mm and 1.1 mm for RX, RY and RZ, respectively. Large variations of these rotation parameters, for instance in 2001, represent the precision of the realized ITRF orientation through the weekly tracking network. Figure 7.7 shows the estimated ULR4 weekly frame rotation parameters with respect to the cumulated IGS solution. As seen from this figure, ULR4 rotation parameters are in good agreement with the other reprocessed solutions.
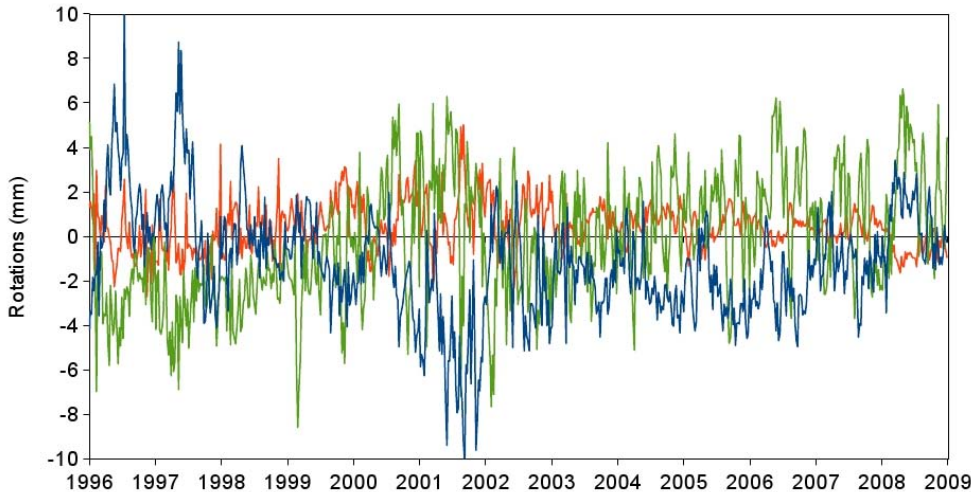
Figure 7.6. ULR4 weekly rotation parameters with respect to ITRF2005.
Rotations are around X (green), Y (blue) and Z (red) axis.

7.2. Terrestrial frame

The terrestrial frame realization is represented here by the estimated station coordinates of the whole network. For an assessment of estimated station velocities see Chapter 8. Since long-term or linearized station positions depend on the estimated velocities and discontinuities applied, here we infer the quality of estimated station coordinates in a weekly basis, that is, analyzing the performance of the ULR4 weekly station coordinate solutions.
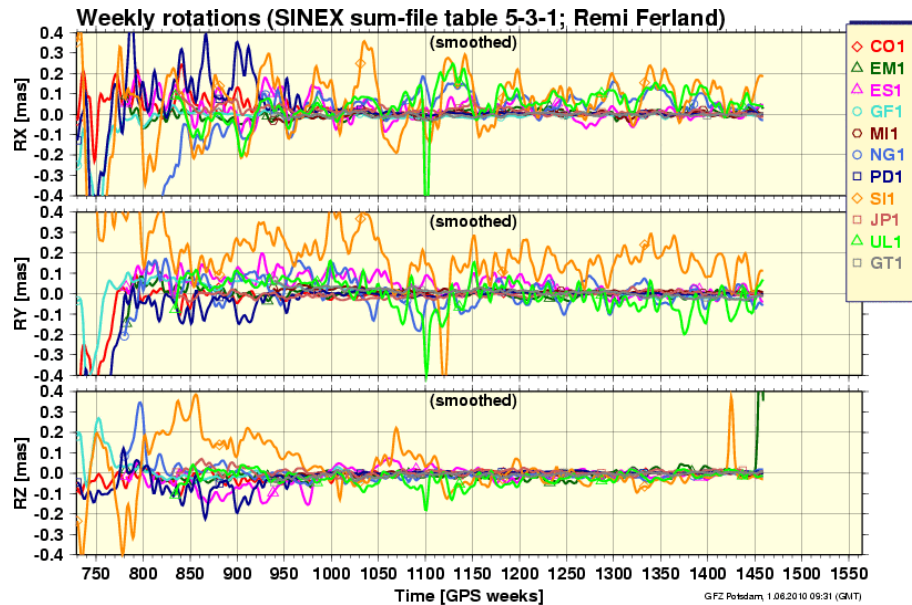
Figure 7.7. Smoothed rotations of contributing IGSr weekly solutions
with respect to IG1 solution[2].

The internal quality of the station coordinates of the ULR4 solution was assessed by analyzing the weighted RMS of the weekly station coordinate residuals with respect to the long-term combined solution expressed in the ITRF2005 (Figure 7.8). The ULR4 weekly WRMS was compared to that obtained from the ULR3 weekly solutions with respect to its own long-term combined solution. This figure shows a clear reduction in the repeatability of ULR4 solution for the horizontal component and a more stable behavior for the vertical component. This reveals a reduced noise level of ULR4 solution with respect to ULR3 (for a deeper correlated noise comparison see section 8.2.2). ULR4 repeatability values are between 1 and 3 mm for the horizontal and between 4 and 6 mm for the vertical component (3D weighted RMS between 2 and 4 mm).
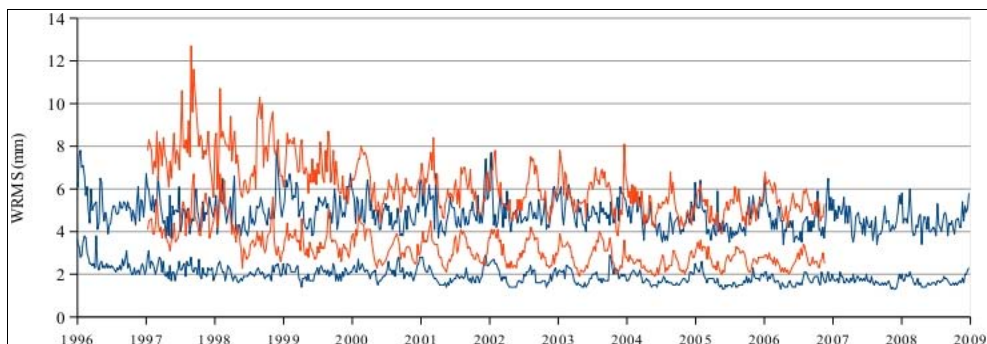
Figure 7.8. Horizontal (bottom) and vertical (top) weighted RMS of the weekly solutions with respect to the long-term solution for both ULR4 (blue) and ULR3 (red) solutions.

The quality of the ULR4 station coordinates was also assessed by comparing them to the weekly solutions contributing to the IGSr. Figure 7.9 shows the RMS of the weekly

station coordinate residuals with respect to the IGSr combination for each component. The repeatability of ULR4 weekly residuals with respect to IGSr are between 1 and 2 mm for the horizontal and between 2 and 4 for the vertical component, respectively. This figure shows that ULR4 weekly solutions (light green line) are in good agreement with the other contributing IGSr solutions. This demonstrates the good quality of the station coordinate estimates of the ULR4 solution.
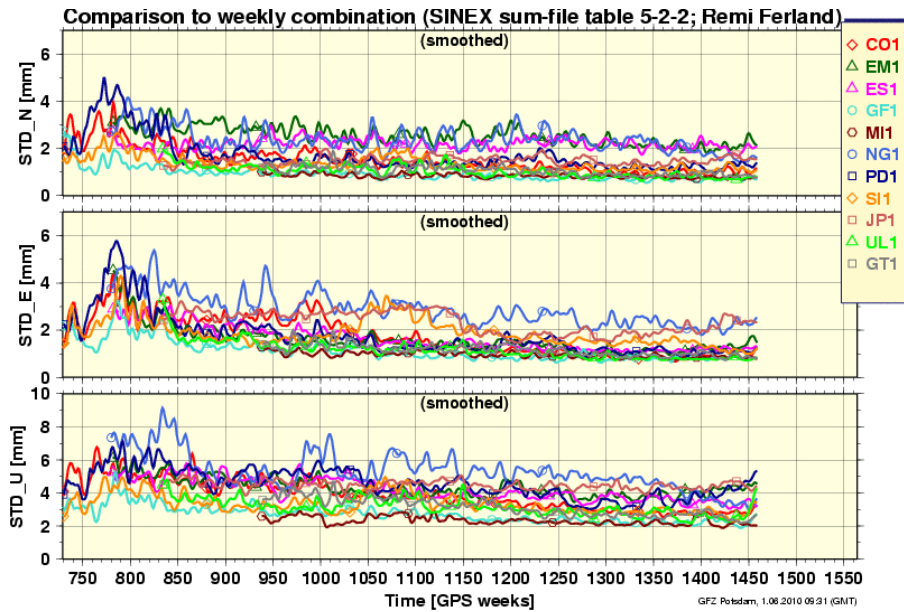
Figure 7.9. Smoothed weighted RMS of contributing IGSr weekly solutions with respect to IG1[2].

7.3. Earth orientation parameters

The Earth orientation parameters (EOP) define the time-varying orientation or transformation between the Earth-fixed terrestrial frame and the celestial (inertial) frame. They comprise the motion of the Celestial Intermediate Pole (CIP) in the celestial system (precession and nutation), the rotation of the Earth around the axis of the pole and the motion of the CIP in the terrestrial system (polar motion or wobble) [*McCarthy and Petit*, 2004]. Variations of these parameters include secular, seasonal, and tidal components. Polar motion variations are mostly related to the redistribution of mass within the Earth system, whereas precession and nutation variations are related primarily to gravitational interactions with external bodies as well as their couplings with internal mass redistributions within the Earth system [*Ray et al.*, 2005].

VLBI is the only technique able to determine all EOP components because it is the only current way to access to the International Celestial Reference Frame (ICRF), which is realized by the coordinates of a set of extragalactic radio sources [*McCarthy and Petit*, 2004]. Especially, VLBI is the only technique accurately providing the rate of spin of the Earth about its polar axis. The related conventional measure of the instantaneous rotation angle of the Earth is the Universal Time (UT1). For the satellite-based geodetic techniques, like GPS, the nutation angles and the diurnal rotation UT1 are not accessible in an absolute sense. For these

geodetic techniques, where satellite orbits are estimated among other parameters, there is a linear relationship between the right ascension of the ascending node of the satellite orbits and the orientation of the Earth in space. That is, the rotation of the Earth is indistinguishable from the rotation of the GPS satellite orbit nodes. However, GPS is sensitive to fast changes in the Earth orientation in space. This way, the excess length-of-day (LOD), equivalent to the discrete change of UT1 over one day, can be observed by GPS. However, any unmodeled forces acting on the geodetic satellites affect the rate of change of the satellite nodes, contaminating then the LOD estimates. It was shown for instance that GPS estimates of LOD contain time-varying biases [*Ray*, 1996]. The rates of change of the nutation angles can also be determined by GPS, but these estimates are not commonly produced [*Ray et al.*, 2005].

We distinguish here the parameters usually estimated by GPS (polar motion, polar motion rates and LOD) as Earth rotation parameters (ERP). From July 3 1994, the IGS ERP standard format consist of discrete integrations of 24h period of polar motion, polar motion rates, and LOD estimates reported at UTC noon epochs. The GPS-related LOD biases are removed before the routine IGS combination from past LOD differences with respect to the IERS Bulletin A values [*Ferland and Piraszewski*, 2009].

ULR4 ERP were not used within the IGSr combination. Therefore, to assess the quality of our estimates, they were compared to the IG1 combined solution. Figure 7.10 show the ULR4 ERP residuals for polar motion, polar motion rates and LOD, respectively, with respect to the combined IG1 ERP solution. The RMS of the ULR4 ERP residuals are at the level of 0.05 mas, 0.3 mas/d, and 0.03 ms, for polar motion, polar motion rates, and LOD, respectively. The same order of polar motion residuals were found within the contributing IGSr solutions with respect to IG1 (e.g., Figure 7.11 for Y component). Slightly smaller residuals for polar motion rates and LOD were found within the contributing IGSr solutions with respect to IGS1 combination. Therefore, we consider that ULR4 ERP values are consistent with the other IGSr contributing solutions.
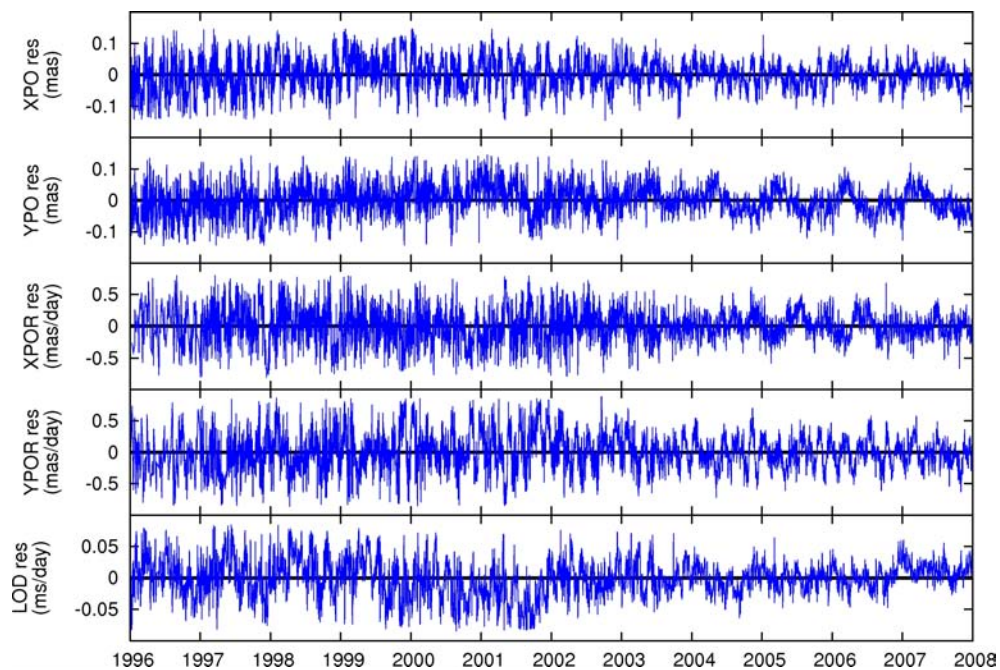
Figure 7.10. ULR4 ERP residuals with respect to IG1 combined solution.
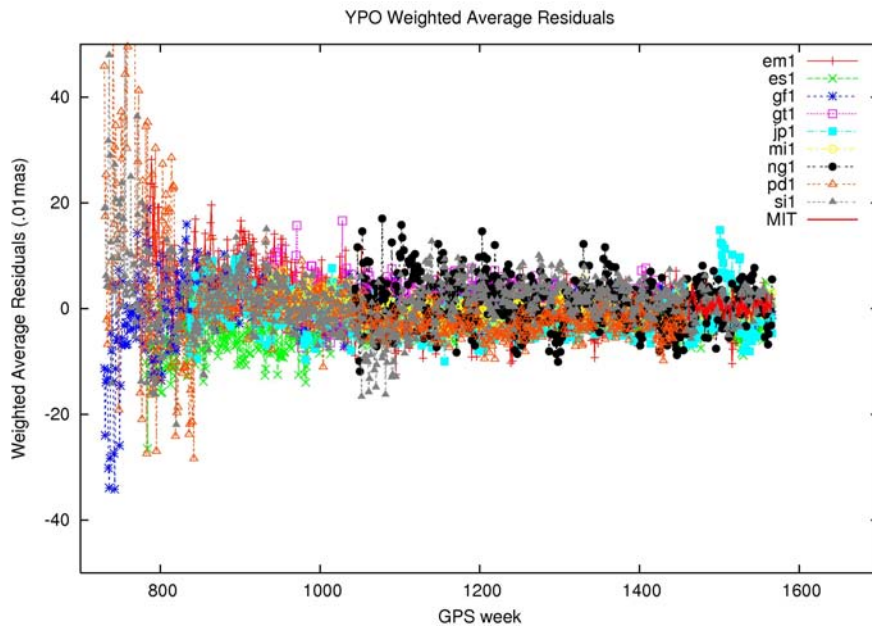
Figure 7.11. Contributing IGSr polar motion residuals for Y
component with respect to IG1 combination[3].
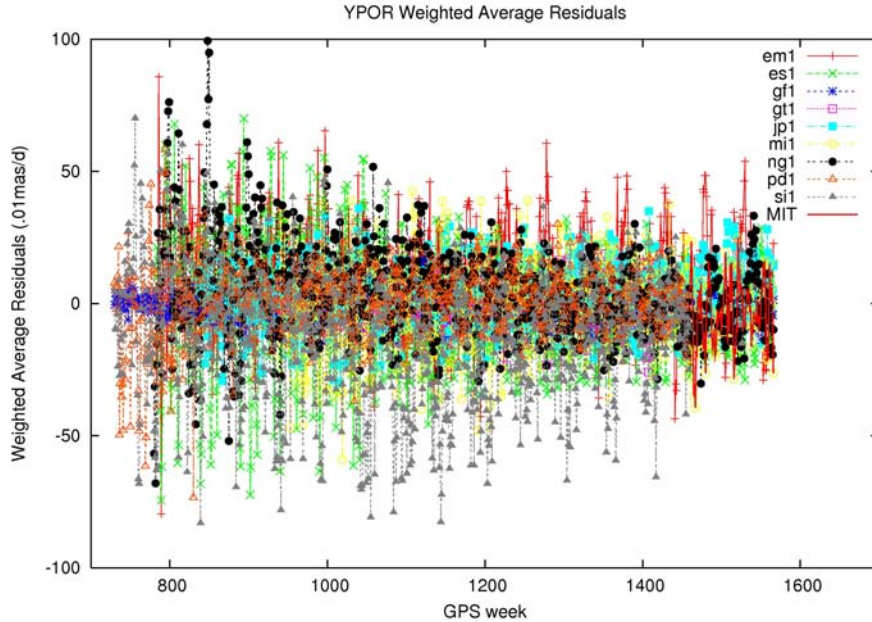
Figure 7.12. Contributing IGSr polar motion rate residuals for Y
component with respect to IG1 combination[3].

7.4. Orbits

As mentioned above, at the GPS satellites altitude, the main error source for orbit determination is the effect of the solar radiation pressure. To account for this non-gravitational effect several additional empiric parameters are usually estimated together with the six
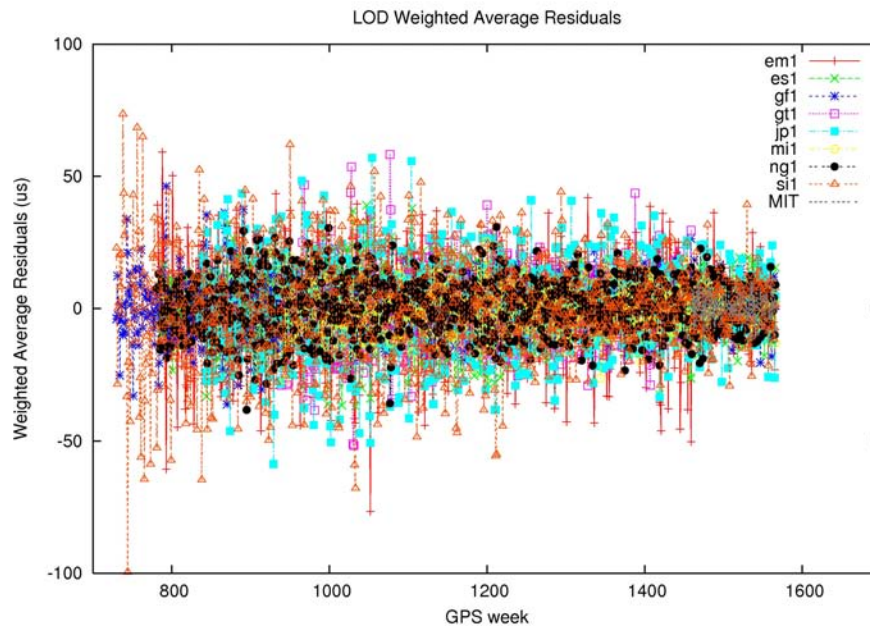
Figure 7.13. Contributing IGSr LOD residuals with respect to IG1 combination[3].

(gravitational) keplerian parameters. From integration of these gravitational and non-gravitational parameters, the satellite position can be extracted at any epoch, usually every 15 minutes, before being exported for further uses, for instance, for IGS orbit combination or to be fixed in regional GPS solutions.

Estimated daily ULR4 orbits were compared to other orbit estimates contributing to the IGSr through a 7-parameter transformation. The smoothed 1D RMS (averaged of the three position components) of ULR4 orbits with respect to the IG1 orbits is shown in Figure 7.14 (UL1, in green). Compared to the other reprocessed orbits, ULR4 orbits are consistent at a level of 4 cm for early data and 2 cm for recent data, respectively. The steadily RMS decay is also consistent between all reprocessed orbits, due mainly to an increased number and quality of tracking sites. Figures 7.15 to 7.21 show the translation, rotation and scale parameters between each reprocessed orbit solution and the combined IG1 orbits. Translations of equatorial components (X and Y) look in good agreement between all solutions. Larger translations are appreciable in Z-axis for ULR4 orbits. As for the apparent geocenter motion, the same discontinuity in Z-translation is likely seen for the ULR4 orbits. This effect is likely due to the parameterization of the non-gravitational forces acting on satellites (see section 7.1.2). Large rotation parameters are also found between some reprocessed orbits, including ULR4 orbits, and the IG1 orbits. This likely represents the poor quality of the daily orbit alignment through the reference network used and the procedure used to combine orbit solutions (see Section 4.2). Finally, ULR4 orbit scale also exhibit large deviations from the IG1 orbits. These scale deviations are clearly related to the different ITRF realizations, as was shown by *Griffiths et al.* [2009][4]. This effect is due to the fact that, before the GPS data processing of the ULR solutions, IGS final orbits (non-reprocessed IGS orbits) were transformed from their respective frame to ITRF2005 to be used as a priori orbits. The scale differences between different ITRF realizations, specially between ITRF97 and ITRF2005

---

4   Available at http://acc.igs.org

(GPS weeks 1021 to 1144) is similar to that found between ULR4 and IG1orbits. Nevertheless, once these orbit frame issues are removed in the IG1 combination, the quality of the ULR4 orbits is reasonably good, as shown in Figure 7.14.
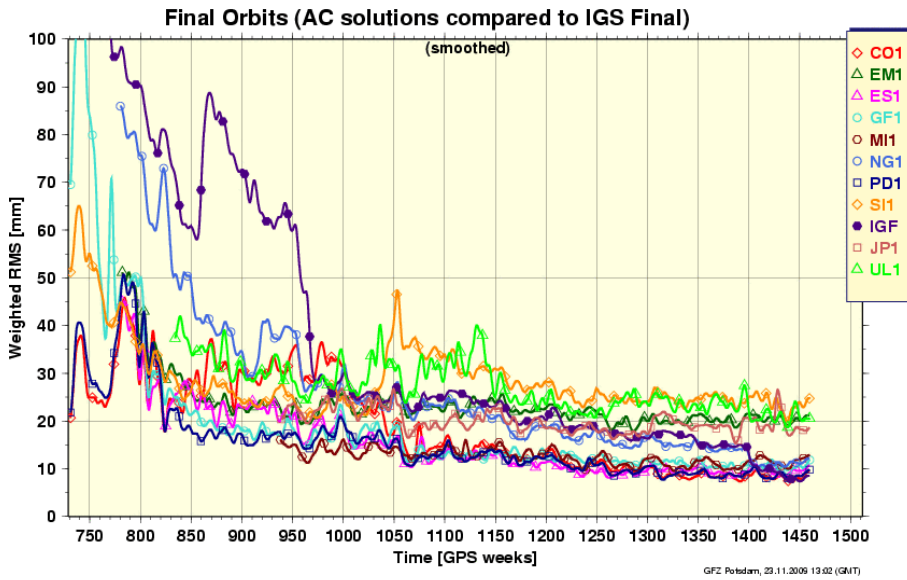
Figure 7.14. Smoothed daily RMS of contributing IGSr orbits with respect to IG1 combined orbits[2].
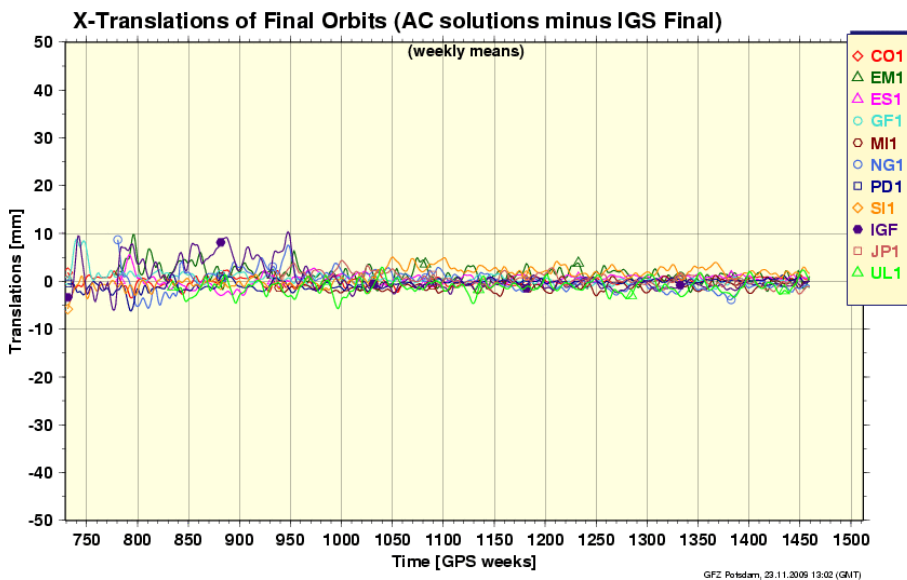
Figure 7.15. Smoothed daily X-translation of contributing IGSr orbits with respect to IG1 combined orbits[2].
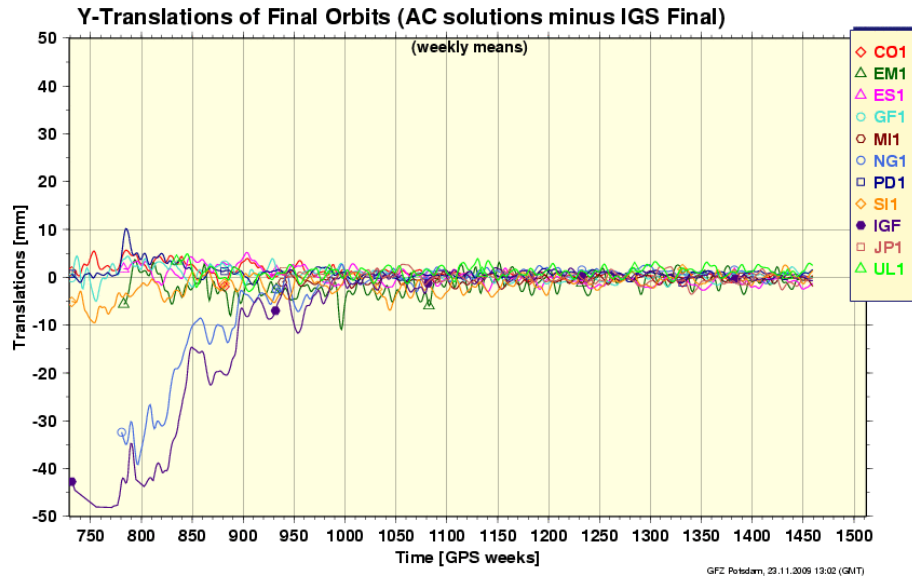
Figure 7.16. Smoothed daily Y-translation of contributing IGSr orbits with respect to IG1 combined orbits[2].
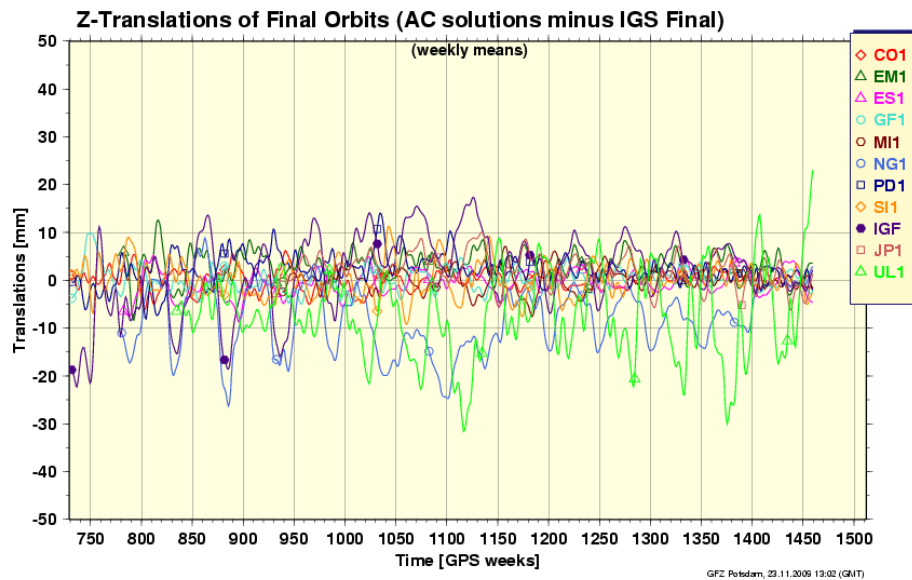
Figure 7.17. Smoothed daily Z-translation of contributing IGSr orbits with respect to IG1 combined orbits[2].
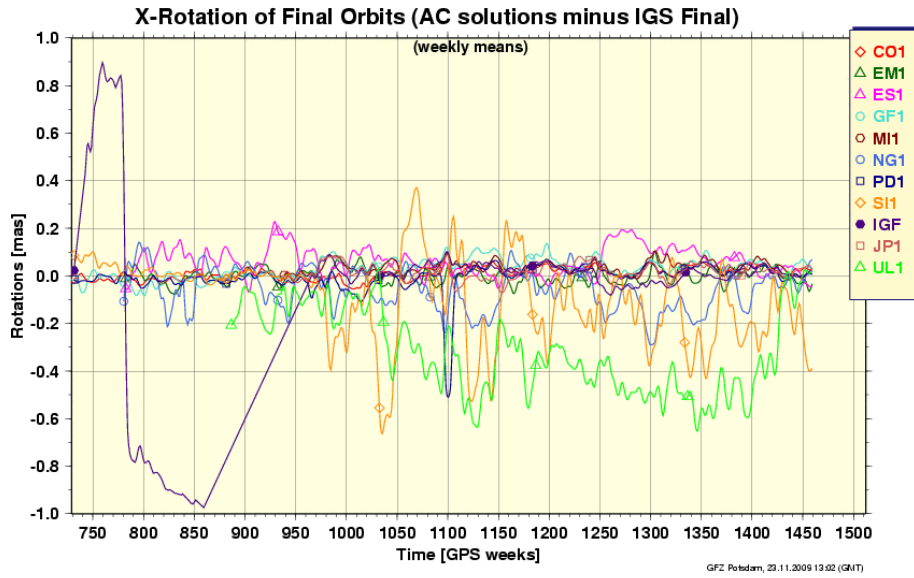
Figure 7.18. Smoothed daily X-rotation of contributing IGSr orbits
with respect to IG1 combined orbits[2].
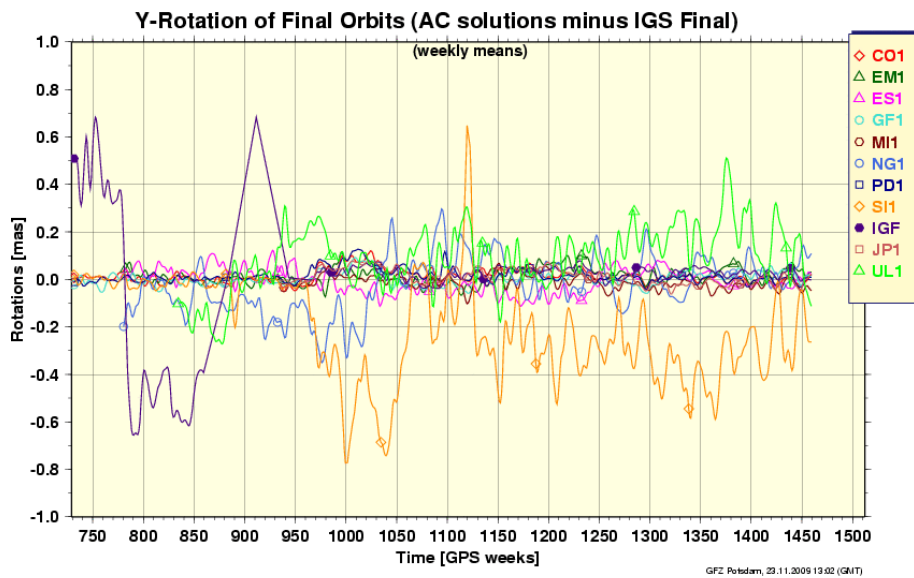
Figure 7.19. Smoothed daily Y-rotation of contributing IGSr orbits
with respect to IG1 combined orbits[2].
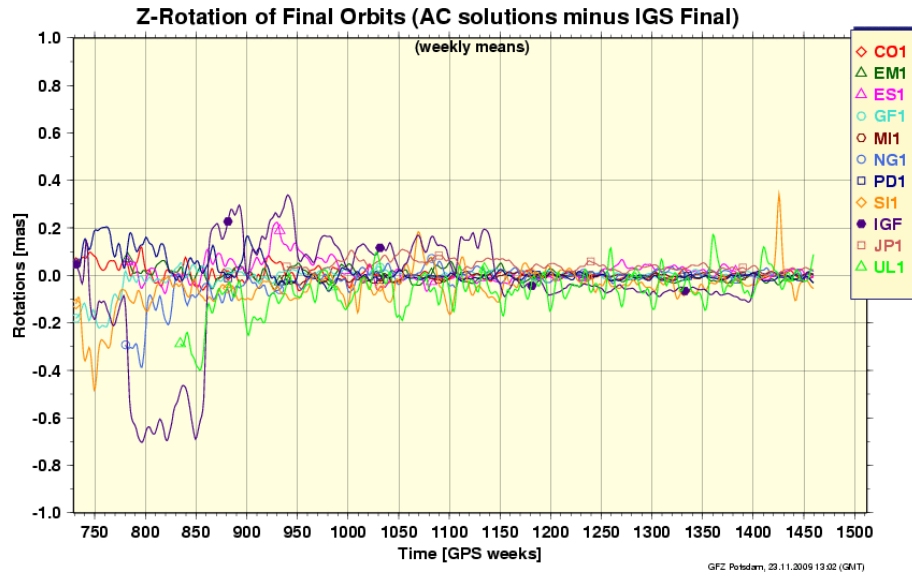
Figure 7.20. Smoothed daily Z-rotation of contributing IGSr orbits with respect to IG1 combined orbits[2].
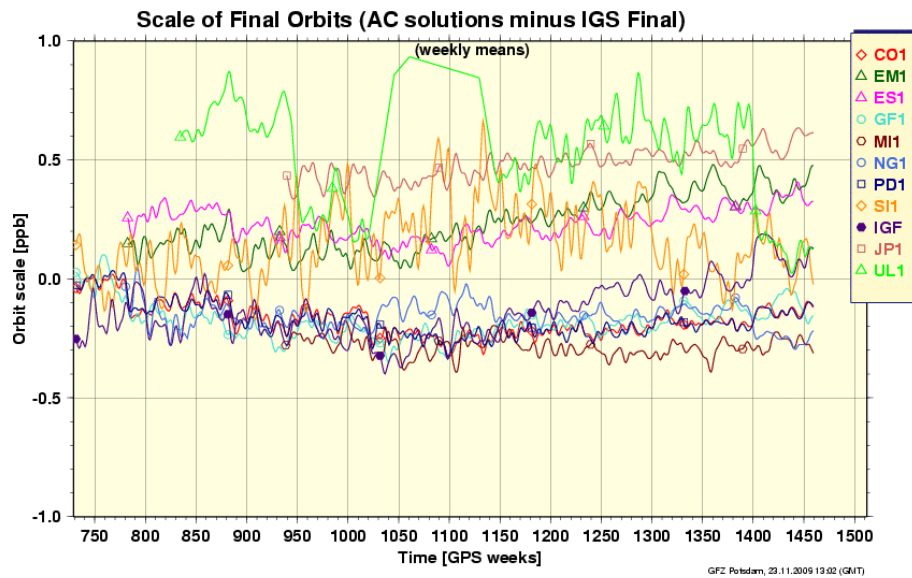
Figure 7.21. Smoothed daily scale of contributing IGSr orbits with respect to IG1 combined orbits[2].

7.5. Summary

In this chapter the geodetic quality of several ULR4 derived products was addressed. These products include station positions, apparent geocenter motion, ERP and orbits. In an external validation, some of these products were combined/compared by the IGS to the high-end estimates of the IGS Analysis Centers and other groups participating to the first IGS reanalysis campaign. The upgrade of the combination strategy implemented (see Chapter 4) allowed us to estimate the apparent geocenter motion for the first time of any past ULR solution. ERP and orbits, although previously estimated in past ULR solutions, were now made available (exported and compared) for the first time. Since ULR apparent geocenter motion, ERP and orbits were extracted for the first time, only the station positions were internally validated through comparison between ULR4 and ULR3 solutions.

The ULR4 frame origin is not significantly biased with respect to ITRF2005 origin. The amplitude of the annual ULR4 geocenter variations agrees well with SLR estimates for the equatorial components (X and Y). For the Z axis, larger variations were found which are mainly related to systematic errors of the GPS technique and also to the network shift approach used here. Compared with other estimates participating to the IGSr, ULR4 agreement is reasonably good. A possible discontinuity on the apparent geocenter motion in Z component deserves further research. It was also found that unaccounted surface loading, coupled with a non-uniform network repartition, is mainly aliased into an annual scale variation of 1.8 mm of amplitude. We found that estimating or not the scale parameter when transforming fiducial-free GPS solutions into a reference frame did not severely affect the apparent geocenter estimates. This spurious scale variation actually corrupts the estimates of annual signals in the station position residuals. Since no long-term scale drift was found, this parameter was not estimated when stacking weekly station solutions. This way, the estimated seasonal signals of the station positions are closer to the true signals caused by surface loading.

For the estimated ULR4 station positions, a clear reduction and improved stability of the weekly repeatability was found with respect to last ULR3 solution. Compared to the IG1 values, ULR4 station positions were found to perform at the same level as the best IGS AC solutions.

For the estimated ULR4 ERP, their residuals with respect to the IG1 combined solution were 0.05 mas, 0.3 mas/day and 0.03 ms/day for polar motion, polar motion rates and LOD, respectively. These residuals are at the same level to those found for the other reprocessed solutions participating in the IGSr.

For the estimated ULR4 orbits, a 1D RMS of 2-4 cm was found with respect to IG1 orbits, in agreement with the other reprocessed orbits participating in the IGSr. For all the reprocessed orbits, X and Y translation parameters with respect to IG1 orbits agree well. However, larger Z translation, rotation and scale variations were found for ULR4 orbits. Large orbit Z-translations, and even a possible discontinuity, seem to be coupled with the estimated apparent geocenter motion on the Z component. This effect might come from the estimation of the non-gravitational parameters and deserves further research. Large rotations of 6-12 mm with respect to combined IG1 orbits indicate that daily orientation of ULR4 orbits, realized through a set of IGS reference frame stations, is not optimal. Both features should be addressed in future ULR solutions.

8. Vertical velocity field

The vertical velocity field and the procedure followed to select the stations to be retained for further analysis are described in Section 8.1. This velocity field is first compared to the previous velocity field estimated at the ULR Consortium (ULR3 solution) (Section 8.2). Second, the geodetic quality of the estimated velocities is further assessed by means of a comparison with the preliminary (at time of writing) ITRF2008 solution (Section 8.3) and a multi-technique comparison (Section 8.4). In Section 8.5 we use the ULR4 velocity field to correct vertical motions at tide gauges with long-term sea level rise records. Finally, a summary of the chapter is given (Section 8.6).

8.1. Selection of the stations in the ULR4 velocity field

Figure 8.1 shows the geographic distribution of the network of stations used in the ULR4 solution. This network is composed by 316 permanent GPS stations. Among them, 216 are co-located within 15 km with a tide gauge (CGPS@TG). From these 216 CGPS@TG, 81 are committed to the IGS TIGA pilot project [*Schöne et al.*, 2009]. In addition, among the 316 stations, 124 are IGS Reference Frame stations used to realize the reference frame [*Kouba et al.*, 1998] and to improve the network geometry within the continents. This network is clearly not evenly distributed, with large concentration of stations in North America, Europe and Japan, whereas other continents like South America, Africa and Asia are under-sampled.
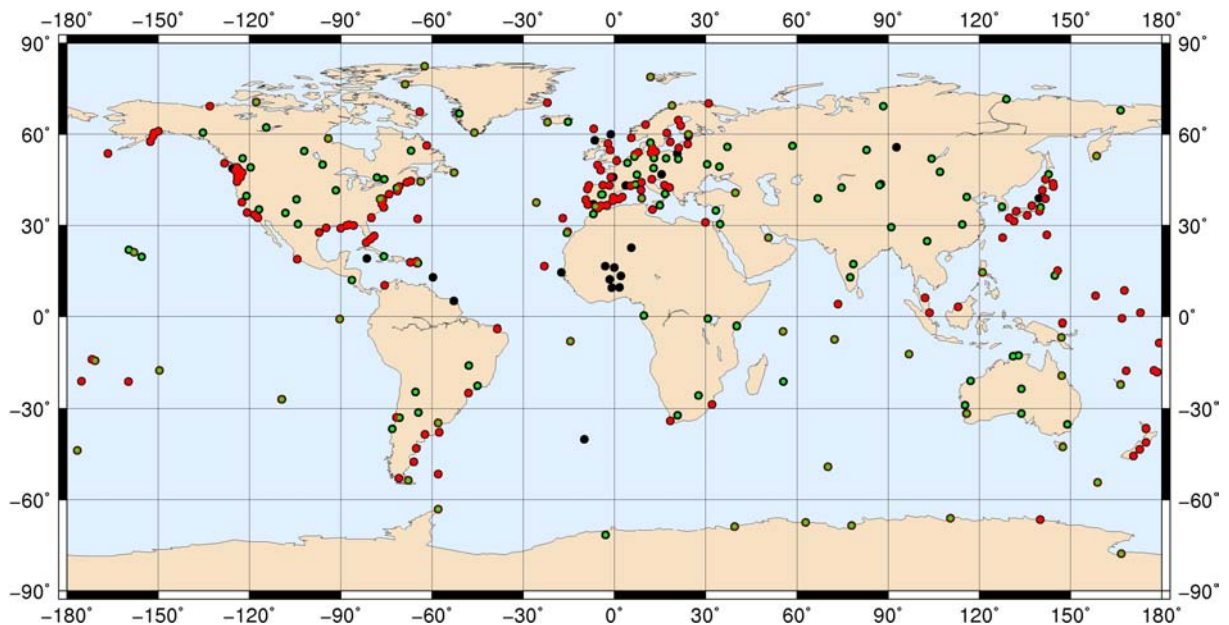
Figure 8.1. ULR4 tracking network (black dots). Red dots represent CGPS@TG stations and green dots represent IGS05 reference frame stations.

The GPS data analyzed here spanned from 1st January 1994 to 31st December 2008. After the input data quality check, the number of daily processed stations increases from a minimum of 25 in 1994 and to a maximum of 239 in 2006 (see Figure 3.9). After this maximum, the number of daily available stations begins to drop due to decommissioning of

older stations. As seen in that figure, GPS processing for 1994 and 1995 years presented a noticeable loss of resolved ambiguities involving, therefore, a quality loss of the estimated parameters. Some of the sharp rise and decrease offsets observed in the percentage of resolved ambiguities for the 1994-1996 period are related to constellation tests involving the activation/deactivation of the P encryption code known as anti-spoofing (GPS Notice Advisory to Navstar Users (NANU)[1]). The source of some other offsets, however, remains unknown, but from Figure 3.9 is clear that they are not related to a change of the network size. At the very start of the stacking process (Chapter 5), the number of outliers found for 1994 and 1995 years was extremely large compared to those found in the rest of available period. We decided to not further include these years of data in the stacking. This finally led a combination of 13 years of data, from 1st January 1996 to 31st December 2008, or 678 weekly solutions between GPS weeks 0834 and 1511.

Figure 8.2 shows a histogram of the number of stations with respect to their data span. About 25% of the stations have a time span larger than 12 years. However, to assess velocity confidence from data span, and thus to select the stations retained in the velocity field, the inter-discontinuities (soln) lengths were examined instead of the total time series lengths. Even if a station has a long time series, station velocities are estimated by soln and then, if no velocity discontinuity is suspected to be present, the different estimated velocities are constrained to result in an unique station velocity estimate (see Section 5.1). Thus, if the maximum soln length of a station did not reach 2.5 years of data, the station was not retained. For such stations, their estimated velocity was not considered reliable due to the expected presence of seasonal signals (see Section 5.2). This way, velocities estimated from the shortest time series or time series with a large number of offsets were not taken into account. From the original 316 stations, 28 stations for which the longest soln has less than 2.5 years of data were rejected. In addition, 5 more stations with soln longer than 2.5 years but less than 50% of available data were also rejected (POR1 13%, TGCV 16%, MALA 19%, VALP 19% and MANZ 49%). These stations with long time series but relatively few data run the risk of having unnoticed offsets that could dramatically bias their velocity estimation (see Section 5.1). Finally, 7 more stations having some velocity discontinuity where also rejected (MANA, NYAL, NTUS, KEN1, P205, P203 and MAC1). For these stations it was not possible to derive reliably a long term velocity. These criteria led to a total number of 275 stations retained in the ULR4 velocity field, which fulfill all the a priori requirements for high geodetic quality.

Figure 8.3 (a and b) shows the estimated vertical velocities of the 275 stations in the ULR4 velocity field. The maximum uplift velocity is 11.6 mm/yr at SELD (Alaska) and HOFN (Iceland) stations. The maximum subsidence is -8.1 mm/yr at GOUG (South Atlantic). At first sight, it is noticeable that large areas show consistent velocities. For instance, there are clear vertical gradients in North American, European and Japanese regions. Note that these areas coincide with the most populated areas of the tracking network. These gradients have been related mainly to Glacial Isostatic Adjustment (GIA) in Europe [*Johansson et al.*, 2002; *Nocquet et al.*, 2005] and North America [*Calais et al.*, 2006; *Sella et al.*, 2007]. Finally, there are some estimated velocities that do not seem to be consistent with nearby stations. Examples of this are KELY (Greenland), LAMA (Poland) or TONG (South Pacific). This indicates the presence of local effects (geophysical or artificial) or biases superimposed to regional or global geophysical effects.

---

1 http://www.navcen.uscg.gov/GPS/nanu.htm
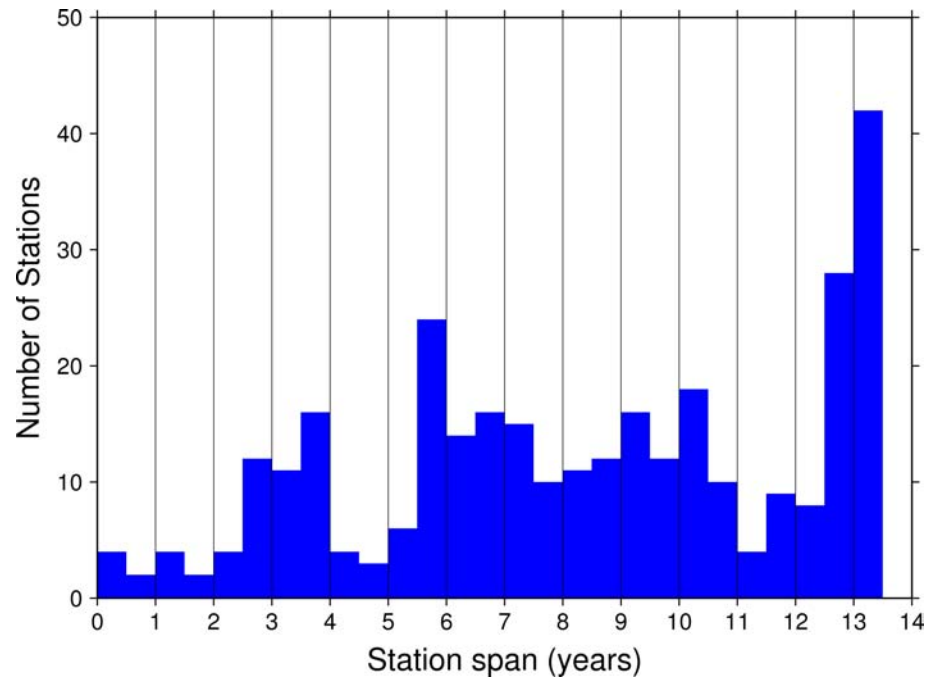
Figure 8.2. Number of stations in ULR4 solution with respect to time series length.
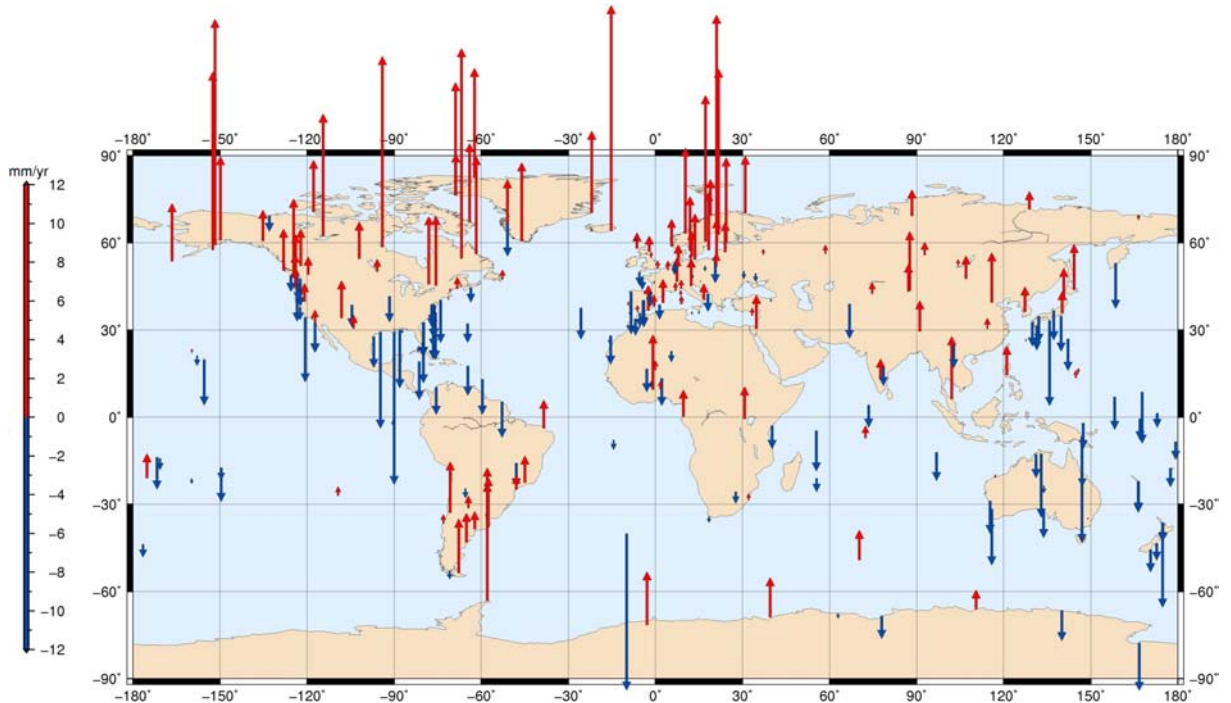
Figure 8.3a. ULR4 vertical velocity field. Red color represents uplift and blue color represents subsidence.
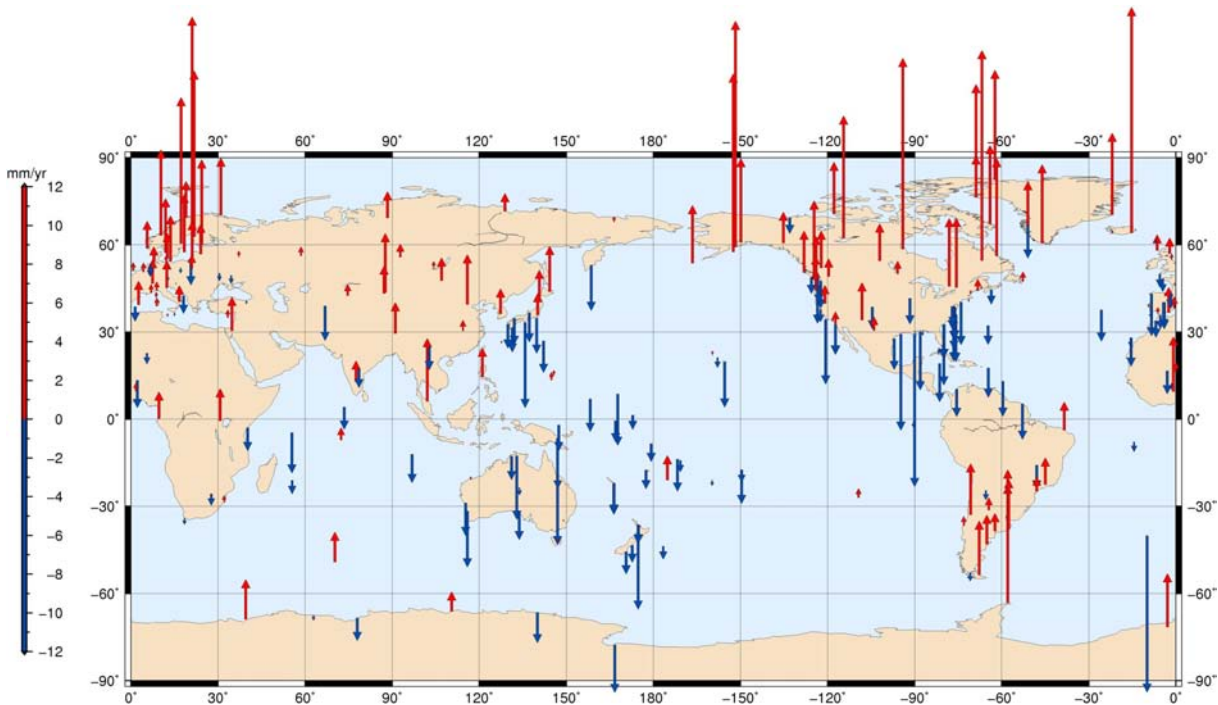
Figure 8.3b. ULR4 vertical velocity field. Red color represents uplift and blue color represents subsidence.

8.2. Comparison of ULR3 and ULR4 vertical velocity fields

In order to compare both ULR3 and ULR4 vertical velocity fields, 180 common stations with more than 2.5 years of data in both solutions were extracted. Since discontinuities applied in both solutions were not exactly the same for each station, only one soln was extracted per station. For each extracted soln in both solutions, the maximum length and matching epochs were ensured. These extracted velocities and their uncertainties were then compared.

8.2.1. Velocity comparison

Velocities extracted from ULR3 and ULR4 solutions were compared by removing the frame differences between them. Although both solutions are expressed in the ITRF2005 reference frame, using a different set of datum stations for the frame alignment can lead to different velocity fields. This way, a 14-parameter transformation was estimated between both extracted solutions and the vertical velocity differences were then analyzed. Differences obtained from this comparison contains exclusively the combined effect of the different data span used for each solution and the different data processing and combination procedures followed in each solution.

The weighted RMS of the vertical velocity differences is 1 mm/yr, with a maximum of 4.2 mm/yr at PERT station. For 56% of the stations, the differences are below 0.5 mm/yr and for 93% below 2 mm/yr (see Figure 8.4). These velocity differences were then compared with their uncertainties (see Figure 8.5). For 94% of the stations, the differences were below 3σ (86% below 2σ). For the remaining 6% of stations with significant differences, they were due

to the use of different discontinuities and inter-station velocity constraints. It is noticeable in Figure 8.5 that ULR4 uncertainties are smaller than ULR3 ones (see more details in next Section 8.2.2). Finally, by examining the rates of the transformation parameters between both solutions, and also by comparing ULR3 and ULR4 velocities without 14-parameter transformation, the effect of the different realization of the ITRF2005 was estimated to be 0.2 mm/yr. This effect is nevertheless not significant with respect to the mean velocity field uncertainty (see Section 6).
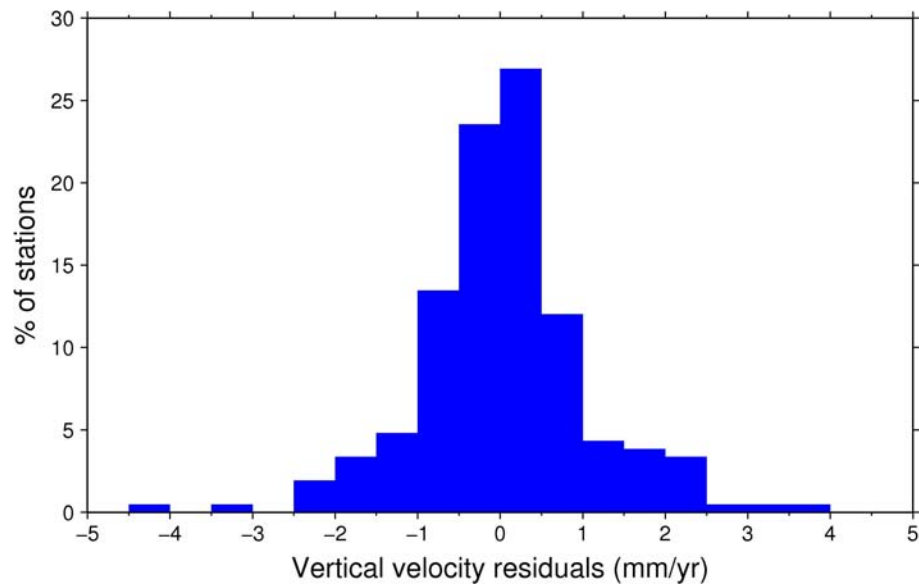
Figure 8.4. Histogram of vertical velocity differences between ULR3
and ULR4 solutions.
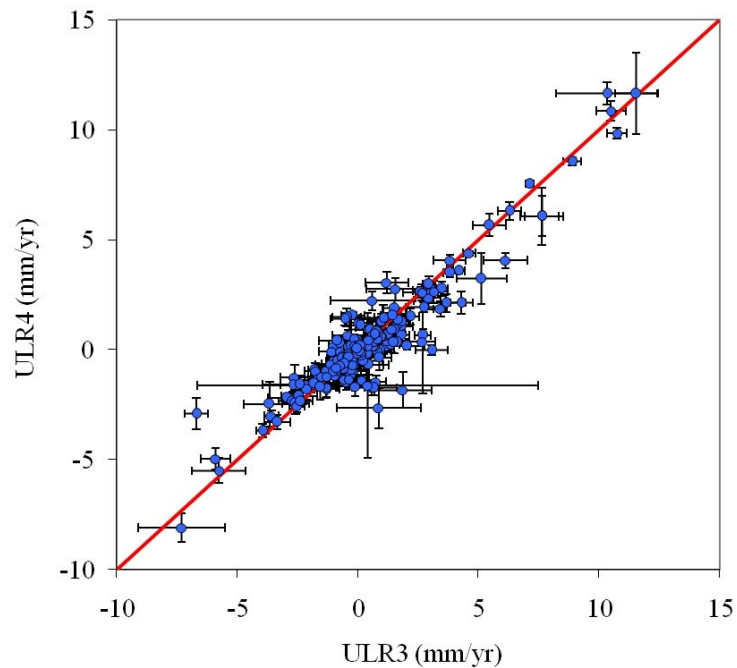
Figure 8.5. Vertical velocity differences between ULR3 and ULR4
solutions. Velocity uncertainties are 1σ.

8.2.2. Velocity uncertainty comparison

In order to properly compare both ULR3 and ULR4 velocity field uncertainties, the 180 retained common time series of ULR4 solution were analyzed with CATS using the same procedure than for ULR3 solution. That is, for the ULR4 time series we removed the seasonal periods and up to 5 fixed harmonics of the 1.04 cpy GPS draconitic period. Then, as for the ULR3 solution, a combination of constant white noise and power law noise models was used to estimate the uncertainties. Furthermore, to avoid the impact of different time series duration and data epoch (see section 6.3.4) between both solutions (ULR4 has 3 years more of data), the 180 time series of the ULR4 solution were windowed to the same time period of ULR3 solution (1997.0-2007.0). This way, only data processing differences (from the GPS data processing to solution combination and discontinuities applied) will arise. Possible differences resulting from the input data and from the different noise analysis strategies are thus avoided. Following this procedure, median noise amplitudes for ULR3 solution were 2.4 mm and 8.0 mm for white and power law, respectively; for ULR4 solution we found 2.0 mm and 6.1 mm for white and power law, respectively. The reduction of noise amplitudes is clearly appreciable, especially for the colored noise component.

Figure 8.6 shows the histograms of the vertical velocity uncertainties of ULR3 and modified ULR4 solutions using the common 180 stations. The improvement in precision of the new solution is noticeable. The median vertical velocity uncertainties for these 180 stations are 0.29 mm/yr and 0.44 mm/yr for ULR4 and ULR3, respectively. This represents a factor ~1.5 of improvement of the internal precision for the ULR4 data processing methodology with respect to the ULR3. Figure 8.7 shows the histogram of the vertical velocity uncertainty differences between both solutions (ULR3 minus ULR4). The mean velocity uncertainty difference is 0.20 ± 0.04 mm/yr.
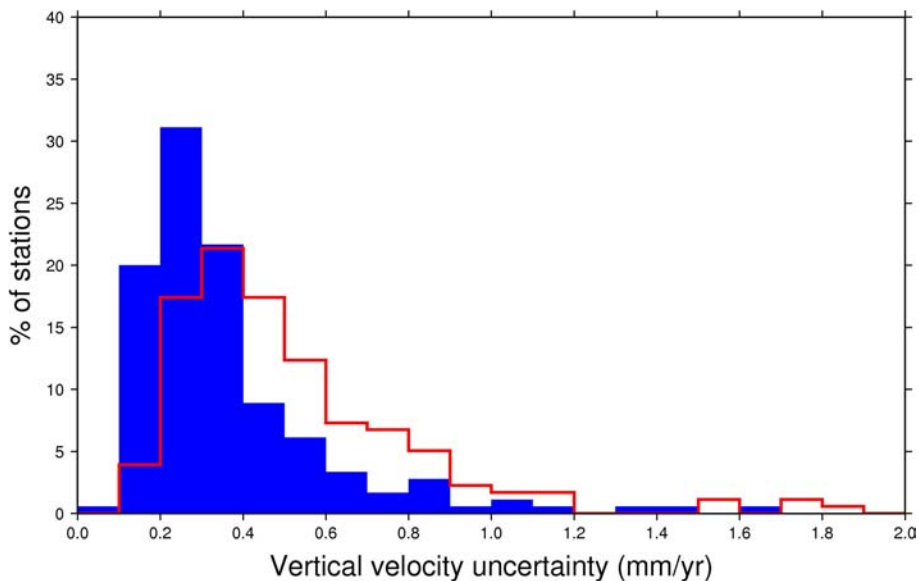
Figure 8.6. Histogram of modified ULR4 solution (blue) and ULR3
solution (red) vertical velocity uncertainties for 180 common stations.
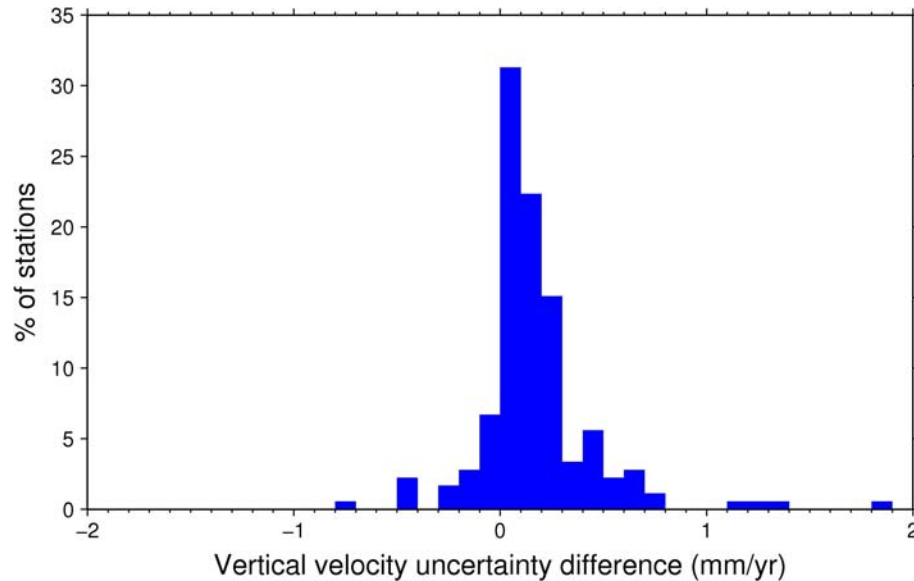
Figure 8.7. Histogram of vertical velocity uncertainty differences
between modified ULR4 and ULR3 solutions for 180 common
stations. Values are ULR3 minus ULR4.

8.3. Comparison with multi-technique vertical velocity fields

ULR4 solution was simultaneously compared to the International VLBI Service (IVS)[2], International Laser Ranging Service (ILRS)[3] and International DORIS Service (IDS)[4] long-term solutions submitted to the ITRF2008 realization. The comparison was then limited to 79 stations co-located with any of those techniques. To compare all these solutions, a combination was performed similarly to an ITRF-type combination following the IERS Product Center[5] procedure, where the IGS long-term solution was replaced by the ULR4 solution. There are, however, two differences with respect to that ITRF-type combination. First, to highlight the velocity differences between the different technique estimations, all velocities within a site were constrained at the level of 0.1 mm/yr sigma level. This way, velocity residuals will indicate a disagreement between co-located stations. The origin of this disagreement cannot, however, be assigned to any co-located station unless at least three techniques are simultaneously available. Second, local ties between co-located stations were unconstrained at 1 m level to avoid their impact on the combined velocities.

The WRMS of the vertical velocity differences of the ULR4 solution with respect to the multi-technique combined one is 0.5 mm/yr, with 96% of the differences smaller than 1 mm/yr (Figure 8.8). The maximum difference was found to be 3.2 mm/yr for THU1 station, which is known to have an unstable GPS monumentation[6]. These velocity differences were compared against the ULR4 uncertainties (see Chapter 6). For 94% of the stations, the differences were below 3σ (87% below 2σ). For the remaining 6% of stations, their significant velocity differences were not confidently assigned to any specific co-located technique.

2   http://ivscc.gsfc.nasa.gov
3   http://ilrs.gsfc.nasa.gov
4   http://ids-doris.org
5   http://itrf.ensg.ign.fr
6   http://igscb.jpl.nasa.gov/mail/igsmail/2002/msg00546.html
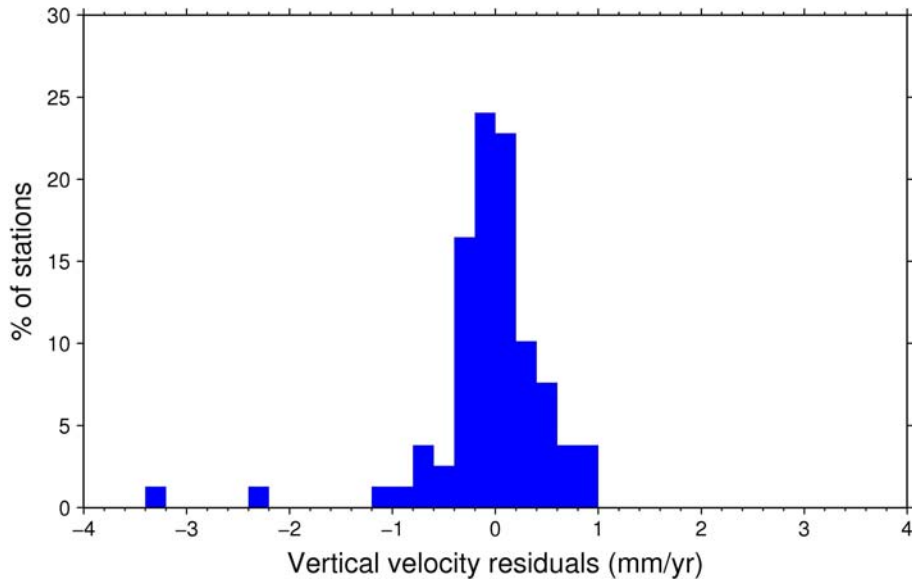
Figure 8.8. Histogram of vertical velocity differences between ULR4
solution and multi-technique combined solution.

8.4. Comparison with the ITRF2008 vertical velocity field

This comparison is similar to that of the previous Section 8.3, but here, ULR4 solution was compared with the preliminary ITRF2008 (ITRF2008P) solution. That is, the (still not official at the time of writing) new reference frame which was computed by combining the IGS, IDS, ILRS and IVS long-term submitted solutions. This way, the comparison was mainly between the ULR4 solution and the IGS long-term solution submitted to ITRF2008. Note, however, that IGS velocities in the ITRF2008P are affected by constraints applied between co-located techniques, so they are not rigorously the IGS long-term estimated velocities, but the IGS velocities of the ITRF2008P solution. In addition, both solutions (ULR4 and IGS) are not fully independent, since the ULR solution contributed to the IGS combined solution submitted to the ITRF through the reprocessing campaign[7]. Thus, ITRF2008P solution contains several non-IGS stations that were analyzed by few Analysis Centers or even by any, except ULR. Thus, to increase the independence of both solutions (ITRF2008P and ULR4) only those stations analyzed by a large number of Analysis Centers were considered here. Those stations correspond to the 120 IGS reference frame (IGS05[8]) stations analyzed in the ULR4 solution.

The weighted RMS of the vertical velocity residuals after a 14-parameter transformation between the ULR4 and the IGS-ITRF2008P solutions is 0.6 mm/yr, with 92% of the differences smaller than 1 mm/yr (Figure 8.9). The maximum difference was found to be 3.2 mm/yr for KUNM station. These velocity differences were compared against the ULR4 uncertainties (Chapter 6). For 90% of the stations, the differences were below 3σ (82% below 2σ). For the remaining 10% of stations with significant differences, they are suspected to be due to different discontinuities and inter-station velocity constraints. The effect of seasonal signals on estimated velocities (only accounted for in the ULR4 solution) is also a source of

---

7   http://acc.igs.org/reprocess.html
8   http://igscb.jpl.nasa.gov/mail/igsmail/2006/msg00178.html

disagreement. For instance, for HYDE station the vertical velocity difference found between ULR4 and IGS solutions is -1.9 mm/yr (ULR4 minus IGS), being the same velocity difference found in ULR4 solution when analyzing the impact of seasonal signals on estimated velocities. This large difference is likely due to the coupled effect of seasonal signals and offset amplitude estimation (see Section 5.2 for more details).
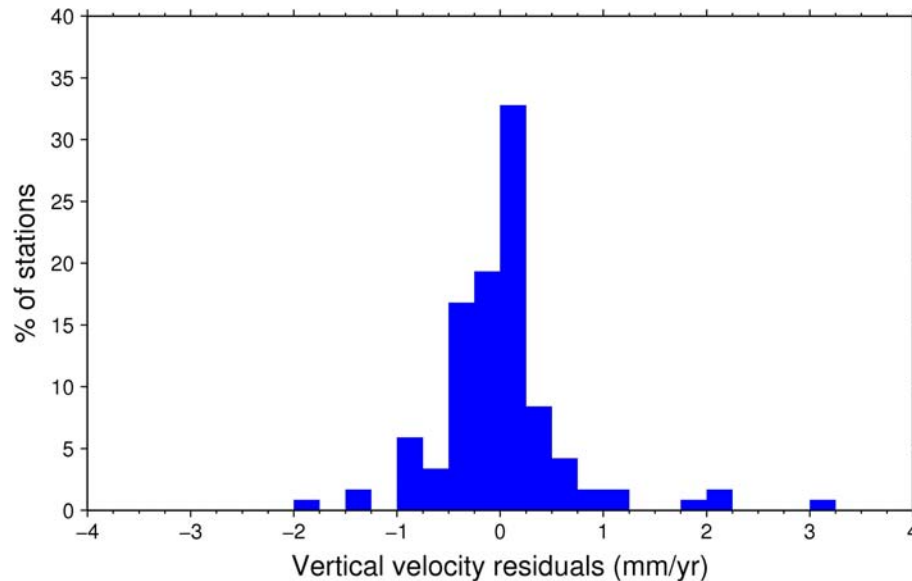
Figure 8.9. Histogram of vertical velocity differences between ULR4 and IGS-ITRF2008P solutions.

8.5. Sea level application

ULR4 vertical velocities were used to correct vertical movements from tide gauge records in order to extract the absolute (geocentric) long-term sea level variation at those tide gauges. The selected tide gauges were the same set used in *Wöppelmann et al.* [2007, 2009]. This set is composed of 27 RLR[9] tide gauges with time series longer than 60 years and more than 85% of valid data. All these tide gauges have a co-located GPS station within less than 20 km. Fernandina tide gauge (used in the above-mentioned studies) was discarded due to a misleading with the co-located GPS station identification. Following these studies, the tide gauges were distributed in 10 regions where absolute sea level trends are expected to be consistent [*Douglas*, 2001]. By computing a mean sea level rise of each region (instead of the mean of all individual tide gauges) we lessen a possible bias in the global sea level rise estimation resulting from the different sampling of the oceans and the regional variability (see Section 1.1).

Using this approach and the ULR4 vertical velocity field to correct vertical movements at tide gauges, we obtained a global-average rate of geocentric sea level rise for the twentieth century of 1.34 ± 0.17 mm/yr. This value is consistent with recent estimates [e.g., *Church and White*, 2006; *Holgate*, 2007; *Wöppelmann et al.*, 2007] but, in addition, is closer to the sum of independent climate contributors (see Section 1.2). Disagreement between this sum and the value estimated here is about 0.2 mm/yr. This estimation would help

---

9   http://www.psmsl.org/data/obtaining/

to close the sea level budget and the so-called sea level enigma.

Furthermore, ULR4-corrected sea level trends were compared with past ULR-corrected estimations published in the above-mentioned studies (ULR1, ULR2 and ULR3 solutions). In those studies, GIA corrections were also applied using the ICE5G (VM2) model [*Peltier*, 2004].

The rationale of such a comparison is as follows. If we assume that, for long-term sea level records, sea level regional variability vanishes, then, dispersion of sea level trends should reach a null value if vertical movements at tide gauges are correctly removed. Conversely, if we assume that sea level regional variability has some effect even for long-term sea level records, then, dispersion of sea level trends will never be null. However, in this case, if we succeed in eliminating completely the other source of global sea level rise error, that is, vertical movements at tide gauges, the dispersion of the sea level trends should be reduced with respect to the dispersion without any correction applied. Therefore, the dispersion of the sea level trends can be used to evaluate if the applied correction is performing better, allowing us to compare different ULR solutions.

Table 8.1 shows the dispersion (root mean squared) of the sea level trends without correction of vertical movements at tide gauges (relative sea level trends), and using GIA corrections or several sets of GPS corrections (different ULR solutions). Dispersion is shown for the individual and for the regional-averaged sea level trends. From this table, several important conclusions can be extracted. First, the dispersion of the sea level trends is reduced when vertical motions at tide gauges are taken into account, confirming our precedent hypothesis. Second, GPS corrections perform better than GIA corrections. This is mainly due to the fact that GPS velocities include a wide range of movements not considered in the GIA models. Third, ULR4 solution is the best of the compared corrections. Fourth, for ULR4 solution, both individual and regional dispersion reach a similar value. This fact might indicate the upper bound of a regional variability effect on global sea level rise. This last conclusion, actually an hypothesis, needs further research and is out of the scope of this work.

Finally, Figure 8.10 shows a graphical representation of these findings. Seven tide gauges records located in two regions (North Europe and North America) are plotted without correction, with GIA correction and with ULR4 correction. The agreement of the ULR4-corrected sea level trends is high within and also between both regions showing the appropriateness of the GPS correction to derive absolute sea level rise estimates at tide gauges.

Table 8.1. Dispersion of the individual and regional sea level trends using different corrections for vertical motions at tide gauges. Values in mm/yr. Non-ULR4 values extracted from *Wöppelmann et al.* [2009].

	No correction	GIA correction	GPS correction			
			ULR1	ULR2	ULR3	ULR4
RMS individual	2.05	1.49	1.15	1.06	0.98	0.59
RMS regional	1.37	0.98	0.91	0.83	0.60	0.55
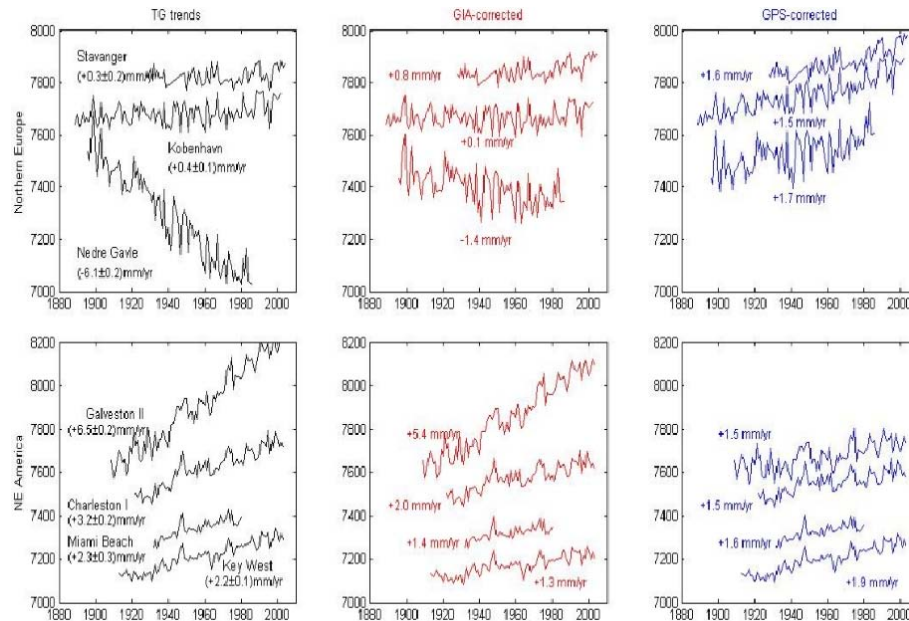
Figure 8.10. Tide gauge time series without correction (left), with GIA correction (middle) and with GPS (ULR4) correction (right) for North Europe (top) and North America (bottom).

8.6. Summary

This chapter has shown that, globally, the estimated velocities of the ULR4 solution are not significantly different from the last estimates of the ULR3 solution, even with differences about 1 mm/yr. However, ULR4 has proven to be more precise than ULR3 by a 1.5 factor. The increased precision comes entirely from an improved data processing and combination strategy. This improvement, seen as a noise content reduction, can also indirectly affect velocity estimation as unnoticed discontinuities could be revealed. Thus, the different discontinuities applied are the main reason for the velocity differences between both velocity fields. Since almost the same software and data has been used in both (extracted) solutions, this should be seen as an internal cross-validation of former and present-day procedures at the ULR Consortium. However, when applied to long-term relative sea level records, ULR4 performing is significantly better.

For a velocity field comparison as independent as possible, we also compared ULR4 velocities to those derived from the four main space geodetic high-end solutions, namely, the long-term IGS, IDS, ILRS and IVS solutions submitted to the ITRF2008 realization. Results show that, for the station sets used, velocity differences are not significant for most stations. Neglecting ULR4 velocity uncertainties, the level of disagreement for ULR4 velocities is at the level of 0.5-0.6 mm/yr. This disagreement accounts for errors contained in all compared solutions (IGS, IDS, ILRS, IVS and ULR4), for instance, the unaccounted effect of seasonal signals (see Section 5.2) when IGS-ITRF2008P velocities were estimated. This shows that the mean uncertainty of ~0.3 mm/yr estimated for ULR4 velocities (see Section 6.4) is adequate. This results were presented in *Santamaría-Gómez et al.* [2010].

Finally, we applied the ULR4 vertical velocity field to correct relative sea level trends of 27 high quality long-time running tide gauges. Comparison with past ULR solutions

applied to the same data set shows that ULR4 solution better removes the effect of vertical motions at tide gauges. Using these corrected sea level trends, the global sea level rise for the twentieth century has been estimated in 1.34 ± 0.17 mm/yr. This value, though consistent with the stated value of the AR4, is closer to the sum of individual climate contributors (difference of 0.2 mm/yr), probably closing the "attribution problem" of the sea level budget.

Conclusion and perspectives

The end of my PhD coincides with the release of the new ULR4 solution of the ULR TIGA Analysis Center. This solution constitutes a major improvement of existing vertical velocity fields in various aspects. It comprises a global network of more than 300 stations, spanning the period 1996 to 2009. The estimated global vertical velocity field is composed of 275 stations from which 178 are co-located with a tide gauge (CGPS@TG stations). The mean vertical velocity uncertainty is 0.3-0.5 mm/yr. This value was estimated from the time-correlated noise content analysis and also from the comparison with other high-end velocity solutions, as those formed by the main four space geodetic techniques (VLBI, SLR, DORIS and GPS). This uncertainty level shows the appropriateness of this vertical velocity field for several geophysical applications like transforming relative to absolute sea level trends, constraining GIA models, or studying regional tectonic phenomena. For instance, ULR4 vertical velocities removed long-term vertical land motion of a set of worldwide selected tide gauges in a more robust way than other GPS or GIA corrections. Absolute sea level trends derived from this velocity field would be then used for future long-term sea level rise and satellite altimetry calibration studies. At present, this velocity field contributes to develop a methodology aiming to densify the ITRF velocity field through the IAG Working Group on Regional Dense Velocity Fields. It also contributes to extend the new ITRF2008 to tide gauges acting thus as a link between the geodetic and oceanographic observing networks. Since tide gauges represent terrestrial and maritime national vertical references, to express heights and depths respectively, therefore, ULR4 solution also contributes towards a worldwide unified height system. This is, to our knowledge, the first attempt to release a global vertical velocity field including so many stations co-located with tide gauges with such a level of accuracy and homogeneity. Reaching such a goal was, however, quite a challenging task.

Indeed, estimating vertical crustal rates with an accuracy better than 1 mm/yr to meet the oceanographic and geodynamic community requirements is not a straightforward matter. There is a broad range of errors affecting velocity estimates. Starting with the GPS data processing itself, we tested different antenna phase center and tropospheric delay models which can change vertical velocities by more than 0.5 mm/yr (0.7 mm/yr and 0.2 mm/yr, respectively). We also developed a better geometric distribution of the sub-networks which caused a slightly smaller, but significant (0.4 mm/yr), vertical velocity change.

Concerning the time series analysis, we confirmed that the biggest sources of error for velocity estimation are the effect of hidden offsets or discontinuities on position time series and the uncertainty of the International Terrestrial Reference Frame (ITRF) definition. With respect to offsets, our major recommendation would be to carefully examine every time series to detect, estimate and remove as far as possible all the significant offsets and velocity discontinuities. Seasonal signals, coupled with offsets, also showed to cause significant velocity differences. We found that, although seasonal signals have a small effect (0.2 mm/yr) for most of the stations with long (>4.5 years) time series, these seasonal signals should be always removed as they can change the estimated offsets amplitude. Changing the offsets amplitude can result in a velocity change of more than 1 mm/yr depending on the offset amplitude change, its position in time series and the time series length. The velocity estimation method used may be improved in the future to allow offset amplitudes and

seasonal signals to be estimated consistently. Such approach should be carefully studied because estimating seasonal signals for very short time series would probably lead to a biased velocity, which can propagate to other stations through the spatial correlation of the estimated parameters.

When estimating a new velocity field, one should address the effect of the reference frame in which estimated velocities are expressed. The geosciences scientific community has been using the different ITRF releases for more than twenty years now. The ULR4 velocity field was estimated with respect to the origin defined by the ITRF2005. Estimating vertical crustal velocities with an accuracy better than 1 mm/yr means therefore knowing the time evolution of such origin (actually the Earth's center of mass) with the same accuracy requirement. In addition, for vertical rates, precise knowledge of the secular ITRF scale is even more needed. Currently, the (conservative) accuracy of the ITRF definition is estimated to be at the level of 0.5 mm/yr for the scale rate and more than 1 mm/yr for the origin rate. Combined, the uncertainty translated to vertical velocities ranges between 0.5 mm/yr and more than 1.5 mm/yr depending on the site latitude. Reducing these uncertainties below the mm/yr level will probably be major and most challenging goal of the 21st century geodesy.

We also showed how time-correlated noise content in time series affects velocity precision. Improvements of the GPS data modeling and processing clearly reduced the amplitude of the correlated noise content. However, the noise analyses we carried out indicate that even an homogeneous data reprocessing, using a thoroughly adapted processing strategy, still results in significant time-correlated noise content in position time series. Moreover, the correlated noise type remains unchanged after the processing improvements implemented. This shows that there is a deeper technique-related noise source to be investigated. Several issues are currently pointed out within the international GPS community. Such forthcoming developments include improving the modeling of non-gravitational effects on satellites such as solar radiation or Earth's surface albedo; reducing the station-dependent effects such as multipath or monument long-term instability; modeling the sub-daily effects at the observation level such as atmospheric tidal loading or EOP variations; modeling higher orders of the ionospheric refraction; or combining different GNSS systems at the observation level.

Future improvements in any of these issues would reduce the time-correlated noise level in position time series which will have a twofold benefit for velocity estimates. First, it will improve the estimated velocity precision. Second, since offsets and velocity discontinuities are unmasked when noise level is reduced, it will also improve the velocity accuracy. This way, noise analyses aiming at exploring systematic error sources are beneficial to improve the estimated GPS velocities.

Further noise analyses are currently being carried out to explain why early data have larger correlated-noise amplitudes. Those tests will be published by A. Santamaría-Gómez, M.-N. Bouin, X. Collilieux and G. Wöppelmann, "Correlated Errors in GPS Position Time Series: Implications for Velocity Estimates", Journal of Geophysical Research (in revision).

With the ULR4 solution the ULR TIGA Analysis Center has participated in the first IGS reanalysis campaign which let us gauge our processing performance with respect to the best GPS solutions available. To cope with this new framework, ULR combination strategy was fully reviewed and upgraded. Results of this comparison were very promising and fruitful. This opens a new front for improving future ULR solutions. However, the obtained ULR products should further improve their self-consistency (e.g., orbits, EOP and terrestrial frame) to be fully comparable to the ones obtained by the IGS Analysis Centers.

Ablain, M., A. Cazenave, G. Valladeau, and S. Guinehut (2009), A new assessment of the error budget of global mean sea level rate estimated by satelllite altimetry over 1993-2008, Ocean Science, 5, 193-201.

Agnew, D. (1992), The time domain behavior of power law noises, Geophys. Res. Lett., 19, 333– 336.

Altamimi, Z., P. Sillard, and C. Boucher (2002), ITRF2000: A new release of the International Terrestrial Reference Frame for earth science applications, J. Geophys. Res., 107(B10), 2214, doi:10.1029/2001JB000561.

Altamimi, Z., X. Collilieux, J. Legrand, B. Garayt, and C. Boucher (2007), ITRF2005: A new release of the International Terrestrial Reference Frame based on time series of station positions and Earth Orientation Parameters, J. Geophys. Res., 112, B09401, doi:10.1029/2007JB004949.

Altamimi, Z., X. Collilieux, and C. Boucher (2008), Accuracy Assessment of the ITRF Datum Definition, in Proceedings of VI Hotine-Marussi Symposium of Theoretical and Computational Geodesy, IAG Symposia, vol. 132, edited by P. Xu, J. Liu, and A. Dermanis, pp. 101– 110, Springer, New York.

Amiri-Simkooei, A. R., C. C. J. M. Tiberius, and P. J. G. Teunissen (2007), Assessment of noise in GPS coordinate time series: Methodology and results, J. Geophys. Res., 112, B07413, doi:10.1029/2006JB004913.

Argus, D. F., and W. R. Peltier (2010), Constraining models of postglacial rebound using space geodesy: a detailed assessment of model ICE-5G (VM2) and its relatives, Geophys. J. Int., 181(2), 697–723, doi:10.1111/j.1365-246X.2010.04562.x.

Ashkenazi, V., R.M. Bingley, and H. Dodson (1994), The determination of tide gauge heights in the United Kingdom by GPS, in: W. E. Carter (Ed.), Report of the Surrey Workshop of the IAPSO Tide Gauge Bench Mark Fixing Committee held at the Deacon Laboratory, Godalming, UK, 13–15 December 1993, pp. 71–75.

Bar-Sever, Y. E., P. M. Kroger, and J. A. Borjesson (1998), Estimating horizontal gradients of tropospheric path delay with a single GPS receiver, J. Geophys. Res., 103 (B3), 5019–5035.

Beavan, J. (2005), Noise properties of continuous GPS data from concrete pillar geodetic monuments in New Zealand and comparison with data from U.S. deep drilled braced monuments, J. Geophys. Res., 110, B08410, doi:10.1029/2005JB003642.

Becker, M., S. Zerbini, T. Baker, B. Bürki, J. Galanis, J. Garate, I. Georgiev, H. Kahle, V. Kotzev, V. Lobazov, I. Marson, M. Negusini, B. Richter, G. Veis, and P. Yuzefovich (2002), Assessment of height variations by GPS at Mediterranean and Black Sea coast tide gauges from the SELF projects, Global Planet. Change, 34, 1–2, 5–35.

Beckley, B. D., F. G. Lemoine, S. B. Luthcke, R. D. Ray, and N. P. Zelensky (2007), A reassessment of global rise and regional mean sea level trends from TOPEX and Jason-1 altimetry based on revised reference frame and orbits, Geophys. Res. Lett., 34, L14608, doi:10.1029/2007GL030002.

Bennett, R. A. (2008), Instantaneous deformation from continuous GPS: contributions from quasi-periodic loads, Geophys. J. Int., 174, 1052-1064, doi: 10.1111/j.1365-246X.2008.03846.x.

Berg, H. (1948), Allgemeine meteorologie, Dümmlers, Bonn.

Berge-Nguyen, M., A. Cazenave, A. Lombard, W. Llovel, J. Viarre, and J. F. Cretaux (2008), Reconstruction of past decades sea level using thermosteric sea level, tide gauge, satellite altimetry and ocean reanalysis data, Global. Planet. Change, 62, 1–13.

Bergeot, N., M. N. Bouin, M. Diament, B. Pelletier, M. Régnier, S. Calmant, and V. Ballu (2009), Horizontal and vertical interseismic velocity fields in the Vanuatu subduction zone from GPS measurements: Evidence for a central Vanuatu locked zone, J. Geophys. Res., 114, B06405, doi:10.1029/2007JB005249.

Bevis, M., W. Scherer, and M. Merrifield (2002), Technical issues and ecommendations related to the installation of continuous GPS stations at tide gauges, Mar. Geod., 25 (1–2), 87–99.

Blewitt, G. (2003), Self-consistency in reference frames, geocenter definition, and surface loading of the solid Earth, J. Geophys. Res., 108(B2), 2103, doi:10.1029/2002JB002082.

Blewitt, G., and D. Lavallée (2000), Effect of annually repeating signals on geodetic velocity estimates, paper presented at The Tenth General Assembly of the WEGENER Project (WEGENER 2000), San Fernando, Spain, 18 − 20 Sept.

Blewitt, G., and D. Lavallée (2002), Effect of annual signals on geodetic velocity, J. Geophys. Res., 107, doi:10.1029/2001JB000570.

Blewitt, G., Y. Back, and G. Gendt (1993), Regional clusters and distributed processing, in Proceedings of the IGS Analysis Center workshop, October 12th-14th 1993, Ottawa, Canada, edited by J. Kouba, pp. 62-91, Int. GPS. Serv. Cent. Bur., Pasadena, Calif.

Blewitt, G., Z. Altamimi, J. Davis, R. Gross, C. Kuo, F. Lemoine, R. Neilan, H.-P. Plag, M. Rothacher, C. K. Shum, M. G. Sideris, T. Schöne, P. Tregoning, and S. Zerbini (2006), Geodetic observations and global reference frame contributions to understanding sea level rise and variability, in Proceedings of the WCRP Workshop "Understanding Sea-Level Rise and Variability", UNESCO, Paris, pp. 145–170. 6–9 June 2006.

Boehm, J., and H. Schuh (2004), Vienna mapping functions in VLBI analyses, Geophys. Res. Lett., 31, L01603, doi:10.1029/2003GL018984.

Boehm, J, B. Werl, and H. Schuh (2006a), Troposphere mapping functions for GPS and very long baseline interferometry from European Centre for Medium-Range Weather Forecasts operational analysis data, J. Geophys. Res., 111, B02406, doi:10.1029/2005JB003629.

Boehm, J., A. Niell, P. Tregoning, and H. Schuh (2006b), Global Mapping Function (GMF): a newempirical mapping function based on numerical weather model data, Geophys. Res. Lett., 33, L07304, doi:10.1029/2005GL025546.

Boehm, J., R. Heinkelmann, and H. Schuh (2006c), Neutral atmosphere delays: empirical models versus discrete time series from numerical weather models, in Proceedings of IAG Symposium Geodetic Reference Frame (GRF2006), Munich, Germany, 9–13 October 2006.

Boehm, J., P. J. MendesCerveira, H. Schuh, and P. Tregoning (2007a), The impact of mapping functions for the neutral atmosphere based on numerical weather models in GPS data analysis, in Tregoning P, Rizos C (eds) IAG symposium series, vol. 130. Springer, Heidelberg, pp 837–843.

Boehm, J., R. Heinkelmann, and H. Schuh (2007b), Short note: a global model of pressure and temperature for geodetic applications, J. Geod., doi:10.1007/s00190-007-0135-3.

Boehm, J., H. Schuh, P. J. Mendes Cerveira, and R. Heinkelmann (2008), Reference pressure for the Global Geodetic Observing System GGOS, IVS memorandum 2008-002v01. ftp://ivscc.gsfc.nasa.gov/pub/memos/ivs-2008-002v01.pdf.

Boehm, J., J. Kouba, and H. Schuh (2008b), Forecast Vienna Mapping Functions 1 for real-time analysis of space geodetic observations, J. Geod., 83, 397–401, DOI 10.1007/s00190-008-0216-y.

Bos, M. S., R. M. S. Fernandes, S. D. P. Williams, and L. Bastos (2008), Fast error analysis of continuous GPS observations, J. Geod., 82, 157-166, doi: 10.1007/s00190-007-0165-x.

Boucher, C. (1979), Les transformations géométriques entre systèmes géodésiques, Rapport Technique de l'IGN, RT/G 3.

Bouin, M.-N., and G. Wöppelmann (2010), Land motion estimates from GPS at tide gauges: a geophysical evaluation, Geophys. J. Int., 180, 193-209, doi: 10.1111/j.1365-246X.2009.04411.x.

Bruyninx, C., Z. Altamimi, M. Becker, M. Craymer, L. Combrinck, A. Combrink, J. Dawson, R. Dietrich, R. Fernandes, R. Govind, T. Herring, A. Kenyeres, R. King, C. Kreemer, D. Lavallée, J. Legrand, L. Sánchez, G. Sella, Z. Shen, A. Santamaría-Gómez, and G. Wöppelmann (in press), A dense global velocity field based on GNSS observations: preliminary results, Proceedings of the International Association of Geodesy General Assembly, Buenos Aires, Argentina, August 31-September 4, 2009.

Cabanes, C., A. Cazenave, and C. Le Provost (2001b), Sea level rise during past 40 years determined from satellite and in situ observations, Science, 294, 840–842.

Calais, E. (1999), Continuous GPS measurements across the western Alps, 1996– 1998, Geophys. J. Int., 138, 221– 230.

Calais, E., J. Y. Han, C. DeMets, and J. M. Nocquet (2006), Deformation of the North American plate interior from a decade of continuous GPS measurements, J. Geophys. Res., 111, B06402, doi:10.1029/2005JB004253.

Cardellach, E., P. Elósegui, and J. L. Davis (2007), Global distortion of GPS networks associated with satellite antenna model errors, J. Geophys. Res., 112, B07405, doi:10.1029/2006JB004675.

Carter, W. E., D. G. Aubrey, T. F. Baker, C. Boucher, C. Le Provost, D. T. Pugh, W. R. Peltier, M. Zumberge, R. H. Rapp, R. E. Shutz, K. O. Emery, and D. B. Enfield (1989), Geodetic fixing of tide gauge benchmarks, Woods Hole Oceanographic Institution Technical Report, WHOI-89-31, 44 pp.

Carter, W. E. (1994), Report of the Surrey Workshop of the IAPSO Tide Gauge Bench Mark Fixing Committee, Report of a meeting held 13–15 December 1993 at the Institute of Oceanographic Sciences Deacon Laboratory, NOAA Technical Report NOSOES0006. 81 pp.

Cazenave, A., and W. Llovel (2010), Contemporary Sea Level Rise, Annu. Rev. Mar. Sci., 2, 145–73. 10.1146/annurev-marine-120308-081105.

Cazenave, A., and R. S. Nerem (2004), Present-day sea level change: Observations and causes, Rev. Geophys., 42, RG3001, doi:10.1029/2003RG000139.

Cazenave, A., A. Lombard, and W. Llovel (2008), Present-day sea level rise: A synthesis, Comptes Rendus Geoscience, 340(11), 761.

Chen, G., and T. A. Herring (1997), Effects of atmospheric azimuthal asymmetry on the analysis of space geodetic data, J. Geophys. Res., 102 (B9), 20 489–20 502.

Chen, J. L., C. R. Wilson, R. J. Eanes, and R. S. Nerem (1999), Geophysical interpretation of observed geocenter variations, J. Geophys. Res., 104(B2), 2683– 2690.

Choi, K., A. Bilich, K. M. Larson, and P. Axelrad (2004), Modified sidereal filtering: Implications for high-rate GPS positioning, Geophys. Res. Lett., 31, L22608, doi:10.1029/2004GL021621.

Church, J. A., and N. J. White (2006), A 20th century acceleration in global sea-level rise. Geophys. Res. Lett., 33, L01602, doi:10.1029/2005GL024826.

Church, J. A., N. J. White, R. Coleman, K. Lambeck, and J. X. Mitrovica (2004), Estimates of the regional distribution of sea-level rise over the 1950 to 2000 period, J. Clim., 17, 2609–2625.

Collilieux, X. (2004), Comparaison de CATREF & Globk pour la comparaison de Repère de Référence Terrestre, Rapport de DEA, Observatoire de Paris.

Collilieux, X. (2008), Analyse des series temporelles de positions des stations de géodésie spatiale: Application au Repère International de Référence Terrestre (ITRF), Thèse de Doctorat de l'Observatoire de Paris.

Collilieux, X., Z. Altamimi, D. Coulot, J. Ray, and P. Sillard (2007), Comparison of very long baseline interferometry, GPS, and satellite laser ranging height residuals from ITRF2005 using spectral and correlation methods, J. Geophys. Res., 112, B12403, doi:10.1029/2007JB004933.

Collilieux, X., Z. Altamimi, J. Ray, T. van Dam, and X. Wu (2009), Effect of the satellite laser ranging network distribution on geocenter motion estimation, J. Geophys. Res., 114, B04402, doi:10.1029/2008JB005727.

Davis, J. L., and J. X. Mitrovica (1996), Glacial Isostatic Adjustment and the Anomalous Tide Gauge Record From Eastern North America, Nature, 379, 331-333.

Davis, J. L., T. A. Herring, I. I. Shapiro, A. E. E. Rogers, and G. Elgered (1985), Geodesy by radio interferometry: Effects of atmospheric modeling errors on estimates of baseline length, Radio Sci., 20, 1593–1607.

DeMets, C., R. G. Gordon, D. F. Argus, and S. Stein (1994), Effect of recent revisions of the geomagnetic reversal timescale on estimates of current plate motions, Geophys. Res. Lett., 21(20), 2191–2194.

Dong, D., P. Fang, Y. Bock, M. K. Cheng, and S. Miyazaki (2002), Anatomy of apparent seasonal variations from GPS-derived site position time series, J. Geophys. Res., 107(B4), 2075, doi:10.1029/2001JB000573.

Dong, D., T. Yunck, and M. Heflin (2003), Origin of the International Terrestrial Reference Frame, J. Geophys. Res., 108(B4), 2200, doi:10.1029/2002JB002035.

Donnelly, J. P., P. Cleary, P. Newby, and R. Ettinger (2004), Coupling instrumental and geological records of sea-level change: Evidence from southern New England of an increase in the rate of sea-level rise in the late 19th century, Geophys. Res. Lett., 31(5), L05203, doi:10.1029/2003GL018933.

Douglas, B. C. (2001), Sea level change in the era of the recording tide gauge, in Sea Level Rise, History and Consequences, ed. B. C. Douglas, M. S. Kearney, S. P. Leatherman, pp. 37–64, San Diego, CA, Academic Press.

Douglas, B. C., and W. R. Peltier (2002), The puzzle of global sea-level rise, Physics Today, 55(3), 35-40.

Douglas, B. C. (2008), Concerning evidence for fingerprints of glacial melting, J. Coastal Res., 24, 218– 227.

Eanes, R. J. and S. Bettadpur (1995), The CSR 3.0 global ocean tide model, Technical Memorandum CSR-TM-95-06, Center for Space Research, University of Texas, Austin, TX.

Elosegui, P., J. L. Davis, R. T. K. Jaldehag, J. M. Johansson, A. E. Niell, and I. I. Shapiro (1995), Geodesy using the Global Positioning System: The effects of signal scattering on estimates of site position, J. Geophys. Res., 100(B6), 9921–9934, doi:10.1029/95JB00868.

Emery, K. O., and D. G. Aubrey (1991), Sea levels, land levels, and tide gauges, Springer Verlag, 237 pp.

Estey, L. H. and C. M. Meertens (1999), TEQC: the multi-purpose toolkit for GPS/GLONASS data, GPS Solutions, 3 (1), 44-49.

Ferland, R. (2006), From Relative to Absolute Antenna Phase Center Calibration: The effect on SINEX products, in Proceedings of the IGS Workshop 2006, Darmstadt, Germany.

Ferland, R., and M. Piraszewski (2009), The IGS-combined station coordinates, earth rotation parameters and apparent geocenter, J. Geod., 83, 385-392, doi:10.1007/s00190-008-0295-9.

Fiedler, J. W., and C. P. Conrad (2010), Spatial variability of sea level rise due to water impoundment behind dams, Geophys. Res. Lett., 37, L12603, doi:10.1029/2010GL043462.

Ge, M., G. Gendt, G. Dick, F. P. Zhang, and C. Reigber (2005), Impact of GPS satellite antenna offsets on scale changes in global network solutions, Geophys. Res. Lett., 32, L06310, doi:10.1029/2004GL022224.

Gelb, A. (1994), Applied Optimal Estimation, 374 pp., MIT Press, Cambridge, Mass.

Gehrels, W. R., G. A. Milne, J. R. Kirby, R. T. Patterson, and D. F. Daniel (2004), Late Holocene sea-level changes and isostatic crustal movements in Atlantic Canada, Quat. Int., 120, 79-89.

Griffiths, J., G. Gendt, T. Nischan, and J. Ray (2009), Assesment of the orbits from the 1st IGS reprocessing campaign, paper presented at the 2009 AGU Fall Meeting, 10 -14 December 2009, San Francisco, CA, Paper #G13A-04.

Heftin, M., W. Bertiger, G. Blewitt, A. Freedman, K. Hurst, S. Lichten, U. Lindqwister, Y. Vigue, F. Webb, T. Yunck, and J. Zumberge (1992), Global Geodesy Using GPS Without Fiducial Sites, Geophys. Res. Lett., 19, 131-134.

Hernandez-Pajares, M., J. M. Juan, J. Sanz, and R. Ors (2007), Secondorder ionospheric term in GPS: Implementation and impact on geodetic estimates, J. Geophys. Res., 112, B08417, doi:10.1029/2006JB004707.

Herring, T. A., R. W. King, and S. C. McClusky (2006a), GAMIT: ReferenceManual Version 10.34. Internal Memorandum, Massachusetts Institute of Technology, Cambridge.

Herring, T. A., R. W. King, and S. C. McClusky (2006b), GLOBK: Global Kalman filter VLBI and GPS analysis program Version 10.3. Internal Memorandum, Massachusetts Institute of Technology, Cambridge.

Holgate, S. J. (2007), On the decadal rates of sea level change during the twentieth century, Geophys. Res. Lett., 34, L01602, doi:10.1029/2006GL028492.

Hopfield, H. S. (1969), Two-quadratic tropospheric refractivity profile for correcting satellite data, J. Geophys. Res., 74, 4487–4499.

Imbrie, J., and K. P. Imbrie (1979), Ice Ages: Solving the Mystery, Harvard University Press, Cambridge, 224pp.

Jansen, E., J. Overpeck, K. R. Briffa, J.-C. Duplessy, F. Joos, V. Masson-Delmotte, D. Olago, B. Otto-Bliesner, W. R. Peltier, S. Rahmstorf, R. Ramesh, D. Raynaud, D. Rind, O. Solomina, R. Villalba and D. Zhang (2007), Palaeoclimate, in Climate Change 2007: The Physical Science Basis. Contribution of Working Group I to the Fourth Assessment Report of the Intergovernmental Panel on Climate Change [Solomon, S., D. Qin, M. Manning, Z. Chen, M. Marquis, K. B. Averyt, M. Tignor and H.L. Miller (eds.)]. Cambridge University Press, Cambridge, United Kingdom and New York, NY, USA.

Jevrejeva, S., J. C. Moore, A. Grinsted, and P. L. Woodworth (2008), Recent global sea level acceleration started over 200 years ago?, Geophys. Res. Lett., 35, L08715, doi:10.1029/2008GL033611.

Johnson, H. O., and D. C. Agnew (1995), Monument motion and measurements of crustal velocities, Geophys. Res. Lett., 22(21), 2905– 2908.

Johansson, J.M., J. L. Davis, H.-G. Scherneck, G. A. Milne, M. Vermeer, J. X. Mitrovica, R. A. Bennett, B. Jonsson, G. Elgered, P. Elósegui, H. Koivula, M. Poutanen, B. O. Rönnäng, and I. I. Shapiro (2002), Continuous GPS measurements of postglacial adjustment in Fennoscandia: 1. Geodetic results, J. geophys. Res., 107(B8), 2157, doi:10.1029/2001JB000400.

Kalman, R. E. (1960), A New Approach to Linear Filtering and Prediction Problems, Transactions of the ASME–Journal of Basic Engineering, 82 (Series D), 35-45.

Kass, W. G., R. L. Dulaney, J. Griffiths, S. Hilla, J. Ray, and J. Rohde (2009), Global GPS data analysis at the National Geodetic Survey, J. Geod., 83(3-4), 289-295.

Khan, S. A., J. Wahr, E. Leuliette, T. van Dam, K. M. Larson, and O. Francis (2008), Geodetic measurements of postglacial adjustments in Greenland, J. Geophys. Res., 113, B02402, doi:10.1029/2007JB004956.

King, M. A., and C. S. Watson (2010), Long GPS coordinate time series: Multipath and geometry effects, J. Geophys. Res., 115, B04403, doi:10.1029/2009JB006543.

Kouba, J., J. Ray, and M. M.Watkins (1998), IGS reference frame realization, 1998 IGS Analysis Center Workshop Proceedings, edited by J. M. Dow et al., pp. 139–172, European Space Operations Center, Darmstadt, Germany.

Kouba, J. (2007), Implementation and testing of the gridded Vienna Mapping Function 1, J. Geod., doi:10.1007/s00190-007-0170-0.

Kouba, J. (2009), Testing of Global Pressure/Temperature (GPT) Model and Global Mapping Function (GMF) in GPS analyses, J. Geod., 83, 3–4, 199–208. doi:10.1007/s00190-008-0229-6.

Lambeck, K. (2002), Sea-level change from mid-Holocene to recent time: An Australian example with global implications, in Ice Sheets, Sea Level and the Dynamic Earth [Mitrovica, J.X., and L.A. Vermeersen (eds.)]. Geodynamic Series Vol. 29, American Geophysical Union, Washington, DC, pp. 33–50.

Lambeck, K., M. Anzidei, F. Antonioli, A. Benini, and A. Esposito (2004), Sea level in Roman time in the Central Mediterranean and implications for recent change, Earth Planet. Sci. Lett., 224, 563–75.

Langbein, J. (2004), Noise in two-color electronic distance meter measurements revisited, J. Geophys. Res., 109, B04406, doi:10.1029/2003JB002819.

Langbein, J. (2008), Noise in GPS displacement measurements from Southern California and Southern Nevada, J. Geophys. Res., 113, B05405, doi:10.1029/2007JB005247.

Langbein, J., and H. Johnson (1997), Correlated error in geodetic time series: Implications for time-dependent deformation, J. Geophys. Res., 102(B1), 591– 604.

Lavallée, D. A., T. van Dam, G. Blewitt, and P. J. Clarke (2006), Geocenter motions from GPS: A unified observation model, J. Geophys. Res., 111, B05405, doi:10.1029/2005JB003784.

Legrand, J., N. Bergeot, C. Bruyninx, G. Wöppelmann, M.-N. Bouin, and Z. Altamimi (2010), Impact of regional reference frame definition on geodynamic interpretations, Journal of Geodynamics, 49, 116-122, doi:10.1016/j.jog.2009.10.002.

Lemoine, F. G., S. C. Kenyon, J. K. Factim, R. G. Trimmer, N. K. Pavlis, D. S. Chinn, C. M. Cox, S. M. Klosko, S. B. Luthcke, M. H. Torrence, Y. M. Wang, R. G. Williamson, E. C. Pavlis, H. Rapp, and T. R. Olson (1998), The development of the joint NASA GSFC and the National Imagery and Mapping Agency (NIMA) Geopotential Model EGM 96, Pub. Goddard Space Flight Center.

Leuliette, E. W., and L. Miller (2009), Closing the sea level rise budget with altimetry, Argo, and GRACE, Geophys. Res. Lett., 36, L04608, doi:10.1029/2008GL036010.

Le Treut, H., R. Somerville, U. Cubasch, Y. Ding, C. Mauritzen, A. Mokssit, T. Peterson, and M. Prather (2007), Historical Overview of Climate Change, in Climate Change 2007: The Physical Science Basis. Contribution of Working Group I to the Fourth Assessment Report of the Intergovernmental Panel on Climate Change [Solomon, S., D. Qin, M. Manning, Z. Chen, M. Marquis, K. B. Averyt, M. Tignor and H. L. Miller (eds.)]. Cambridge University Press, Cambridge, United Kingdom and New York, NY, USA.

Llovel, W., A. Cazenave, P. Rogel, and M. Berge-Nguyen (2009), 2-D reconstruction of past sea level (1950–2003) using tide gauge records and spatial patterns from a general ocean circulation model, in revision, Clim. Past., 5, 1-11.

Lyard, F., F. Lefevre, T. Letellier, and O. Francis (2006), Modelling the global ocean tides: modern insights from FES2004, Ocean Dynamics, 56, 394-415.

MacMillan, D. S. (1995), Atmospheric gradients from very long baseline interferometry observations, Geophys. Res. Lett., 22, 1041-1044.

Mader, G. L. (1999), GPS antenna calibration at the National Geodetic Survey, GPS Sol., 3(1), 50-48, doi:10.1007/PL00012780.

Mao, A., C. G. A. Harrison, and T. H. Dixon (1999), Noise in GPS coordinate time series, J. Geophys. Res., 104, 2797– 2816.

Marini, J. W. (1972), Correction of satellite tracking data for an arbitrary atmospheric profile, Radio Sci., 7, 223-231.

Mazzotti, S., C. Jones, and R. E. Thomson (2008), Relative and absolute sea level rise in western Canada and northwestern United States from a combined tide gauge-GPS analysis, J. Geophys. Res., 113, C11019, doi:10.1029/2008JC004835.

McCarthy, D., and G. Petit (2004), IERS Technical Note 32, IERS Conventions (2003), Technical report, Verlag des Bundesamts fur Kartographie und Geodasie, Frankfurt am Main, Germany.

Mignard, F. (2005), Famous, frequency analysis mapping on usual sampling, technical report, Obs. de la Cote d'Azur Cassiopée, Nice, France.

Milankovitch, M. (1941), Kanon der Erdbestrahlungen und seine Anwendung auf das Eiszeitenproblem. Belgrade. English translation by Pantic, N., 1998: Canon of Insolation and the Ice Age Problem, Alven Global, 636 pp.

Miller, L., and B. C. Douglas (2004), Mass and volume contributions to 20th century global sea level rise, Nature, 428, 406–409, doi:10.1038/nature02309.

Miller, L., and B. C. Douglas (2006), On the rate and causes of twentieth century sea-level rise, Philos. Trans. R. Soc. Lond., A 364, 805–820.

Milne, G. A., J. L. Davis, J. X. Mitrovica, H.-G. Scherneck, J. M. Johansson, M. Vermeer, and H. Koivula (2001), Space-Geodetic Constraints on Glacial Isostatic Adjustment in Fennoscandia, Science 23 March 2001, Vol. 291. no. 5512, pp. 2381-2385 DOI: 10.1126/science.1057022.

Mitchum, G. T. (2000), An improved calibration of satellite altimetric heights using tide gauge sea levels wtih adjustment for land motion, Marine Geodesy, 23, 145-166.

Mitrovica, J. X., M. E. Tamisiea, J. L. Davis, and G. A. Milne (2001), Recent mass balance of polar ice sheets inferred from patterns of global sea-level change, Nature, 409(6823), 1026-1029.

Munk, W. (2002), Twentieth century sea level: An enigma, in Proceedings of the National Academy of Sciences of the United States of America, 99(10), 6550.

Niell, A. E. (1996), Global mapping functions for the atmosphere delay at radio wavelengths, J. Geophys. Res., 101, 3227 − 3246, doi:10.1029/95JB03048.

Niell, A. E., A. J. Coster, F. S. Solheim, V. B. Mendes, P. C. Toor, R. B. Langley, and C. A. Upham (2001), Comparison of Measurements of Atmospheric Wet Delay by Radiosonde, Water Vapor Radiometer, GPS, and VLBI, Journal of Atmospheric and Oceanic Technology, 18, 830-850.

Niell, A. E. (2006), Interaction of Atmosphere Modeling and VLBI Analysis Strategy, in International VLBI Service for Geodesy and Astrometry 2006, General Meeting Proceedings, edited by Dirk Behrend and Karen Baver, NASA/CP-2006-214140.

Neilan, R., P. A. Van Scoy, and P. L. Woodworth (1998), Proceedings of the Workshop on Methods for Monitoring Sea Level : GPS and Tide Gauge Benchmark Monitoring, GPS Altimeter Calibration. Workshop Organised By the IGS and PSMSL, Jet Propulsion Laboratory, 17–18 March 1997. 202 pp.

Nicholls, R. J., P. P. Wong, V. R. Burkett, J. O. Codignotto, J. E. Hay, R. F. McLean, S. Ragoonaden, and C. D. Woodroffe (2007), Coastal systems and low-lying areas. Climate Change 2007: Impacts, Adaptation and Vulnerability. Contribution of Working Group II to the Fourth Assessment Report of the Intergovernmental Panel on Climate Change, M. L. Parry, O. F. Canziani, J. P. Palutikof, P. J. van der Linden and C. E. Hanson, Eds., Cambridge University Press, Cambridge, UK, 315-356.

Nocquet, J.M., E. Calais, and B. Parsons, (2005), Geodetic constraints on glacial isostatic adjustment in Europe, Geophys. Res. Lett., 32, L06308, doi:10.1029/2004GL022174.

Papoulis, A., and S. U. Pillai (2002), Probability, Random Variables and Stochastic Processes, McGraw-Hill, 4th edition.

Paulson, A., S. Zhong, and J. Wahr (2007), Inference of mantle viscosity from GRACE and relative sea level data, Geophys. J. Int. 171:497–508.

Peltier, W. R. (2001), Global glacial isostatic adjustment and modern instrumental records of relative sea level history, in Sea Level Rise: History and Consequences, edited by B. Douglas, et al., 65-95 pp., Int. Geophys. Ser. Academic, San Diego.

Peltier, W. R. (2002), On eustatic sea level history: Last Glacial Maximum to Holocene, Quat. Sci. Rev., 21, 1–3, 377–396.

Peltier, W. R. (2004), Global glacial isostasy and the surface of the ice-age earth: The ice-5G (VM2) model and grace, Annual Review of Earth and Planetary Sciences, 32, 111-149.

Peltier, W. R., and R. G. Fairbanks (2006), Global glacial ice volume and last glacial maximum duration from an extended Barbados sea level record, Quat. Sci. Rev., 25, 3322-3337.

Penna, N. T., M. A. King, and M. P. Stewart (2007), GPS height time series: Short-period origins of spurious long-period signals, J. Geophys. Res., 112, B02402, doi:10.1029/2005JB004047.

Petrie, E. J., M. A. King, P.Moore, and D. A. Lavallée (2010), Higher order ionospheric effects on the GPS reference frame and velocities, J. Geophys. Res., 115, B03417, doi:10.1029/2009JB006677.

Plag, H. P. (2006), Recent relative sea level trends: An attempt to quantify forcing factors, Philos. Trans. R. Soc. Lond., A 364:1841–69.

Prandi, P., A. Cazenave, and M. Becker (2009), Is coastal mean sea level rising faster than the global mean? A comparison between tide gauges and satellite altimetry over 1993–2007, Geophys. Res. Lett., 36, L05602, doi:10.1029/2008GL036564.

Press, W. H., B. P. Flannery, S. A. Teukolsky, and W. T. Vetterling (1992), Numerical Recipes, 818 pp., Cambridge Univ. Press, New York.

Ray, J. R. (1996), Measurements of length of day using the Global Positioning System, J. Geophys. Res., 101, B9, 20141-20149.

Ray, J., D. Dong, and Z. Altamimi (2004), IGS reference frames: status and future improvements, GPS Solutions, 8, 251-266, doi:10.1007/s10291-004-0110-x.

Ray, J., J. Kouba, and Z. Altamimi (2005), Is there utility in rigorous combinations of VLBI and GPS Earth orientation parameters?, J. Geod. 79(9), 505-511, doi: 10.1007/s00190-005-0007-7.

Ray, J., Z. Altamimi, X. Collilieux, and T. Van Dam (2008), Anomalous harmonics in the spectra of GPS position estimates, GPS Solut., 12(1), 55–64, doi:10.1007/s10291-007-0067-7.

Rothacher, M., and G. Mader (2003), Receiver and satellite antenna phase center offsets and variations. In: Tetreault P, Neilan R, Gowey K (eds) Proc. 2002 IGS Network, Data and Analysis Centre Workshop, Ottawa, pp. 141–152.

Saastamoinen, J. (1972), Atmospheric correction for the troposphere and stratosphere in radio ranging of satellites, in The Use of Artificial Satellites for Geodesy in Geodesy, Geophys. Monogr. Ser., vol. 15, edited by S. W. Henriksen, A. Mancini, and B. H. Chovitz, pp. 247–251, AGU, Washington, D. C.

Sanchez, L., and M. Krügel (2006), The role of the TIGA project in the unification of classical height systems, presented at the international IAG/FIG symposium on "Geodetic Reference Frames", GRF, 9–14 October 2006, Munich, Germany.

Santamaría, A., M.-N. Bouin, and G. Wöppelmann (2008a), New strategy for reprocessing a global GPS network at the ULR TIGA Analysis Centre, paper presented at the European Geosciences Union meeting, Vienna, 13 – 18 April, 2008.

Santamaría, A., M.-N. Bouin, G. Wöppelmann, and C. Letetrel (2008b), Variations à long terme du niveau de la mer dans un référentiel absolu: Apport de 10 ans de GPS, oral presentation at the Colloque CNFGG-G2 "L'eau dans tous ses Etats, visions spatiales", Paris, 17 – 18 November 2008.

Santamaría, A., M.-N. Bouin, and G. Wöppelmann (2009a), Impact of sub-network configuration on global scale GPS processing, paper presented at the European Geosciences Union meeting, Vienna, 19 – 24 April, 2009.

Santamaría, A., M.-N. Bouin, and G. Wöppelmann (2009b), Overview of current GPS processing strategy at ULR TIGA Analysis Center, oral presentation at the TIGA Splinter Meeting of the XI Session of the GLOSS Group of Experts, Paris, 11 – 15 May 2009.

Santamaría-Gómez, A., M.-N. Bouin, G. Wöppelmann, and X. Collilieux (2010), Accuracy of the ULR4 global GPS vertical velocity field for geophysical applications, oral presentation at the Symposium on Vertical Rates from GNSS, Newcastle, 2 July 2010.

Santamaría-Gómez. A., M-.N. Bouin, and G. Wöppelmann (in press), Improved GPS data analysis strategy for tide gauge benchmark monitoring, Proceedings of the International Association of Geodesy General Assembly, Buenos Aires, Argentina, August 31-September 4, 2009.

Scargle, J. D. (1982), Studies in astronomical time series analysis, II, Statistical aspects of spectral analysis of unevenly spaced points, Astrophs J., 263, 835–853.

Schenewerk, M. S., T. M. van Dam, and R. S. Nerem (1999), Seasonal motion in the Annapolis, Maryland GPS monument, GPS Solutions, Vol. 2, Num. 3, pp. 41-49.

Schmid, R., and M. Rothacher (2003), Estimation of elevation-dependent satellite antenna phase center variations of GPS satellites, J. Geod. 77(7-8), 440-446 doi:10.1007/s00190-003-0339-0

Schmid, R., M. Rothacher, D. Thaller, and P. Steigenberger (2005), Absolute phase center corrections of satellite and receiver antennas: Impact on global GPS solutions and estimation of azimuthal phase center variations of the satellite antenna, GPS, 9, doi:10.1007/s10291-005-0134-x.

Schmid, R., P. Steigenberger, G. Gendt, M. Ge, and M. Rothacher (2007), Generation of a consistent absolute phase-center correction model for GPS receiver and satellite antennas, J. Geod., 81, 781–798.

Schmid, R., X. Collilieux, F. Dilssner, R. Dach, and M. Schmidtz (2010), Updated phase center corrections for satellite and receiver antennas, paper presented at the IGS Workshop 2010, 28 June – 1 July, 2010, Newcastle, UK.

Schoene, T. (2006), Linking GPS to tide gauges and tide gauge benchmarks, World Climate Research Program Workshop on understanding sea-level rise and variability, 6–9 June 2006, UNESCO/IOC, Paris, France.

Schöne, T., N. Schön, and D. Thaller (2009), IGS Tide Gauge Benchmark Monitoring Pilot Project (TIGA): scientific benefits, J. Geod., 83, 249–261.

Sella, G. F., S. Stein, T. H. Dixon, M. Craymer, T. S. James, S. Mazzotti, and R. K. Dokka (2007), Observation of glacial isostatic adjustment in ''stable'' North America with GPS, Geophys. Res. Lett., 34, L02306, doi:10.1029/2006GL027081.

Shackleton, N. J. (2000), The 100,000-year ice-age cycle identified and found to lag temperature, carbon dioxide, and orbital eccentricity, Science, 289, 1897–1902.

Snay, R., M. Cline, W. Dillinger, R. Foote, S. Hilla, W. Kass, J. Ray, J. Rohde, G. Sella, and T. Soler (2007), Using global positioning system-derived crustal velocities to estimate rates of absolute sea level change from North American tide gauge records, J. Geophys. Res., 112, B04409, doi:10.1029/2006JB004606.

Solomon, S., D. Qin, M. Manning, Z. Chen, M. Marquis, K. B. Averyt, M. Tignor, and H. L. Miller (2007), Contribution of Working Group I to the Fourth Assessment Report of the Intergovernmental Panel on Climate Change, Cambridge University Press, Cambridge, United Kingdom and New York, NY, USA, 996 pp..

Steigenberger, P., J. Boehm, and V. Tesmer (2009), Comparison of GMF/GPT with VMF1/ECMWF and implications for atmospheric loading, J. Geod., doi:10.1007/s00190-009-0311-8, in press.

Stewart, M. P., N. T. Penna, and D. D. Lichti (2005), Investigating the propagation mechanism of unmodelled systematic errors on coordinate time series estimated using least squares, J. Geod., 79(8), 479–489, doi:10.1007/s00190-005-0478-6.

Tamisiea, M. E., J. X. Mitrovica, G. A. Milne, and J. L. Davis (2001), Global geoid and sea level changes due to present-day ice mass fluctuations, J. Geophys. Res., 106(B12), 30,849–30,863.

Teferle, F. N., R. M. Bingley, A. H. Dodson, T. F. Baker (2002), Application of the dual-CGPS concept to monitoring vertical land movements at tide gauges, Physics and Chemistry of the Earth, 27, 32-34, pp. 1401-1406.

Tesmer, V., J. Boehm, R. Heinkelmann, and H. Schuh (2007), Effect of different tropospheric mapping functions on the TRF, CRF and position time-series estimated from VLBI, J. Geod., doi:10.1007/s00190-006-0126-9.

Tregoning, P., P. J. Morgan, and R. Coleman (2004), The effect of receiver firmware upgrades on GPS vertical timeseries. Cah. Cent. Eur. Geodyn. Seismol., 23, 37–46.

Tregoning, P., and T. van Dam (2005), Atmospheric pressure loading corrections applied to GPS data at the observation level, Geophys. Res. Lett., 32, L22310, doi:10.1029/2005GL024104.

Tregoning, P., and T. A. Herring (2006), Impact of a priori zenith hydrostatic delay errors on GPS estimates of station heights and zenith total delays, Geophys. Res. Lett., 33, L23303, doi:10.1029/2006GL027706.

Tregoning, P., and C. Watson (2009), Atmospheric effects and spurious signals in GPS nalyses, J. Geophys. Res., 114, B09403, doi:10.1029/2009JB006344.

Tushingham, A. M., and W. R. Peltier (1991), Ice-3g - a New Global-Model of Late Pleistocene Deglaciation Based Upon Geophysical Predictions of Postglacial Relative Sea-Level Change, Journal of Geophysical Research-Solid Earth and Planets, 96(B3), 4497.

van Dam, T. M., G. Blewitt, and M. Heflin (1994), Detection of atmospheric pressure loading using the Global Positioning System, J. Geophys. Res., 99, 23,939-23,950.

van Dam, T., J. Wahr, P. C. D. Milly, A. B. Shmakin, G. Blewitt, D. Lavallée, and K. Larson (2001), Crustal displacements due to continental water loading, Geophys. Res. Lett., 28, 651–654.

van Dam, T., J. Wahr, and D. Lavallée (2007), A comparison of annual vertical crustal displacements from GPS and Gravity Recovery and Climate Experiment (GRACE) over Europe, J. Geophys. Res., 112, B03404, doi:10.1029/2006JB004335.

Vergnolle, M., M.-N. Bouin, L. Morel, F. Masson, S. Durand, J. Nicolas, and S. A. Melachroinos (2008), GPS estimates of ocean tide loading in NW-France: determination of ocean tide loading constituents and comparison with a recent ocean tide model, Geophys. J. Int., 173, 444–458, doi: 10.1111/j.1365-246X.2008.03734.x.

Vigue, Y., S. M. Lichten, G. Blewitt, M. B. Heflin, and R. P. Malla (1992), Precise determination of Earth's center of mass using measurements from the Global Positioning System, Geophys. Res. Lett., 19, 1487–1490.

Waelbroeck, C., L. Labeyriea, E. Michel, J. C. Duplessy, J. F. McManus, K. Lambeck, E. Balbon and M. Labracherie (2002), Sea-level and deep water temperature changes derived from benthic foraminifera isotopic records, Quat. Sci. Rev., 21(1–3), 295–305.

Watson, C., P. Tregoning, and R. Coleman (2006), Impact of solid Earth tide models on GPS coordinate and tropospheric time series, Geophys. Res. Lett., 33, L08306, doi:10.1029/2005GL025538.

Wilbanks, T. J., P. Romero Lankao, M. Bao, F. Berkhout, S. Cairncross, J.-P. Ceron, M. Kapshe, R. Muir-Wood, and R. Zapata-Marti (2007), Industry, settlement and society. Climate Change 2007: Impacts, Adaptation and Vulnerability. Contribution of Working Group II to the Fourth Assessment Report of the Intergovernmental Panel on Climate Change, M. L. Parry, O. F. Canziani, J. P. Palutikof, P. J. van der Linden and C. E. Hanson, Eds., Cambridge University Press, Cambridge, UK, 357-390.

Williams, S. D. P. (2003a), Offsets in Global Positioning System time series, J. Geophys. Res., 108(B6), 2310, doi:10.1029/2002JB002156.

Williams, S. D. P. (2003b), The effect of coloured noise on the uncertainties of rates estimated from geodetic time series, J. Geod., 76, 483– 494.

Williams, S. D. P., and P. Willis (2006), Error analysis of weekly station coordinates in the DORIS network, J. Geod., 80, 525-539, doi: 10.1007/s00190-006-0056-6.

Williams, S. D. P., Y. Bock, P. Fang, P. Jamason, R. M. Nikolaidis, L. Prawirodirdjo, M. Miller, and D. J. Johnson (2004), Error analysis of continuous GPS position time series, J. Geophys. Res., 109, B03412, doi:10.1029/2003JB002741.

Williams, S. D. P. (2008), CATS: GPS coordinate time series analysis software, GPS Solutions, 12(2), 147–153.

Woodworth, P. L. (2003), Some comments on the long sea level records from the Northern Mediterranean, J. Coast. Res., 19(1), 212-217.

Woodworth, P. L. (2006), Some important issues to do with long-term sea level change, Philos. Trans. R. Soc., Ser. A, 364, 787– 803.

Wöppelmann, G., S. McLellan, M.-N. Bouin, Z. Altamimi, and L. Daniel (2004), Current GPS data analysis at CLDG for the IGS TIGA Pilot Project, Cahiers du Centre Européen Géodynamique & de Sismologie, 23, 149–154.

Wöppelmann, G., B. Martin Miguez, M. N. Bouin, and Z. Altamimi (2007), Geocentric sea level trend estimates from GPS analyses at relevant tide gauges worldwide, Glob. Planet. Change, 57, 396–406.

Wöppelmann, G., M.-N. Bouin, and Z. Altamimi (2008), Terrestrial reference frame implementation in global GPS analysis at TIGA ULR consortium, Physics and Chesmistry of the Earth, 33, 3-4, 217-224.

Wöppelmann, G., C. Letretel, A. Santamaría, M. N. Bouin, X. Collilieux, Z. Altamimi, S. Williams, and B. Martín Míguez (2009), Rates of sea-level change over the past century in a geocentric reference frame, Geophys. Res. Lett., 36(L12607).

Wyatt, F. K. (1982), Displacements of surface monuments: Horizontal motion, J. Geophys. Res., 87(B2), 979– 989.

Wyatt, F. K., S. T. Morrisey, and D. C. Agnew (1988), Shallow borehole tilt: a reprise, J. Geophys. Res., 93(B8), 9197-9201.

Wyatt, F. K. (1989), Displacements of surface monuments: Vertical motion, J. Geophys. Res., 94(B2), 1655– 1664.

Yan, H., W. Chen, Y. Zhu, W. Zhang, and M. Zhong (2009), Contributions of thermal expansion of monuments and nearby bedrock to observed GPS height changes, Geophys. Res. Lett., 36, L13301, doi:10.1029/2009GL038152.

Zerbini, S., H.-P. Plag, T. Baker, M. Becker, H. Billiris, B. Bürki, H.-G. Kahle, I. Marson, L. Pezzoli, B. Richter, C. Romagnoli, M. Sztobryn, P. Tomasi, M. Tsimplis, G. Veis, and G. Verrone (1996), Sea level in the Mediterranean: a first step towards separation of crustal movements and absolute sea-level variations, Global Planet. Change, 14, 1–2, 1 – 48.

Zhang, J., Y. Bock, H. Johnson, P. Fang, S. Williams, J. Genrich, S. Wdowinski, and J. Behr (1997), Southern California permanent GPS geodetic array: Error analysis of daily position estimates and site velocities, J. Geophys. Res., 102(B8), 18035–18055.

Zhang, F. P., G. Gendt, M. Ge, and J. Wuensch (2004), Vertical rate of crustal motion at tide gauges derived by GPS, Geophys. Res. Abstr., 6, 03344.

Zhang, F. P., G. Gendt, and M. Ge (2007), GPS data processing at GFZ for monitoring the vertical motion of global tide gauge benchmarks, Technical report for projects TIGA and SEAL, GeoForschungsZentrum Potsdam, Scientific Technical Report STR07/02, p. 28.

Zhu, S. Y., F.-H. Massmann, Y. Yu, and C. Reigber (2003), Satellite antenna phase center offsets and scale errors in GPS solutions, J. Geod., 76, 668–672, doi:10.1007/s00190-002-0294-1.

ANNEXES

A1. ULR3 strategy summary

```
===============================================================================
|                      ULR ANALYSIS STRATEGY SUMMARY                          |
|                      (template version 2.0, 07 Aug. 2006)                   |
===============================================================================
| Analysis Center   | French Consortium of                                   |
|                   | University of La Rochelle, UMR 6250 LIENSs             |
|                   | and IGN's geodetic research laboratory LAREG           |
|                   |                                                        |
|                   |  Université de La Rochelle                             |
|                   |  Bat.  ILE                                             |
|                   |  2 rue Olympe de Gouges                                |
|                   |  17000 LA ROCHELLE                                     |
|-------------------------------------------------------------------------------|
| Contact people    | Guy Woppelmann                                         |
|                   |      e-mail: gwoppelm@univ-lr.fr                       |
|                   | Marie-Noelle Bouin                                     |
|                   |      e-mail: Marie-Noelle.Bouin@meteo.fr              |
|                   | Alvaro Santamaria Gomez                                |
|                   |      e-mail: asantamaria@fomento.es                   |
|-------------------------------------------------------------------------------|
| Software used     | GAMIT v. 10.21 for GPS observations processing         |
|                   | CATREF for station coordinate solutions combination    |
|                   |        and alignment to ITRF2005                       |
|-------------------------------------------------------------------------------|
| GNSS system(s)    | GPS                                                    |
|-------------------------------------------------------------------------------|
| Final products    | ulrWWWW7.snx weekly SINEX file                         |
| generated for     |                                                        |
| GPS Week 'WWWW'   |                                                        |
| day of Week 'n'   |                                                        |
| (n=0,1,...,6)     |                                                        |
|-------------------------------------------------------------------------------|
| Preparation date  | 2008-07-15 (original updated version)                  |
|-------------------------------------------------------------------------------|
| Modification dates|                                                        |
|-------------------------------------------------------------------------------|
| Effective date    | 1997-01-01/2006-11-18 (GPSW 886/1401)                  |
| for data analysis |                                                        |
===============================================================================


===============================================================================
|                      MEASUREMENT MODELS                                     |
|-------------------------------------------------------------------------------|
| Preprocessing     | Five sub-networks including up to 50 stations manually |
|                   | selected with worlwide distribution.                   |
|                   | Small RINEX files (less than 6 hours of observations)  |
|                   | are discarded.                                         |
|-------------------------------------------------------------------------------|
| Basic observable  | Double-differenced carrier phase with ionosphere-free  |
|                   | combination of L1 and L2 carriers (LC or L3). Code     |
|                   | pseudoranges are used to obtain receiver clock offsets |
|                   | and in the ambiguity resolution with the               |
|                   | Melbourne-Wuebbena widelane method. Non-redundant      |
```

```
|                   | baselines are estimated.                          |
|                   |---------------------------------------------------|
|                   | Elevation angle cutoff: 10 degrees                |
|                   | Sampling rate: 30 seconds for cleaning            |
|                   |              5 minutes for parameter estimation   |
|                   | Weighting: at first inversion phases are weighted by |
|                   |            elevation angle, then the scatter of the  |
|                   |            phase residuals are estimated by station and|
|                   |            are used in the second inversion where    |
|                   |            phases are weighted by elevation angle and |
|                   |            by station. Phases are not satellite-     |
|                   |            dependent weighted.                    |
|                   | Code biases: C1 & P2' corrected to P1 & P2 using  |
|                   |            receiver type dependent monthly tables from |
|                   |            http://www.qiub.unibe.ch/ionosphere/p1c1.dcb|
|-------------------------------------------------------------------------|
| Modeled           | Double-differenced carrier phase with ionosphere-free |
| observables       | linear combination applied.                       |
|-------------------------------------------------------------------------|
|*Satellite antenna| SV-specific z-offsets & block-specific x- & y-offsets |
| -center of mass   | (from manufacturers) from file igs_test05.atx based on |
| offsets           | GFZ/TUM analyses using fixed IGb00 coordinates (see |
|                   | IGSMail #5149, 12 May 2005).                       |
|-------------------------------------------------------------------------|
|*Satellite antenna| Block-specific nadir angle-dependent "absolute" PCVs |
| phase center      | applied from file igs_test05.atx; no azimuth-dependent |
| corrections       | corrections applied (see IGSMail #5149, 12 May 2005 |
|-------------------------------------------------------------------------|
|*Satellite clock   | 2nd order relativistic correction for non-zero    |
| corrections       | orbit ellipticity (-2*R*V/c) applied              |
|-------------------------------------------------------------------------|
| GPS attitude      | GPS satellite yaw attitude model: applied (Bar-Server, |
| model             | 1995) based on nominal yaw rates.                 |
|-------------------------------------------------------------------------|
|*RHC phase         | Phase wind-up applied according to Wu et al. (1993) |
| rotation corr.    |                                                   |
|-------------------------------------------------------------------------|
|*Ground antenna    | "Absolute" elevation- & azimuth-dependent (when   |
| phase center      | available) PCVs & L1/L2 offsets from ARP applied from |
| offsets &         | file igs_test05.atx                               |
| corrections       | (see IGSMail #5149, 12 May 2005).                 |
|-------------------------------------------------------------------------|
|*Antenna radome    | Calibration applied if given in file igs_test05.atx; |
| calibrations      | otherwise radome effect neglected (radome => NONE) |
|-------------------------------------------------------------------------|
|*Marker -> antenna| dN,dE,dU eccentricities from site logs applied to  |
| ARP eccentricity  | compute station marker coordinates                |
|-------------------------------------------------------------------------|
| Troposphere       | Met data input: Standard temperature and          |
| a priori model    |                 height dependent pressure data    |
|                   |---------------------------------------------------|
| (parameter        | Zenith delay: Saastamoinen (1972) "dry" + "wet" using |
|  estimation is    |               synthesized input met data          |
|  below)           |---------------------------------------------------|
|                   | Mapping function: GMF (Boehm et al., 2006) dry & wet |
|                   |---------------------------------------------------|
|                   | Horiz. grad. model: no a priori gradient model is used |
|-------------------------------------------------------------------------|
|*Ionosphere        | 1st order effect: accounted for by using the ionosphere|
```

```
|                     |                           free linear combination (LC or L3)  |
|                     |----------------------------------------------------------------|
|                     | 2nd order effect: no corrections applied                       |
|                     |----------------------------------------------------------------|
|                     | Other effects:    no other corrections applied                 |
|---------------------|----------------------------------------------------------------|
|*Tidal               |*Solid Earth tide: IERS 2003 (dehanttideinel.f routine, |
| displacements       |                based on Chap. 7.1.2)                   |
|                     |----------------------------------------------------------------|
|                     |*Permanent tide: zero-frequency contribution left in    |
| (IERS Conventions|                    tide model, NOT in site coordinates    |
| 2003, Ch. 4, eqn |----------------------------------------------------------------|
| 11 contributions)|*Solid Earth pole tide: IERS 2003; mean pole removed    |
|                     |                by linear trend (Ch. 7, eqn 23a & 23b)  |
|                     |----------------------------------------------------------------|
|                     |*Oceanic pole tide: no model is applied                 |
|                     |----------------------------------------------------------------|
|                     |*Ocean tide loading: IERS Conventions 2003 (updated     |
|                     |                Ch. 7, 2006) using site-dependent       |
|                     |                amplitudes & phases for 11 main tidal   |
|                     |                constituents from the Scherneck & Bos   |
|                     |                web-based Ocean Tide Loading provider   |
|                     |                using the CSR4.0 ocean tide model;      |
|                     |                CMC corrections applied to SP3 orbits.  |
|                     |----------------------------------------------------------------|
|                     |*Ocean tide geocenter: site-dependent coeffs corrected  |
|                     |                for center of mass motion of whole      |
|                     |                Earth; CMC corrections also applied     |
|                     |                to SP3 orbits.                          |
|                     |----------------------------------------------------------------|
|                     | Atmosphere tides: not applied                          |
|---------------------|----------------------------------------------------------------|
|*Non-tidal           | Atmospheric pressure:  not applied                     |
| loadings            |----------------------------------------------------------------|
|                     | Ocean bottom pressure: not applied                     |
|                     |----------------------------------------------------------------|
|                     | Surface hydrology:     not applied                     |
|                     |----------------------------------------------------------------|
|                     | Other effects:         none applied                    |
|---------------------|----------------------------------------------------------------|
|*Earth orientation| Ocean tidal: diurnal/semidiurnal variations in x,y, &  |
| variations          |         UT1 applied according to IERS 2003.            |
|                     |----------------------------------------------------------------|
| (near 12 & 24 hr | Atmosphere tidal: S1, S2, S3 tides not applied         |
| only; longer        |----------------------------------------------------------------|
| period tidal        | High-frequency nutation: prograde diurnal polar motion |
| corrections         |         corrections applied using IERS routine         |
| should not be       |         (IERS 2003, Table 5.1)                         |
| applied)            |----------------------------------------------------------------|
|                     |                                                        |
| [NOTE: effects are included in observation model as well as in the       |
|  transformation of orbits from inertial to terrestrial frame]            |
================================================================================


================================================================================
|                           REFERENCE FRAMES                                   |
|------------------------------------------------------------------------------|
| Time argument    | GPS time as given by observation epochs, which is         |
|                  | offset by only a fixed constant (approx.) from TT/TDT     |
```

```
|---------------------------------------------------------------------------|
| Inertial       | Geocentric; mean equator and equinox of 2000 Jan 1.5     |
| frame          | (J2000.0)                                                |
|---------------------------------------------------------------------------|
| Terrestrial    | ITRF2005 applying the Minimal Constraint Approach on     |
|                | the 7 transformation parameters between ITRF2005 datum   |
|                | (comprising up to 91 IGS05 stations) and the station     |
|                | coordinate solutions. CATREF (Altamimi et al. 2007)      |
|---------------------------------------------------------------------------|
| Tracking       | Tracking network is global: up to 225 stations, among    |
| network        | which 160 are CGPS@TG and 91 are IGS05 stations.         |
|                | Stations are distributed into 5 subnetworks with up to   |
|                | 50 globally distributed stations each.                   |
|                | Subnetworks are combined (and aligned to ITRF2005) to    |
|                | form daily solutions by applying the above mentionned    |
|                | approach with up to 20 globally distributed IGS05 RF     |
|                | stations in the ITRF2005 datum.                          |
|                | Daily solutions are combined and aligned to ITRF2005     |
|                | using the same approach to form the weekly solutions     |
|---------------------------------------------------------------------------|
| Interconnection| Precession: IAU 1976 Precession Theory                   |
| (EOP parameter |----------------------------------------------------------|
| estimation is  | Nutation: IAU 1980 Nutation Theory                       |
| below)         |----------------------------------------------------------|
|                | A priori EOPs: UT1 and polar motion interpolated from    |
|                |               IERS Bulletin B.                           |
|===========================================================================|


|===========================================================================|
|                            ORBIT MODELS                                   |
|---------------------------------------------------------------------------|
| Geopotential   | EGM96 degree and order 9;                                |
| (static)       | C21 & S21 modeled according to polar motion variations   |
|                | (IERS 2003, Chap. 6)                                     |
|                |----------------------------------------------------------|
|                | GM=398600.4415 km**3/sec**2 (for TT/TDT time argument)   |
|                |----------------------------------------------------------|
|                | AE = 6378136.3 m                                         |
|---------------------------------------------------------------------------|
| Tidal variations|*Solid Earth tides: C20,C21,S21,C22, and S22 as in IERS  |
| in geopotential |    (1992); n=2 order-dependent Love numbers & frequency  |
|                |    dependent corrections for 6 (2,1) tides according to  |
|                |    R. Eanes communication (1995)                         |
|                |----------------------------------------------------------|
|                | Ocean tides: no model applied                            |
|                |----------------------------------------------------------|
|                |*Solid Earth pole tide: no model applied in orbit models  |
|                |----------------------------------------------------------|
|                | Oceanic pole tide: no model applied                      |
|---------------------------------------------------------------------------|
| Third-body     | Sun & Moon as point masses                               |
| forces         |----------------------------------------------------------|
|                | Ephemeris: Generated from the MIT PEP program            |
|                |----------------------------------------------------------|
|                | GM_Sun              132712440000.0000  km**3/sec**2      |
|                | GM_Moon                     4902.7989  km**3/sec**2      |
|---------------------------------------------------------------------------|
| Solar radiation| A priori: nominal block-dependent constant direct        |
| pressure model |          acceleration; Berne 9-parameter SRP model       |
```

		with direct, y-axis, B-axis scales and once-
		per-revolution accelerations (sine & cosine
		terms) along each of the three axes.
(parameter		---
estimation is		Earth shadow model: umbra & penumbra included
below)		---
		Earth albedo: not applied

		Moon shadow model: umbra & penumbra included

		Satellite attitude: model of Bar-Sever applied (see
		IGSMail #0591, 9 May 1994); using
		nominal yaw rates.

		Other forces: none applied
*Relativitic	Dynamical correction: not applied
effects		(see IERS 2003, Ch. 10, eqn 1)

		Gravitational time delay: IERS 2003, Ch. 11, eqn 17
		applied
Numerical	Adams-Moulton fixed-step, 11-pt predictor-corrector
integration	with Nordsieck variable-step starting procedure (see
	Ash, 1972 and references therein).

		Integration step-size: 75 s; tabular interval: 15 min.

		Starter procedure: Runge-Kutta Formulation; initial
		conditions taken from prior orbit solution at 12:00

		Arc length: 24 hours (00:00:00 - 23:59:30 GPS time)

ESTIMATED PARAMETERS (& APRIORI VALUES & CONSTRAINTS)
Adjustment	Weighted least squares method to generate loosely
	constrained solutions and covariance matrices that
	are passed to CATREF Software for combination and
	alignment to the ITRF2005.
Data span	24 hours used for each daily analysis
	(00:00:00 - 23:59:30 GPS time)
*Station	Free network strategy (constraints to a priori values
coordinates	are between 1 m. and 100 m., no station is fixed). All
	station coordinates are adjusted, relative to the a
	priori values from ITRF2005.snx
Satellite clocks	Estimated using one-way phase data aligned with
	pseudorange.

		No clk files are printed out.
Receiver clocks	Estimated during clock estimation.
Orbits	Geocentric position and velocity, solar radiation
	pressure scales and once-per-revolution perturbation

	terms. Radiation pressure scaling factors and perturbation terms are estimated for each of the orthogonal directions: satellites - sun, body centered Y, and orthogonal third directions estimated as constant offsets for each one-day arc; plus once-per-rev sine/cosine terms are estimated with apriori values from the prior day. The constraints are 0.01 ppm or 20 cm for initial conditions and 0.01% for the direct radiation-presssure, y-bias, third axis coefficients and the once-per-rev parameters.
	Orbits estimated per global sub-network are not combined. No sp3 files are printed out.
Satellite attitude	No attitude parameters are adjusted
Troposphere	Zenith delay: residual delays are adjusted for each station assuming mostly dominated by "wet" component and parameterized by a piecewise linear, continuous model with 2 hour intervals.
	Mapping function: GMF (Boehm et al., 2006) wet function used to estimate zenith delay residuals.
	Zenith delay epochs: each even-integer hour
	Gradients: one N-S & one E-W gradient parameter for each day and each station, with continuous linear variation during the day; 0.03 m. at 10 degree elevation 1 sigma constraint is applied at all stations. Mapping function from Chen and Herring (1997) is used.
Ionospheric correction	Not estimated
Ambiguity	Real-valued double-differenced phase cycle ambiguities adjusted except when they can be resolved confidently in which case they are fixed using the Melboune-Wuebbena widelane to resolve L1-L2 cycles and then estimation to resolve L1 and L2 cycles.
*Earth orientation parameters (EOP)	Daily x & y pole offsets, pole-rates, UT1 and LOD. x and y pole estimated as piece-wise, linear offsets. A priori vaules from IERS Bulletin B. Constraints are 0.001 arcsec (~3 cm) for Wobble, 0.0005 arcsec/day (~1.5 cm/day) for Wobble rate, 0.00001 sec for UT1 and 0.0001 sec/day for LOD.
Other parameters	None

REFERENCES
Altamimi, Z., X. Collilieux, J. Legrand, B. Garayt & C. Boucher, ITRF2005:

| A new release of the International Terrestrial Reference Frame based on |
| time series of station positions and Earth Orientation Parameters. |
| J. Geophys. Res. 112(B9), 2007. |
| |
| Ash, M.E., Deter,ination of Earth satellite orbits, Tech. Note 1972-5, |
| Lincoln Laboratory, MIT, 19 April 1972. |
| |
| Bar-Sever, Y.E., New GPS attitude model, IGS Mail #591, 1995, |
| http://igscb.jpl.nasa.gov/mail/igsmail/1994/msg00166.html |
| |
| Boehm, J., A.E. Niell, P. Tregoning, & H. Schuh, Global Mapping Function |
| (GMF): A new empirical mapping function based on numerical weather |
| model data, Geophys. Res. Lett., 33, L07304, doi: 10.1029/2005GL025545, |
| 2006. |
| |
| Boehm, J., R. Heinkelmann, & H. Schuh, Short Note: A global model of |
| pressure and temperature for geodetic applications, J. Geod., |
| doi:10.1007/s00190-007-0135-3, 2007. |
| |
| Chen, G. and T.A. Herring, Effects of atmospheric azimuthal asymmetry of |
| the analysis of space geodetic data, J. Geophys. Res., 102, 20, 489-20, |
| 502, 1997. |
| |
| IERS Conventions 2003, D.D. McCarthy & G. Petit (editors), IERS Technical |
| Note 32, Frankfurt am Main: Verlag des Bundesamts fuer Kartographie und |
| Geodaesie, 2004. (see also updates at website) |
| |
| Saastamoinen, J., Atmospheric correction for the troposphere and |
| stratosphere in radio ranging of satellites, in The Use of Artificial |
| Satellites for Geodesy, Geophys. Monogr. Ser. 15 (S.W. Henriksen et al.,|
| eds.), AGU, Washington, D.C., pp.247-251, 1972. |
| |
| Wu, J.T., S.C. Wu, G.A. Hajj, W.I. Bertiger, & S.M. Lichten, Effects of |
| antenna orientation on GPS carrier phase, Manuscripta Geodaetica,18, |
| 91-98, 1993. |
==

A2. ULR4 strategy summary

```
================================================================================
|                       ULR ANALYSIS STRATEGY SUMMARY                          |
|                      (template version 2.0, 07 Aug. 2006)                    |
================================================================================
| Analysis Center   | French Consortium of                                     |
|                   | University of La Rochelle, UMR 6250 LIENSs               |
|                   | and IGN's geodetic research laboratory LAREG             |
|                   |                                                          |
|                   |  Université de La Rochelle                               |
|                   |  Bat.  ILE                                               |
|                   |  2 rue Olympe de Gouges                                  |
|                   |  17000 LA ROCHELLE                                       |
|-------------------------------------------------------------------------------|
| Contact people    | Guy Woppelmann                                           |
|                   |       e-mail: gwoppelm@univ-lr.fr                        |
|                   | Marie-Noelle Bouin                                       |
|                   |       e-mail: Marie-Noelle.Bouin@meteo.fr               |
|                   | Alvaro Santamaria Gomez                                  |
|                   |       e-mail: asantamaria@fomento.es                     |
|-------------------------------------------------------------------------------|
| Software used     | GAMIT/GLOBK v.10.34  for GPS observations processing     |
|                   |                      and daily combination of sub-networks|
|                   | CATREF    for weekly station coordinates combination     |
|-------------------------------------------------------------------------------|
| GNSS system(s)    | GPS                                                      |
|-------------------------------------------------------------------------------|
| Final products    | ulrWWWW7.snx weekly SINEX file                           |
| generated for     | ulrWWWWn.sp3 daily orbit & satellite clock files        |
| GPS Week 'WWWW'   | ulrWWWWn.clk daily station and SV clock files           |
| day of Week 'n'   | ulrWWWW7.erp weekly ERP file of daily values            |
| (n=0,1,...,6)     |                                                          |
|-------------------------------------------------------------------------------|
| Preparation date  | 2009-01-01 (updated version)                            |
|-------------------------------------------------------------------------------|
| Modification dates| 2009-01-01: Refined pre-processing of RINEX files       |
|                   |             Sampling rate from 5 min to 3 min            |
|                   |             Antenna calibration file from igs_test05    |
|                   |                to igs05_1515.atx                        |
|                   |             GMF to VMF1 mapping function                 |
|                   |             Standard to GPT model met data              |
|                   |             CSR4.0 to FES2004 ocean tide model          |
|                   |             Only NNR constraints in datum definition    |
|                   |             Static to dynamic subnetworks definition    |
|                   |             IAU 1980 to IAU 2000 nutation theory        |
|                   |             One to two gradients per day estimates      |
|                   |             Loose a priori constraints on Wobble        |
|-------------------------------------------------------------------------------|
| Effective date    | 1997-01-01/2007-12-31 (GPSW 886/1459)                   |
| for data analysis |                                                          |
================================================================================


================================================================================
|                          MEASUREMENT MODELS                                  |
|-------------------------------------------------------------------------------|
```

Preprocessing	Very small compressed RINEX files (less than 50KB) are directly discarded. Small compressed RINEX files (between 50KB and 100KB) are analyzed with TEQC and files with less than 5000 observations are discarded.
Basic observable	Double-differenced carrier phase with ionosphere-free combination of L1 and L2 carriers (LC or L3). Code pseudoranges are used to obtain receiver clock offsets and in the ambiguity resolution with the Melbourne-Wuebbena widelane method. Non-redundant baselines are estimated.
	Elevation angle cutoff: 10 degrees Sampling rate: 30 seconds for cleaning 3 minutes for parameter estimation Weighting: at first inversion phases are weighted by elevation angle, then the scatter of the phase residuals are estimated by station and are used in the second inversion where phases are weighted by elevation angle and by station. Phases are not satellite-dependent weighted. Code biases: C1 & P2' corrected to P1 & P2 using receiver type dependent monthly tables from http://www.qiub.unibe.ch/ionosphere/p1c1.dcb
Modeled observables	Double-differenced carrier phase with ionosphere-free linear combination applied.
*Satellite antenna -center of mass offsets	SV-specific z-offsets & block-specific x- & y-offsets (from manufacturers) from file igs05_1515.atx based on GFZ/TUM analyses using fixed IGb00 coordinates (see IGSMail #5149, 12 May 2005).
*Satellite antenna phase center corrections	Block-specific nadir angle-dependent "absolute" PCVs applied from file igs05_1515.atx; no azimuth-dependent corrections applied (see IGSMail #5149, 12 May 2005).
*Satellite clock corrections	2nd order relativistic correction for non-zero orbit ellipticity (-2*R*V/c) applied
GPS attitude model	GPS satellite yaw attitude model: applied (Bar-Server, 1995) based on nominal yaw rates.
*RHC phase rotation corr.	Phase wind-up applied according to Wu et al. (1993)
*Ground antenna phase center offsets & corrections	"Absolute" elevation- & azimuth-dependent (when available) PCVs & L1/L2 offsets from ARP applied from file igs05_1515.atx (see IGSMail #5149, 12 May 2005).
*Antenna radome calibrations	Calibration applied if given in file igs05_1515.atx; otherwise radome effect neglected (radome => NONE)
*Marker -> antenna ARP eccentricity	dN,dE,dU eccentricities from site logs applied to compute station marker coordinates
Troposphere	met data input: synthesized met data from GPT model,

a priori model	Boehm et al. (2007), with relative humidity set to 50% for all sites.
(parameter estimation is below)	Zenith delay: dry values by station extracted from VMF1 grid at ellipsoidal surface, height corrections using Saastamoinen (1972) with GPT met data. wet values using Saastamoinen (1972) with GPT met data.
	Mapping function: VMF1 (Boehm et al., 2006) dry & wet.
	Horiz. grad. model: no a priori gradient model is used
*Ionosphere	1st order effect: accounted for by using the ionosphere free linear combination (LC or L3)
	2nd order effect: no corrections applied
	Other effects: no other corrections applied
*Tidal displacements	*Solid Earth tide: IERS 2003 (dehanttideinel.f routine, based on Chap. 7.1.2)
	*Permanent tide: zero-frequency contribution left in tide model, NOT in site coordinates
(IERS Conventions 2003, Ch. 4, eqn 11 contributions)	*Solid Earth pole tide: IERS 2003; mean pole removed by linear trend (Ch. 7, eqn 23a & 23b)
	*Oceanic pole tide: no model is applied
	*Ocean tide loading: IERS Conventions 2003 (updated Ch. 7, 2006) using site-dependent amplitudes & phases for 11 main tidal constituents from the Scherneck & Bos web-based Ocean Tide Loading provider using the FES2004 ocean tide model; CMC corrections applied to SP3 orbits.
	*Ocean tide geocenter: site-dependent coeffs corrected for center of mass motion of whole Earth; CMC corrections also applied to SP3 orbits.
	Atmosphere tides: not applied
*Non-tidal loadings	Atmospheric pressure: not applied
	Ocean bottom pressure: not applied
	Surface hydrology: not applied
	Other effects: none applied
*Earth orientation variations	Ocean tidal: diurnal/semidiurnal variations in x,y, & UT1 applied according to IERS 2003.
(near 12 & 24 hr	Atmosphere tidal: S1, S2, S3 tides not applied

```
| only; longer    |---------------------------------------------------------|
| period tidal    | High-frequency nutation: prograde diurnal polar motion  |
| corrections     |          corrections applied using IERS routine         |
| should not be   |             (IERS 2003, Table 5.1)                      |
| applied)        |---------------------------------------------------------|
|                                                                             |
| [NOTE: effects are included in observation model as well as in the          |
|  transformation of orbits from inertial to terrestrial frame]               |
===============================================================================


===============================================================================
|                          REFERENCE FRAMES                                   |
|-----------------------------------------------------------------------------|
| Time argument   | GPS time as given by observation epochs, which is         |
|                 | offset by only a fixed constant (approx.) from TT/TDT     |
|-----------------------------------------------------------------------------|
| Inertial        | Geocentric; mean equator and equinox of 2000 Jan 1.5      |
| frame           | (J2000.0)                                                 |
|-----------------------------------------------------------------------------|
| Terrestrial     | ITRF2005 reference frame realized through the set of up|
| frame           | to 126 station coordinates and velocities given in the   |
|                 | IGS internal realization IGS05.snx (aligned to           |
|                 | ITRF2005).  Reference sites may be removed from the      |
|                 | realization if the standard deviation of their           |
|                 | position estimates deviates too much from the median     |
|                 | sigma of the remaining reference sites or if their       |
|                 | position estimate deviates by more than 4-sigma from     |
|                 | the apriori value. Conditions are applied iteratively.   |
|                 | The datum is specified only for orientation using NNR    |
|                 | constraints wrt IGS05 coordinates.                       |
|-----------------------------------------------------------------------------|
| Tracking        | Tracking network is global: up to 299 stations, among    |
| network         | which 200 are CGPS@TG and 126 are IGS05 stations.        |
|                 | Stations are dynamically distributed into daily sub-     |
|                 | networks, based on geometry and on data availibily.      |
|                 | The subnetworks are equitably filled out up to 50        |
|                 | stations maximum. 6 common stations are dynamically      |
|                 | selected from the available IGS05 stations for daily     |
|                 | subnetworks combination.                                 |
|-----------------------------------------------------------------------------|
| Interconnection | Precession: IAU 1976 Precession Theory                   |
| (EOP parameter  |----------------------------------------------------------|
| estimation is   | Nutation: IAU 2000 Nutation Theory                       |
| below)          |----------------------------------------------------------|
|                 | A priori EOPs: UT1 and polar motion interpolated from    |
|                 |            IERS Bulletin B.                              |
===============================================================================


===============================================================================
|                             ORBIT MODELS                                    |
|-----------------------------------------------------------------------------|
| Geopotential    | EGM96 degree and order 9;                                |
| (static)        | C21 & S21 modeled according to polar motion variations   |
|                 | (IERS 2003, Chap. 6)                                     |
|                 |----------------------------------------------------------|
|                 | GM=398600.4415 km**3/sec**2 (for TT/TDT time argument)   |
|                 |----------------------------------------------------------|
|                 | AE = 6378136.3 m                                         |
|-----------------------------------------------------------------------------|
```

```
| Tidal variations |*Solid Earth tides: C20,C21,S21,C22, and S22 as in IERS |
| in geopotential  |    (1992); n=2 order-dependent Love numbers & frequency |
|                  |    dependent corrections for 6 (2,1) tides according to  |
|                  |    R. Eanes communication (1995)                         |
|                  |----------------------------------------------------------|
|                  | Ocean tides: no model applied                            |
|                  |----------------------------------------------------------|
|                  |*Solid Earth pole tide: no model applied in orbit models|
|                  |----------------------------------------------------------|
|                  | Oceanic pole tide: no model applied                      |
|------------------------------------------------------------------------------|
| Third-body       | Sun & Moon as point masses                               |
| forces           |----------------------------------------------------------|
|                  | Ephemeris: Generated from the MIT PEP program            |
|                  |----------------------------------------------------------|
|                  | GM_Sun              132712440000.0000  km**3/sec**2      |
|                  | GM_Moon                      4902.7989  km**3/sec**2      |
|------------------------------------------------------------------------------|
| Solar radiation  | A priori: nominal block-dependent constant direct        |
| pressure model   |           acceleration; Berne 9-parameter SRP model      |
|                  |           with direct, y-axis, B-axis scales and once-   |
|                  |           per-revolution accelerations (sine & cosine    |
|                  |           terms) along each of the three axes.           |
| (parameter       |----------------------------------------------------------|
| estimation is    | Earth shadow model: umbra & penumbra included            |
| below)           |----------------------------------------------------------|
|                  | Earth albedo:      not applied                           |
|                  |----------------------------------------------------------|
|                  | Moon shadow model:  umbra & penumbra included            |
|                  |----------------------------------------------------------|
|                  | Satellite attitude: model of Bar-Sever applied (see      |
|                  |                     IGSMail #0591, 9 May 1994); using    |
|                  |                     nominal yaw rates.                   |
|                  |----------------------------------------------------------|
|                  | Other forces:      none applied                          |
|------------------------------------------------------------------------------|
|*Relativitic      | Dynamical correction: not applied                        |
| effects          |                       (see IERS 2003, Ch. 10, eqn 1)     |
|                  |----------------------------------------------------------|
|                  | Gravitational time delay: IERS 2003, Ch. 11, eqn 17      |
|                  |                           applied                        |
|------------------------------------------------------------------------------|
| Numerical        | Adams-Moulton fixed-step, 11-pt predictor-corrector      |
| integration      | with Nordsieck variable-step starting procedure (see     |
|                  | Ash, 1972 and references therein).                       |
|                  |----------------------------------------------------------|
|                  | Integration step-size: 75 s; tabular interval: 15 min.   |
|                  |----------------------------------------------------------|
|                  | Starter procedure: Runge-Kutta Formulation; initial      |
|                  | conditions taken from prior orbit solution at 12:00      |
|                  |----------------------------------------------------------|
|                  | Arc length: 24 hours (00:00:00 - 23:59:30 GPS time)      |
================================================================================


================================================================================
|          ESTIMATED PARAMETERS (& APRIORI VALUES & CONSTRAINTS)               |
|------------------------------------------------------------------------------|
| Adjustment       | Weighted least squares to generate loosely constrained   |
|                  | covariance matrices and solutions that are passed        |
```

	to a Kalman filter (GLOBK) for subnetwork combinations and orbits determination, and then to a weighted least squares (CATREF) adjustment for weekly commbinations.
Data span	24 hours used for each daily analysis (00:00:00 - 23:59:30 GPS time)
*Station coordinates	Free network strategy (constraints to a priori values are between 1 m. and 100 m., no station is fixed). All station coordinates are adjusted, relative to the a priori values, either from IGS05.snx or from a previous ULR solution expressed in the ITRF2005.
Satellite clocks	Estimated using one-way phase data aligned with pseudorange. Time reference is defined by an ensemble average over selected hydrogen maser sites (only of the first subnetwork) fit to broadcast ephemeris clocks.
	sp3 clock files: Estimated values included 30 seconds sampling for clock files.
Receiver clocks	Estimated during clock estimation.
Orbits	Geocentric position and velocity, solar radiation pressure scales and once-per-revolution perturbation terms. Radiation pressure scaling factors and perturbation terms are estimated for each of the orthogonal directions: satellites - sun, body centered Y, and orthogonal third directions estimated as constant offsets for each one-day arc; plus once-per-rev sine/cosine terms are estimated with apriori values from the prior day. The constraints are 0.01 ppm or 20 cm for initial conditions, 5% for the direct and y-bias and 1% for the third axis bias and the once-per-rev parameters.
	sp3 files: orbits transformed to crust-fixed (rotating) frame accounting for geocenter motions due to ocean tides and for subdaily tidal EOP variations.
Satellite attitude	No attitude parameters are adjusted
Troposphere	Zenith delay: residual delays are adjusted for each station assuming mostly dominated by "wet" component and parameterized by a piecewise linear, continuous model with 2 hour intervals.
	Mapping function: VMF1 (Boehm et al. 2006) wet function used to estimate zenith delay residuals.
	Zenith delay epochs: each even-integer hour
	Gradients: two N-S & two E-W gradient parameter for each day and each station, with continuous linear variation during the day; 0.03 m. at 10 degree elevation 1 sigma constraint is

```
|                 |           applied at all stations. Mapping function  |
|                 |           from Chen and Herring (1997) is used.      |
|-----------------------------------------------------------------------|
| Ionospheric     | Not estimated                                       |
| correction      |                                                     |
|-----------------------------------------------------------------------|
| Ambiguity       | Real-valued double-differenced phase cycle ambiguities |
|                 | adjusted except when they can be resolved confidently |
|                 | in which case they are fixed using the Melboune-    |
|                 | Wuebbena widelane to resolve L1-L2 cycles and then  |
|                 | estimation to resolve L1 and L2 cycles.             |
|-----------------------------------------------------------------------|
|*Earth orientation| Daily x & y pole offsets, pole-rates, UT1 and LOD. |
| parameters (EOP) | x and y pole estimated as piece-wise, linear offsets. |
|                 | A priori values from IERS Bulletin B. Constraints are |
|                 | 0.032 arcsec (~1 m) for Wobble, 0.0032 arcsec/day   |
|                 | (~10 cm/day) for Wobble rate, 0.00002 sec for UT1 and |
|                 | 0.02 sec/day for LOD.                               |
|-----------------------------------------------------------------------|
| Other           | none                                                |
| parameters      |                                                     |
=========================================================================
```

```
=========================================================================
|                           REFERENCES                                  |
|-----------------------------------------------------------------------|
| Ash, M.E. (1972), Determination of Earth satellite orbits, Tech. Note |
|    1972-5, Lincoln Laboratory, MIT, 19 April 1972.                    |
|                                                                       |
| Bar-Sever, Y.E. (1995), New GPS attitude model, IGS Mail #591, 1995,  |
|    http://igscb.jpl.nasa.gov/mail/igsmail/1994/msg00166.html          |
|                                                                       |
| Boehm, J., B. Werl, and H. Schuh (2006), Troposphere mapping function for |
|    GPS and very long baseline interferometry from European Centre for |
|    Medium-Range Weather Forecasts operational analysis data. J. Geophys. |
|    Res., 111, B02406.                                                 |
|                                                                       |
| Boehm, J., R. Heinkelmann, and H. Schuh (2007), Short Note: A global model|
|    of pressure and temperature for geodetic applications, J. Geod.,   |
|    doi:10.1007/s00190-007-0135-3.                                     |
|                                                                       |
| Chen, G. and T.A. Herring (1997), Effects of atmospheric azimuthal    |
|    asymmetry of the analysis of space geodetic data, J. Geophys. Res., 102.|
|                                                                       |
| IERS Conventions 2003, D.D. McCarthy & G. Petit (editors), IERS Technical |
|    Note 32, Frankfurt am Main: Verlag des Bundesamts fuer Kartographie und |
|    Geodaesie, 2004.  (see also updates at website)                    |
|                                                                       |
| Saastamoinen, J. (1972), Atmospheric correction for the troposphere and |
|    stratosphere in radio ranging of satellites, in The Use of Artificial |
|    Satellites for Geodesy, Geophys. Monogr. Ser. 15 (S.W. Henriksen et al.,|
|    eds.), AGU, Washington, D.C., pp.247-251, 1972.                    |
|                                                                       |
| Wu, J.T., S.C. Wu, G.A. Hajj, W.I. Bertiger, and S.M. Lichten (1993), |
|    Effects of antenna orientation on GPS carrier phase, Manuscripta   |
|    Geodaetica,18, 91-98, 1993.                                        |
=========================================================================
```

B. ULR4 vertical velocity field

```
Column "Site", GPS station acronym.
Column "DOMES", GPS station number.
Column "Lon", degrees, longitude of the GPS station.
Column "Lat", degrees, latitude of the GPS station.
Column "T_GPS", years, Length of the GPS time series.
Column "Data", percentage of data in the time series.
Column "V_GPS", mm/yr, GPS vertical velocity.
Column "S_GPS", mm/yr, GPS vertical velocity uncertainty.
Column "MODEL", stochastic model used to estimate uncertainty.
```

Site	DOMES	Lon	Lat	T_GPS	Data	V_GPS	S_GPS	MODEL
ABER	13231M001	357.9198	56.9684	10.28	93.7	0.81	0.11	vw+pl
ACOR	13434M001	351.6011	43.1723	8.96	93.4	-2.19	0.18	vw+gm
AJAC	10077M005	8.7626	41.7362	8.54	91.5	0.30	0.13	vw+pl
ALAC	13433M001	359.5188	38.1518	9.40	93.1	0.60	0.11	vw+pl
ALBH	40129M003	236.5125	48.1986	13.01	99.2	0.15	0.18	vw+fn
ALGO	40104M002	281.9286	45.7635	13.01	97.5	3.51	0.22	vw+fn
ALIC	50137M001	133.8855	-23.5289	12.83	97.4	-0.39	0.28	vw+fn
ALME	13437M001	357.5406	36.6680	7.61	98.7	1.30	0.16	vw+pl
ALRT	40162M001	297.6595	82.4443	6.45	97.4	5.66	0.51	vw+fn
AMC2	40472S004	255.4754	38.6154	10.19	99.1	-1.14	0.27	vw+fn
ANP1	49908S101	283.3908	38.8222	6.28	94.9	-1.27	0.41	vw+fn
AOML	49914S001	279.8378	25.5845	6.37	98.3	-0.68	0.44	vw+fn
ARP3	49878S003	262.9410	27.6797	10.35	96.6	-1.60	0.32	vw+fn
ARTU	12362M001	58.5605	56.2523	9.39	97.7	0.47	0.27	vw+pl
ASC1	30602M001	345.5879	-7.8987	11.37	69.2	-0.51	0.38	vw+fn
ASPA	50503S006	189.2776	-14.2341	7.38	91.6	-0.60	0.20	vw+pl
AUCK	50209M001	174.8344	-36.4188	12.99	99.4	-0.94	0.25	vw+fn
AV09	99997S001	193.4582	53.6922	4.28	87.7	2.99	0.56	vw+fn
BAHR	24901M002	50.6081	26.0570	12.09	99.5	0.03	0.23	vw+fn
BARB	43401S001	300.3909	13.0033	3.21	74.6	-1.82	1.05	vw+fn
BARH	49927S001	291.7783	44.2027	10.24	93.5	0.62	0.24	vw+fn
BILI	12363M001	166.4380	67.9425	9.27	94.2	0.29	0.46	vw+fn
BJFS	21601M001	115.8925	39.4197	9.19	98.0	2.58	0.42	vw+fn
BOR1	12205M002	17.0735	52.0906	13.00	99.2	-0.29	0.15	vw+pl
BORK	14268M001	6.7474	53.3796	6.59	99.1	-0.51	0.42	vw+fn
BRAZ	41606M001	312.1221	-15.8461	12.31	91.7	-1.25	0.35	vw+fn
BRMU	42501S004	295.3037	32.1966	13.01	91.4	-0.98	0.14	vw+fn
BRST	10004M004	355.5034	48.1893	10.16	88.2	-0.64	0.22	vw+fn
BRUS	13101M004	4.3592	50.6092	13.01	98.7	0.48	0.16	vw+pl
BUDP	10101M003	12.5000	55.5597	5.61	100.	1.27	0.34	vw+pl
CAGL	12725M003	8.9728	38.9476	12.81	95.6	0.41	0.22	vw+fn
CANT	13438M001	356.2019	43.2799	7.60	97.3	-0.09	0.23	vw+fn
CART	41902M001	284.4661	10.3233	8.54	63.7	-1.43	0.35	vw+fn
CAS1	66011M001	110.5197	-66.1413	12.98	90.5	1.01	0.38	tw+fn
CASC	13909S001	350.5815	38.5058	10.63	96.6	0.18	0.16	vw+fn
CEDU	50138M001	133.8098	-31.6944	11.27	93.0	-1.48	0.33	vw+fn
CEUT	13449M001	354.6887	35.7135	5.06	94.6	-0.70	0.61	vw+fn
CHA1	49851S001	280.1571	32.5827	7.84	98.7	-1.71	0.48	vw+fn
CHAT	50207M001	183.4342	-43.7635	12.99	99.3	-0.68	0.23	vw+fn
CHIZ	10020M001	359.5923	45.9412	8.18	95.8	0.13	0.22	vw+fn
CHPI	41609M003	315.0148	-22.5505	5.64	92.4	1.38	0.59	vw+fn

CHUR	40128M002	265.9113	58.5882	13.01	98.4	9.84	0.26	vw+fn
CKIS	50213M003	200.1994	-21.0716	7.30	77.9	-0.28	0.48	vw+fn
CNMR	50512M001	145.7431	15.1324	5.39	89.6	0.25	0.54	vw+fn
COCO	50127M001	96.8340	-12.1092	12.53	95.6	-1.47	0.31	vw+fn
CONZ	41719M002	286.9745	-36.6593	6.62	98.4	0.48	1.93	vw+rw
CORD	41511M001	295.5300	-31.3572	6.75	67.8	0.64	0.46	vw+fn
CRO1	43201M001	295.4157	17.6454	13.01	93.9	-1.53	0.32	vw+fn
DAEJ	23902M002	127.3745	36.2158	9.78	98.7	1.29	0.33	vw+fn
DARW	50134M001	131.1327	-12.7606	12.48	79.7	-1.22	0.56	vw+pl
DAV1	66010M001	77.9726	-68.4461	12.89	95.9	-1.18	0.34	vw+fn
DGAR	30802M001	72.3702	-7.2215	12.63	79.5	0.64	0.27	vw+fn
DJOU	99902M001	1.6616	9.6284	3.34	100.	0.42	0.96	wh+fn
DRAO	40105M002	240.3750	49.1323	13.01	99.1	0.91	0.26	vw+fn
DUBO	40137M001	264.1338	50.0695	12.19	98.1	0.66	0.29	vw+fn
DUBR	11901M001	18.1104	42.4583	8.26	65.9	-0.92	0.31	vw+fn
DUCK	49846S001	284.2488	35.9990	6.62	94.3	-2.43	0.49	vw+fn
DUM1	91501M001	140.0019	-66.5248	10.98	89.2	-1.58	0.42	wh+fn
DUNT	50212S001	170.6294	-45.6220	9.06	89.0	-1.16	0.29	vw+fn
EISL	41703M003	250.6167	-26.9923	9.09	85.4	0.43	0.71	vw+fn
EPRT	49928S001	293.0079	44.7163	10.24	88.3	0.17	0.18	vw+pl
FLIN	40135M001	258.0220	54.5439	12.56	98.5	1.90	0.36	vw+fn
FORT	41602M001	321.5744	-3.8516	10.28	98.2	1.45	0.57	vw+fn
FTS1	49893S001	236.0439	46.0126	12.08	98.8	2.54	0.20	vw+fn
GAL1	49872S001	265.2632	29.1658	7.48	80.9	-4.96	0.47	vw+fn
GALA	42005M001	269.6964	-0.7377	6.76	85.6	-0.36	0.59	vw+fn
GAO1	99903M001	359.9940	16.1490	3.33	90.9	0.50	0.74	wh+fn
GCGT	80401M001	278.6206	19.1733	3.55	99.8	-1.98	0.19	vw+pl
GENO	12712M002	8.9211	44.2270	10.43	94.8	0.47	0.23	vw+fn
GETI	22703M001	102.1055	6.1848	3.74	88.1	3.24	1.15	vw+fn
GLPS	42005M002	269.6963	-0.7380	5.97	87.3	-0.35	0.19	vw+pl
GLPT	49467M001	283.5005	37.0633	9.13	98.6	-2.56	0.27	vw+fn
GLSV	12356M001	30.4967	50.1750	10.83	98.2	-0.40	0.22	vw+pl
GODE	40451M123	283.1732	38.8336	13.01	98.1	-1.00	0.23	vw+fn
GOLD	40405S031	243.1108	35.2436	13.01	92.0	-0.05	0.13	vw+gm
GOUG	30608M001	350.1193	-40.1590	10.10	86.9	-8.09	0.65	vw+fn
GRAS	10002M006	6.9206	43.5626	13.01	92.3	0.44	0.12	vw+pl
GRAZ	11001M002	15.4935	46.8752	9.02	98.3	-0.08	0.30	vw+fn
GRIS	99995S001	270.0427	29.1017	3.31	83.9	-7.86	0.66	vw+fn
GUAM	50501M002	144.8684	13.5017	13.01	95.4	0.40	0.34	vw+fn
GUAO	21612M003	87.1773	43.2791	6.54	99.6	1.42	0.19	vw+pl
HARB	30302M009	27.7072	-25.7362	3.97	100.	-0.62	0.79	vw+fn
HARV	40420M101	239.3179	34.2900	13.01	86.4	-3.34	0.52	vw+pl
HELG	14264M001	7.8931	53.9916	8.76	99.1	0.80	0.29	vw+fn
HLFX	40120M001	296.3887	44.4911	6.02	99.6	-0.75	0.34	wh+fn
HNLC	49970S001	202.1355	21.1733	11.51	86.7	-0.53	0.18	tw+pl
HNPT	49913S001	283.8696	38.4013	12.95	92.9	-1.64	0.21	vw+fn
HOB2	50116M004	147.4387	-42.6129	12.89	96.5	0.20	0.44	vw+pl
HOFN	10204M002	344.8021	64.1165	11.50	96.8	11.64	1.84	vw+rw
HOLB	40130M001	231.8650	50.4515	13.01	88.8	2.14	0.52	vw+pl
HOLM	40148M001	242.2388	70.6161	7.33	99.6	2.68	0.17	vw+pl
HRAO	30302M004	27.6870	-25.7393	12.25	86.2	-0.15	0.25	vw+fn
HYDE	22307M001	78.5509	17.3077	6.16	98.3	-0.98	0.28	vw+pl
IBIZ	13454S001	1.4490	38.7233	3.02	97.1	-0.76	0.36	wh+pl
IISC	22306M002	77.5704	12.9369	12.99	90.3	1.06	0.47	vw+pl
IRKT	12313M001	104.3162	52.0325	12.97	97.5	0.35	0.33	vw+fn
ISPA	41703M007	250.6556	-26.9691	4.87	90.1	0.47	0.41	vw+pl
JAB1	50136M001	132.8939	-12.5768	11.05	68.1	-3.28	0.33	vw+fn
JOZE	12204M001	21.0315	51.9106	13.00	98.0	0.70	0.11	vw+pl
KARR	50139M001	117.0972	-20.8531	12.49	98.3	0.16	0.46	vw+pl

```
KELS  49662M001  237.1039   45.9259   9.92   98.7  -0.90   0.27   vw+fn
KELY  43005M001  309.0552   66.8486   5.66   97.1  -1.73   0.33   vw+pl
KELY  43005M002  309.0552   66.8486   7.28   96.6   2.23   0.42   vw+pl
KERG  91201M002   70.2555  -49.1612  13.01   94.7   1.55   0.17   vw+pl
KIRI  50305M001  172.9229    1.3455   6.40   85.3  -0.75   0.48   vw+fn
KIT3  12334M001   66.8854   38.9465  13.01   88.6  -1.79   0.37   vw+fn
KLPD  10802M001   21.1189   55.5360   3.39   96.6   1.88   0.38   vw+gm
KODK  40419S003  207.4986   57.5611   6.23   58.7   9.19   2.74   vw+fn+rw
KOKB  40424M004  200.3351   21.9923  12.94   95.8   0.23   0.33   vw+fn
KOUR  97301M210  307.1940    5.2172  13.01   91.3  -1.85   0.82   vw+pl
KSTU  12349M002   92.7938   55.8146   7.06   76.5   0.67   0.27   vw+pl
KUNM  21609M001  102.7972   24.8824  10.22   97.5  -1.20   0.39   vw+fn
KWJ1  50506M001  167.7302    8.6647   6.35   82.4  -2.65   0.91   tw+fn
KYW1  49852S001  278.3470   24.4370  10.76   91.7  -0.30   0.11   vw+pl
LAE1  51002M001  146.9932   -6.6294   5.55   96.6  -5.50   0.57   wh+fn
LAGO  13903M001  351.3316   36.9140   8.34   94.2  -0.30   0.16   vw+fn
LAMA  12209M001   20.6699   53.7090   9.00   93.4  -1.13   0.25   vw+pl
LAMP  12706M002   12.6057   35.3180   9.38   95.8   0.16   0.31   vw+fn
LAUT  50804M002  177.4466  -17.4982   7.09   82.1  -0.98   0.38   vw+fn
LHAZ  21613M002   91.1040   29.4922   9.27   91.3   1.61   0.31   vw+fn
LPGS  41510M001  302.0677  -34.7264  13.01   92.8   2.60   0.38   tw+fn
LROC  10023M001  358.7807   45.9667   7.10   98.2   0.01   0.21   vw+fn
LYTT  50214S001  172.7222  -43.4137   9.12   80.9  -0.89   0.36   vw+fn
MADR  13407S012  355.7503   40.2393   3.99   99.9  -1.31   0.69   vw+fn
MALD  22901S001   73.5263    4.1607   6.83   73.2  -1.15   0.57   vw+fn
MALI  33201M001   40.1944   -2.9759  12.70   96.1  -1.20   0.44   vw+fn
MALL  13444M001    2.6246   39.3638   7.60   99.8   1.22   0.20   vw+pl
MAR6  10405M002   17.2585   60.4302   9.83   97.8   7.54   0.15   vw+pl
MARS  10073M008    5.3538   43.0867  10.45   95.9  -0.04   0.25   vw+fn
MAS1  31303M002  344.3667   27.6054  12.99   94.7  -0.38   0.19   vw+fn
MATE  12734M008   16.7045   40.4590  13.01   99.0   0.83   0.20   vw+fn
MAW1  66004M001   62.8707  -67.4689  12.98   95.9  -0.29   0.30   vw+fn
MBAR  33901M001   30.7379   -0.5974   7.45   63.8   1.67   0.23   vw+pl
MCM4  66001M003  166.6693  -77.7589  13.00   98.3  -2.46   1.02   vw+pl
MDO1  40442M012  255.9850   30.5120  13.01   98.7   0.70   0.27   vw+fn
MDVJ  12309M005   37.2145   55.8429   6.55   96.2   0.30   0.88   vw+fn
METS  10503S011   24.3953   60.0513  13.01   98.7   4.39   0.10   vw+pl
MKEA  40477M001  204.5437   19.6791  12.25   97.4  -2.34   0.24   vw+fn
MOB1  49863S001  271.9759   30.0604  11.87   97.3  -3.01   0.26   vw+fn
MPLA  41521M001  302.4689  -37.8490   5.33   66.1   2.56   0.68   vw+fn
NAIN  40164M001  298.3113   56.3597   6.03   95.6   5.01   0.20   vw+pl
NANO  40138M001  235.9135   49.1045  13.01   97.9   1.07   0.24   vw+fn
NAUR  50701M001  166.9256   -0.5480   5.50   59.2  -1.10   0.77   vw+fn
NEAH  40139M001  235.3751   48.1066  12.99   87.7   4.06   0.25   vw+fn
NEIA  41620M001  312.0750  -24.8731   6.94   86.7   0.75   0.48   vw+fn
NEWL  13273M103  354.4572   49.9135  10.24   92.8  -0.67   0.12   vw+pl
NEWP  49666M001  235.9381   44.3926  10.76   88.5   1.09   0.24   vw+fn
NIAM  99904M001    2.1832   13.3923   3.58   97.9  -1.42   0.68   vw+fn
NICO  14302M001   33.3964   34.9601  11.62   81.4   0.41   0.23   vw+fn
NKLG  32809M002    9.6721    0.3515   8.74   98.0   1.36   0.44   vw+fn
NLIB  40465M001  268.4251   41.5805  13.00   98.7  -1.34   0.29   vw+fn
NOT1  12717M004   14.9898   36.6913   8.28   99.3  -0.18   0.18   vw+pl
NOUM  92701M003  166.4102  -22.1352   9.21   99.0  -1.61   0.29   vw+fn
NPRI  49684S001  288.6725   41.3189   8.15   96.6  -0.13   0.26   vw+fn
NRC1  40114M001  284.3762   45.2618  13.01   91.7   3.59   0.13   vw+pl
NRIL  12364M001   88.3598   69.2346   8.27   99.4   1.37   0.47   vw+fn
NRMD  92701M005  166.4849  -22.0939   2.61  100.  -1.55   1.15   vw+fn
NSTG  13216M001  358.5601   54.8264   9.07   81.3   0.31   0.28   vw+fn
OHI2  66008M005  302.0987  -63.1664   6.87   84.8   6.07   0.92   wh+fn
```

OHI3	66008M006	302.0986	-63.1664	5.89	87.8	6.07	0.82	vw+fn
OHIG	66008M001	302.0997	-63.1660	6.08	73.1	6.07	1.29	vw+fn
ONSA	10402M004	11.9255	57.2204	13.01	99.4	2.80	0.11	vw+pl
OUAG	99907M001	358.4875	12.2762	2.58	100.	-0.31	0.46	vw+pl
P201	21776S001	141.6853	45.2154	5.74	98.1	-0.02	0.23	vw+pl
P202	21777S001	144.2858	43.8271	5.56	98.9	2.36	0.27	wh+pl
P204	21779S001	140.7245	41.5905	5.71	99.0	1.46	0.20	vw+pl
P206	21781S001	139.8249	34.7384	5.53	99.8	-1.81	0.45	vw+fn
P207	21782S001	137.2246	36.5778	5.57	99.7	-1.52	0.44	vw+fn
P208	21783S001	135.7732	33.2991	5.74	99.8	-4.41	0.47	wh+fn
P209	21784S001	132.0662	34.7169	5.53	99.8	-1.36	0.22	vw+pl
P210	21785S001	129.8662	32.5603	5.74	98.8	-1.23	0.57	wh+fn
P211	21786S001	131.4093	31.4055	5.59	99.7	-1.26	0.58	wh+fn
P212	21787S001	127.6652	26.0611	5.54	99.9	0.14	0.18	wh+pl
P213	21732S006	142.1946	26.9382	5.69	98.0	-1.63	3.29	wh+rw
PAPE	92201M011	210.4273	-17.4228	4.94	83.8	-1.75	0.55	vw+fn
PARC	41716S001	289.1201	-52.9521	9.99	53.1	-0.43	0.31	vw+fn
PBL1	49891S001	237.5811	37.6667	8.15	92.6	-0.63	0.35	vw+fn
PCLA	99992S001	272.8106	30.3011	4.88	98.9	-0.23	0.59	vw+fn
PDEL	31906M004	334.3372	37.5616	8.69	94.8	-1.62	0.18	vw+fn
PERT	50133M001	115.8852	-31.6299	12.99	95.9	-2.90	0.70	vw+pl
PETP	12355M002	158.6071	52.8817	10.22	98.4	-2.34	0.35	vw+fn
PGC5	40129M007	236.5489	48.4576	3.99	99.4	-2.33	0.77	wh+fn
PIE1	40456M001	251.8811	34.1226	13.01	95.9	1.93	0.22	vw+fn
PIMO	22003M001	121.0777	14.5419	9.79	89.6	1.48	0.41	vw+fn
PLO3	49886S003	242.7570	32.4908	9.73	98.0	-1.53	0.35	vw+fn
PLO5	49886S999	242.7570	32.4908	2.53	97.7	-1.54	0.77	vw+fn
PLUZ	31308M001	344.5924	27.9869	3.31	99.5	-1.49	0.41	vw+pl
PNCY	49584S001	274.3218	30.0375	6.61	99.4	0.03	0.38	vw+fn
PNGM	51006M001	147.3660	-2.0296	6.63	72.2	-1.34	0.39	vw+fn
POHN	51601M001	158.2101	6.9138	5.66	79.5	-1.69	0.59	vw+fn
POL2	12348M001	74.6943	42.4881	13.01	92.9	0.58	0.22	vw+fn
POLV	12336M001	34.5429	49.4126	7.53	99.7	-0.44	0.54	vw+fn
POR4	49842S004	289.2905	42.8791	5.27	90.9	0.22	0.43	vw+fn
POTS	14106M003	13.0661	52.1931	13.01	99.2	0.17	0.16	vw+pl
PRMI	82002M001	292.9546	17.8578	2.76	100.	0.05	1.01	vw+fn
QAQ1	43007M001	313.9522	60.5508	6.60	97.8	4.06	0.35	vw+fn
QIKI	40166M001	295.9663	67.4232	4.44	100.	4.02	0.54	vw+fn
QUIN	40433M004	239.0556	39.7852	12.94	90.5	0.95	0.66	vw+pl
RABT	35001M002	353.1457	33.8199	8.61	97.0	-0.85	0.24	vw+fn
RAMO	20703S001	34.7631	30.4293	10.55	97.5	1.74	0.25	vw+fn
RBAY	30315M001	32.0784	-28.6334	8.21	53.7	0.36	2.33	vw+rw
REUN	97401M003	55.5717	-21.0788	9.92	77.6	-0.70	0.32	vw+fn
REYK	10202M001	338.0445	63.9874	12.93	97.6	0.16	0.24	vw+fn
RIGA	12302M002	24.0588	56.7725	9.83	96.9	1.55	0.22	vw+pl
RIOG	41507M004	292.2489	-53.6018	8.00	99.1	2.77	0.32	vw+fn
RWSN	41513M001	294.8928	-43.1068	8.92	92.1	1.51	0.36	vw+fn
SAMO	50603M001	188.2616	-13.7600	7.49	76.0	-1.67	0.46	vw+fn
SANT	41705M003	289.3314	-32.9744	13.01	97.9	2.64	0.51	vw+pl
SASS	14281M001	13.6433	54.3315	5.91	96.9	2.35	0.53	vw+fn
SCCC	49851S999	280.0620	32.6080	3.78	98.8	-3.14	0.24	vw+gm
SCH2	40133M002	293.1674	54.6507	11.32	96.0	10.85	0.44	vw+fn
SCOA	10088M002	358.3183	43.2032	3.04	91.4	-0.77	0.70	vw+fn
SCOR	43006M002	338.0497	70.3638	3.90	97.8	4.21	0.87	wh+fn
SCUB	40701M001	284.2377	19.8886	8.97	71.1	0.08	0.41	vw+fn
SEAT	40457M002	237.6905	47.4623	12.98	91.1	-1.39	0.27	vw+fn
SELD	99996S001	208.2933	59.2770	8.17	96.1	11.66	0.51	vw+fn
SEY1	39801M001	55.4794	-4.6426	11.95	53.1	-2.10	0.62	vw+fn
SFER	13402M004	353.7944	36.2806	12.72	92.5	0.33	0.17	vw+fn

```
SHEE  13236M001    0.7434   51.2580  11.76  93.2   0.40  0.31  vw+fn
SHK1  49473M001  285.9884   40.2816  10.29  96.4  -2.20  0.32  vw+fn
SHK5  99994S002  285.9884   40.2816   2.66  100.  -2.20  2.00  vw+rw
SIMO  30307M001   18.4396  -34.0093   7.39  56.8  -0.34  0.36  vw+fn
SIO3  40460M004  242.7496   32.6895  13.01  96.0   0.65  0.24  tw+fn
SKE0  10426M001   21.0483   64.7310   3.61  99.8  11.05  0.33  vw+gm
SOL1  49907S001  283.5461   38.1318  11.53  96.2  -2.11  0.30  vw+fn
STAS  10330M001    5.5986   58.8476   7.78  98.0   1.39  0.30  vw+fn
STJO  40101M001  307.3223   47.4036  13.01  99.0   0.49  0.18  vw+fn
SUTH  30314M002   20.8105  -32.2065  10.70  94.5   0.00  0.24  vw+fn
SWTG  99999S001  353.6111   58.0350   3.29  90.8   0.81  0.23  wh+rw
SYOG  66006S002   39.5837  -68.8779  12.98  97.1   2.06  0.30  vw+fn
TAKL  50216S001  174.7699  -36.6591   5.98  70.2  -0.94  0.42  vw+fn
TAMA  99905M001  359.1383    9.4915   2.68  78.6   2.83  1.30  vw+fn
TAMP  99908M001    5.5296   22.6556   2.80  95.1  -0.57  0.85  vw+fn
THTI  92201M009  210.3936  -17.4666  10.54  93.8  -0.66  0.37  vw+fn
THU1  43001M001  291.2120   76.4499   7.05  88.6   2.13  0.40  vw+pl
THU3  43001M002  291.1750   76.4496   6.59  100.   5.82  1.18  vw+fn+rw
TIDB  50103M108  148.9800  -35.2177  13.01  92.9   0.10  0.13  tw+pl
TIXI  12360M001  128.8664   71.5191  10.22  96.9   0.93  0.24  vw+pl
TOMB  99906M001  357.0025   16.6249   2.54  92.0  -1.20  1.10  vw+fn
TONG  50902M001  184.8208  -21.0156   6.84  82.1   1.28  0.34  vw+fn
TORS  10108S001  353.2355   61.8636   4.35  89.0  -0.23  0.35  vw+pl
TOW2  50140M001  147.0557  -19.1497  13.01  98.2  -0.72  0.26  vw+fn
TRAB  20808M001   39.7756   40.8043   7.97  96.9  -0.18  0.37  wh+fn
TRDS  10331M001   10.3192   63.2169   8.16  98.8   4.43  0.43  vw+fn
TRO1  10302M006   18.9396   69.5370  10.80  98.8   1.86  0.35  vw+fn
TSEA  99993S001  210.1050   61.0245   9.10  85.5   4.31  0.44  vw+fn
TSKB  21730S005  140.0875   35.9226  13.01  99.1   1.11  0.23  vw+fn
TUKT  40165M001  227.0057   69.3114   5.35  97.4  -0.82  0.45  vw+fn
TUVA  51101M001  179.1966   -8.4691   6.97  75.3  -0.93  0.25  vw+fn
UCLU  40140M001  234.4584   48.7349   3.99  97.0  -0.84  0.66  vw+fn
ULAB  24201M001  107.0523   47.6736   7.99  89.9   1.18  0.17  vw+pl
UNSA  41514M001  294.5924  -24.5816   8.99  91.8  -0.50  0.46  vw+fn
URUM  21612M001   87.6007   43.6157   6.17  96.6   3.05  0.49  vw+fn
USNA  49908S001  283.5206   38.7953   9.93  97.6  -1.72  0.34  vw+fn
USNO  40451S003  282.9338   38.7310  11.66  98.2  -1.16  0.26  vw+fn
VAAS  10511M001   21.7706   62.8051   9.83  93.0   8.57  0.19  vw+pl
VALE  13439M001  359.6624   39.2921   7.61  88.4  -0.08  0.11  vw+pl
VARS  10322M002   31.0312   70.2141   7.78  99.5   2.96  0.31  vw+fn
VBCA  41512M001  297.7308  -38.5131   8.81  85.5   0.92  0.45  vw+fn
VENE  12741M001   12.3320   45.2446  10.92  94.0   1.40  0.28  vw+gm
VESL  66009M001  357.1582  -71.5586  10.38  81.6   2.76  0.51  vw+fn
VILL  13406M001  356.0480   40.2537  13.01  97.0  -1.38  0.35  vw+pl
VIS0  10423M001   18.3673   57.4797   9.83  97.6   2.98  0.36  vw+fn
VTIS  49956M001  241.7062   33.5352  10.05  97.6   0.18  0.27  vw+fn
WARN  14277M002   12.1014   53.9869   5.88  97.1   0.34  0.50  vw+fn
WES2  40440S020  288.5067   42.4216  13.00  93.0   0.06  0.21  vw+fn
WGTT  50208S004  174.7816  -41.0997   9.04  96.6  -3.68  0.30  vw+fn
WHIT  40136M001  224.7779   60.5862  12.56  97.9   1.61  0.48  vw+fn
WILL  40134M001  237.8322   52.0504  13.00  93.7   1.91  0.36  vw+fn
WSRT  13506M005    6.6045   52.7293  11.51  99.0  -0.55  0.18  vw+pl
WTZR  14201M010   12.8789   48.9537  12.95  98.7  -0.16  0.24  vw+fn
WUHN  21602M001  114.3573   30.3635  12.80  96.2   0.55  0.38  vw+fn
YAR1  50107M004  115.3470  -28.8835   6.38  96.7  -1.70  0.56  vw+fn
YELL  40127M003  245.5193   62.3229  13.01  95.1   6.31  0.40  vw+fn
ZIMM  14001M004    7.4653   46.6851  13.01  99.1   1.25  0.24  vw+fn
```

C. ULR4 discontinuity set

```
SITE  SOLNS  DOY YEAR      EAST           NORTH            UP
----  -----  --- ----  ---------------  ---------------  ---------------
0194  01-02  164 2008     8.0 +/-  0.2    -3.3 +/-  0.3     2.9 +/-  0.9
ABER  01-02  076 2000    -1.1 +/-  0.2    -0.7 +/-  0.2     3.6 +/-  0.6
ACOR  01-02  006 2000     3.2 +/-  0.2     6.3 +/-  0.2    -2.0 +/-  0.8
ACOR  02-03  157 2002     1.2 +/-  0.2    -1.5 +/-  0.2    -9.4 +/-  0.8
ACOR  03-04  240 2003    -0.9 +/-  0.2    -0.5 +/-  0.2     8.0 +/-  0.8
ACOR  04-05  077 2007    -1.4 +/-  0.2    -2.9 +/-  0.2    -4.2 +/-  0.6
ALAC  01-02  151 2006    -5.5 +/-  0.1     1.6 +/-  0.2    -0.6 +/-  0.5
ALBH  01-02  274 2002    -0.3 +/-  0.1    -0.2 +/-  0.1     4.0 +/-  0.4
ALBH  02-03  238 2003     6.2 +/-  0.1     0.6 +/-  0.1   -12.0 +/-  0.4
ALEX  01-02  233 2003   -17.9 +/-  0.5    -1.2 +/-  0.5    -3.4 +/-  2.3
ALEX  02-03  194 2006    10.0 +/-  0.3     0.3 +/-  0.3     0.3 +/-  1.4
AMC2  01-02  244 1999    -3.3 +/-  0.2    -4.2 +/-  0.2    -0.5 +/-  0.7
AMC2  02-03  165 2002    -0.8 +/-  0.1     2.6 +/-  0.2     6.1 +/-  0.5
AMC2  03-04  274 2007     1.9 +/-  0.2     6.6 +/-  0.2     1.1 +/-  0.6
AOML  01-02  318 2002     2.2 +/-  0.2    -1.5 +/-  0.2     5.2 +/-  0.8
ARP3  01-02  238 1999   -12.1 +/-  0.2     0.4 +/-  0.2     1.0 +/-  0.7
ASPA  01-02  275 2008     3.4 +/-  0.8     3.2 +/-  0.6   -15.8 +/-  2.7
AUCK  01-02  307 2005     3.5 +/-  0.1    -1.1 +/-  0.1   -10.0 +/-  0.4
AUCK  02-03  314 2007     0.1 +/-  0.2    -5.3 +/-  0.2    39.0 +/-  0.5
BARH  01-02  086 2007     3.7 +/-  0.1     3.6 +/-  0.2   -12.1 +/-  0.5
BINT  01-02  109 2001     2.8 +/-  0.8    -1.3 +/-  0.6     9.0 +/-  2.7
BOR1  01-02  151 1999     3.7 +/-  0.1     0.3 +/-  0.1    -4.2 +/-  0.4
BRAZ  01-02  118 1998     3.5 +/-  0.3     3.4 +/-  0.2    12.9 +/-  1.1
BRFT  01-02  175 2007     1.3 +/-  0.2    -6.0 +/-  0.2    -4.1 +/-  0.7
BRMU  01-02  071 2003    -4.1 +/-  0.2    -5.2 +/-  0.1     7.2 +/-  0.6
BRST  01-02  162 2003    -0.8 +/-  0.2     0.8 +/-  0.2     3.0 +/-  0.7
BRST  02-03  076 2005    -3.4 +/-  0.2     3.9 +/-  0.2     2.2 +/-  0.6
BRST  03-04  207 2006     4.2 +/-  0.2    -7.2 +/-  0.2    -8.1 +/-  0.6
BRST  04-05  163 2008    -3.6 +/-  0.2     5.5 +/-  0.2     5.4 +/-  0.6
BRUS  01-02  118 2000    -0.4 +/-  0.1    -3.7 +/-  0.1     2.0 +/-  0.4
BRUS  02-03  010 2004    -4.5 +/-  0.1     0.8 +/-  0.1     1.3 +/-  0.4
CAGL  01-02  192 2001     5.9 +/-  0.1     1.3 +/-  0.1    -4.0 +/-  0.5
CANT  01-02  254 2003    -4.8 +/-  0.2     4.0 +/-  0.2     0.9 +/-  0.7
CAS1  01-02  051 1997     0.7 +/-  0.3    -4.4 +/-  0.4    42.4 +/-  1.1
CAS1  02-03  303 1997     1.7 +/-  0.3     6.4 +/-  0.3   -36.6 +/-  1.0
CASC  01-02  271 1999    -1.8 +/-  0.2    -1.7 +/-  0.2    -0.5 +/-  0.7
CASC  02-03  061 2008     2.8 +/-  0.1    -0.1 +/-  0.2     1.7 +/-  0.5
CEUT  01-02  062 2005    -1.1 +/-  0.2     9.0 +/-  0.2    -5.0 +/-  0.8
CHUR  01-02  034 2005     1.6 +/-  0.1     3.4 +/-  0.1     3.4 +/-  0.3
CHUR  02-03  088 2008    -3.8 +/-  0.1     2.8 +/-  0.2    -1.3 +/-  0.4
CNMR  01-02  195 2005   -34.1 +/-  0.4    22.9 +/-  0.3    -6.0 +/-  1.6
CNMR  02-03  036 2008     4.8 +/-  0.4    -0.7 +/-  0.4   -22.5 +/-  1.6
COCO  01-02  170 2000    34.8 +/-  0.2   -10.2 +/-  0.2     7.6 +/-  0.6
COCO  02-03  255 2007     2.8 +/-  0.2     9.4 +/-  0.1     1.3 +/-  0.5
CONZ  01-02  137 2005    -0.7 +/-  0.2    -5.3 +/-  0.2    -3.9 +/-  0.7
CORD  01-02  074 2001     2.7 +/-  0.3    -2.4 +/-  0.3    -4.9 +/-  1.4
CRO1  01-02  273 1999    -0.6 +/-  0.2    -0.9 +/-  0.2    -8.5 +/-  0.8
CRO1  02-03  105 2000     1.2 +/-  0.3     1.4 +/-  0.2    24.8 +/-  2.1
CRO1  03-04  319 2000    -2.1 +/-  0.2    -2.2 +/-  0.2   -15.1 +/-  2.0
DAKA  01-02  336 2004    -3.9 +/-  0.3     6.6 +/-  0.3    -4.9 +/-  1.1
DAKA  02-03  023 2007     4.2 +/-  0.4    -9.4 +/-  0.3    -7.8 +/-  1.4
DAV1  01-02  273 1999     2.4 +/-  0.2     3.8 +/-  0.2     5.3 +/-  0.7
```

```
DAV1   02-03  213  2007    -1.1  +/-  0.2     6.1  +/-  0.2      2.7  +/-   0.5
DGAR   01-02  305  1996     9.6  +/-  0.7     5.4  +/-  0.6     -0.8  +/-   2.4
DGAR   02-03  361  2004    10.7  +/-  0.2     4.6  +/-  0.2     -1.6  +/-   0.7
DUBO   01-02  008  1997    -2.8  +/-  0.2    -0.3  +/-  0.3    -12.4  +/-   0.8
DUBO   02-03  277  1999     1.7  +/-  0.1     6.0  +/-  0.1    -20.7  +/-   0.4
DUBR   01-02  240  2005     6.3  +/-  0.2     5.0  +/-  0.3     -3.6  +/-   0.9
DUBR   02-03  022  2007     8.5  +/-  0.3     7.7  +/-  0.3     15.5  +/-   0.9
DUCK   01-02  106  2003    -4.8  +/-  0.2   -13.6  +/-  0.2    -11.4  +/-   0.9
DUCK   02-03  262  2003   -16.2  +/-  0.3    -7.0  +/-  0.3     -1.9  +/-   1.1
DUCK   03-04  022  2004    -6.7  +/-  0.4     5.7  +/-  0.4      1.3  +/-   1.6
DUM1   01-02  084  1998    18.1  +/-  0.4    14.0  +/-  0.4     -0.2  +/-   1.1
DUNT   01-02  358  2004     2.6  +/-  0.2     3.8  +/-  0.2     -0.9  +/-   0.6
EISL   01-02  003  2002     6.6  +/-  0.3     1.3  +/-  0.2     -7.3  +/-   1.2
EISL   02-03  038  2003     1.3  +/-  0.3    -0.6  +/-  0.2     -6.3  +/-   1.3
EPRT   01-02  253  2000     0.5  +/-  0.1    -0.3  +/-  0.2     10.1  +/-   0.5
EPRT   02-03  024  2002     3.6  +/-  0.1    -0.8  +/-  0.2    -13.0  +/-   0.5
EPRT   03-04  192  2004     8.0  +/-  0.2     4.5  +/-  0.2     -8.2  +/-   0.7
FLIN   01-02  007  1997     1.6  +/-  0.2    -3.0  +/-  0.2      3.3  +/-   0.6
FORT   01-02  080  2000     0.4  +/-  0.3    -3.2  +/-  0.3    -26.0  +/-   1.3
FTS1   01-02  340  1996    -0.8  +/-  0.2    -2.3  +/-  0.2     -7.3  +/-   0.6
FUNC   01-02  093  2008    -5.7  +/-  0.4    -4.1  +/-  0.4      1.1  +/-   1.6
GENO   01-02  244  2000    -1.0  +/-  0.1     0.5  +/-  0.2     -9.2  +/-   0.6
GLPS   01-02  282  2008    -2.3  +/-  0.3    -1.8  +/-  0.3     -5.9  +/-   0.9
GLPT   01-02  273  1997    -1.2  +/-  0.3    -1.1  +/-  0.3     11.2  +/-   1.4
GLSV   01-02  317  2007     3.1  +/-  0.1    -5.5  +/-  0.2     -2.3  +/-   0.4
GODE   01-02  239  1998     1.9  +/-  0.1     1.8  +/-  0.1     -6.1  +/-   0.5
GOLD   01-02  289  1999   -10.5  +/-  0.1    -4.3  +/-  0.1      4.5  +/-   0.5
GOUG   01-02  205  2007    16.1  +/-  0.3    -5.3  +/-  0.3     24.4  +/-   2.1
GRAS   01-02  113  2003     5.8  +/-  0.1     1.7  +/-  0.1      2.3  +/-   0.5
GRAZ   01-02  177  1996     0.4  +/-  0.3    -3.0  +/-  0.3     -3.6  +/-   0.9
GRAZ   02-03  152  2001    -3.5  +/-  0.1    -1.1  +/-  0.2      0.4  +/-   0.5
GUAM   01-02  285  2001     2.7  +/-  0.3    -4.0  +/-  0.2     -1.8  +/-   1.0
GUAM   02-03  116  2002     1.9  +/-  0.3   -15.9  +/-  0.2     -7.9  +/-   1.0
HARB   01-02  332  2007     0.0  +/-  0.3     2.3  +/-  0.2     -2.5  +/-   0.9
HARV   01-02  253  1999    -1.7  +/-  0.1     0.4  +/-  0.1     12.9  +/-   0.5
HIL1   01-02  208  2006    -3.3  +/-  0.3     9.1  +/-  0.3     -2.0  +/-   1.1
HNLC   01-02  286  2004    -0.1  +/-  0.2    -1.2  +/-  0.2      0.2  +/-   0.7
HNPT   01-02  143  2000     3.4  +/-  0.1     2.7  +/-  0.1      0.0  +/-   0.6
HNPT   02-03  165  2007    -0.8  +/-  0.1     3.1  +/-  0.2     61.3  +/-   0.5
HOB2   01-02  225  1998     0.0  +/-  1.1    -0.1  +/-  1.2   -149.6  +/-  23.4
HOB2   02-03  299  1998    -0.1  +/-  1.1     2.0  +/-  1.2    145.7  +/-  23.4
HOB2   03-04  358  2004     4.1  +/-  0.1    -4.5  +/-  0.2     -2.9  +/-   0.5
HOFN   01-02  264  2001    -0.6  +/-  0.1    -1.0  +/-  0.2     46.6  +/-   0.5
HOLB   01-02  023  2002     1.8  +/-  0.1     3.0  +/-  0.2    -25.1  +/-   0.5
HOLB   02-03  351  2003    -1.3  +/-  0.1     1.3  +/-  0.2      5.3  +/-   0.5
HRAO   01-02  324  2004     2.0  +/-  0.2    -2.6  +/-  0.2      5.5  +/-   0.6
HRAO   02-03  045  2006    -1.8  +/-  0.2    -0.1  +/-  0.2     -6.7  +/-   0.5
HRAO   03-04  045  2008    10.0  +/-  0.2    16.0  +/-  0.2     -1.6  +/-   0.6
HYDE   01-02  361  2004     8.1  +/-  0.2    -2.5  +/-  0.2     -2.3  +/-   0.8
HYDE   02-03  330  2007     1.9  +/-  0.2    -9.8  +/-  0.2      0.8  +/-   0.8
IISC   01-02  246  2004     4.4  +/-  0.3     3.0  +/-  0.3      2.8  +/-   1.1
IISC   02-03  361  2004    11.9  +/-  0.3    -5.8  +/-  0.3    -10.4  +/-   1.1
JAB1   01-02  331  2001     0.2  +/-  0.3     0.0  +/-  0.2     13.2  +/-   1.0
JAB1   02-03  063  2003     1.2  +/-  0.3    -3.9  +/-  0.2     -1.7  +/-   0.9
JAB1   03-04  053  2007     6.0  +/-  0.4    -2.3  +/-  0.4     13.2  +/-   1.9
JOZE   01-02  337  2004    -3.8  +/-  0.1     0.5  +/-  0.2     -0.9  +/-   0.5
JOZE   02-03  001  2006    -0.5  +/-  0.1    -0.3  +/-  0.2      0.6  +/-   0.5
KELS   01-02  008  1998    -5.7  +/-  0.3    -1.4  +/-  0.3     11.8  +/-   1.2
KEN1   01-02  307  2002    -1.7  +/-  0.2   -18.8  +/-  0.2     -9.0  +/-   0.7
```

```
KERG  01-02  091 1999      2.5 +/-  0.2       4.0 +/-  0.2       3.0 +/-  0.7
KERG  02-03  318 2002     -0.8 +/-  0.2       1.5 +/-  0.2     -11.4 +/-  0.8
KERG  03-04  249 2008     18.0 +/-  0.4      11.9 +/-  0.4     -14.3 +/-  1.2
KODK  01-02  016 2003      9.4 +/-  0.2      -1.0 +/-  0.3      -0.4 +/-  0.9
KOKB  01-02  267 2002    -25.4 +/-  0.2     -39.4 +/-  0.2      12.7 +/-  0.6
KOKB  02-03  139 2004     22.3 +/-  0.2      40.5 +/-  0.1      -9.4 +/-  0.5
KOUR  01-02  005 1998     -0.9 +/-  0.3      -1.8 +/-  0.2       9.8 +/-  1.2
KOUR  02-03  030 2002      0.8 +/-  0.2      -0.7 +/-  0.2      18.6 +/-  0.8
KUNM  01-02  040 2003      1.3 +/-  0.2       4.8 +/-  0.2      16.5 +/-  1.0
KUNM  02-03  361 2004     -5.7 +/-  0.2      -7.3 +/-  0.2      -3.7 +/-  0.9
LAMA  01-02  100 2000     16.2 +/-  0.2     -18.0 +/-  0.3       2.2 +/-  1.1
LAMA  02-03  280 2000    -22.0 +/-  0.2      14.9 +/-  0.3     -13.1 +/-  1.1
LHAZ  01-02  280 2008      6.4 +/-  0.3      -0.5 +/-  0.3      -3.1 +/-  1.1
LWTG  01-02  262 2006     -2.6 +/-  0.2       0.6 +/-  0.3      -1.4 +/-  0.9
MAC1  01-02  358 2004     -4.3 +/-  0.3     -15.4 +/-  0.4      -5.5 +/-  1.0
MAC1  02-03  083 2005     -0.7 +/-  0.3      -4.6 +/-  0.4       4.6 +/-  1.0
MALD  01-02  149 2000     -6.4 +/-  0.4      35.2 +/-  0.3      26.7 +/-  1.3
MALI  01-02  296 1997    -15.7 +/-  0.3       6.6 +/-  0.2       2.5 +/-  1.1
MALI  02-03  165 2001      1.0 +/-  0.3      -3.9 +/-  0.2       6.4 +/-  1.0
MALL  01-02  226 2003     -5.8 +/-  0.2     -13.4 +/-  0.2      -1.0 +/-  0.6
MANA  01-02  283 2004     -8.8 +/-  0.4      -6.4 +/-  0.3      11.5 +/-  1.3
MANZ  01-02  319 2002    -62.4 +/-  0.5      54.3 +/-  0.4       1.2 +/-  1.7
MANZ  02-03  016 2003      1.4 +/-  0.5    -133.7 +/-  0.5      30.2 +/-  1.9
MANZ  03-04  142 2003   -382.1 +/-  0.4     193.3 +/-  0.4     -15.7 +/-  1.7
MANZ  04-05  204 2004    317.7 +/-  0.4    -205.9 +/-  0.3      18.2 +/-  1.4
MARS  01-02  087 2003     -5.8 +/-  0.1       5.7 +/-  0.2       0.9 +/-  0.6
MARS  02-03  210 2004      5.8 +/-  0.1      -3.4 +/-  0.2       1.5 +/-  0.6
MAS1  01-02  226 1999     -1.3 +/-  0.1       3.9 +/-  0.1       1.6 +/-  0.6
MAS1  02-03  190 2008      2.4 +/-  0.2       6.8 +/-  0.2      -0.7 +/-  0.7
MATE  01-02  102 1996     -0.5 +/-  0.5      -1.0 +/-  0.5     -28.8 +/-  1.8
MATE  02-03  191 1996     -0.6 +/-  0.4       4.2 +/-  0.3      28.6 +/-  1.4
MATE  03-04  169 1999      7.9 +/-  0.1      -0.3 +/-  0.1      -1.0 +/-  0.4
MATE  04-05  329 2008     -5.0 +/-  0.4       2.9 +/-  0.4       3.1 +/-  1.4
MBAR  01-02  241 2002      1.8 +/-  0.3       3.3 +/-  0.3       5.3 +/-  1.0
MBAR  02-03  086 2008     -0.4 +/-  0.3       0.0 +/-  0.3      -6.9 +/-  0.9
MCM4  01-02  028 1999     -0.7 +/-  0.1      -1.5 +/-  0.1      39.4 +/-  0.5
MCM4  02-03  003 2002     -1.7 +/-  0.1      -0.3 +/-  0.1     -15.2 +/-  0.5
MDO1  01-02  342 2004     -3.6 +/-  0.1       2.6 +/-  0.1      -9.6 +/-  0.5
MKEA  01-02  288 2006    -10.4 +/-  0.2       2.8 +/-  0.1      -4.6 +/-  0.5
NANO  01-02  009 2003      0.2 +/-  0.1       5.7 +/-  0.1      -6.1 +/-  0.5
NCDK  01-02  348 2004     10.7 +/-  0.2      -7.3 +/-  0.2      -2.5 +/-  0.9
NEAH  01-02  109 2005      1.6 +/-  0.1       0.6 +/-  0.2      -5.1 +/-  0.5
NEWL  01-02  169 2003     -0.1 +/-  0.1       0.3 +/-  0.2       2.7 +/-  0.5
NEWL  02-03  087 2008     -3.3 +/-  0.3      -8.6 +/-  0.4      -1.3 +/-  1.1
NEWP  01-02  066 1998      8.2 +/-  0.3       1.7 +/-  0.3      10.0 +/-  1.0
NIAM  01-02  238 2005      1.2 +/-  0.3       5.0 +/-  0.2     -10.4 +/-  0.9
NICO  01-02  233 1999     -4.1 +/-  0.2       2.7 +/-  0.2       3.5 +/-  0.6
NICO  02-03  163 2008     -0.8 +/-  0.2       6.5 +/-  0.2       1.9 +/-  0.7
NOUM  01-02  327 2001     -6.5 +/-  0.2       0.2 +/-  0.2      -7.5 +/-  0.7
NOVJ  01-02  332 2002     -0.2 +/-  0.3       0.8 +/-  0.3     -16.5 +/-  1.2
NSTG  01-02  129 2001      0.4 +/-  0.3       0.2 +/-  0.3       7.7 +/-  1.0
NSTG  02-03  095 2002      0.6 +/-  0.2      -0.6 +/-  0.2      -9.9 +/-  0.8
NTUS  01-02  301 1999      2.6 +/-  0.4       0.1 +/-  0.3      -6.7 +/-  1.2
NTUS  02-03  053 2001     -0.9 +/-  0.4      -5.7 +/-  0.4      -1.0 +/-  1.3
NYAL  01-02  249 2001     -1.7 +/-  0.1      -5.6 +/-  0.1       2.3 +/-  0.3
OHI3  01-02  310 2007     -2.4 +/-  0.2      -0.6 +/-  0.2      -5.4 +/-  0.5
ONSA  01-02  033 1999      0.6 +/-  0.1      -0.2 +/-  0.1     -12.0 +/-  0.3
P201  01-02  268 2003     15.4 +/-  0.2     -34.4 +/-  0.3      -0.1 +/-  0.7
P201  02-03  333 2004     -2.8 +/-  0.2      -8.3 +/-  0.2       3.6 +/-  0.6
```

```
P202  01-02  268 2003    12.1 +/-  0.3    -52.6 +/-  0.3     -6.9 +/-  1.0
P202  02-03  333 2004     6.4 +/-  0.2    -23.1 +/-  0.2     -0.6 +/-  0.7
P202  03-04  033 2006    -1.8 +/-  0.2     -3.2 +/-  0.3     -1.2 +/-  0.8
P203  01-02  268 2003   203.8 +/-  0.4     18.5 +/-  0.4      0.3 +/-  1.3
P203  02-03  333 2004   100.1 +/-  0.7    -62.4 +/-  0.9     -1.8 +/-  2.5
P204  01-02  268 2003    48.7 +/-  0.2     -1.3 +/-  0.3     -6.0 +/-  0.8
P205  01-02  228 2005    -3.0 +/-  0.5    -23.0 +/-  0.6     10.9 +/-  1.9
P205  02-03  165 2008   -17.8 +/-  0.2     -1.8 +/-  0.3      1.9 +/-  0.9
P207  01-02  249 2004     0.8 +/-  0.2    -11.6 +/-  0.3      1.7 +/-  0.8
P207  02-03  081 2007    -9.9 +/-  0.2      6.3 +/-  0.3      2.6 +/-  0.8
P208  01-02  249 2004   -13.2 +/-  0.2    -12.8 +/-  0.2    -10.0 +/-  0.7
P210  01-02  242 2007    -1.0 +/-  0.5      5.6 +/-  0.5     -3.5 +/-  1.9
P210  02-03  333 2007    -3.5 +/-  0.5     14.1 +/-  0.5     -9.7 +/-  1.9
P213  01-02  045 2008    21.5 +/-  0.2     -7.1 +/-  0.2      3.3 +/-  0.8
PDEL  01-02  348 2006     2.7 +/-  0.2      6.3 +/-  0.2      1.2 +/-  0.6
PDEL  02-03  097 2008    -0.4 +/-  0.2      1.1 +/-  0.2      6.1 +/-  0.6
PERT  01-02  156 2001     0.4 +/-  0.2      4.9 +/-  0.2    -17.6 +/-  0.6
PERT  02-03  156 2003    -0.1 +/-  0.2     -4.4 +/-  0.2     -4.7 +/-  0.6
PETP  01-02  020 2005    -4.3 +/-  0.2      6.0 +/-  0.2     -3.2 +/-  0.6
PETP  02-03  307 2005    -1.9 +/-  0.2      0.5 +/-  0.2    -10.5 +/-  0.6
PETP  03-04  179 2007    -4.3 +/-  0.1     12.5 +/-  0.2     -4.8 +/-  0.5
PIE1  01-02  023 2007    -4.6 +/-  0.1      5.4 +/-  0.1    -13.6 +/-  0.4
PIMO  01-02  345 1999    -3.2 +/-  0.3     -0.5 +/-  0.3     -2.7 +/-  1.5
PIMO  02-03  361 2004    -6.8 +/-  0.3      1.5 +/-  0.2     -3.2 +/-  1.1
POR1  01-02  035 1999  -153.4 +/-  1.1  -3338.4 +/-  1.0     82.2 +/-  4.4
POTS  01-02  232 1999     0.3 +/-  0.1     -1.2 +/-  0.1     -7.7 +/-  0.4
QAQ1  01-02  248 2003     4.2 +/-  0.2     -1.3 +/-  0.2      5.0 +/-  0.7
QAQ1  02-03  364 2003    -4.8 +/-  0.2      5.2 +/-  0.2      0.9 +/-  0.7
QUIN  01-02  091 1998    -4.5 +/-  0.2      4.7 +/-  0.2     -8.5 +/-  0.7
RAMO  01-02  199 2000   -16.2 +/-  0.2     -9.5 +/-  0.1     -1.2 +/-  0.5
RAMO  02-03  077 2004    15.3 +/-  0.1      6.1 +/-  0.1     -9.2 +/-  0.5
REYK  01-02  169 2000    -7.4 +/-  0.2      9.9 +/-  0.2     -8.6 +/-  0.6
REYK  02-03  164 2003    -3.6 +/-  0.1      0.3 +/-  0.2    -14.9 +/-  0.6
REYK  03-04  073 2008     4.0 +/-  0.2      1.8 +/-  0.3      3.2 +/-  1.0
REYK  04-05  150 2008    -7.1 +/-  0.3      3.8 +/-  0.3      5.7 +/-  1.1
RIGA  01-02  013 2005     5.0 +/-  0.1      0.2 +/-  0.1     -4.1 +/-  0.5
RIGA  02-03  142 2006    -5.1 +/-  0.1     -0.3 +/-  0.1     -0.9 +/-  0.5
RIGA  03-04  350 2007    -1.1 +/-  0.2      2.5 +/-  0.2     -0.3 +/-  0.6
SANT  01-02  199 1996    -4.2 +/-  0.4     -0.2 +/-  0.4      4.2 +/-  1.4
SANT  02-03  315 1998    -4.2 +/-  0.2      1.1 +/-  0.2      1.8 +/-  0.6
SCH2  01-02  280 2008    -3.0 +/-  0.2      8.5 +/-  0.3      4.9 +/-  0.8
SEAT  01-02  142 1998    -3.4 +/-  0.2     -3.1 +/-  0.2     10.9 +/-  0.6
SEAT  02-03  249 2002    -0.5 +/-  0.1      0.3 +/-  0.1      3.4 +/-  0.5
SELD  01-02  138 2006    11.2 +/-  0.2      2.5 +/-  0.2    -31.6 +/-  0.6
SFER  01-02  035 1998     0.4 +/-  0.5      4.8 +/-  0.5      9.9 +/-  2.7
SFER  02-03  153 1998     6.5 +/-  0.4     -2.2 +/-  0.4     -4.2 +/-  2.2
SFER  03-04  064 2002     4.6 +/-  0.1     -7.2 +/-  0.1      1.7 +/-  0.5
SFER  04-05  156 2003    -8.5 +/-  0.1      6.4 +/-  0.1      1.8 +/-  0.5
SFER  05-06  195 2005    -6.0 +/-  0.1     -2.1 +/-  0.1      4.8 +/-  0.5
SIO3  01-02  013 1998     3.1 +/-  0.1     -4.6 +/-  0.1      9.8 +/-  0.5
SIO3  02-03  289 1999     1.9 +/-  0.2      9.0 +/-  0.2      2.5 +/-  0.7
SIO3  03-04  103 2000     0.2 +/-  0.2      2.5 +/-  0.2     10.5 +/-  0.7
SIO3  04-05  249 2007    -3.4 +/-  0.1      1.7 +/-  0.1     -5.4 +/-  0.5
SOL1  01-02  242 2000    -0.2 +/-  0.2      0.1 +/-  0.2     -3.1 +/-  0.8
SOL1  02-03  334 2006    -0.6 +/-  0.2     -0.1 +/-  0.2      3.7 +/-  0.7
SPLT  01-02  054 2006    -8.3 +/-  0.2     -2.4 +/-  0.2      2.6 +/-  0.7
STAS  01-02  122 2007     2.5 +/-  0.1     -0.3 +/-  0.1     -6.2 +/-  0.4
STJO  01-02  214 1996    -1.5 +/-  0.2     -3.0 +/-  0.3     -2.4 +/-  0.8
SUTH  01-02  153 2004     4.5 +/-  0.1      1.1 +/-  0.1     -1.5 +/-  0.4
```

```
SYOG   01-02   026 2007      -1.5 +/-   0.2       0.9 +/-   0.2     -11.7 +/-   0.6
THU1   01-02   175 2001      -3.9 +/-   0.3      -3.4 +/-   0.3       9.1 +/-   2.6
TIDB   01-02   178 1996      -0.9 +/-   0.4       5.7 +/-   0.3     -18.3 +/-   1.1
TONG   01-02   123 2006      81.6 +/-   0.3      23.5 +/-   0.3     -11.5 +/-   1.2
TORS   01-02   085 2002      -4.8 +/-   0.2       2.7 +/-   0.3      -0.6 +/-   0.9
TRDS   01-02   127 2007       0.8 +/-   0.1       5.1 +/-   0.2      -3.2 +/-   0.5
TRO1   01-02   139 2000       2.3 +/-   0.1       2.5 +/-   0.2       0.6 +/-   0.5
TRO1   02-03   195 2004     -10.2 +/-   0.1      -4.6 +/-   0.1       7.4 +/-   0.5
TSEA   01-02   307 2002     -13.6 +/-   0.2     -13.7 +/-   0.2      -4.1 +/-   0.7
TSKB   01-02   235 2000       7.1 +/-   0.2       3.6 +/-   0.2      -8.6 +/-   0.6
TSKB   02-03   128 2008       8.9 +/-   0.2      -1.1 +/-   0.2      -2.2 +/-   0.6
URUM   01-02   267 1999       0.7 +/-   0.2      -0.4 +/-   0.3     -13.2 +/-   0.9
USNA   01-02   136 2001      -0.2 +/-   0.2       0.3 +/-   0.2       4.5 +/-   0.7
USNA   02-03   340 2001      -3.1 +/-   0.2      -1.1 +/-   0.2       7.7 +/-   0.7
VALE   01-02   055 2005       1.5 +/-   0.2      -5.3 +/-   0.2      -1.2 +/-   0.6
VANU   01-02   113 2004      -7.0 +/-   0.3      -2.6 +/-   0.3       1.2 +/-   1.1
VANU   02-03   258 2005      -8.4 +/-   0.3      -0.4 +/-   0.3       4.0 +/-   1.2
VANU   03-04   157 2008      -4.3 +/-   0.3      -1.0 +/-   0.3      -4.3 +/-   1.0
VENE   01-02   274 1997       0.9 +/-   0.3      -3.2 +/-   0.3      34.6 +/-   1.4
VENE   02-03   231 1999      -0.2 +/-   0.2       0.7 +/-   0.2     -53.4 +/-   1.0
VENE   03-04   032 2001       6.2 +/-   0.2       4.1 +/-   0.2      93.0 +/-   0.9
VENE   04-05   301 2005      -5.6 +/-   0.1       3.1 +/-   0.2      -7.2 +/-   0.5
VESL   01-02   101 2002      -0.5 +/-   0.2      -1.1 +/-   0.2     -14.1 +/-   0.7
VIGO   01-02   082 2007       0.1 +/-   0.3      -0.8 +/-   0.3       4.0 +/-   1.0
VILL   01-02   057 1998      -0.7 +/-   0.2      -0.5 +/-   0.2      -0.5 +/-   0.6
VILL   02-03   113 2001      -2.1 +/-   0.2      -0.6 +/-   0.2      -0.9 +/-   0.6
VILL   03-04   272 2004      -1.8 +/-   0.2       2.9 +/-   0.2       2.2 +/-   0.6
VTIS   01-02   162 2004      -0.2 +/-   0.1      -0.5 +/-   0.1      -4.6 +/-   0.5
WARN   01-02   295 2003       3.1 +/-   0.1       3.0 +/-   0.2       3.9 +/-   0.5
WARN   02-03   025 2008       0.2 +/-   0.2       1.0 +/-   0.2       0.4 +/-   0.6
WES2   01-02   181 1997      -8.0 +/-   0.2       8.3 +/-   0.2       1.1 +/-   0.6
WES2   02-03   152 1998      10.8 +/-   0.1      -8.8 +/-   0.2      -2.4 +/-   0.5
WES2   03-04   235 2000      -9.5 +/-   0.1       3.9 +/-   0.2      -6.4 +/-   0.7
WES2   04-05   208 2001      -0.3 +/-   0.2      -5.1 +/-   0.2       8.6 +/-   0.8
WES2   05-06   283 2002       0.3 +/-   0.2      -0.2 +/-   0.2      -5.7 +/-   0.6
WGTT   01-02   358 2004       3.1 +/-   0.2       3.3 +/-   0.2       0.1 +/-   0.7
WHIT   01-02   296 2002       6.3 +/-   0.1       1.2 +/-   0.1       6.2 +/-   0.3
WSRT   01-02   076 1998       0.8 +/-   0.1      -0.6 +/-   0.2       3.9 +/-   0.4
WUHN   01-02   128 1997       1.3 +/-   0.5      -2.1 +/-   0.4       2.8 +/-   1.8
WUHN   02-03   189 1999      -3.0 +/-   0.3       3.5 +/-   0.2      -4.8 +/-   1.1
WUHN   03-04   069 2000       7.5 +/-   0.2       2.8 +/-   0.2      -0.4 +/-   1.1
WUHN   04-05   026 2002      -0.8 +/-   0.2       0.2 +/-   0.2      43.7 +/-   0.7
YELL   01-02   235 1996       0.0 +/-   0.2       2.0 +/-   0.2     -19.6 +/-   0.8
YSSK   01-02   319 2006      11.5 +/-   0.2       0.3 +/-   0.3       0.9 +/-   0.7
ZIMM   01-02   310 1998       5.1 +/-   0.1       0.2 +/-   0.1      -2.4 +/-   0.4
```

D. Publications

D1. Santamaría-Gómez. A., M-.N. Bouin, and G. Wöppelmann (in press), Improved GPS data analysis strategy for tide gauge benchmark monitoring, Proceedings of the International Association of Geodesy General Assembly, Buenos Aires, Argentina, August 31-September 4,2009.

D2. Wöppelmann, G., C. Letetrel, A. Santamaría, M.-N. Bouin, X. Collilieux, Z. Altamimi, S. D. P. Williams, and B. Martín Miguez (2009), Rates of sea-level change over the past century in a geocentric reference frame, Geophys. Res. Lett., 36, L12607, doi:10.1029/2009GL038720.

D3. Bruyninx, C., Z. Altamimi, M. Becker, M. Craymer, L. Combrinck, A. Combrink, J. Dawson, R. Dietrich, R. Fernandes, R. Govind, T. Herring, A. Kenyeres, R. King, C. Kreemer, D. Lavallée, J. Legrand, L. Sánchez, G. Sella, Z. Shen, A. Santamaría-Gómez, G. Wöppelmann (in press), A Dense Global Velocity Field based on GNSS Observations: Preliminary Results, Proceedings of the International Association of Geodesy General Assembly, Buenos Aires, Argentina, August 31-September 4,2009.

D4. Legrand, J., N. Bergeot, C. Bruyninx, G. Wöppelmann, A. Santamaría-Gómez, M.-N. Bouin, Z. Altamimi (in press), Comparison of Regional and Global GNSS Positions, Velocities and Residual Time Series, Proceedings of the International Association of Geodesy General Assembly, Buenos Aires, Argentina, August 31-September 4,2009.

D5. Santamaría, A., M.-N. Bouin, and G. Wöppelmann (2008), New strategy for reprocessing a global GPS network at the ULR TIGA Analysis Centre, paper presented at the European Geosciences Union meeting, Vienna, 13 − 18 April, 2008.

D6. Santamaría, A., M.-N. Bouin, and G. Wöppelmann (2009), Impact of sub-network configuration on global scale GPS processing, paper presented at the European Geosciences Union meeting, Vienna, 19 − 24 April, 2009.

Improved GPS data analysis strategy for tide gauge benchmark monitoring

Alvaro Santamaría-Gómez
Instituto Geográfico Nacional, c/ General Ibañez Ibero 3, 28071, Madrid, Spain
Institut Géographique National, LAREG/GRGS, 6 - 8 av. Blaise Pascal, 77455, Champs-sur-Marne, France

Marie-Noëlle Bouin
Institut Géographique National, LAREG/GRGS, 6 - 8 av. Blaise Pascal, 77455, Champs-sur-Marne, France
CNRM/CMM, Météo France, 13 rue du Chatellier, CS 12804, 29228 Brest, France

Guy Wöppelmann
Université de La Rochelle-CNRS, UMR 6250 LIENSS, 2 rue Olympe de Gouges, 17000, La Rochelle, France

Abstract. The University of La Rochelle (ULR) TIGA Analysis Center (TAC) completed a new global reprocessed solution spanning 13 years with more than 300 GPS permanent stations, 216 of them being co-located with tide gauges. A state-of-the-art GPS processing strategy was applied, in particular, the station sub-networks used in the daily processing were optimally built. Station vertical velocities were estimated in the ITRF2005 reference frame by stacking the weekly position estimates. Outliers, offsets and discontinuities in time series were carefully examined. Vertical velocities uncertainties were assessed in a realistic way by analysing the type and amplitude of the noise content in the residual position time series. The comparison shows that the velocity uncertainties have been reduced by a factor of 2 with respect to previous ULR solutions. The analysis of this solution and its by-products shows the high geodetic quality achieved in terms of homogeneity, precision and consistency with respect to other top-level geodetic solutions.

Keywords: GPS, tide gauges, ITRF.

1 Introduction

In order to estimate long-term geocentric sea level rise, tide gauges trends must be corrected for the long-term vertical displacements of the land upon which they are settled. In addition, for proper satellite altimeter calibration purposes, tide gauges trends must be referred to a common, global and stable reference frame, such as the latest realization of the International Terrestrial Reference Frame (ITRF) [Altamimi et al., 2007].

These long-term vertical displacements can be corrected by modelling geological processes as the Global Isostatic Adjustment (GIA) [e.g. Douglas, 2001] or directly from continuous geodetic observations at or near tide gauges. This second method should be preferred as it takes into account local displacements (geological, anthropogenic or whatever), not accounted for in the GIA models. Within the different geodetic techniques used for this purpose (GPS, DORIS and absolute gravity), GPS is the most widespread. Recent studies [Wöppelmann et al., 2009; Bouin and Wöppelmann, 2010] have shown that correcting the tide gauge trends using continuous GPS stations (cGPS@TG) improves the consistency of the sea level rates. To this aim, the International GNSS Service (IGS) Tide Gauge Benchmark Monitoring Pilot Project (TIGA) was established in 2001 [Schöne et al., 2009]. Since 2002, the ULR consortium contributes to the TIGA project as an Analysis and Data Center [Wöppelmann et al., 2004].

Several global vertical velocity field solutions (ULR solutions hereafter) were released with different station networks, time spans and processing strategies [Wöppelmann et al., 2007; 2009]. In this paper, we present the fourth ULR solution based on an homogeneous reprocessing of a larger global network of 316 stations, spanning an increased period of 13 years (January 1996 to December 2008). This solution comes out with a new data analysis strategy, including a new sub-network design and combination. The troposphere and ocean tide modelisation were also improved. Both GPS processing and vertical velocity estimation strategies are described; realistic uncertainties are estimated by analysing the noise content of time series. Finally, the quality of the solution is assessed and discussed.

2 Data analysis strategy

2.1 Data

The global tracking network consists of 316 GPS stations. 216 of them are cGPS@TG, including 81 stations committed to TIGA. Also 124 of them are IGS reference frame (RF) stations used for realizing the reference frame [Kouba et al., 1998] and for improving the network geometry.
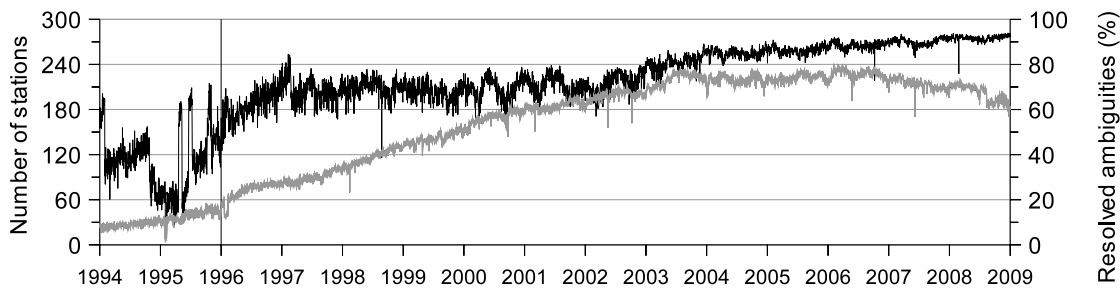
Fig. 1 Number of daily available stations (grey) and percentage of daily resolved ambiguities (black).

This network was processed over the period 1st January 1994 to 31st December 2008. Small RINEX files (less than 5 hours of observation) were rejected. This quality check procedure yielded a number of daily available stations between a minimum of 25 in 1994 (53 in 1996) and a maximum of 239 in 2006 (grey line in Figure 1). 1994 and 1995 were finally not retained in the solution due to a lack of fixed ambiguities and therefore quality (black line in Figure 1) and they will not be further considered.

2.2 Improved network geometry

GPS processing time increases exponentially with the number of stations. To overcome this limitation, it is usual to split the whole network in several sub-networks, to process each sub-network independently and then to combine the sub-network solutions into a unique daily solution.

Historic ULR solutions (ULR1 to ULR3 solutions) used five global, manually-selected, permanent sub-networks over the entire data span ("static sub-networks" hereafter). Using this approach, the a priori stations included in each sub-network were always the same, whether or not their data were available for a specific day, making the geometry worse when their data were missing, and therefore, possibly yielding an unnecessary large number of sub-networks in the processing (always five). This static configuration was changed in the ULR4 solution into a new station distribution approach resulting in global, automatic, daily-variable sub-networks ("dynamic sub-networks" hereafter), with up to 50 stations per sub-network.

Shorter baselines improves ambiguity resolution [Steigenberger et al., 2006]. With the dynamic approach, all daily available stations were distributed into the strictly necessary number of sub-networks, ensuring optimal dense sub-networks. Thus, the number of dynamic sub-networks used grows from 1 in 1996 to 6 in 2003. Moreover, to obtain global geometrically well-distributed sub-networks for optimal orbit estimation, each station is assigned to the sub-network where it is more isolated, i.e. reducing the baselines. In this way, "deserted" areas of each sub-network are iteratively being "populated".

In addition, six daily-variable common IGS RF stations, with more than 12h of observation, are included in each dynamic sub-network to combine the solutions. Northernmost and southernmost stations are always selected and then four other globally well-distributed stations are added.

Static versus dynamic approaches were compared by processing two solutions using the same stations and processing strategy except for the stations distribution. Figure 2 shows that using dynamic sub-networks clearly increases the percentage of resolved ambiguities as the number of available stations decreases, up to 20% in 1997 (Figure 2). The 10% offset in the percentage of resolved ambiguities observed at the end of 1999 for both appraches is related to the use of code bias corrections (see section 2.3), only available for post-2000 year period when the test was performed.

2.3 Models and parameterization

Double-differenced ionosphere-free carrier phase data is analysed using GAMIT software version 10.34 [Herring et al., 2006a]. The elevation cut-off angle is set to 10°, avoiding mismodelling of low-elevation troposphere and phase center variations (PCV) of relative-to-absolute antenna calibration. Sampling rate is set to 3 minutes. Carrier phase observations are weighted in two iterations: by elevation angle first and then by elevation angle and by station, accounting for the station phase residuals
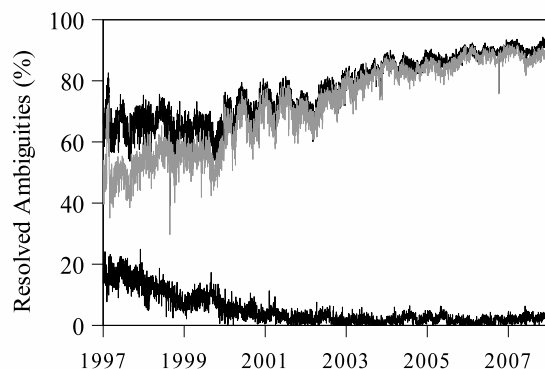
Fig. 2 Resolved ambiguities for static (grey), dynamic sub-networks (top black) and the difference (bottom black).

from the first iteration. Code bias corrections are applied for the whole period using monthly tables from the Astronomical Institute of the University of Bern (AIUB) [IGSMAIL-2827 (2000) at http://igscb.jpl.nasa.gov/mail/]. Real-valued double differenced phase cycle ambiguities are adjusted except when they can be resolved confidently. In this case, they are fixed using the Melbourne-Wübbena wide-lane to resolve L1-L2 cycles and then estimation to resolve L1 and L2 cycles. For satellite antennas, satellite-specific z-offsets [Ge et al., 2005] and block-specific nadir angle-dependent absolute PCV [Schmid et al., 2007] are applied. For receiver antennas, L1/L2 offsets and azimuth-dependent, when available, and elevation-dependent absolute PCV are applied. A priori zenith hydrostatic (dry) delay values are extracted by station from the ECMWF meteorological model through the VMF1 grids [Boehm et al., 2006]. Residual delays are adjusted for each station assuming mostly dominated by the wet component and parameterized by a piecewise linear, continuous model with 2 hour intervals. Both dry and wet VMF1 mapping functions are used. One gradient is estimated for each day and each station. Solid Earth tides are corrected following IERS Conventions (2003) [McCarthy and Petit, 2004]. Ocean tide loading is corrected using FES2004 model [Lyard et al., 2006]. No atmospheric tide nor non-tidal corrections were applied. Earth orientation parameters (EOP) are daily estimated as a piecewise, linear model with a priori values from IERS Bulletin B. UT1-UTC offsets are highly constrained to their a priori values. Satellite positions and velocities are adjusted in 24 hours arcs taking IGS final orbits [Dow et al., 2005] as a priori. Solar radiation pressure parameters are estimated using the Berne model [Beutler et al., 1994].

2.4 Data processing scheme and reference frame

Each dynamic sub-network is processed independently using GAMIT software. The daily sub-network solutions are combined into a daily solution (by estimating only translations and rotations) using GLOBK [Herring et al., 2006b] by means of the estimated orbital parameters, the estimated positions of the six common stations and their estimated zenith tropospheric path delays. Daily loose solutions are constrained by no-net-rotation (NNR) constraints with respect to ITRF2005 and combined into a weekly solution using CATREF software [Altamimi et al., 2007]. These weekly solutions are aligned to ITRF2005 using NNR constraints with all IGS RF stations available, whereas inner constraints [Altamimi et al., 2007] are used for scale and translation, in order to preserve the weekly apparent geocenter motion information.

All the weekly solutions for the whole period (GPS weeks 0834 to 1512), are then combined into a long-term solution using CATREF. This long-term solution (ULR4) is aligned to ITRF2005 using minimal constraints over all the transformation parameters with a selected set of IGS RF stations called datum. The 68 stations retained in the datum were selected based on their data availability (at least present in 80% of the whole processed period) and their quality as follows. Firstly, stations with known or suspected velocity discontinuities were rejected, and secondly, in an iterated process, stations showing large position and velocity residuals with respect to ITRF2005 values were also rejected. Thresholds for positions were set to 0.5 cm in horizontal and 1.5 cm in vertical. The larger value in the vertical component is due to the fact that ITRF2005 GPS coordinates were estimated with a relative PCV model. Station differences using the absolute PCV model are estimated to be within this range. Thresholds for velocity residuals were set to 1.5 mm/yr and 2 mm/yr respectively.

The residual position time series of each station were visually examined. To avoid biased velocities, all discontinuities (significant offsets and velocity changes) were detected, identified if possible, and removed using ITRF2005 discontinuities as a priori. Then, all outliers were removed in an iterative process, from bigger to smaller magnitude (depending on the time series noise), down to a minimum of 2 cm for residuals and 4 for normalized residuals.

3 Results

3.1 Vertical rates

The vertical velocity fields of ULR4 and ULR3 [Wöppelmann et al., 2009] solutions were compared using a common set of 170 stations with more than 4.5 years of data. Figure 3 shows that most of the velocity differences are below 1 mm/yr (RMS of 0.8 mm/yr), except some stations for which larger differences are due to different discontinuities on their
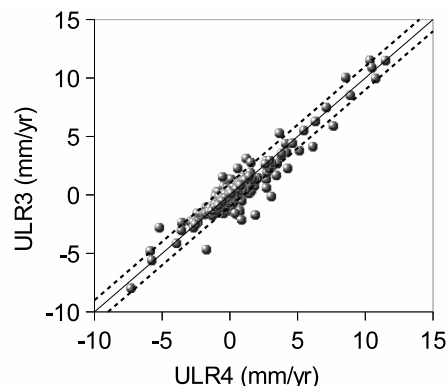
Fig. 3 Vertical velocity difference between ULR3 and ULR4. Dashed lines represent $\pm 1 mm/yr$.

time series. The mean difference between both velocity fields is 0.16 ± 0.06 mm/yr which is related to the different datum used to aling the solutions. This misalignment is under the internal precision of the ITRF2005.

From the complete ULR4 solution, 224 stations with more than 4.5 years of data were retained. For these stations, their estimated velocities are confidently not influenced by seasonal signals [Blewitt and Lavallée, 2002]. Nevertheless, the rate uncertainties estimated with a standard least squares algorithm (based on a Gaussian white noise process) are clearly optimistic by a factor of 3-11 [Zhang et al., 1997; Mao et al., 1999]. More realistic uncertainties of the estimated velocities must account for correlated noise present in the time series.

A noise analysis was performed using the Maximum Likelihood Estimation (MLE) technique (CATS software, [Williams, 2008]). Vertical velocity uncertainties were estimated using a white noise plus power law noise model. To avoid biased adjustments, time series were previously examined for periodic signals. Besides the annual and semi-annual terms, we also found and removed up to six harmonics of the GPS "draconitic" period described by Ray et al., 2007. Figure 4 shows the histogram of the realistic vertical velocity uncertainties of the ULR4 solution with respect to the realistic uncertainties estimated for the ULR3 solution also using CATS. The improvement is close to a factor of 2. Also the factor of optimism of the formal uncertainties with respect to the realistic ones is 2-3, quite smaller than the above-mentioned values. This is due to the improvement and consistency of the processing strategy presented here, which results in a noticeable reduction of the correlated noise content for the ULR4 solution compared to previous solutions.

3.2 Weekly repeatability

The internal quality of the ULR4 solution was assessed by analysing the repeatability of the weekly position solutions. Figure 5 shows the repeatability
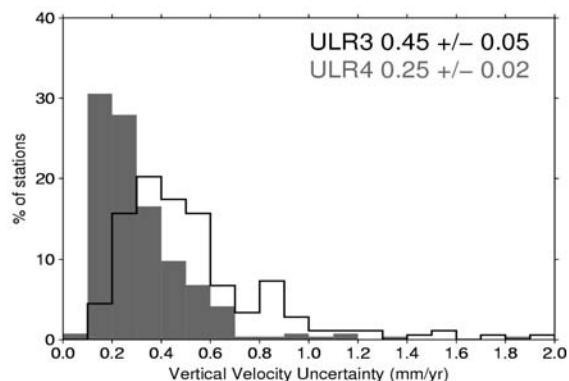
Fig. 4 Histogram of estimated uncertainties for ULR4 (grey) and ULR3 (black) solutions and their median values.
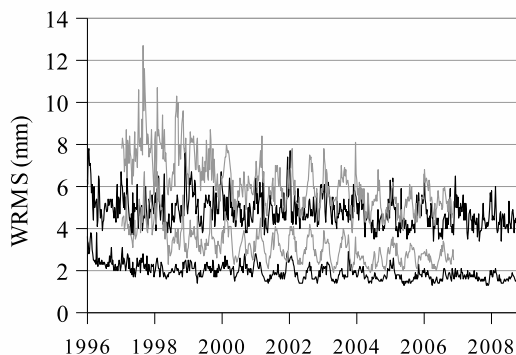
Fig. 5 Horizontal (bottom) and vertical (top) weighted RMS of the weekly solutions with respect to the long-term solution for both ULR4 (black) and ULR3 (grey) solutions.

of the time series (mean values of the weighted RMS of the weekly positions with respect to the long-term combined positions) for ULR4 and ULR3 solutions. Horizontal and vertical repeatabilities are improved in the ULR4 solution. Moreover, for the whole reprocessed period vertical repeatabilities are more stable, showing the improved ULR4 time consistency. ULR4 repeatability values are between 1 and 3 mm for the horizontal and between 4 and 6 mm for the vertical component (3D weighted RMS between 2 and 4 mm). These values are fully consistent with those of the IGS combined solution [Altamimi and Collilieux, 2008], showing that ULR4 solution is comparable in quality with the ITRF2005.

3.3 Origin and scale

As a satellite technique, GPS estimated origin should be coincident with the Earth's center of mass. However this affirmation is not completely fulfilled due to remaining GPS-specific systematic errors, as the modelling of the solar radiation pressure coefficients or the unaccounted effect of higher ionospheric orders [Hernández-Pajares et al., 2007].

We have estimated here apparent geocenter motion using the network shift or geometric approach [Lavallée et al., 2006]. Figure 6 shows the translation and scale parameters of the weekly solutions with respect to the long-term combined solution aligned to the ITRF2005. Translation trends are not significant, showing the consistency of the secular origin definition with respect to the ITRF2005. The scale shows no trend either, as this parameter is completely dependent on the ITRF2005 scale definition through the satellites antenna z-offset corrections. For intercomparison purposes, an annual signal was estimated for each transformation parameter (Table 1).

Compared to SLR results [Collilieux et al., 2009], the annual amplitudes of the equatorial components (X and Y) and the scale are fully consistent. However, the amplitude of the Z component is twice larger. Regarding the annual phase, the scale
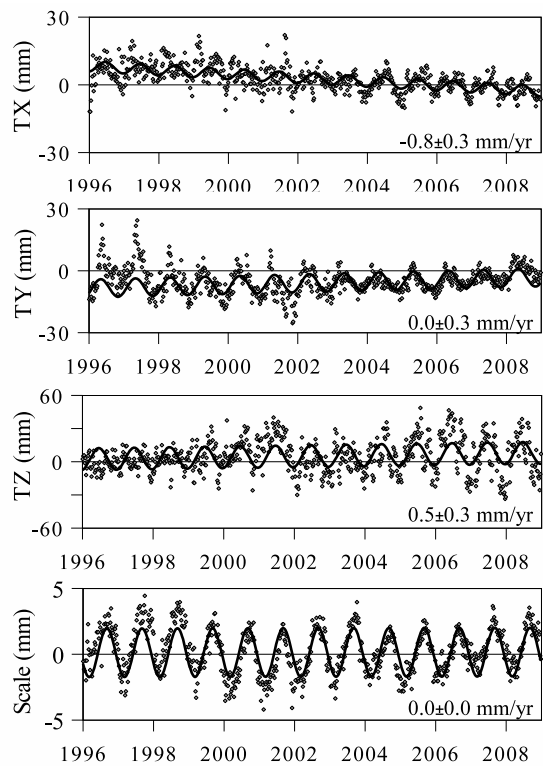
Fig. 6 Weekly translation and scale parameters with respect to the ITRF2005. Also their trends and annual signal are traced.

Table 1. Annual signal of apparent geocenter and scale

	Amplitude (mm)	Phase (deg)
TX	2.3 ± 0.2	164.6 ± 5.4
TY	4.2 ± 0.3	122.2 ± 3.5
TZ	9.9 ± 0.8	171.3 ± 3.5
Scale	1.8 ± 0.1	243.2 ± 1.6

parameter is fully consistent, but all translational parameters show a shift of about $137°$ (4.5 months). Compared to other GPS results [Lavallée et al., 2006], the amplitude of the Z component and both equatorial phases are consistent. The phase of Z component exhibits larger solution-dependent variations. Both issues point probably at the above-mentioned GPS systematic errors and also at the poor performance of the network shift method used with a not-well distributed global network [Lavallée et al., 2006].

3.4 Orbits

The estimated ULR4 orbits were compared with the current official non-reprocessed IGS final orbits [Dow et al., 2005]. A classic 7-parameter Helmert transformation was applied between both 24h-arc sets. 1D RMS differences (the average of the three RMS components) were estimated for each common observed satellite and then the median daily RMS value was extracted and traced (black line, Figure 7).
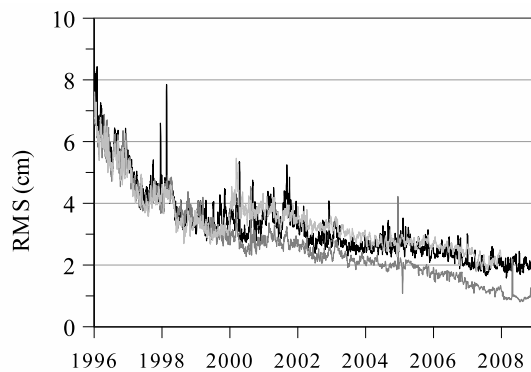
Fig. 7 7-day smoothed daily RMS between final IGS orbits and ULR (black), SIO/SOPAC (light grey) and CODE/AIUB (dark grey) reprocessed orbits.

We show that ULR and IGS orbits are in good agreement with each other, from 8.5 cm in 1996 to 1.5 cm in 2009. The same range of differences was obtained between IGS orbits and reprocessed orbits from SIO/SOPAC IGS Analysis Center (light grey line). Some smaller differences were obtained with reprocessed CODE/AIUB IGS Analysis Center (dark grey line) for the post-2000 period. This demonstrates that the ULR4 orbits are of the same quality as the reprocessed orbits of some of the IGS Analysis Centers.

4 Concluding remarks

The new ULR4 solution is based on an homogeneous reprocessing of a global GPS network of 316 stations spanning up to 13 years of data. The processing strategy was improved with respect to past ULR solutions. Special attention was paid to the sub-network geometry distribution, which clearly improves the quality of the reprocessing by increasing the number of resolved ambiguities. The analysis of the results and by-products of this solution (vertical velocities, repeatability, transformation parameters and orbits) shows the high geodetic quality achieved. The state-of-the-art GPS processing strategy implemented fulfils the IGS requirements and recommendations. Thereby, in addition to the IGS TIGA project, the ULR consortium is participating with its latest solution to the first IGS reanalysis campaign, enabling an invaluable extension of IGS and ITRF reference frames towards tide gauges. Also, the ULR consortium is contributing to the Working Group on Regional Dense Velocity Fields of the International Association of Geodesy Subcommision 1.3. [Bruyninx, submitted, this issue]. Further studies will be carried out in order to assess the geophysical usefulness of this solution. For example, this global and accurate vertical velocity field may be used to separate vertical land motion trends from relative sea level trends as recorded by tide gauges.

References

Altamimi, Z. and Collilieux, X. (2008). IGS contribution to ITRF. *J. Geod.*, 83(3-4):375–383.

Altamimi, Z., Collilieux, X., Legrand, J., Garayt, B., and Boucher, C. (2007). ITRF2005: A new release of the International Terrestrial Reference Frame based on time series of station positions and Earth Orientation Parameters. *J. Geophys. Res.*, 112(B09401).

Beutler, G., Brockmann, E., Gurtner, W., Hugentobler, U., Mervart, L., and Rothacher, M. (1994). Extended orbit modeling techniques at the CODE Processing Center of the International GPS Service for Geodynamics (IGS): theory and initial results. *Manuscripta Geodaetica*, (19):367–386.

Blewitt, G. and Lavallée, D. (2002). Effect of annual signals on geodetic velocity. *J. Geophys. Res.*, 107(B02145).

Boehm, J., Werl, B., and Schuh, H. (2006). Troposphere mapping functions for GPS and very long baseline interferometry from European Centre for Medium-Range Weather Forecasts operational analysis data. *J. Geophys. Res.*, 111(B02406).

Bouin, M.-N. and Wöppelmann, G. (2010). Land motion estimates from GPS at tide gauges: a geophysical evaluation. *Geophys. J. Int.*, (180):193–209.

Bruyninx, C. e. a. A dense global velocity field based on GNSS observations: preliminary results. *Submitted, this issue*.

Collilieux, X., Altamimi, Z., Ray, J., van Dam, T., and Wu, X. (2009). Effect of the satellite laser ranging network distribution on geocenter motion estimation. *J. Geophys. Res.*, 114(B02145).

Douglas, B. (2001). *Sea level change in the era of the recording tide gauge*, volume 75 of *International. Geophysics Series*. Academic, San Diego, California.

Dow, J. M., Neilan, R. E., and Gendt, G. (2005). The International GPS Service: Celebrating the 10th anniversary and looking to the next decade. *Adv. Space Res.*, 36:320–326.

Ge, M., Gendt, G., Dick, G., Zhang, F., and Reigber, C. (2005). Impact of GPS satellite antenna offsets on scale changes in global network solutions. *Geophys. Res. Lett.*, 32(L06310).

Hernández-Pajares, M., Juan, J. M., Sanz, J., and Orús, R. (2007). Second-order ionospheric term in GPS: Implementation and impact on geodetic estimates. *J. Geophys. Res.*, 112(B08417).

Herring, T. A., King, R. W., and McClusky, S. C. (2006a). GAMIT: Reference Manual Version 10.34. *Internal Memorandum, Massachusetts Institute of Technology, Cambridge*.

Herring, T. A., King, R. W., and McClusky, S. C. (2006b). GLOBK: Global Kalman filter VLBI and GPS analysis program Version 10.3. *Internal Memorandum, Massachusetts Institute of Technology, Cambridge.*

Kouba, J., J.R., R., and Watkins, M. (1998). IGS Reference Frame realization.IGS 1998 Analysis Center Workshop - Proceedings Darmstadt. page 139.

Lavallée, D., van Dam, T., Blewitt, G., and Clarke, P. (2006). Geocenter motions from GPS: A unified observation model. *J. Geophys. Res.*, 111(B05405).

Lyard, F., Lefevre, F., Letellier, T., and Francis, O. (2006). Modelling the global ocean tides: modern insights from FES2004. *Ocean Dynamics*, 56:394–415.

Mao, A., Harrison, C. G. A., and Dixon, T. H. (1999). Noise in GPS coordinate time series. *J. Geophys. Res.*, 104:2797–2816.

McCarthy, D. and Petit, G. (2004). IERS Technical Note 32 - IERS Conventions (2003). Technical report, Verlag des Bundesamts fur Kartographie und Geodasie, Frankfurt am Main, Germany.

Ray, R., Altamimi, Z., Collilieux, X., and Van Dam, T. (2007). Anomalous harmonics in the spectra of GPS position estimates. *GPS Solutions*, 12(1):55–64.

Schmid, R., Steigenberger, P., Gendt, G., Ge, M., and Rothacher, M. (2007). Generation of a consistent absolute phase-center correction model for GPS receiver and satellite antennas. *J. Geod.*, 81:781–798.

Schöne, T., Schön, N., and Thaller, D. (2009). IGS Tide Gauge Benchmark Monitoring Pilot Project (TIGA): scientific benefits. *J. Geod.*, 83:249–261.

Steigenberger, P., Rothacher, M., Dietrich, R., Fritsche, M., Rülke, A., and Vey, S. (2006). Reprocessing of a global GPS network. *J. Geophys. Res.*, 111(B05402).

Williams, S. D. P. (2008). CATS: GPS coordinate time series analysis software. *GPS Solutions*, 12(2):147–153.

Wöppelmann, G., Letretel, C., Santamaría, A., Bouin, M.-N., Collilieux, X., Altamimi, Z., Williams, S., and Martín Míguez, B. (2009). Rates of sea-level change over the past century in a geocentric reference frame. *Geophys. Res. Lett.*, 36(L12607).

Wöppelmann, G., Martín Míguez, B., Bouin, M.-N., and Altamimi, Z. (2007). Geocentric sea-level trend estimates from GPS analyses at relevant tide gauges world-wide. *Global and Planetary Change*, 57(3-4):396–406.

Wöppelmann, G., McLellan, S., Bouin, M.-N., Altamimi, Z., and Daniel, L. (2004). Current GPS data analysis at CLDG for the IGS TIGA Pilot Project. *Cahiers du Centre Européen Géodynamique & de Sismologie*, 23:149–154.

Zhang, J., Bock, Y., Johnson, H., Fang, P., Williams, S., Genrich, J., Wdowinski, S., and Behr, J. (1997). Southern California Permanent GPS Geodetic Array: Error analysis of daily position estimates and site velocities. *J. Geophys. Res.*, 102:18035–18056.

Rates of sea-level change over the past century in a geocentric reference frame

G. Wöppelmann,[1] C. Letetrel,[1] A. Santamaria,[2,3] M.-N. Bouin,[3,4] X. Collilieux,[3] Z. Altamimi,[3] S. D. P. Williams,[5] and B. Martin Miguez[6]

[1] The results from a carefully implemented GPS analysis, using a strategy adapted to determine accurate vertical station velocities, are presented. The stochastic properties of our globally distributed GPS position time series were inferred, allowing the computation of reliable velocity uncertainties. Most uncertainties were several times smaller than the $1-3$ mm/yr global sea level change, and hence the vertical velocities could be applied to correct the long tide gauge records for land motion. The sea level trends obtained in the ITRF2005 reference frame are more consistent than in the ITRF2000 or corrected for Glacial-Isostatic Adjustment (GIA) model predictions, both on the global and the regional scale, leading to a reconciled global rate of geocentric sea level rise of 1.61 ± 0.19 mm/yr over the past century in good agreement with the most recent estimates. **Citation:** Wöppelmann, G., C. Letetrel, A. Santamaria, M.-N. Bouin, X. Collilieux, Z. Altamimi, S. D. P. Williams, and B. Martin Miguez (2009), Rates of sea-level change over the past century in a geocentric reference frame, *Geophys. Res. Lett.*, *36*, L12607, doi:10.1029/2009GL038720.

1. Introduction

[2] Estimates of global-scale sea level rise over the past century are mainly based on long tide gauge records. The range of estimates published in the literature is rather wide (1 to 3 mm/yr), with figures converging towards 1.8 mm/yr [e.g., *Church and White*, 2006; *Douglas*, 2001; *Holgate*, 2007; *Jevrejeva et al.*, 2008]. To a large extent the origin of the differences lies in the methods used to correct the tide gauge records for vertical displacements of the land upon which they are located [e.g., *Woodworth*, 2006]. While most analyses have included corrections for Glacial-Isostatic Adjustment (GIA) effects, many other land motion processes, for example, associated with plate tectonics, volcanism, sediment compaction, or underground fluid extraction, have not been accounted for, except by excluding the possibly affected tide gauge records from consideration in the studies. Furthermore, the GIA models contain uncertainties in the knowledge of some geophysical parameters, which can yield to large differences in the magnitude and sign of the vertical displacement predictions [e.g., *Woodworth*, 2006].

[3] Encouraging results were recently obtained on global scales [e.g., *Steigenberger et al.*, 2006; *Wöppelmann et al.*, 2007], showing that the GPS technique in continuous mode and the reference frame realization have reached the maturity to provide useful information to account for land motion in tide gauge records. However, the issue remains challenging. To be useful site displacements at tide gauges should be monitored with standard errors several times smaller than the estimated $1-3$ mm/year rates of global sea level rise. The use of a consistent analysis strategy throughout the whole observation data span is demonstrated to be mandatory [e.g., *Steigenberger et al.*, 2006] to prevent GPS products (in particular GPS velocities) from being contaminated with spurious signals that make questionable any geophysical interpretation [e.g., *Penna et al.*, 2007]. In this study, we extended the *Wöppelmann et al.* [2007] results, providing consistent position time series at tide gauges over a longer data span of up to 10 years, based on the recent ITRF2005 reference frame [*Altamimi et al.*, 2007].

2. Data Analysis
2.1. GPS Observations and Processing

[4] We analyzed GPS observations from a global network of 227 stations using a consistent processing strategy over the whole period from January 1997 to November 2006. Among the stations, 160 are co-located within 15 km of a tide gauge, and 91 are used by the International GNSS Service (IGS) for the reference frame implementation. The electronic supplement provides a map showing the stations distribution (Figure S1[1]). We used the GAMIT software version 10.21 [*King and Bock*, 2006], estimating station coordinates, satellite orbits, Earth orientation parameters (EOPs), and zenith tropospheric delay parameters as a piecewise linear model with nodes every 2 hours. Daily observation files were grouped into five subnets with up to 50 stations each. To ensure the optimal estimation of satellite orbital parameters, as well as the alignment to the ITRF2005 reference frame, the subnet stations were globally distributed. Loosely constrained daily subnet solutions were produced using a priori site coordinates in the ITRF2005 reference frame; a priori orbits from the IGS; and a priori EOPs from the IERS Bulletin B. The daily subnet solutions (station coordinates with full co-variances) were combined and aligned to the ITRF2005 by means of minimum constraints using the CATREF Software [*Altamimi et al.*, 2002, 2007]. The obtained global daily solutions were combined into weekly solutions in a second step. The weekly solutions were provided to the TIGA pilot project [*Schöne*

---
[1]LIENSS, UMR6250, Université de La Rochelle, La Rochelle, France.
[2]Instituto Geográfico Nacional, Madrid, Spain.
[3]LAREG/IGN et GRGS, Marne-la-Vallée, France.
[4]Météo-France, CMM, CNRM, Brest, France.
[5]Proudman Oceanographic Laboratory, Liverpool, UK.
[6]Intergovernmental Oceanographic Commission of UNESCO, Paris, France.

---
[1]Auxiliary materials are available in the HTML. doi:10.1029/2009GL038720.

et al., 2009]. The particular set of stations used to define the reference frame was chosen to provide optimal stability over the entire reanalysis period. More details on the GPS data processing strategy used in this study and implemented by the University of La Rochelle (ULR) analysis centre can be found in the electronic supplement (Text 01). An important feature to outline is the use of absolute antenna phase centre corrections for satellites and receivers [*Schmid et al.*, 2007].

2.2. Noise Characteristics and Velocity Error Estimates

[5] Previous works [e.g., *Mao et al.*, 1999; *Williams et al.*, 2004] demonstrated the presence of significant time-correlated noise in the de-trended GPS position time series residuals. An important consequence is that formal errors on the GPS-derived velocities are grossly underestimated by factors of 5 to 11 if correlations are not properly accounted for [e.g., *Mao et al.*, 1999]. To assign more realistic uncertainties on the GPS velocities, we carefully examined the noise content in our series by the maximum likelihood estimation (MLE) technique using CATS software [*Williams*, 2008]. These series were the non-linear post-fit residuals obtained from the combination of the whole GPS weekly station coordinates solutions over the 10-year period [*Wöppelmann et al.*, 2007, equation (1), p. 401]. They were previously inspected for outliers and offsets using an iterative approach described in the electronic supplement (Text S2).

[6] A combination of power-law plus white noise model turned out to provide the most likely stochastic description of our GPS position series. This finding was consistent with former results [e.g., *Mao et al.*, 1999; *Williams et al.*, 2004]. The estimated spectral indexes were close to −1 (flicker noise), whatever the positioning component. Furthermore, the noise levels were significantly reduced (30 to 40% in the vertical component) compared to previous global network solutions using similar data spans [e.g., *Williams et al.*, 2004]. The average noise levels were 2.6 ± 0.4 mm and 8.2 ± 1.0 mm/yr^0.25 for the white- and power law noises, respectively. They support the results obtained by *Feissel-Vernier et al.* [2007] on a preliminary (shorter) version of our reprocessed GPS solutions with an independent noise analysis method (Allan variance). For completeness and further investigations, the electronic supplement provides the vertical GPS velocities in the ITRF2005 and their "CATS" error bars (Table S1). It includes details of the noise analysis for 180 out of the 227 stations that fulfilled the time series selection criteria of 3.5 years of minimum length with more than 70% of valid data in the time series [*Blewitt and Lavallée*, 2002].

2.3. From ITRF2000 to ITRF2005 Reference Frame

[7] *Wöppelmann et al.* [2007] expressed their long-term cumulative solution in the ITRF2000 [*Altamimi et al.*, 2002], the most recent and robust realization available at that time. In the meantime, three additional observation years were computed at ULR, and the ITRF2005 was released [*Altamimi et al.*, 2007]. Using the ITRF2005 datum and the ITRF2000 as a priori reference frames, starting from the GAMIT loosely constrained subnet solutions in our processing scheme (section 2), resulted in two different solutions over the 10-year period, hereafter ULR2 (using

ITRF2000) and ULR3 (using ITRF2005). The *Wöppelmann et al.* [2007] solution over the shorter 6.7-year period is called ULR1, hereafter. Figure S2 of the auxiliary material shows differences up to 2 mm/yr in the vertical velocities between the two ULR2 and ULR3 solutions (Figure S2, top). A 14-parameter transformation was estimated using the 227 stations in both GPS solutions, yielding a translation rate along the Z-axis of -1.7 ± 0.2 mm/yr and a drift in the scale of 0.13 ± 0.03 ppb/yr. These estimates are consistent with *Altamimi et al.* [2007]. The Z-translation rate between the two frames impacts the vertical velocity of any site at latitude ϕ by $1.7 \times \sin(\phi)$ mm/yr, whereas the scale rate results in a vertical velocity change of about 0.8 mm/yr. Applying these reference frame corrections to the ULR2 solution resulted in differences not statistically significant in the vertical velocities with respect to the ULR3 solution (Figure S2, bottom), thus they were only due to the use of two different reference frames. The transformation parameters between each weekly GPS solution and the combined one expressed in the ITRF2005 (translations and scale factor) showed that our processing scheme implemented the ITRF2005 reference frame at the $1-2$ mm level accuracy on a weekly basis (Figure S3).

3. Rates of Sea-Level Change

3.1. Results

[8] The GPS vertical velocities were used to correct for the land motion affecting the tide gauge records to derive absolute (geocentric) changes in sea level (Figure 1). This exercise was carried out at coastal sites with tide gauge records fulfilling the *Douglas* [2001] selection criteria in determining a global rate of sea level rise. That is, tide gauge records were required to contain more than 85% of valid data over a time span of at least 60 years. The final number of records complying with the selection criteria was identical to the number of records used by *Douglas* [2001], as it was for the number of regions, respectively 27 and 10 (Figure 1), if the Fernandina record was discarded (see discussion). The tide gauge records and their analysis were presented by *Wöppelmann et al.* [2007]. The results are summarized in Table 1, and completed with the 3-year extended ULR solutions presented in section 3.2 (ULR2 and ULR3). The tide gauge and GPS error estimates were each of comparable size, supporting the exercise of applying the GPS vertical velocities for land motion corrections. The "CATS" error bars (section 2.2) are shown for the 'best' vertical GPS velocity field (ULR3).

[9] Although the above mentioned error estimates take into account the noise properties of the GPS position time series, they remain an intra-technique estimate. From herein, intra and inter-regional agreement of the sea level trends will be regarded as a most robust estimate of uncertainty.

3.2. Discussion

[10] In estimating absolute sea level trends, we assumed that land motion is essentially linear on the time span considered here (100 years). This assumption is supported by the very small scatter of the acceleration term in the tide gauge records longer than $50-60$ years, suggesting that vertical land motion rates are nearly constant at most sites [*Douglas*, 2001, Figure 3.16, p. 61]. Observational evidence for acceleration was only detected in reconstructions of
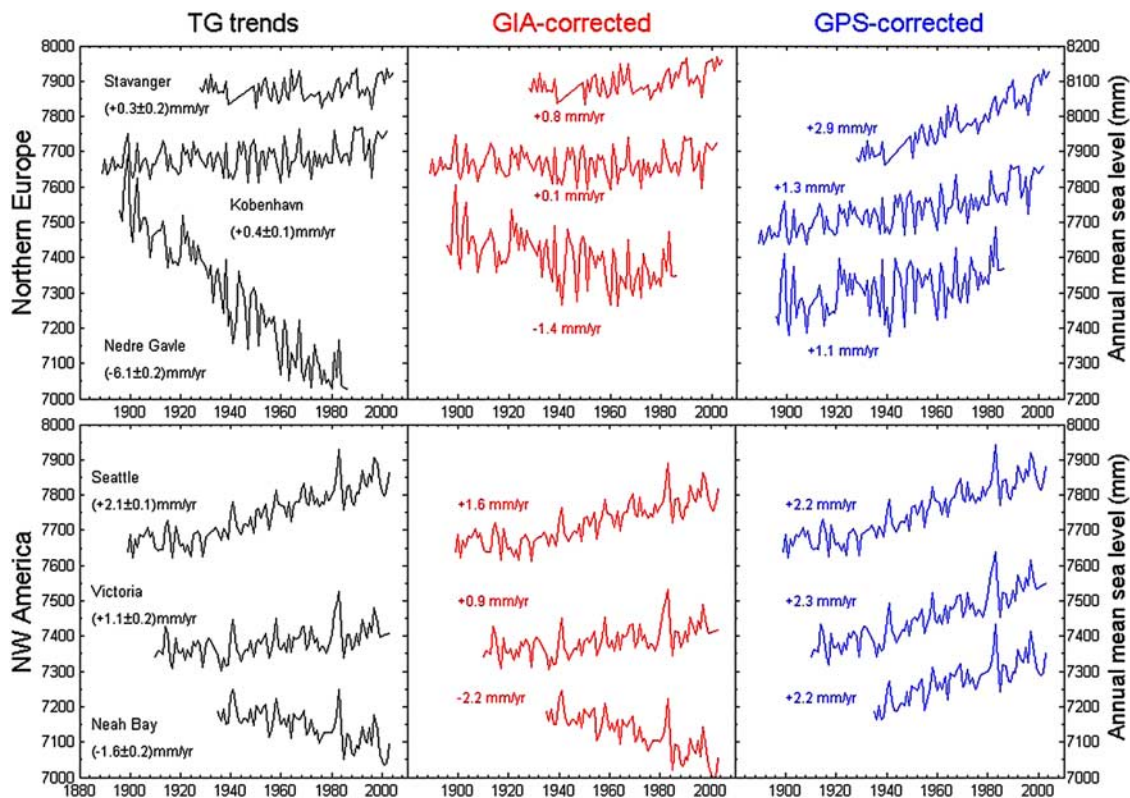
Figure 1. Time series of annual mean sea-level values from: (left) tide gauges; (middle) tide gauges corrected for GIA using *Peltier* [2004] ICE5G (VM2) model predictions; and (right) GPS-corrected tide gauge records in the ITRF2005 reference frame; in (top) Northern Europe and (bottom) North West America. The time series are displayed with arbitrary offsets for presentation purposes (units are in mm).

global sea level curves using large amounts of data [*Church and White*, 2006; *Jevrejeva et al.*, 2008]. In addition, we assumed that the local vertical displacements of the relatively close observation points (tide gauges and GPS antennae) are under the sub-mm per year level. The validity of this second working hypothesis is raised, especially at Fernandina, where the land motion corrections failed to provide an agreement with the other stations in the South-East North America region. In absence of repeated high-precision levelling data between the GPS antenna and the tide gauge benchmarks, the hypothesis was necessitated in our exercise.

[11] Table 2 summarises the scatter of the individual-, and regional rates of sea level change as measured by the standard deviation statistic. It reveals a slight but steady progress in the land motion corrections performed by the successive ULR solutions. *Wöppelmann et al.* [2007] already noted that GPS corrections provided figures that were more in agreement within a region than GIA corrections from *Peltier* [2004] (e.g., Figure 1). However, the most striking improvement shown here is the significant reduction in the scatter of the regionally averaged sea level trends using ITRF2005 (ULR3 solution, Table 2). Progresses were definitely made in the reference frame realization when shifting to ITRF2005. In contrast, the 3-year data extension barely reduced this scatter using ITRF2000 (ULR1 to ULR2), suggesting that the limitation was more in the

analysis strategy (models, reference frame) than in the data span. This remark is consistent with the predicted standard errors that were obtained for the GPS vertical velocities as a function of the time span of the GPS data (Figure S4). For comparison, the predicted standard errors were also plotted assuming a pure white noise, or using the best noise characteristics observed by *Williams et al.* [2004] in previous global network solutions using similar data spans. GPS analyses have thus reached the maturity to provide useful information for separating land motion from sea level changes recorded by tide gauges, in particular the most underrated and difficult to model effects that are sediment compaction and land subsidence associated with coastal reclamation, development and withdrawal of underground water (Figure 1). Such effects are very site specific, but are sufficiently frequently associated with harbours and tide gauge sites to raise serious concerns on the validity of global averages obtained from uncorrected secular trends.

[12] There might be a limit in the reduction of the scatter of long term sea level trends, however. The issue is the subject of an extensive scientific debate. Sea level rise is expected to vary spatially as a result of the redistribution of melt-water within the Earth system [e.g., *Mitrovica et al.*, 2001]. These variations are long wavelength (>1000 km), and could explain that using ITRF2005 or ITRF2000 did not change significantly the scatter of the geocentric sea-level trends within a region. However, the GPS-corrected

Table 1. Relative and Absolute Sea Level Trends From Tide Gauge Records Using Different Vertical Velocity Fields Computed at ULR[a]

Groups of Stations	Span (yr)	Tide Gauges (TG) Trend (mm/yr)	GPS/TG Dist. (m)	Span (yr)	ULR1 Trend (mm/yr)	TG+ULR1 Trend (mm/yr)	Span (yr)	ULR2 Trend (mm/yr)	TG+ULR2 Trend (mm/yr)	ULR3 Trend (mm/yr)	TG+ULR3 Trend (mm/yr)
North Sea + English Channel											
ABERDEEN I+II	103	0.58 ± 0.10	2	6.7	0.15	0.73	8.2	−0.10	0.48	0.67 ± 0.22	1.25
NEWLYN	87	1.69 ± 0.11	10	6.7	−1.04	0.65	8.1	−0.90	0.79	−0.21 ± 0.27	1.48
BREST	83	1.40 ± 0.05	350	6.7	−1.18	0.22	8.0	−1.18	0.22	−0.54 ± 0.77	0.86
Atlantic											
CASCAIS	97	1.22 ± 0.10	84	6.7	−0.58	0.64	8.1	−0.37	0.85	0.12 ± 0.19	1.34
LAGOS	61	1.35 ± 0.18	138	5.3	−0.32	1.03	6.6	−0.59	0.76	−0.10 ± 0.29	1.25
Mediterranean											
MARSEILLE	105	1.27 ± 0.09	5	6.7	−0.32	0.95	8.3	0.34	1.61	0.82 ± 0.37	2.09
GENOVA	78	1.20 ± 0.07	1000	6.6	−0.26	0.94	8.3	−0.61	0.59	−0.16 ± 0.85	1.04
New Zealand											
AUCKLAND II	85	1.30 ± 0.13	5	3.9	1.61	2.91	5.3	1.47	2.77	−0.87 ± 0.48	0.43
PORT LYTTELTON	101	2.08[b] ± 0.11	2	5.8	1.21	3.29	7.0	1.66	3.74	−0.59 ± 0.35	1.49
Pacific											
HONOLULU	99	1.46 ± 0.13	5	6.5	0.46	1.92	8.6	0.12	1.58	−0.15 ± 0.36	1.31
SW North America											
LA JOLLA	72	2.11 ± 0.16	700	6.7	−1.36	0.75	9.8	−0.75	1.36	−0.38 ± 0.62	1.73
LOS ANGELES	78	0.86 ± 0.15	2200	6.7	−0.64	0.22	7.9	−0.67	0.19	−0.30 ± 0.48	0.56
SE North America											
CHARLESTON I	82	3.23 ± 0.16	8200	4.8	−1.80	1.43	6.9	−1.76	1.47	−1.31 ± 0.44	1.92
FERNANDINA	83	2.00 ± 0.13	5500	6.7	−4.28	−2.28	9.4	−3.99	−1.99	−3.58 ± 0.30	−1.58
GALVESTON II	94	6.47 ± 0.17	4200	4.5	−6.85	−0.38	5.9	−6.30	0.17	−5.89 ± 0.61	0.58
MIAMI BEACH	45	2.29 ± 0.26	4800	5.2	0.92	3.21	6.7	0.08	2.37	0.46 ± 0.61	2.75
KEY WEST	90	2.23 ± 0.10	16000	6.7	−0.50	1.73	9.4	−0.97	1.26	−0.59 ± 0.38	1.64
NE North America											
EASTPORT	63	2.07 ± 0.16	800	6.2	1.39	3.46	8.1	1.48	3.55	2.07 ± 0.87	4.14
NEWPORT	70	2.48 ± 0.14	500	6.1	−0.18	2.3	7.3	−0.18	2.3	0.42 ± 0.37	2.9
HALIFAX	77	3.29 ± 0.11	3100	2.8	−1.57	1.72	3.9	−1.5	1.79	−0.72 ± 0.31	2.57
ANNAPOLIS	70	3.46 ± 0.17	100	6.7	−0.12	3.34	8.9	0.19	3.65	0.69 ± 0.94	4.15
SOLOMON'S ISL.	62	3.36 ± 0.19	200	6.7	−3.36	0.00	9.8	−2.92	0.44	−2.43 ± 0.69	0.93
Northern Europe											
STAVANGER	63	0.27 ± 0.17	16000	4.7	0.23	0.50	6.0	1.81	2.08	2.68 ± 0.82	2.95
KOBENHAVN	101	0.32 ± 0.12	7300	2.6	−0.08	0.24	3.9	0.25	0.57	0.97 ± 0.35	1.29
NEDRE GAVLE	90	−6.05 ± 0.23	11000	6.4	6.22	0.17	7.7	6.46	0.41	7.12 ± 0.19	1.07
NW North America											
VICTORIA	86	1.10 ± 0.15	12000	6.7	0.68	1.78	9.8	0.65	1.75	1.20 ± 0.23	2.30
NEAH BAY	65	−1.59 ± 0.22	7800	6.7	4.21	2.62	8.8	3.28	1.69	3.82 ± 0.69	2.23
SEATTLE	104	2.06 ± 0.11	5900	6.7	−0.57	1.49	8.8	−0.42	1.64	0.14 ± 0.31	2.20

[a]The sites are grouped into regions according to *Douglas* [2001]. The columns TG+ULR represent the GPS−corrected tide gauge trend with the different ULR solutions (see text for details).
[b][from *Hannah*, 2004].

trends were different in ITRF2005 or ITRF2000 due to the systematic differences between the frames (section 2.3); leading to different values of regionally averaged sea level trends, and scatter (Table 2).

[13] In contrast, *Douglas* [2008] found no conclusive evidence of glacial melting fingerprints in any of the long tide gauge records that were used by most authors in their determinations of global sea level rise. The assumption that

Table 2. Scatter of the Individual-, and Regional Rates of Sea-Level Change as Measured by the Standard Deviation Statistic Using Different Land Motion Corrections[a]

Land Motion Correction at the Tide Gauges	No Correction	GIA-Corrected ICE5G (VM2)	GPS-Corrected ULR 1	GPS-Corrected ULR 2	GPS-Corrected ULR 3
Scatter of the individual rates of sea-level change	2.05 mm/yr	1.49 mm/yr	1.32 mm/yr (1.15)	1.23 mm/yr (1.06)	1.15 mm/yr (0.98)
Scatter of the regional rates of sea-level change	1.37 mm/yr	0.98 mm/yr	0.93 mm/yr (0.91)	0.87 mm/yr (0.83)	0.62 mm/yr (0.60)

[a]See text for details on the ULR solutions. The figures in parentheses correspond to the removal of Fernandina record from the statistics.

underlies the studies which aim at estimating a secular rate of global sea level rise is that the longer the period of sea level variation, the greater the spatial extent of that signal.

[14] Furthermore, *Prandi et al.* [2009] did not find any significant difference between coastal and global mean sea level rise, comparing tide gauges and satellite altimetry data over 1993–2007. Using *Douglas* [2001] approach and our best estimates of land motion from GPS (ULR3 corrections) yielded a global-average rate of geocentric sea-level rise for the past century which is in good agreement with the recent estimates (e.g., 1.7 mm/yr [*Church and White*, 2006; *Holgate*, 2007]). Including or discarding the anomalous Fernandina record resulted in an estimate of 1.55 ± 0.19 mm/yr or 1.61 ± 0.19 mm/yr, respectively. The approach is therefore robust (see also figures in parenthesis in Table 2), and gave further support to the *Douglas* [2001] morphological grouping of tide gauges, which was based on their correlation at low frequencies with their neighbours. Despite the different time spans, our estimate of global sea level rise appeared to be in good agreement with the sum of steric sea level and land ice contributions estimated by *Leuliette and Miller* [2009] over the recent period of 2003–2007 (1.5 mm/yr) using altimetry, Argo, and GRACE gravity observations.

4. Conclusions

[15] Although there might be a natural limit in the reduction of the scatter of long term sea level trends due to the variability of sea level rise, the geodetic approach is reducing this long-term spatial variability by taking into account the land motion at the tide gauges, whatever the origin of the land motion. The significantly improved results, shown in this paper, give further evidence for a reduction of technique errors and analysis artefacts thanks to the utilization of a fully consistent processing strategy throughout the entire 10-year GPS data span. Improving the analysis strategy proved to be more relevant than extending the data span. Many of our GPS vertical velocities were estimated with uncertainties several times smaller than the 1–3 mm/yr associated with global sea level change, taking into account the stochastic properties of the GPS position time series. Hence, they could be applied to correct the long tide gauge records for land motion, leading to an updated GPS-corrected estimate of global-scale sea level rise which is in agreement with previous ones [e.g., *Church and White*, 2006].

[16] Other studies may benefit from our new global GPS velocity field, for instance to compare with satellite altimetry data, which requires to monitor the tide gauges in the same geocentric reference frame. The uncertainty introduced by land motion in radar altimeter calibration using tide gauges is estimated to be about 0.4 mm/yr [*Mitchum*, 2000]. We are looking forward to seeing results from the application of our GPS velocity field in such investigations. These will certainly provide invaluable feedback to further assess the performance of our results, but are beyond the scope of this paper.

[17] Last but not least, improving our understanding of sea-level rise and variability, as well as reducing the associated uncertainties, depends critically on the availability of a stable global reference frame. The accuracy of its origin and scale is the main factor limiting the determination of geocentric sea level trends today. Progressively improving the frame's accuracy is an important continued mission and effort of international services like the IGS.

References

Altamimi, Z., P. Sillard, and C. Boucher (2002), ITRF2000: A new release of the International Terrestrial Reference Frame for earth science applications, *J. Geophys. Res.*, *107*(B10), 2214, doi:10.1029/2001JB000561.

Altamimi, Z., X. Collilieux, J. Legrand, B. Garayt, and C. Boucher (2007), ITRF2005: A new release of the International Terrestrial Reference Frame based on time series of station positions and Earth Orientation Parameters, *J. Geophys. Res.*, *112*, B09401, doi:10.1029/2007JB004949.

Blewitt, G., and D. Lavallée (2002), Effect of annual signals on geodetic velocity, *J. Geophys. Res.*, *107*(B7), 2145, doi:10.1029/2001JB000570.

Church, J. A., and N. J. White (2006), A 20th century acceleration in global sea-level rise, *Geophys. Res. Lett.*, *33*, L01602, doi:10.1029/2005GL024826.

Douglas, B. C. (2001), Sea level change in the era of the recording tide gauge, in *Sea Level Rise: History and Consequences*, *Int. Geophys. Ser.*, vol. 75, edited by B. Douglas, M. Kearney, and S. Leatherman, chap. 3, pp. 37–64, Academic, San Diego, Calif.

Douglas, B. C. (2008), Concerning evidence for fingerprints of glacial melting, *J. Coastal Res.*, *24*, 218–227.

Feissel-Vernier, M., O. De Viron, and K. Le Bail (2007), Stability of VLBI, SLR, DORIS, and GPS positioning, *Earth Planets Space*, *59*, 475–497.

Hannah, J. (2004), An updated analysis of long-term sea level change in New Zealand, *Geophys. Res. Lett.*, *31*, L03307, doi:10.1029/2003GL019166.

Holgate, S. J. (2007), On the decadal rates of sea level change during the twentieth century, *Geophys. Res. Lett.*, *34*, L01602, doi:10.1029/2006GL028492.

Jevrejeva, S., J. C. Moore, A. Grinsted, and P. L. Woodworth (2008), Recent global sea level acceleration started over 200 years ago?, *Geophys. Res. Lett.*, *35*, L08715, doi:10.1029/2008GL033611.

King, R. W., and Y. Bock (2006), Documentation for the GAMIT GPS Analysis Software, release 10.2, technical report, Mass. Inst. of Technol., Cambridge.

Leuliette, E. W., and L. Miller (2009), Closing the sea level rise budget with altimetry, Argo, and GRACE, *Geophys. Res. Lett.*, *36*, L04608, doi:10.1029/2008GL036010.

Mao, A., C. G. A Harrison, and T. H. Dixon (1999), Noise in GPS coordinate time series, *J. Geophys. Res.*, *104*, 2797–2816.

Mitchum, G. (2000), An improved calibration of satellite altimetric heights using tide gauge sea-levels with adjustment for land motion, *Mar. Geod.*, *23*, 145–166.

Mitrovica, J. X., M. Tamisiea, J. L. Davis, and G. A. Milne (2001), Recent mass balance of polar ice sheets inferred from patterns of global sea-level change, *Nature*, *409*, 1026–1029.

Penna, N. T., M. A. King, and M. P. Stewart (2007), GPS height time series: Short-period origins of spurious long-period signals, *J. Geophys. Res.*, *112*, B02402, doi:10.1029/2005JB004047.

Peltier, W. R. (2004), Global glacial isostasy and the surface of the Ice-Age Earth: The ICE-5G (VM2) model and GRACE, *Annu. Rev. Earth Planet. Sci.*, *32*, 111–149, doi:10.1146/annurev.earth.32.082503.144359.

Prandi, P., A. Cazenave, and M. Becker (2009), Is coastal mean sea level rising faster than the global mean? A comparison between tide gauges and satellite altimetry over 1993–2007, *Geophys. Res. Lett.*, *36*, L05602, doi:10.1029/2008GL036564.

Schmid, R., P. Steigenberger, G. Gendt, M. Ge, and M. Rothacher (2007), Generation of a consistent absolute phase center correction model for GPS receivers and satellites antennas, *J. Geod.*, *81*, 781–798.

Schöne, T., N. Schön, and D. Thaller (2009), IGS Tide Gauge Benchmark Monitoring Pilot Project (TIGA): Scientific benefits, *J. Geod.*, *83*, 249–261.

Steigenberger, P., M. Rothacher, R. Dietrich, M. Fritsche, A. Rülke, and S. Vey (2006), Reprocessing of a global GPS network, *J. Geophys. Res.*, *111*, B05402, doi:10.1029/2005JB003747.

Williams, S. D. P. (2008), CATS: GPS coordinate time series analysis software, *GPS Solutions*, *12*, 147–153.

Williams, S. D. P., Y. Bock, P. Fang, P. Jamason, R. M. Nikolaidis, L. Prawirodirdjo, M. Miller, and D. J. Johnson (2004), Error analysis of continuous GPS position time series, *J. Geophys. Res.*, *109*, B03412, doi:10.1029/2003JB002741.

Woodworth, P. L. (2006), Some important issues to do with long-term sea level change, *Philos. Trans. R. Soc., Ser. A*, *364*, 787–803.

Wöppelmann, G., B. Martin Miguez, M. N. Bouin, and Z. Altamimi (2007), Geocentric sea-level trend estimates from GPS analyses at relevant tide gauges world-wide, *Global Planet. Change*, *57*, 396–406.

————————————

Z. Altamimi, M.-N. Bouin, X. Collilieux, and A. Santamaria, LAREG/IGN et GRGS, F-77455 Marne-la-Vallée CEDEX, France.

C. Letetrel and G. Wöppelmann, LIENSS, UMR6250, Université de La Rochelle, 2 rue Olympe de Gouges, F-17000 La Rochelle CEDEX, France. (gwoppelm@univ-1r.fr)

B. M. Miguez, Intergovernmental Oceanographic Commission of UNESCO, 1 rue Miollis, F-75732 Paris CEDEX 15, France.

S. D. P. Williams, Proudman Oceanographic Laboratory, Bidston Hill, Liverpool L3 5DA, UK.

A Dense Global Velocity Field based on GNSS Observations: Preliminary Results

C. Bruyninx[1], Z. Altamimi, M. Becker, M. Craymer, L. Combrinck, A. Combrink, J. Dawson, R. Dietrich, R. Fernandes, R. Govind, T. Herring, A. Kenyeres, R. King, C. Kreemer, D. Lavallée, J. Legrand, L. Sánchez, G. Sella, Z. Shen, A. Santamaría-Gómez, G. Wöppelmann

[1] Royal Observatory of Belgium, Av. Circulaire 3, B-1180 Brussels, Belgium
E-mail: C.Bruyninx@oma.be

Abstract. In a collaborative effort with the regional sub-commissions within IAG sub-commission 1.3 "Regional Reference Frames", the IAG Working Group (WG) on "Regional Dense Velocity Fields" (see http://epncb.oma.be/IAG) has made a first attempt to create a dense global velocity field. GNSS-based velocity solutions for more than 6000 continuous and episodic GNSS tracking stations, were proposed to the WG in reply to the first call for participation issued in November 2008. The combination of a part of these solutions was done in a two-step approach: first at the regional level, and secondly at the global level.

Comparisons between different velocity solutions show an RMS agreement between 0.3 mm/yr and 0.5 mm/yr resp. for the horizontal and vertical velocities. In some cases, significant disagreements between the velocities of some of the networks are seen, but these are primarily caused by the inconsistent handling of discontinuity epochs and solution numbers. In the future, the WG will re-visit the procedures in order to develop a combination process that is efficient, automated, transparent, and not more complex than it needs to be.

Keywords. GNSS, velocity field, combination

1 Introduction

The Working Group "Regional Dense Velocity Fields" has been created in 2007 at the IUGG (International Union of Geodesy and Geophysics) General Assembly in Perugia, Italy. It is embedded within IAG (International Association of Geodesy) sub-commission 1.3 on "Regional Reference Frames" where it co-exists with the regional sub-commissions for Europe, South and Central America, North America, Africa, South-East Asia and Pacific, and Antarctica (Drewes et al. 2008).
The long-term goal of the Working Group is to provide a globally referenced dense velocity field based on GNSS observations and linked to the multi-technique global conventional reference frame, the ITRF (International Terrestrial Reference Frame, Altamimi et al., 2007a).

2 Working Group objectives and work plan

2.1 Objectives

The Working Group on "Regional Dense Velocity Fields" joins the efforts of groups processing local/regional/global CORS or repeated GNSS campaigns and set up the following action items:

- define specifications and quality standards for the regional SINEX solutions and relevant meta-data (e.g. description of GNSS equipment and position/velocity discontinuities);
- collect SINEX solutions and their meta-data;
- study in-depth the individual strengths and shortcomings of local/regional and continuous/epoch GNSS solutions to determine site velocities;
- define optimal strategies for the combination of regional and global SINEX solutions;
- provide dense regional velocity fields;
- provide the densification of the ITRF2005 (or its successors);
- encourage participation in related symposia;
- implement a web site in order to provide information on the activities and access to the products of the WG;
- and prepare recommendations and a comprehensive final report on the WG activities at the next IUGG General Assembly in 2011.

2.2 Work plan

The work plan of the WG has been divided into two major parts. During the first part, covering 2007-2009, the WG set up the initial strategy and submission guidelines, collected a first set of test

solutions, and performed a first preliminary velocity combination.

The working group closely links its activities with the regional sub-commissions within IAG sub-commission 1.3. Their expertise, coordination role for their region, and their capability to generate a unique cumulative solution for their region including velocity solutions from third parties (even campaigns) is essential for the WG. The initial WG strategy consisted therefore in a two-step approach. First, region coordinators (one for each region corresponding to the regions of the different regional sub-commissions) gathered sub-regional velocity solutions for their region (in accordance with the WG requirements) and combined these with, where available, the velocity solution from the regional sub-commissions (e.g. EUREF, SIRGAS…) in order to produce one regional combined velocity solution in the SINEX format. Secondly, two combination coordinators -T. Herring (MIT, US) and D. Lavallée (TU Delft, Netherlands)- combined these regional SINEX solutions with the long-term solutions from global networks to generate a preliminary velocity solution tied to the ITRS. The main goal of this preliminary solution was to identify the problems that would arise and help to set strategic choices and guidelines for the future. These guidelines will be used to issue a new solution in the second part of the WG term, 2010-2011. The results of the 2007-2009 period will be presented in this paper.

As mentioned in the introduction, the WG accepts velocity solutions based on CORS and repeated GNSS campaigns (under specific conditions, see Section 3.1).

One of the strategic choices the WG group had to make from the start was to decide whether to (1) stack weekly combined regional and global (position) SINEX solutions to compute the velocities or to (2) combine cumulative regional and global (position+velocity) SINEX solutions. Considering that the WG does not have access to the weekly SINEX of many cumulative velocity solutions, it was decided to go for approach (2). This will allow us combining, if necessary, only velocities (without the positions). In addition, it will allow us a step-wise combination of regional and global solutions; it will also facilitate meta-data management and outlier detection, as these will be done at regional level. And finally, it perfectly fits in the initial frame (using region and combination coordinators) that was set up. The disadvantages of combining cumulative (position+) velocity solutions are however that no coordinate time series will be available to the WG and that it will be necessary to

consistently handle discontinuities, especially on frame-attachment sites.

3   Call for participation

3.1 Initial submission guidelines

In order to allow inclusion of a maximum number of velocity solutions, the WG set up the following guidelines for the contributing solutions:

− minimum 2 years of continuous data or 2 campaign epochs over a 4 year period;
− minimum 2.5 years of continuous data if significant seasonal signals are present;
− significant number of "frame-attachment" sites, preferably observed over a period exceeding 5 years;
− position/velocity discontinuities should be identical to the ones used by the (IGS) International GNSS Service (Dow et al., 2009)
− velocity constraints should be minimal or removable;
− SINEX format should contain full covariance information (an exception is allowed for PPP solutions only providing correlations between individual station coordinates).

The detailed submission guidelines are available from the Working Group web site: http://www.epncb.oma.be/IAG/.

3.2 Call for Participation

A first Call for Participation (CfP) was issued at the end of 2008. Analysts, producing regional and global velocity solutions, were invited to submit their SINEX files to the Working Group. Fig. 1 shows the map with the sites for which solutions that have been proposed following this CfP (black dots); in total more than 6000 sites were proposed.
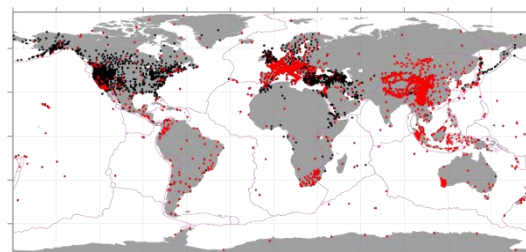
Fig. 1 Map with the sites for which velocity solutions have been proposed to the Working Group up to July 2009 (black dots). In total more than 6000 sites have been proposed. In red: sites used in the first preliminary combination (see section 4).

4 Input for preliminary combination

A preliminary velocity combination has been computed in the summer of 2009. This solution contained contributions from the region coordinators as well as one global solution.

4.1 Regional contributions

Several of the region coordinators prepared a velocity solution for their region to be included in the preliminary combination. The African and South & Central American contributions are based on the contribution of a single analysis center, while the solutions from Europe and South-East Asia & Pacific are combined solutions based on input from several analysis groups. More details are given below:

– *Africa* (see Fig. 2): The solution includes 93 CORS and covers the period from Jan. 1996 till June 2009 (Fernandes et al., 2007). The GNSS data analysis, has been done using GIPSY/OASIS II (Zumberge et al., 1997) by applying the PPP strategy with ambiguity resolution (Blewitt, 2008). GIPSY tools were also used to derive the velocity solutions.
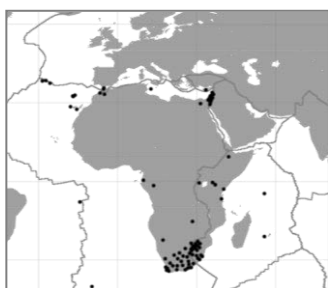
Fig. 2 Sites contributing to the African velocity solution.

– *Europe* (see Fig. 3): The solution includes the velocities estimated from a reprocessing of the EUREF Permanent Network (EPN), maintained by the regional sub-commission for Europe (Bruyninx et al., 2009), complemented with several sub-regional velocity solutions. In total, velocity estimates for 525 sites were obtained, which is more than twice the number of the sites presently included in the EPN. All of the contributing sub-regional solutions were available in the SINEX format and the combination was done with the CATREF software (Altamimi et al. 2007b). The main problem encountered during the combination was the fact that some of the submitted sub-regional solutions did not use any

discontinuities at all (more about this in Section 6).
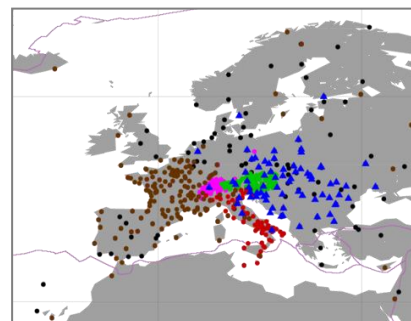
Fig. 3 Sites and solutions included in the European solution: reprocessed EPN ('96-'09) in black, AGNES ('98-09') in pink, AMON ('01-'09) in green, ASI ('97-'09) in red, IGN ('98-'09) in brown, and CEGRN ('94-'07) blue triangles.

– *South and Central America* (see Fig. 4): The solution includes about 128 CORS from the SIRGAS network (Seemüller et al., 2009) and covers the period from 2000 till 2009. The GNSS data processing, as well as the cumulative SINEX solution, have been computed using the Bernese V5.0 software (Beutler et al., 2007).
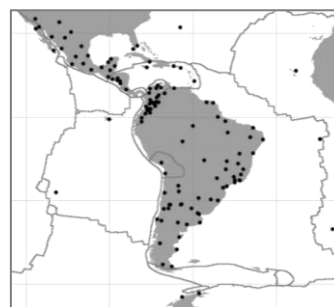
Fig. 4 Sites contributing to the South and Central America velocity solution.

– *South-East Asia and Pacific* (see Fig. 5): The solution comprises 1156 sites resulting of a combination of several sub-regional networks. The combination was done using the CATREF software. In this solution, ensuring the consistent use of station names, particularly four-character identifiers, was a major struggle for many stations. In addition, as indicated in Figure 5, not all solutions were available in full SINEX format.
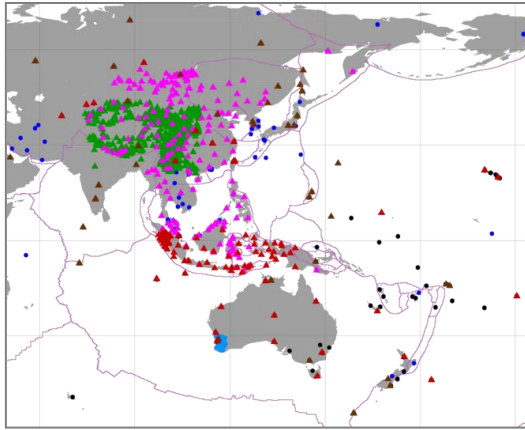
Fig. 5 Sites and solutions contributing to the East-Asia and Pacific velocity solution. Solutions with full SINEX information are indicated with circles: PCGIAP ('97-'06) in dark blue, SW Austr. seism. zone ('02-'06) in light blue, and GeoScience Australia TIGA ('97-'09) in black. The triangles indicate the stations belonging to networks providing velocity-only solutions: Tibet ('98-'04) in green, Asia ('94-04) in pink, Global ('95-'07) in orange, and Indonesia ('91-'01) in red.

4.2 Global contribution

One global solution was included in this first test combination. This solution, from the ULR consortium (Université de La Rochelle and IGN/LAREG) is based on a reprocessing of 299 CORS from Jan. 1996 till Jan. 2009 using the GAMIT software (Herring et al., 2007), see Fig.6.
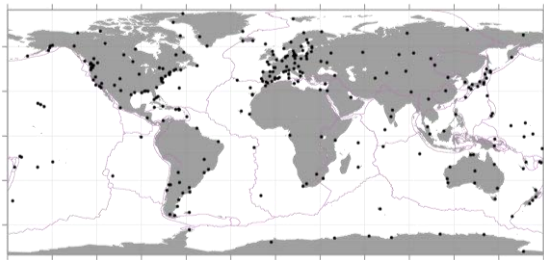
Fig. 6 Sites contributing to the global ULR velocity solution.

Its main objective is the correction of vertical land movements that affect the tide gauge records (Wöppelmann et al. 2009). A key issue to achieve the accuracy requirement of the sea-level application (sub-mm/yr) is the realization of a stable and accurate reference frame. The ULR solution therefore includes a global set of reliable reference frame stations from the IGS. It includes three additional years of data and an improved data analysis strategy with respect to the previous solution (Wöppelmann et al. 2009). See details in Santamaria-Gomez et al. (this issue). The stacking

of the solutions was done with CATREF. The ULR network has several sites common to the regional solutions.

5 Test combination

The submitted regional networks and the global network were combined using two different approaches. First approach was a step-wise one: first a combination of sites that are present in at least 3 solutions was done. Based on the common sites from this combination, re-weighting factors for each SINEX file were estimated. The solution is then iterated with the final weights coming from the χ^2 of the individual solution velocity estimates with respect to the combination, using sites common to at least 2 solutions. The variance weights vary from about 200 to 1.6. The differences are most probably caused by the usage of different software packages and will be investigated in more detail in the future. The second approach consisted in attaching each regional network to the global network (ULR) using frame-attachment sites. This means that the global sites are not changed by the attachment of the regional sites but the regional networks are adjusted. More details on this approach are given in Davis and Blewitt (2000).

Table 1. Agreement between global ULR velocity solution and each of the regional velocity solutions after a Helmert transformation.

Solution	RMS Pos. [mm]		RMS Vel. [mm/yr]		# common (excluded sites)
	Hor.	Up.	Hor.	Up	
Europe	1.68	2.58	0.28	0.44	43(10)
Africa	4.54	4.14	0.92	1.24	12(2)
South & Central America	3.85	4.41	0.74	1.26	25(3)
South-Asia & Pacific	2.12	3.83	0.22	0.47	26(13)

Figure 7 and Table 1 present the first comparisons between each of the regional velocity solutions and the global ULR solution. The comparison was done after performing a Helmert transformation on both positions and velocities (estimating translations and scale, together with their rate). The results clearly show that the European and South-Asia & Pacific solutions agree better with the ULR solution than the SIRGAS and African solutions. This does not necessarily mean that the quality of the latter solutions is worse than the first ones, but reflects more the fact that inconsistent

discontinuity epochs and solution numbers are used between the last two solutions and the ULR. This is confirmed by the fact that the SIRGAS and African solutions also have a significantly larger position RMS w.r.t. to the ULR solution compared to the European and South-Asia & Pacific solution.

Detailed maps of the comparison between the different solutions are available from the WG web site at http://epncb.oma.be/IAG/
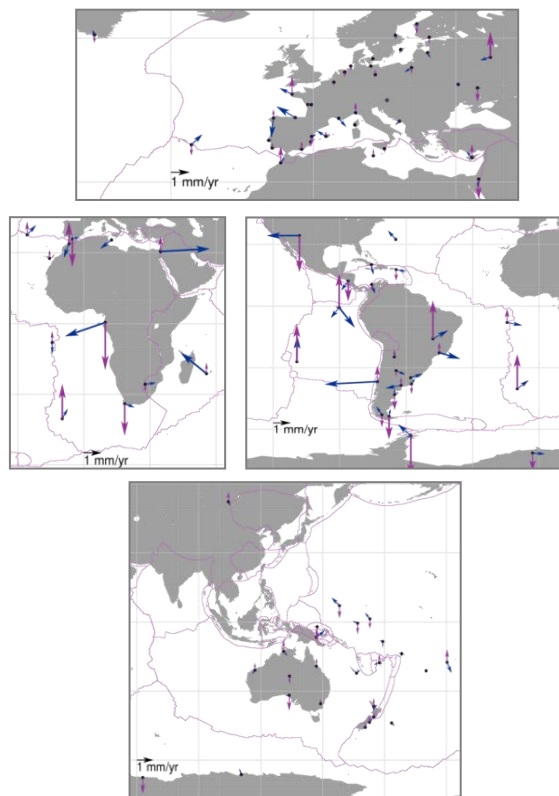
Fig. 7 Differences between global ULR velocity solution and each of the regional velocity solutions after a Helmert transformation. In purple: vertical velocity differences and in blue: horizontal velocity differences. Top: Europe, middle-left: Africa, middle-right: South and Central America, bottom: East-Asia and Pacific.

6 Difficulties

Not all sites included in the contributing solutions have official DOMES numbers assigned by the IERS (International Earth Rotation and Reference Systems Service) and this can make SINEX combination software fail. As a large number of these sites are third party sites without detailed monumentation information, it is impossible to request official IERS DOMES numbers for them. Therefore, the WG implemented a coordinated

approach for attributing virtual DOMES numbers. Moreover, in the case of duplicate station names, a new station identification and virtual DOMES number was assigned in a coordinated way, avoiding overlaps and inconsistencies between the different regions.

Typically, when a position change occurs at a CORS, two different positions are estimated: one before the discontinuity epoch and one after it. Independently of the fact that the position change is associated with a velocity change or not, most stacking is done in a way to estimate, in addition to the two position solutions, also two velocity solutions. Separate velocities may also be estimated but can be linked through constraints if they are statistically compatible, as usually the case for instrument-related discontinuities. This principle is illustrated in Figure 8.
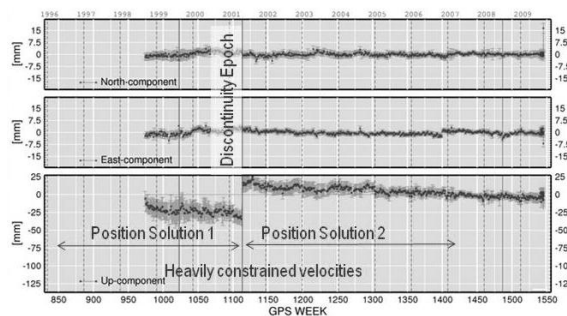
Fig. 8 Principle of the introduction of discontinuity epochs and solution numbers.

When discontinuities occur at reference frame sites or at sites common to different solutions, it is imperative that the same discontinuity epochs and solution numbers are applied during the analysis before combining the solutions. As in this first test, cumulative position+velocity solutions have been combined, the WG asked the analysts producing these solutions to apply the station discontinuities identified by the IGS/ITRF (ftp://macs.geod.nrcan.gc.ca/pub/requests/sinex/discontinuities/ALL.SNX). However, the treatment of discontinuities and velocity changes are subject to interpretation and analysis groups may not necessarily agree on discontinuity epochs.

In practice, the different contributors did not strictly follow the IGS discontinuities, obviously influencing the estimated positions as well as velocities and most probably causing some of the outliers seen in Figure 8. This exercise demonstrated the need to come up with a consensus on the discontinuities. To test a

collaborative approach, a first attempt was made to merge the discontinuities reported by the different groups in one file which can be edited and maintained by the different groups.

In addition, to the "bookkeeping" problems described above, some sub-regional solutions consisted of precise velocity estimates with only approximate coordinates. The implication is that inter-site correlations (not always negligible) are neglected which caused failure of some combination software. Other numerical instabilities were seen due to the equating (or heavily constraining) of velocities before and after a position jump.

7 Summary and outlook

The IAG Working Group on "Regional Dense Velocity Fields" preformed a first test combination of a set of cumulative velocity solutions from regional and global networks in order to identify the main problems when producing a dense velocity field based on multiple cumulative position and velocity solutions. The test identified the urgent need for a consensus on the attribution of discontinuity epochs for stations common to several solutions. Due to the use of different analysis strategies and software packages by the individual contributors, finding such a consensus is a challenge as most probably not the same discontinuities are seen by different people. In addition, the treatment of the post-seismic signals is also subject to interpretation. A possible way to go ahead for the Working Group could be to combine solutions at the weekly level and only deal with the attribution of the discontinuity epochs at the combination level. This would mean that in a first step the weekly global solutions would be combined with to generate a global core network with reliable velocity solutions. In a second step, weekly combined regional solutions (including the sub-regional solutions providing weekly contributions) could be added to this global core network on a weekly basis resulting in a densified core network which could then be used for velocity estimation using one single set of agreed-upon discontinuities. Finally, the remaining cumulative velocity solutions (for which the WG does not have access to weekly position solutions) could be attached to the cumulative densified core network. This approach is one of the alternative procedures which are presently under discussion within the WG.

References

Altamimi, Z., X. Collilieux, J. Legrand, B. Garayt, and C. Boucher (2007a). ITRF2005: A new release of the International Terrestrial Reference Frame based on time series of station positions and Earth Orientation Parameters, *J. Geophys. Res.*, 112, B09401, doi:10.1029/2007JB004949

Altamimi, Z., P. Sillard, and C. Boucher (2007b). CATREF software: Combination and analysis of terrestrial reference frames. LAREG, Technical, Institut Géographique National, Paris, France

Beutler, G., H. Bock, E. Brockmann, R. Dach, P. Fridez, W. Gurtner, H. Habrich, U. Hugentobler, D. Ineichen, A. Jaeggi, M. Meindl, L. Mervart, M. Rothacher, S. Schaer, R. Schmid, T. Springer, P. Steigenberger, D. Svehla, D. Thaller, C. Urschl, R. Weber (2007). Bernese GPS software version 5.0. ed. Urs Hugentobler, R. Dach, P. Fridez, M. Meindl, Univ. Bern

Blewitt, G. (2008), Fixed point theorems of GPS carrier phase ambiguity resolution and their application to massive network processing: Ambizap, J. Geophys. Res., 113, B12410, doi:10.1029/2008JB005736

Bruyninx, C., Z. Altamimi, C. Boucher, E. Brockmann, A. Caporali, W. Gurtner, H. Habrich, H. Hornik, J. Ihde, A. Kenyeres, J. Mäkinen, G. Stangl, H. van der Marel, J. Simek, W. Söhne, J.A. Torres, G. Weber (2009). The European Reference Frame: Maintenance and Products, *IAG Symposia Series, "Geodetic Reference Frames",* Springer, Vol. 134, pp. 131-136, DOI: 10.1007/978-3-642-00860-3_20

Davis, Ph., and G. Blewitt (2000). Methodology for global geodetic time series estimation: A new tool for geodynamics, *JGR*, Vol. 105, NO. B5, pp.11083-11100

Dow, J.M., R.E. Neilan, and C. Rizos (2009), The International GNSS Service in a changing landscape of Global Navigation Satellite Systems, Journal of Geodesy, 83:191–198, DOI: 10.1007/s00190-008-0300-3

Drewes, H., H. Hornik, J. Ádám, S. Rózsa. Eds. (2008). The geodesist handbook 2008. *Journal of Geodesy*, Springer, 82 (11), pp. 661 – 846

Fernandes, R.M.S., J.M. Miranda, B.M.L. Meijninger, M.S. Bos, R. Noomen, L. Bastos, B.A.C. Ambrosius, R.E.M. Riva (2007). Surface Velocity Field of the Ibero-Maghrebian Segment of the Eurasia-Nubia Plate Boundary, *Geophysical Journal International*, 169, pp. 315–324, doi:10.1111/j.1365-246X.2006.03252.x

Herring, T.A., R. W. King, S. C. McClusky (2007). Introduction to GAMIT/GLOBK, Release 10.3, Mass. Instit. of Tech., Cambridge,

Santamaria-Gomez, A., M-N. Bouin, and G. Wöppelmann. An improved GPS data analysis strategy for tide gauge benchmark monitoring. *Submitted, this issue.*

Seemüller, W., M. Seitz, L. Sánchez, H. Drewes (2009). The position and velocity solution SIR09P01 of the IGS Regional Network Associate Analysis Centre for SIRGAS (IGS RNAAC SIR). *DGFI Report* No. 85. DGFI, Munich. Available at http://www.sirgas.org/ index.php?id=97

Wöppelmann, G., C. Letetrel, A. Santamaria, M-N. Bouin, X. Collilieux, Z. Altamimi, S. D. P. Williams, B. Martin Miguez (2009). Rates of sea-level change over the past century in a geocentric reference frame, *GRL*, 36, L12607, doi:10.1029/2009GL038720

Zumberge, J., M. Heflin, D. Jefferson, M. Watkins, F. Webb (1997). Precise point positioning for the efficient and robust analysis of GPS data from large networks, *JGR.* 102, pp. 5005–501

Comparison of Regional and Global GNSS Positions, Velocities and Residual Time Series

J. Legrand [(1)], N. Bergeot[(1)], C. Bruyninx[(1)], G. Wöppelmann[(2)], A. Santamaría-Gómez[(3,4)], M.-N. Bouin[(5)], Z. Altamimi[(3)]

(1) Royal Observatory of Belgium, Avenue Circulaire 3, B-1180 Brussels, Belgium;
(2) UMR LIENSS, Université de La Rochelle-CNRS, 2 rue Olympe de Gouges, 17000 La Rochelle, France;
(3) LAREG/IGN, 6-8 Avenue Blaise Pascal, 77455 Marne-la-Vallée, France
(4) Instituto Geográfico Nacional, c/ General Ibañez Ibero 3, 28071, Madrid, Spain;
(5) CNRM / Centre de Météo Marine, 13 rue du Chatellier, 29604 Brest, France;

E-mail: J.Legrand@oma.be

Abstract. More than ten years (1996-2008) of weekly GPS solutions of 299 globally distributed stations have been used to quantify the impact of the reference frame definition and especially the size of the network on the estimated station positions, velocities, and residual position time series. For that purpose, weekly regional solutions (covering the European region) and global solutions have been respectively stacked to obtain regional and global station positions, velocities, and residual position time series. In both cases, the estimated long-term solutions have been tied to the ITRF2005 under minimal constraints using a selected set of reference stations. This study shows that: (1) regional position and velocity solutions can present biases with respect to each other and to global solutions, while in comparison, global solutions are much more stable; (2) the obtained residual position time series are affected by the size of the network with significantly reduced periodic signals in the regional networks, e.g. a 27% reduction of the annual signals in the height component.

Keywords. Geodesy; Reference Frame; Methodology; GNSS; Station Positions; Velocity Field; Residual position time series.

1 Introduction

Different GNSS reprocessing performed during the last years (Steigenberger 2006; Wöppelmann et al. 2007; 2009; Kenyeres in press) have shown that significant improvements in the quality and homogeneity of the estimated parameters can be obtained. Within the EUREF Permanent Network (EPN; Bruyninx, 2004), recently, a new Special Project (SP) dedicated to the coordination of the EPN re-processing has been set up (Völksen, 2009). This SP will use the consistent high quality GNSS products (e.g. orbits, clocks and Earth rotation parameters) issued from the International GNSS Service (IGS; Dow, 2009) re-processing campaign, to re-process the EPN data. During the project Pilot Phase, optimal processing strategies are investigated such as the need to add (or not) global IGS stations to the EPN re-processing. Indeed, with the improving computing facilities and GNSS data analysis, it has become less demanding to perform a global analysis and regional networks may consider this approach.

In Legrand and Bruyninx (2009a), global and regional station positions solutions were compared and it was demonstrated that positions obtained from global network solutions are less sensitive to the reference frame definition compared to regional solutions. In Legrand et al. (2009b), it was shown that when expressing a GNSS solution in the ITRF2005 (Altamimi et al. 2007a) using minimal constraints, the network effect (due to the size of the GNSS network and the choice of the reference stations) significantly influences the estimated velocity field and consequently might cause incorrect geodynamical interpretations. Consequently, when sub-mm/year accuracy is required, e.g. for a proper interpretation of intraplate deformations or vertical velocities, a global approach should be considered.

In this paper, these studies have been repeated using an enhanced GPS re-processed solution with an enlarged network and, in addition, they were extended to also investigate the impact of

the size and the geometry of the network on the station residual position time series.

2 Input Data

More than ten years (1996-2008) of weekly GPS solutions produced by the ULR consortium (Université de la Rochelle and IGN/LAREG) as its contribution to the Tide Gauge Benchmark Monitoring project of the IGS (TIGA) have been used throughout this paper. The ULR weekly solutions provide station coordinates together with their covariance information for 299 globally distributed continuously observing GNSS stations (Figure 1) from which 265 stations have more than 3.5 years of data.
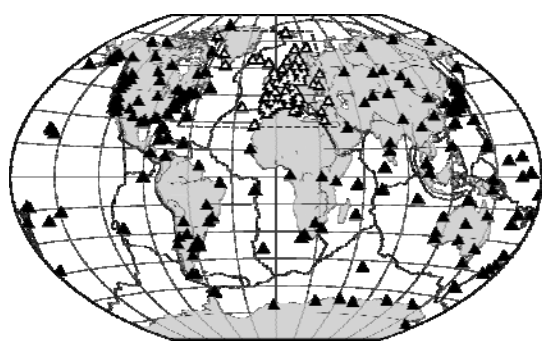
Fig. 1 Global (black triangles) and regional (white triangles) networks used in this study. The dashed area corresponds to Figure 2.

The same parameterization and observation modeling were used over the whole 13-year period, estimating station coordinates, satellite orbits, Earth orientation parameters, and zenith tropospheric delay parameters every 2 hours. IGS absolute phase centre corrections for both the tracking and transmitting antennas were applied (see Santamaria et al. in this issue, for further details on the GNSS reprocessing strategy).

In order to investigate the impact of using regional network instead of a global network, we elaborated several long-term solutions by varying the geographical extension of the network and the reference stations used in the alignment to the ITRF2005. First, regional weekly solutions have been created from the ULR global weekly solutions by extracting the 74 GNSS stations located in Europe, all of them are included in the EUREF Permanent Network (EPN). Then, global and regional cumulative solutions (positions, velocities, and residual time series) were computed by stacking both sets of weekly

(regional and global) solutions. The stacking was performed with CATREF (Altamimi 2007b) and the position and velocity combined solutions (regional and global) were tied to the ITRF2005 under minimal constraints using 14 transformation parameters (translations, rotations, scale and their rates) using a selection of ITRF2005 reference stations. The minimal constraints approach has the advantage of preserving the intrinsic characteristics of the stacked solution (Altamimi, 2003) while avoiding any internal distortion of the original network geometry. The selected reference stations were chosen in such a way that they have a station observation history of at least 3 years in the ITRF, as well as in the ULR time series, show a good agreement with the ITRF2005 solution, and are optimally distributed over the network.

To evaluate the impact of the reference stations on the global and regional velocity fields, several sets of regional and global reference stations were tested. In the global case, we selected 100 reference stations geographically well-distributed over the globe. While in the regional case, the set of reference stations covered only the European region. In order to highlight the instability observed in a regional case, based on the same set of 74 regional stations, two different regional solutions were computed using two sets of reference stations (Figure 2) having a large probability of being used in Europe:

- Selection A: 30 reference stations

- Selection B: 19 stations, subset of selection A with stations located only on the European continent.
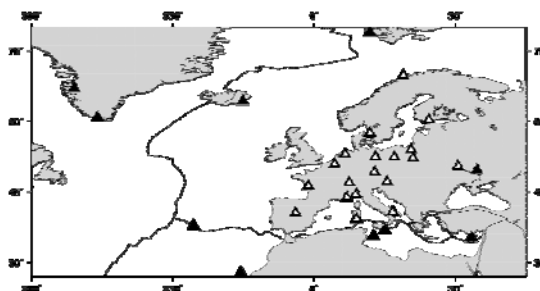
Fig. 2. Stations used for the reference frame alignment of regional solutions. Selection A: stations are indicated with black and white triangles; selection B: stations are indicated with white triangles.

3 Results

In a first step, the cumulative positions and the velocities of the global solution have been compared to the cumulative positions and the velocities of the two regional solutions (at epoch 2003.0). In a second step, a similar comparison was done for the residual position time series. For the common stations, the different cumulative solutions are based on identical weekly positions.

3.1 Positions and Velocities

The differences between the positions obtained using the different networks (see Table 1) can reach 3 mm in the horizontal component and 8 mm in the vertical component. They are due to the network effect and entail a systematic effect on both the horizontal and vertical positions. Nevertheless, these differences are much smaller than in Legrand and Bruyninx (2009a). Indeed, in the previous paper, the authors used a 1-year cumulative solution and found differences reaching 8 mm in the horizontal and 2 cm in the vertical. In this paper, the use of solutions based on a longer time span, 13 years instead of 1 year, allows to stabilize the reference frame definition and entails a better (more stable and reliable) alignment of the solution to the ITRF2005.

Table 1. Statistics on position and velocity differences between Regional A (resp. Regional B) and Global solution for the 74 common stations.

Position differences [mm]		RMS	Max.
Horizontal	Regional A – Global	0.9	2.5
	Regional B – Global	1	3.2
Vertical	Regional A – Global	1.7	7.8
	Regional B – Global	2.1	6.8
Velocity differences [mm/yr]		RMS	Max.
Horizontal	Regional A – Global	0.3	0.6
	Regional B – Global	0.5	1.1
Vertical	Regional A – Global	0.6	1.4
	Regional B – Global	0.6	1.7

Similar systematic effects also affect the horizontal and the vertical velocities (Table 1). They are highlighted in Fig. 3, which shows the horizontal velocity differences between the global solution and the two regional solutions (top: regional A, bottom: regional B). These differences (as well as the ones between the two regional solutions) can be fully explained by a

Euclidean transformation similarity and are due to the so-called network effect.

The vertical velocity differences between the global solution and the two regional solutions (top: regional A, bottom: regional B) in Fig. 4 present a tilt affecting both regional solutions compared to the global solution.
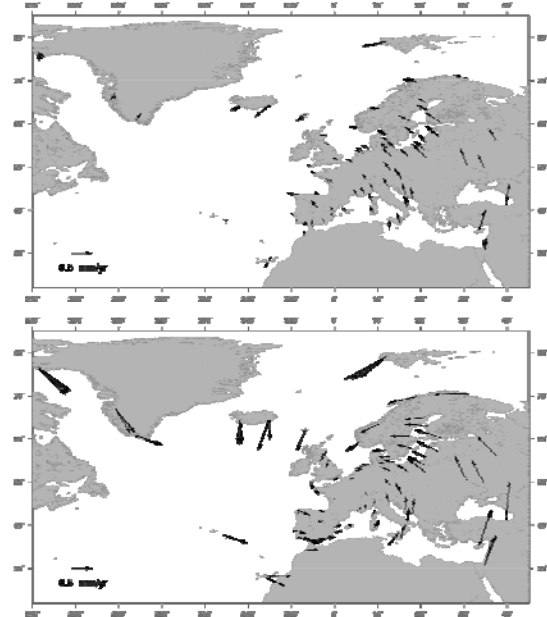
Fig. 3. Difference between global and regional horizontal velocity fields (mm/yr). Top: global versus regional A, bottom: global versus regional B.
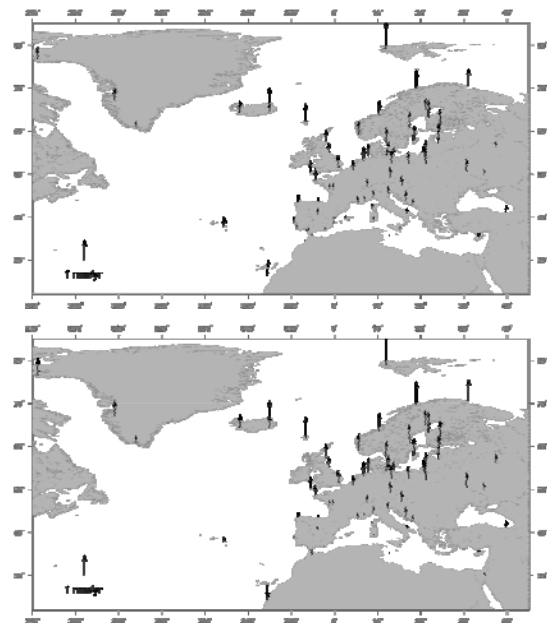
Fig. 4. Difference between global and regional vertical velocity fields (mm/yr). Top: global versus regional A, bottom: global versus regional B.

These results reassert the results in Legrand et al. (2009b). Nevertheless, the impact of the reference frame definition on the derived velocity fields is smaller in the present study than in Legrand et al. (2009b), where the differences between the regional velocity fields and the global velocity field could reach up to 1.3 mm/yr in the horizontal and 2.9 mm/yr in the vertical. The smaller differences obtained in this paper are most probably due to the availability of a larger number of reference stations in good agreement with the ITRF2005. Wöppelmann et al. (2008) investigated the influence of using different sets of reference stations to express a global solution in a given frame and concluded that the best results were obtained using a large global distribution of reference stations mitigating the individual problems at each of the reference stations. Similarly, in a regional network, more reliable velocities are obtained using a larger number of reference stations.

The comparison between regional A and B solution shows that the disagreement between the global and regional solutions (both positions and velocities) is amplified when the reference stations cover a smaller geographical area.

3.3 Time series

In addition to the observed position and velocity differences, the size of the network also affects the residuals position time series. These residual position time series are obtained when removing the estimated site velocity from the weekly positions and provide information on the non-linear site (e.g. seasonal) motions.

The residual time series from regional A and from regional B are identical. Indeed, they depend on the size of the network and stations in the solution, and not on the selected reference stations. Consequently, in the following, only the residual time series from the regional A solution are compared with the global residual time series.

During the stacking, discontinuities have been introduced to account for jumps in the timeseries. A new station position is estimated after each discontinuity and the velocities are usually constrained to be equal before and after a discontinuity. As, only a linear motion was assumed, the RMS of a residual time series reflects the noise, but also the seasonal signals which affect the GNSS stations. In average, the RMS of the regional residual time series is

reduced by about 20% compared to the global residual time series. Fig. 5 shows, for each European station, the difference between the RMS of the global residual time series and the regional residual time series. The mean RMS reduction is 0.75 mm on the vertical component and is maximal in the North-East of Europe. On the horizontal component, the RMS reduction is about 0.25 mm.
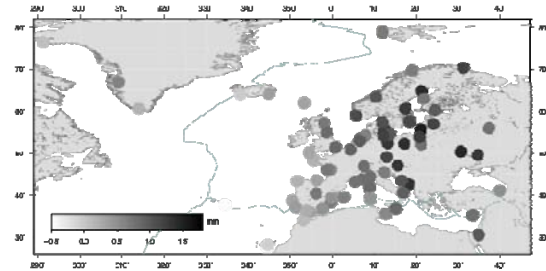
Fig. 5. RMS reduction for the up component (in mm) when processing a regional network instead of a global one.

Fig. 6 illustrates the RMS reduction for the station GLSV (Kiev, Ukraine). The RMS of the height time series obtained with the global network is 5.8 mm compared to 4.3 mm for the regional one; this means that the RMS was reduced by 1.5 mm. The amplitude of the annual (resp. semi-annual) signal is 5.2 mm (resp. 0.9 mm) for the global and 3.8 mm (resp. 0.8 mm) for the regional.
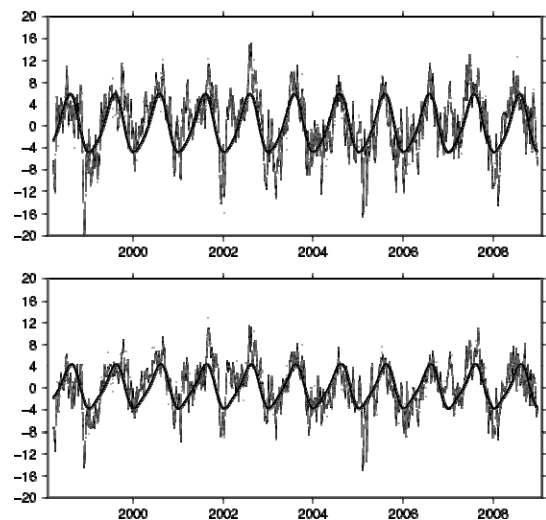
Fig. 6. Residual time series of GLSV: Up component. Top: global, bottom: regional A.

Table 2 gives the mean amplitudes of the annual and semi-annual terms simultaneously fitted on

the residual time series; it evidences an amplitude reduction for all the components when a regional network is considered instead of a global one. For the horizontal components, the annual amplitude decreases by 8% for the east component and 15% for the north component. The semi-annual amplitude is decreased by 9% for both the east and the north components. The up component is the most affected by this reduction: the annual amplitude is decreased by 27% (see Figures 7 and 8 for details) and the semi-annual amplitude is reduced by 15%.

Table 2. Mean amplitudes and standard deviations of the annual and semi-annual terms estimated from the residual time series.

Mean Amplitude [mm]	Global		Regional	
	Annual	Semi-annual	Annual	Semi-annual
East	0.66 ± 0.46	0.23 ± 0.12	0.61 ± 0.44	0.21 ± 0.11
North	0.74 ± 0.68	0.29 ± 0.16	0.63 ± 0.62	0.22 ± 0.14
Up	2.37 ± 1.17	0.93 ± 0.58	1.73 ± 1.04	0.79 ± 0.47
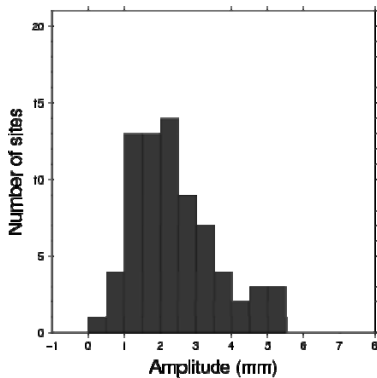
Fig. 7. Histogram of the annual amplitudes observed in the up component time series in Europe with our global network.
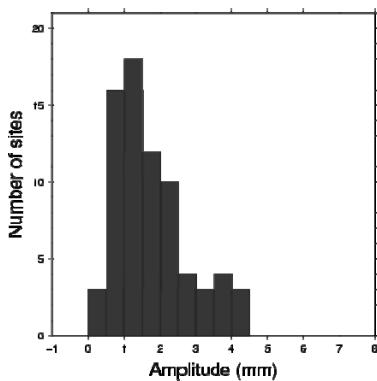
Fig. 8. Histogram of the annual amplitudes observed in the up component time series in Europe with our regional network.

Fig. 9 (resp. Fig. 10) shows the histograms of the phases of the annual signal in the up component for the global network (resp. for the regional network). In the global network, the predominant phase is around 180°, while within the regional network the phases are more randomly distributed.
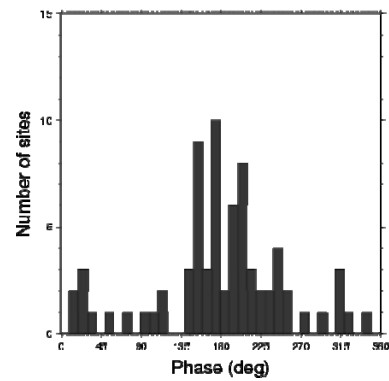
Fig. 9. Histogram of the annual phases observed in the up component time series in Europe with our global network.
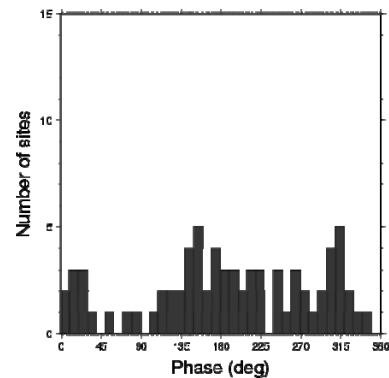
Fig. 10. Histogram of the annual phases observed in the up component time series in Europe with our regional network.

This study shows that our regional network is not able to reliably reconstruct the spatially correlated annual and semi-annual signals. Indeed, during the stacking, these common signals are absorbed by the transformation parameters estimated to align each individual solution to the final combined solution.

4. Conclusion

We investigated the influence of the reference frame definition in terms of reference station

selection and network extension on the cumulative positions, velocities, and residual position time series obtained from a GNSS network which was tied to the ITRF2005 using minimal constraints.

It was shown that, based on identical sets of weekly positions, the estimated long-term positions and velocities can differ (up to 2 mm in the horizontal and 8 mm in the vertical for the positions and up to 0.5 mm/yr in the horizontal and 2 mm/yr in the vertical for the velocities) due to a network effect which depends on the selection of the reference stations. The disagreement between the global and regional solutions (both positions and velocities) is amplified when the regional reference stations cover a smaller geographical area.

In a regional network, the absorption of the common mode signals induces several effects on the residual position time series. The mean RMS of the regional residual time series shows a reduction of about 20% compared to the global residual time series. This RMS reflects not only the noise but also the seasonal signals in the time series. We demonstrated that the regional network underestimates the amplitude of the annual (27% reduction of the annual signal in the height component) and semi-annual signals in all components. In addition, the phase of the annual and semi-annual signals is altered: while in a global network the predominant phase is 180°, this is not the case anymore in a regional network. Consequently, a geophysical interpretation of the seasonal signals observed using a regional network can be more challenging.

References

Altamimi Z. (2003). Discussion on How to Express a Regional GPS Solution in the ITRF. EUREF Publication No. 12, Verlag des Bundesamtes für Kartographie und Geodäsie, Frankfurt am Main, pp. 162-167.

Altamimi, Z., Collilieux, X., Legrand, J., Garayt, B., Boucher, C. (2007a). ITRF2005: A new Release of the International Terrestrial Reference Frame based on Time Series of Station Positions and Earth Orientation Parameters. *J. Geophys. Res.*, 112, B09401, doi:10.1029/2007JB004949.

Altamimi, Z., Sillard, P., Boucher, C. (2007b). CATREF software: Combination and Analysis of Terrestrial Reference Frames. *LAREG Technical*, Institut Géographique National, Paris, France.

Bruyninx, C. (2004). The EUREF Permanent Network; a multidisciplinary network serving surveyors as well as scientists. *GeoInformatics*, Vol 7, pp. 32-35.

Dow, J. M., J.M., ·Neilan, R. E., and Rizos, C. (2009). The International GNSS Service in a changing landscape of Global Navigation Satellite Systems. *Journal of Geodesy* 83:191–198, DOI: 10.1007/s00190-008-0300-3.

Kenyeres A., Legrand J., Figurski M., Bruyninx C., Kaminski P., Habrich H Homogenous Reprocessing of the EPN : First Experiences and Comparisons. Accepted by : *Bulletin of Geodesy and Geomatics*.

Legrand J., Bruyninx C. (2009a). EPN Reference Frame Alignment: Consistency of the Station Positions. *Bulletin of Geodesy and Geomatics*, Vol. LXVIII, No.1, 20-34

Legrand J., Bergeot N., Bruyninx C., Wöppelmann G., Bouin M.-N., Altamimi, Z. (2009b) Impact of Regional Reference Frame Definition on Geodynamic Interpretations, Journal of Geodynamics, Vol. In Press, Accepted Manuscript, pp. -

Santamaría-Gómez, A., M-N. Bouin, G. Wöppelmann. Improved GPS data analysis strategy for tide gauge benchmark monitoring. Submitted, this issue.

Steigenberger, P., Rothacher, M., Dietrich, R., Fritsche, M., Rülke, A., Vey, S. (2006). Reprocessing of a global GPS network. *J. Geophys. Res.*, 111, B05402, doi:10.1029/2005JB003747.

Völksen C. (2009). Draft Charter for the EUREF Working Group on Reprocessing of the EPN, *http://epn-repro.bek.badw.de/Documents /charter_repro.pdf*

Wöppelmann, G., C. Letetrel, A. Santamaria, M.-N. Bouin, X. Collilieux, Z. Altamimi, S. D. P. Williams, and B. Martin Miguez. (2009) Rates of sea-level change over the past century in a geocentric reference frame, *Geophys. Res. Lett.*, 36, L12607, doi:10.1029/2009GL038720.

Wöppelmann G., Bouin, M-N., Altamimi, Z. (2008). Terrestrial reference frame implementation in global GPS analysis at TIGA ULR consortium. *Physics and Chemistry of the Earth*, Parts A/B/C Volume 33, Issues 3-4, Observing and Understanding Sea Level Variations, pp. 217-224.

Wöppelmann G., B. Martin Miguez, M-N. Bouin, Z. Altamimi. (2007). Geocentric sea-level trend estimates from GPS analyses at relevant tide gauges world-wide. *Global Planet. Change*, 57, 396– 406.

New strategy for reprocessing a global GPS network at the ULR TIGA analysis centre

Álvaro Santamaría[1,2], Marie-Noëlle Bouin[3], Guy Wöppelmann[4]

email: asantamaria@fomento.es

[1]Instituto Geográfico Nacional, C/General Ibáñez de Ibero, 3, 28003 Madrid, Spain
[2]Institut Géographique National – LAREG, 6-8 Avenue Blaise Pascal, Champs-Sur-Marne, 77455 France
[3]Météo France, Brest, France
[4]UMR 6250 LIENSS, University of La Rochelle-CNRS, La Rochelle, France

A. Introduction

The GPS Tide Gauge Benchmark Monitoring Pilot Project (TIGA-PP) is a pilot study of the IGS for establishing a service to analyze GPS data from stations at or near tide gauges (CGPS@TG). The primary product of the service would be time series of coordinates for analyzing vertical motions of tide gauges. The service may further contribute to the calibration of satellite altimeters and other oceanographic activities.

The University of La Rochelle (ULR), in close cooperation with the French Geographic Institute (IGN) geodetic laboratory (LAREG), constitutes one of the seven TIGA Analysis Centres (TAC). It aims at processing past, current and future GPS data with a latency of 460 days, and re-computing a selected subset of IGS network stations for improved long-term stability of the reference frame since the inception of the IGS. The ULR processing infrastructure is copes with a network of up to 223 stations and is based on the following scientific software:

- **GAMIT**, used for processing GPS measurements (*Herring et al. 2006a*)
- **CATREF**, used for combining station positions, velocities, EOPs, and defining the reference frame (*Altamimi et al. 2007*).
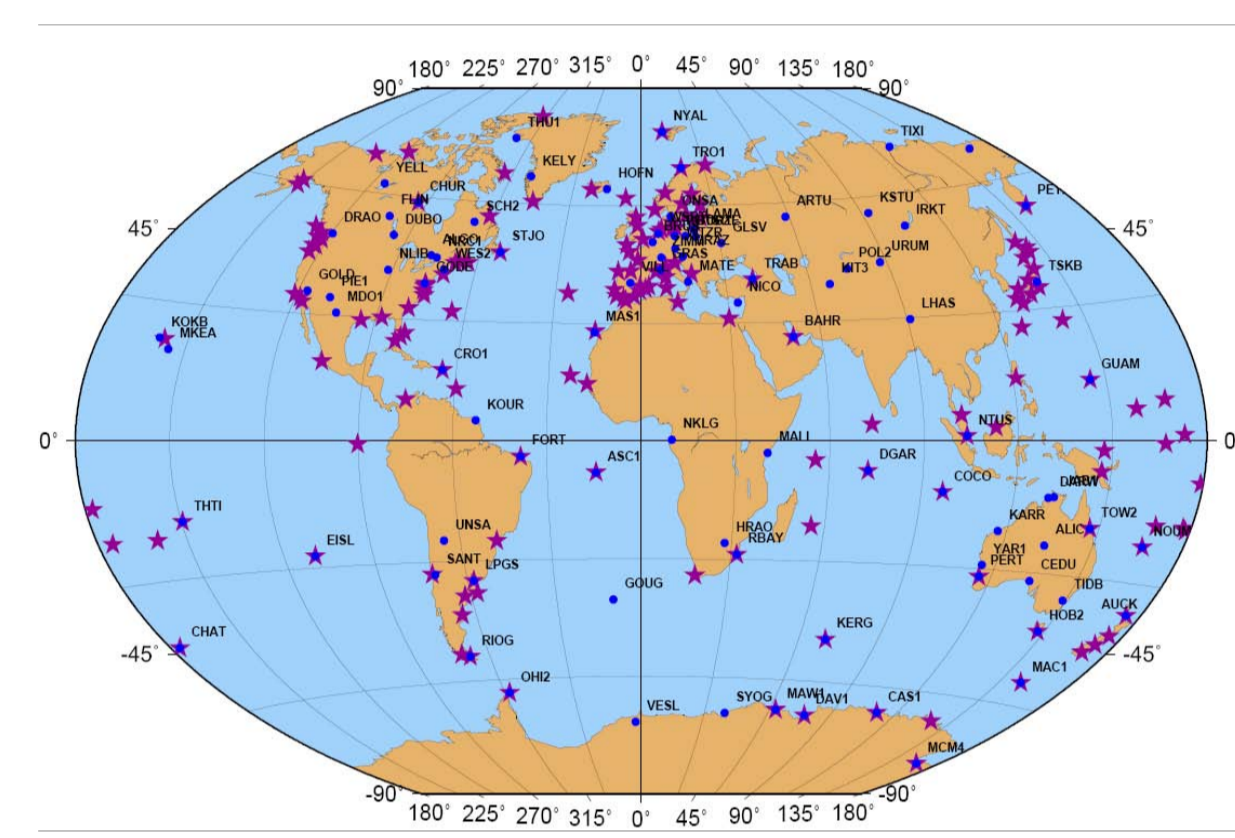
ULR TIGA Analysis Centre Network
★ CGPS@TG
● IGS station

B. Validation of 2006 re-processing

In 2006 the ULR TAC network was extended to reach its current configuration. At the same time, a major advance in the IGS community was made in the antenna phase centre variation model (PCV), from relative to absolute model. This encouraged ULR TAC to re-process the GPS data backwards until 1996. In the new re-processing were included the absolute phase centre variation model and the GMF mapping function from (*Boehm et al. 2006b*).

In order to validate the re-processed solution, two main tests were carried out at IGN/LAREG:

- differences between absolute and relative PCV model (with estimation of orbits)
- differences between GMF and VMF1 mapping functions (with cutoff angle of 10°).

The test network is composed by 42 IGS05 stations globally well distributed and the data span constitutes 1 week per month in 2006 (84 daily solutions). The software used are:

- **GAMIT 10.32**
- **CATREF**
- **SIMILITUDE**: used for comparing station daily solutions without stacking them (D. Coulot, IGN-LAREG).
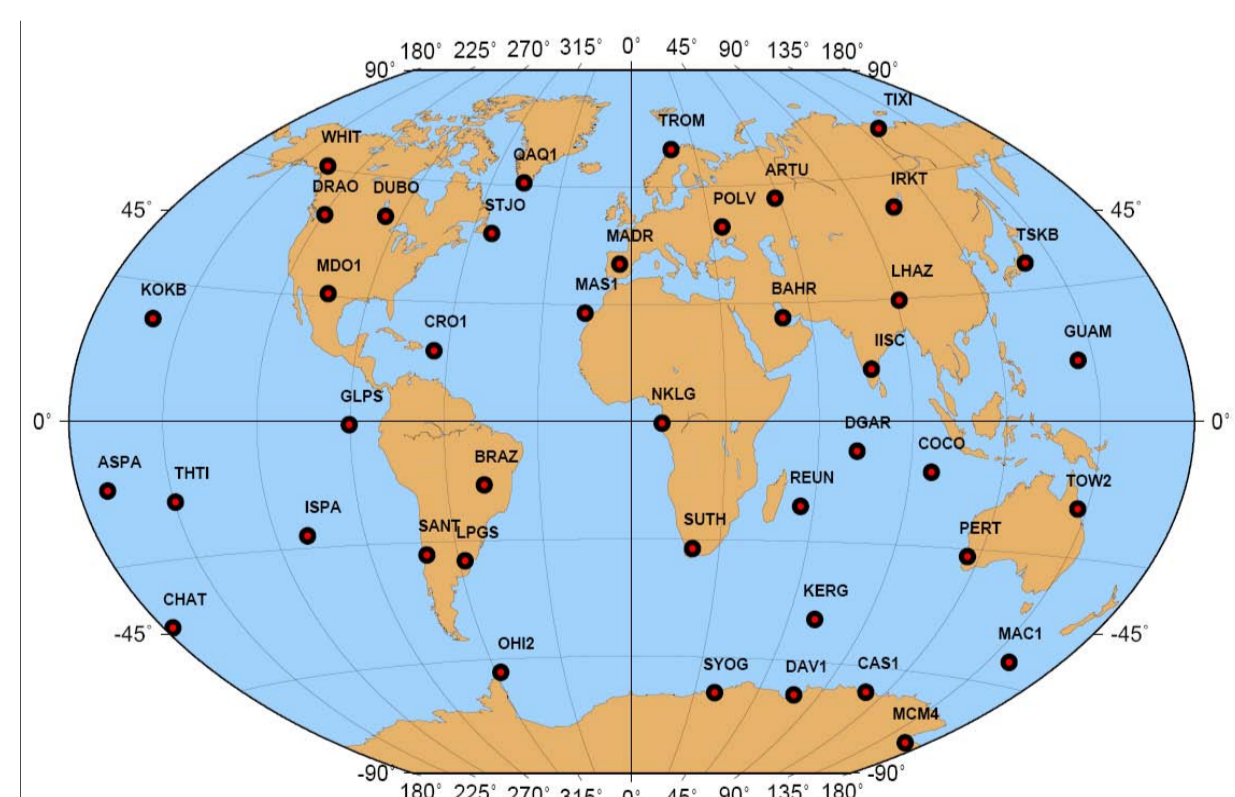
Validation test network

C. Phase Centre Variation test

Estimating the orbits in order to be consistent with each model, the impact of the switch from relative phase centre variations (RPCV) to absolute phase centre variations (APCV) on the reference frame is a:

- scale change of 1,8 ppb (± 0,1) or 11,5 mm at the Equator, corroborating (*Ferland 2006*).

- station specific vertical changes (local effects) up to 1,5 cm (black points are significant differences)

Difference between APCV/RPCV and ITRF2005

Difference between APCV and RPCV
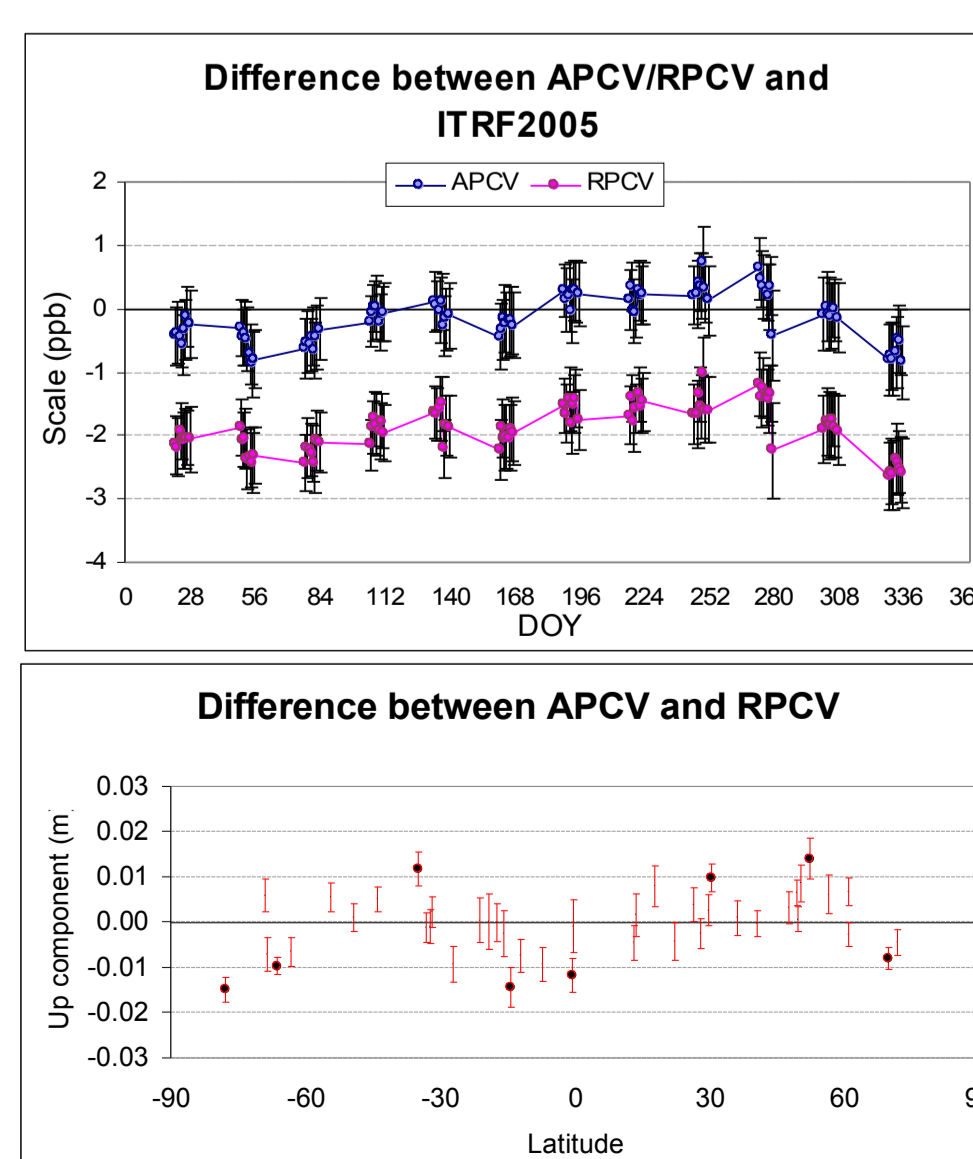
D. Troposphere modelling test

The two mapping functions compared are based on data from ECMWF numerical weather model:

-VMF1 grid: a_h, a_w and $ZHD_{a priori}$ each 6 hours in a global 2°x2,5° grid. (*Boehm et al. 2006a*), (*Kouba 2007*)

- GMF: a_h a_w each 24 hours in the form of spatial spherical harmonic coefficients up to degree and order 9. (*Boehm et al. 2006b*). $ZHD_{a priori}$ were obtained with GPT model (*Boehm et al. 2007*).

The significant (black points) maximum difference is about 2 mm. in the Antarctic continent (MCM4 station).
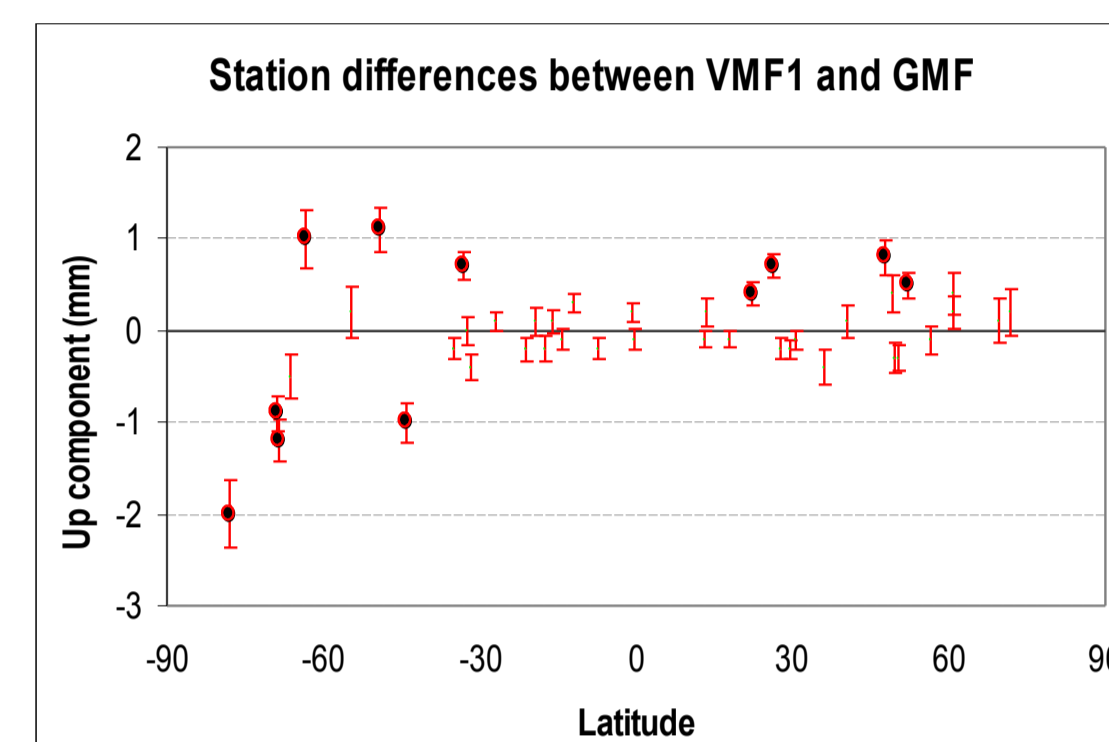
The GPS processing with GMF is faster by 13 min. per daily solution and CPU, that is 5,5 months per CPU for the ULR re-processed solution.

In order to specify if there is a difference in the estimated velocity, we have estimated the relationship between the daily differences of the height component (dH) and the daily differences of the a priori modelled hydrostatic delay (dHD) at 10° for the MCM4 station, which contains the higher difference.
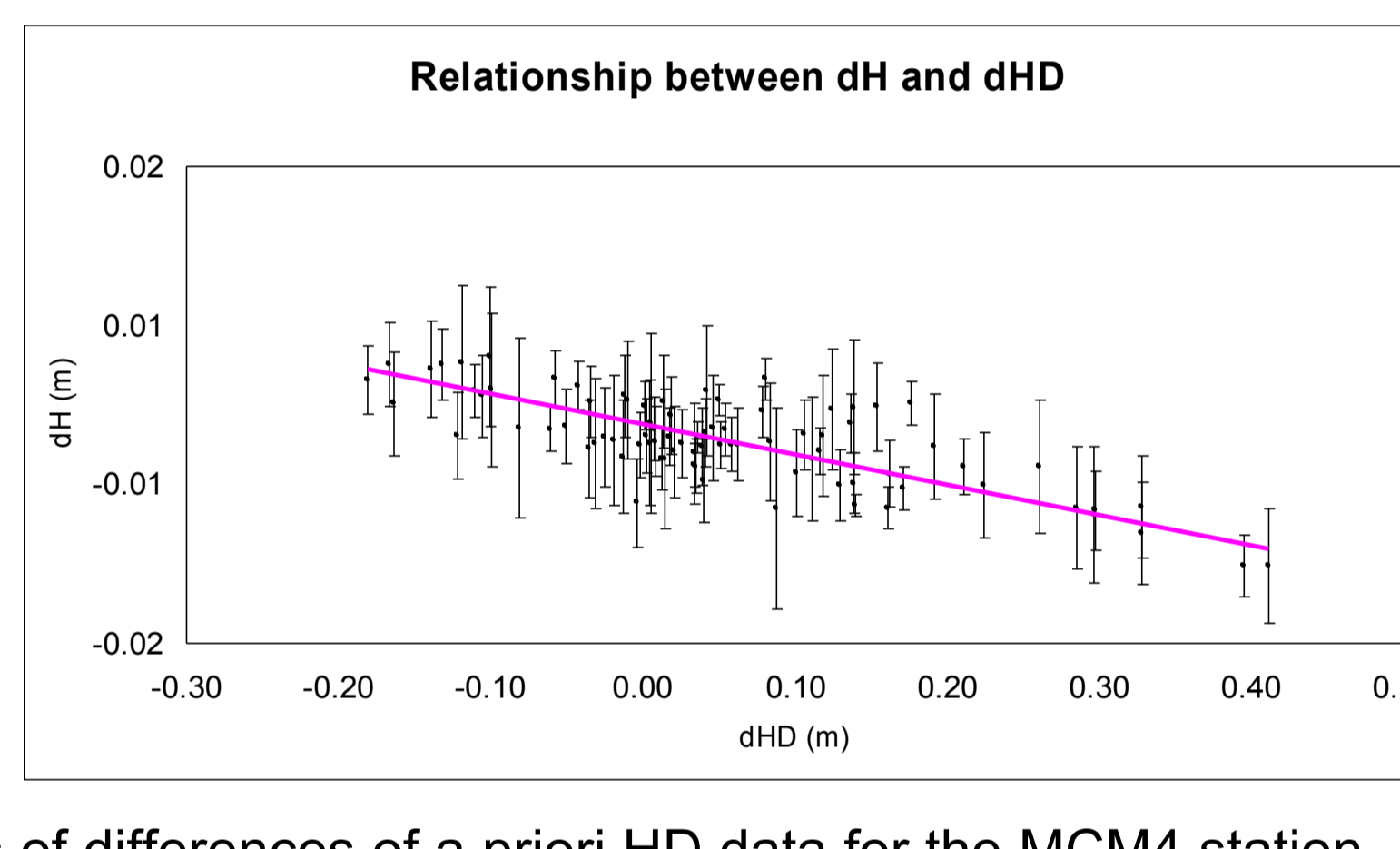
This relationship is defined as:

$$dH = -0.0137 \, dHD - 0.0013$$
$$(\pm 0.0015) \quad (\pm 0.0003)$$

Correlation = -0.76

Station differences between VMF1 and GMF

Relationship between dH and dHD

Using this relationship with 8 years of differences of a priori HD data for the MCM4 station, we verify that there is no velocity difference. Thus we conclude that we can use GMF instead of VMF1.

Height (transformed) differences between VMF1 and GMF in MCM4
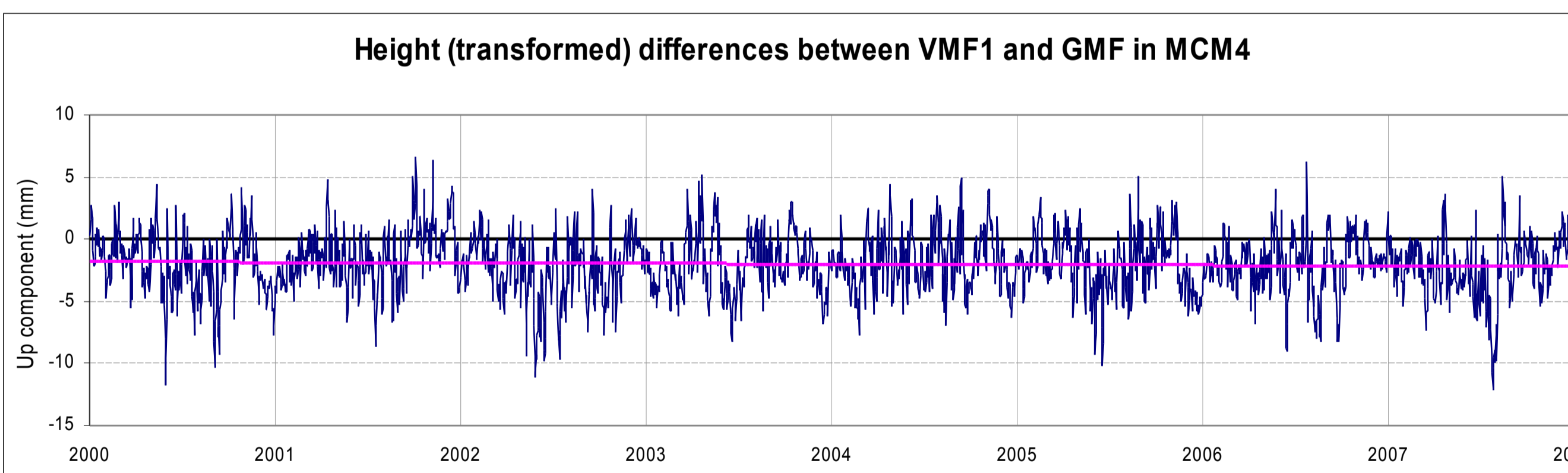
E. Quality of the re-processed solution

In order to characterize the noise process in unevenly sampled re-processed time series, we have used the Lomb-Scargle algorithm (*Press et al. 2001*) for 201 stations having more than 150 data weeks and we have filtered the annual and semi-annual signal.

With a linear regression we have obtained that the type of noise is located between white and flicker noise, with a mean spectral index (α) of -0.6 . Furthermore we have obtained the same anomalous harmonics at 1.04 cpy described in (*Ray et al. 2007*) but with a higher resolution on the 9th harmonic.

In comparison with the stacked IGS solution, using 75 common stations with more than 200 data weeks, we have obtained a significant reduction of the spectral index. As conclusion, this means a noise process less correlated for the ULR re-processed solution.

ULR re-processed spectra

Up spectra for IGS common stations
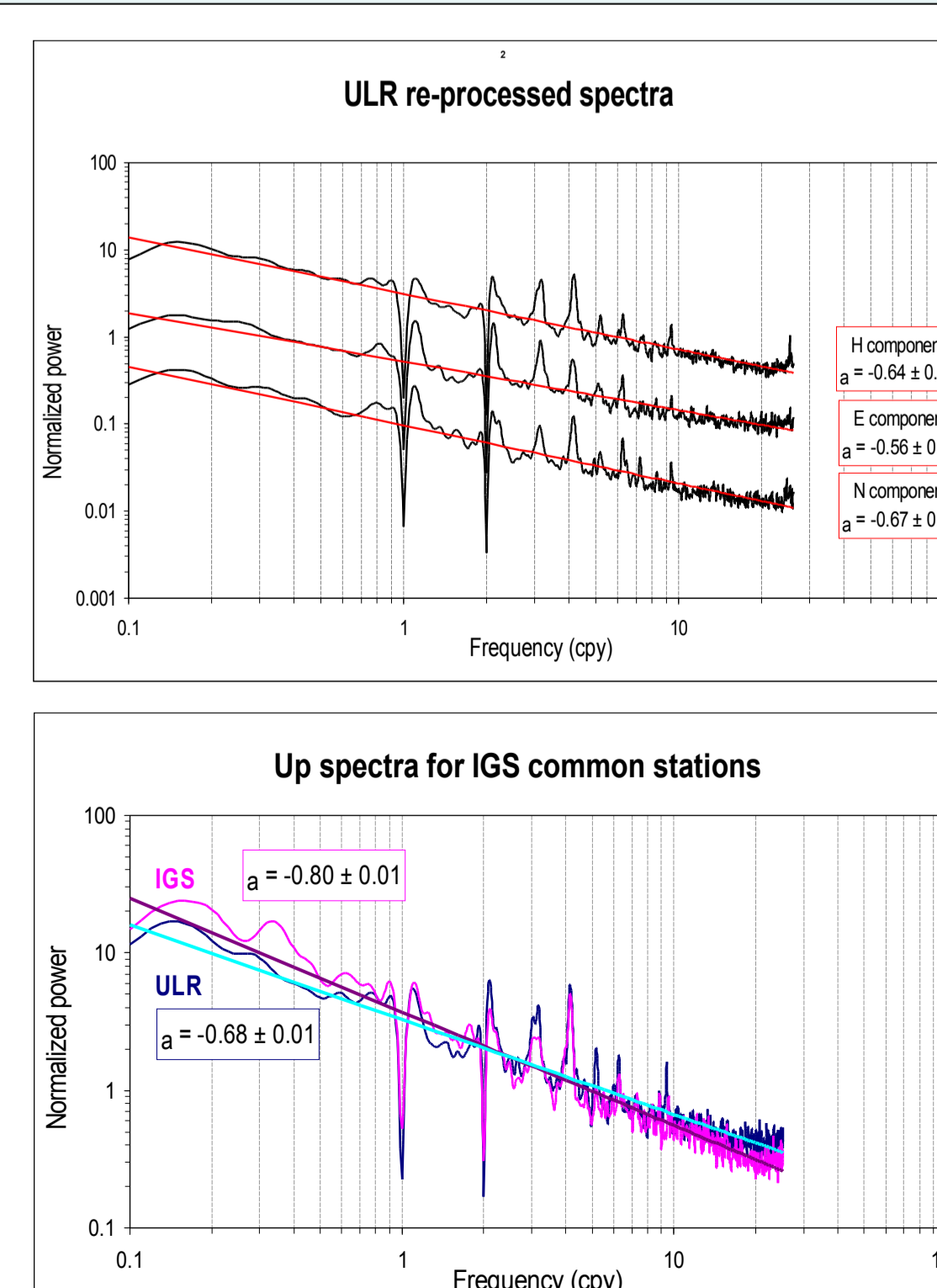
F. Sub-networks and software combination test

Due to the update of the GPS processing software since the last re-processing and the anomalous transformation parameters obtained for the beginning solutions before 1999 where the GPS network was sparse, the ULR TIGA Analysis Centre plans to do a new re-processing.

For this new re-processing special care will be applied in the selection of sub-networks. As TIGA stations suffer from highly concentrated regional networks, mainly in Europe and Japan, this issue needs to be addressed. Furthermore, the regional sub-network scheme will reduce the baseline lengths and therefore should improve the GPS results.

In addition, in this test, we exploit other combination software as GLOBK (*Herring et al. 2006b*) which can be used to combine simultaneously station positions, velocities and EOPs, as well as the sub-networks estimated orbits.

We have therefore 4 solutions to compare:

-Global sub-networks + CATREF

-Regional sub-networks + CATREF

-Global sub-networks + GLOBK

-Regional sub-networks + GLOBK

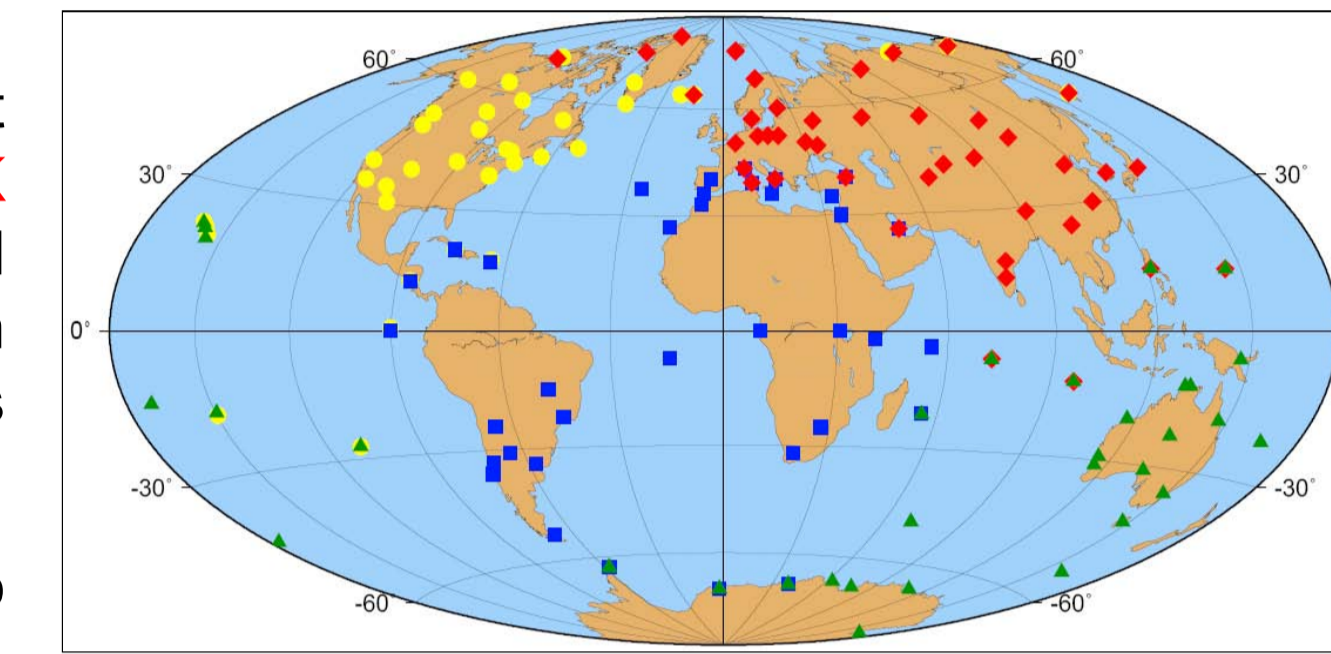The data span is the same as the one described in box B (12 data weeks distributed in 2006).
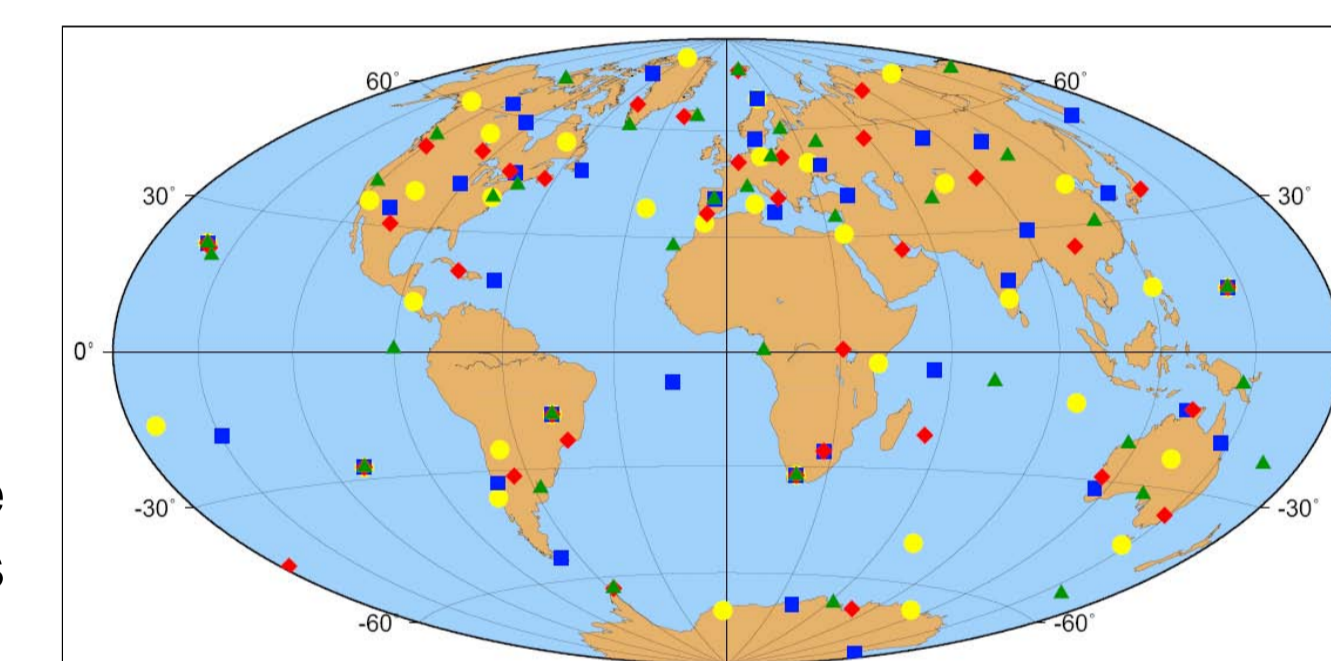
Fig: Regional sub-networks

Fig: Global sub-networks

Following (*Collilieux 2004*), the reference frame for both software can be defined similarly. That was checked with a similarity transformation between both stacked solutions. Thus, hereafter we use CATREF to align and stack the solutions.

As external criteria, in order to decide which strategy involves the most appropriate combination and reference frame definition, we have estimated the stations annual signal in the up component for the 4 solutions and we have compared these annual signals with those obtained from the IGS residuals of the ITRF2005 solution (*Collilieux et al. 2007*).

Examining the stations with the most important annual signals, we conclude that, with the data span used, we are not able to distinguish correctly any difference between both strategies. We will extend the data span for this analysis and will use some geophysical models to compare estimated positions, like post-glacial rebound and gravity GRACE data.

Annual signal in BRAZ station

Annual signal in IRKT station
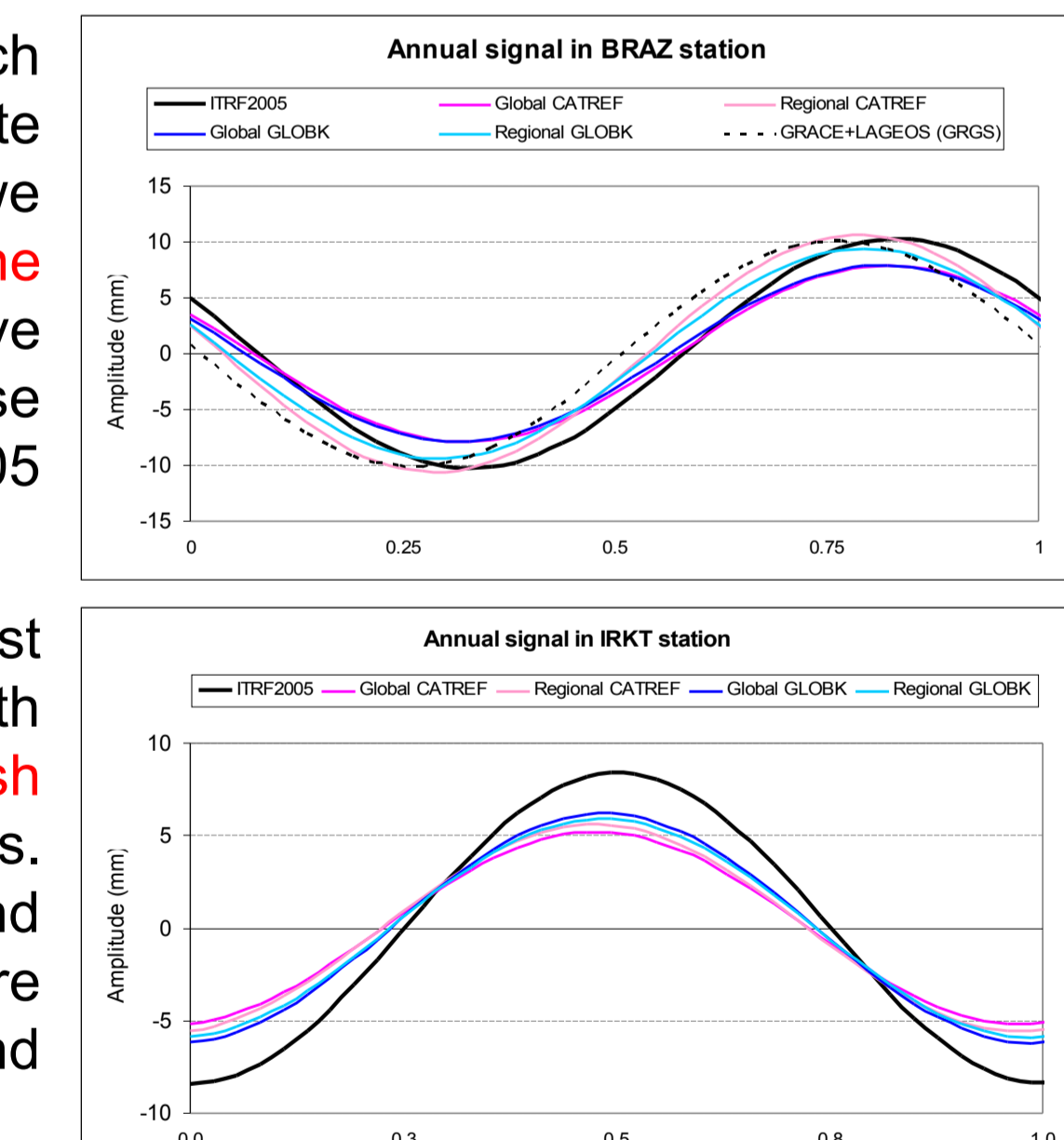
G. References

***Altamimi, Z., Sillard, P. and Boucher, C. (2007): CATREF software documentation. IGN
***Collilieux, X. (2004): Comparison de CATREF & GLOBK pour la comparaison de Repère de Rérérence Terrestre. Rapport de DEA. Observatoire de Paris.
***Collilieux, X., Altamimi, Z., Coulot, D., Ray, J. and Sillard, P. (2007): Comparison of very long baseline interferometry, GPS, and satellite laser ranging height residuals from ITRF2005 using spectral and correlation methods. Jour. of Geophy. Res., 112, B12403, 2007.
***Boehm, J., Werl, B. and Schuh, H. (2006a): Troposphere mapping functions for GPS and very long baseline interferometry from European Centre for Medium-Range Weather Forecasts operational analysis data. Jour. of Geophy. Res., 111.
***Boehm, J., Niell, A., Tregoning, P. and Schuh, H. (2006b): Global Mapping Function (GMF): A new empirical mapping function based on numerical weather model data. Geophys. Res. Lett., 33.
***Boehm, J., Heinkelmann, R. and Schuh, H. (2007): Short Note: A global model of pressure and temperature for geodetic applications. Jour. of Geodesy. DOI: 10.1007/s00190-007-0135-3.
***Herring, T.A., King, R.W. and McClusky, S.C. (2006a): GAMIT Reference Manual, GPS Analysis at MIT. Release 10.3. Mass. Inst. of Technol. Cambridge, MA.
***Herring, T.A., King, R.W. and McClusky, S.C. (2006b): GLOBK Reference Manual, Global Kalman filter VLBI and GPS analysis program. Release 10.3. Mass. Inst. of Technol. Cambridge, MA.
***Ferland, R. (2006): Proposed Update of the IGS Reference Frame Realization. Proc. IGS WS, Darmstadt, Germany, 2006.
***Kouba, J. (2007): Implementation and testing of the gridded Vienna Mapping Function 1 (VMF1). Jour. of Geod., DOI: 10.1007/s00190-007-0170-0
***Press, W.H., Teukolsky, S.A., Vetterling, W.T. and Flannery, B.P. (2001): Numerical recipes in Fortran 77: the art of scientific computing (2nd edn). Vol. 1 of Fortran numerical recipes, Cambridge University Press, Cambridge, pp 569-569
***Ray, J.R., Altamimi, Z., Collilieux, X. and van Dam, T.M. (2007): Anomalous harmonics in the spectra of GPS position estimates. GPS Solutions, DOI:10.1007/s10291-007-0067-7.

Impact of sub-network configuration on global scale GPS processing

Álvaro Santamaría[1,2], **Marie-Noëlle Bouin**[3], **Guy Wöppelmann**[4]
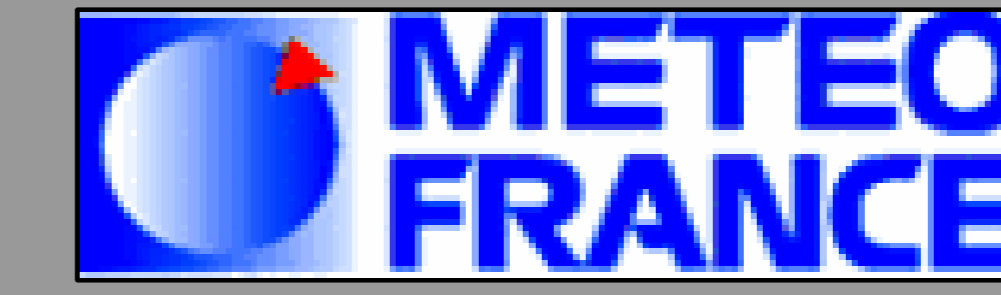
email: asantamaria@fomento.es

[1] Instituto Geográfico Nacional, Madrid, Spain
[2] Institut Géographique National – LAREG, Champs-Sur-Marne, France
[3] Météo France, Brest, France
[4] UMR 6250 LIENSS, University of La Rochelle-CNRS, La Rochelle, France

① ⓘ INTRODUCTION ⓘ

In a global GPS processing, like the reprocessing campaign started by the IGS last year, it is usual to have between 50 and 100 IGS Reference Stations only per day. At the University of La Rochelle (ULR) TIGA Analysis Center (TAC), the daily tracking network processed from 1997 to 2008 varies between 67 and 195 stations (Fig. 1).
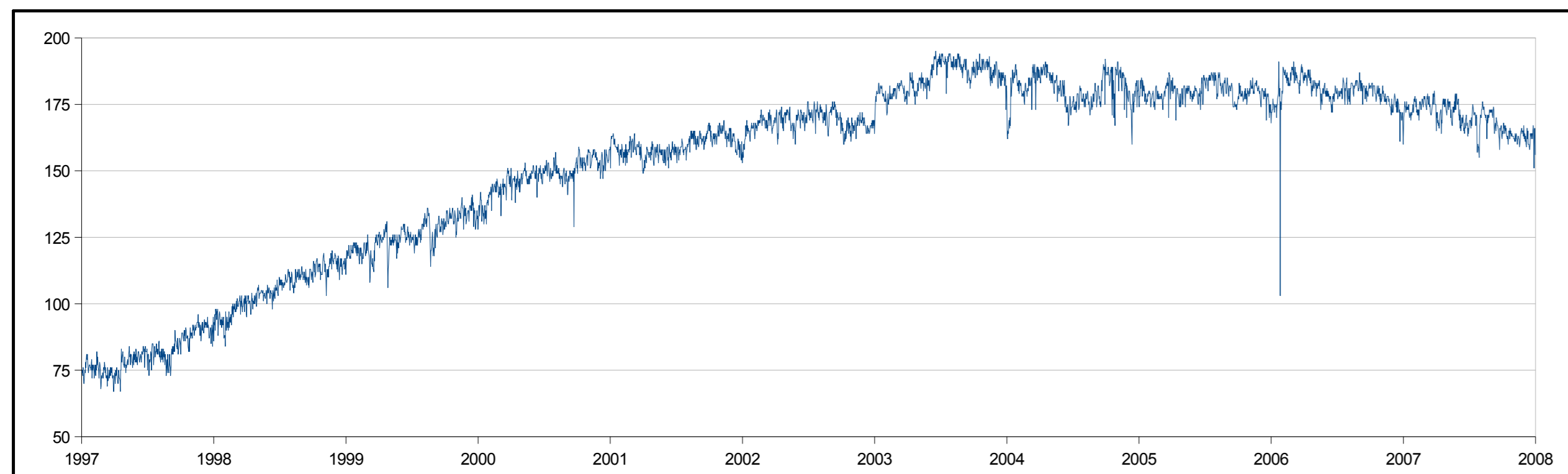
Fig. 1 Daily number of stations evolution at ULR TAC

The GPS processing time increases exponentially with the number of stations available. In order to overcome this limitation, it is usual to split the whole daily network in several sub-networks, process each sub-network independently and then combine again the solutions into a unique daily solution.

Five global, manually-selected, permanent sub-networks, called here "static sub-networks", were used at the ULR TAC for the previous GPS re-processing started in 2006 (Fig. 2 for example), using GAMIT software. With this configuration, the stations included in each sub-network were always the same, even if their data were not available for a specific processing day, making the geometry worse and using an unnecessary number of sub-networks in the processing (Fig. 3).
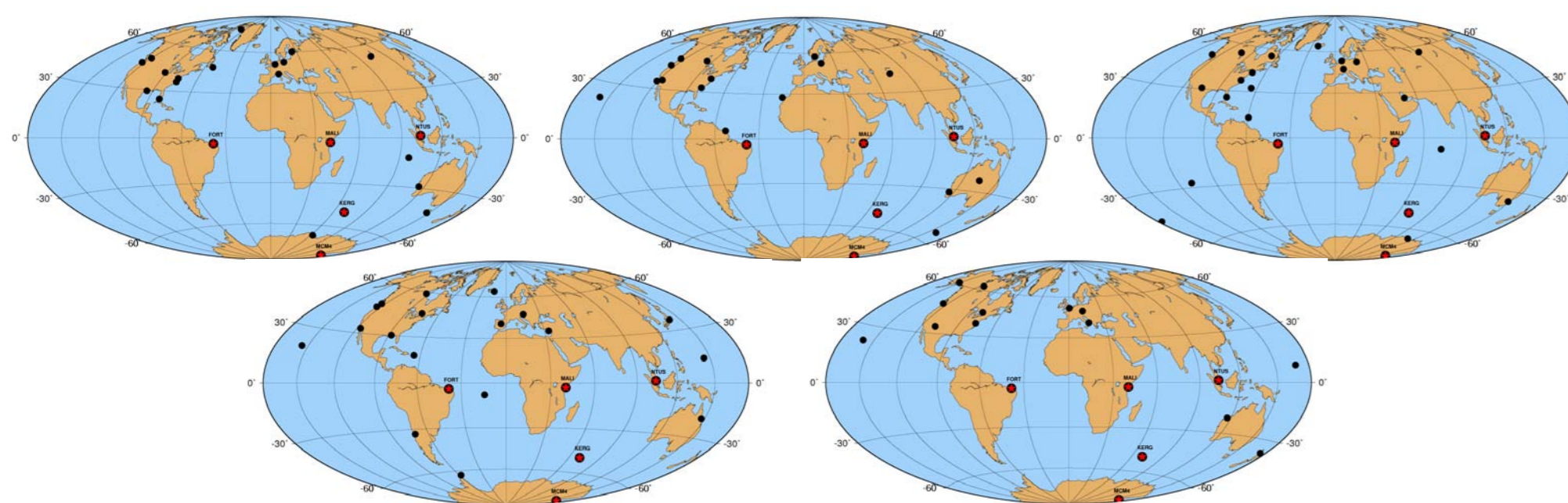
Fig. 2 Static sub-networks for DOY 336 of 1997

This static configuration is compared with a new station distribution using global, automatic, daily-variable sub-networks, called here "dynamic sub-networks", with up to 50 station maximum per sub-network (Fig. 4). These dynamic sub-networks were extracted based on an a priori knowledge of the daily available stations for which data existed and the 3D distance between them, in such a way that nearby stations were distributed in different sub-networks, in order to obtain a regular distribution based on geometry. The stations used to combine the sub-networks were selected dynamically with the same criteria, but using only IGS Reference Frame stations. This procedure came up with six stations retained, usually one station near each North and South Poles and another four near the Equator.
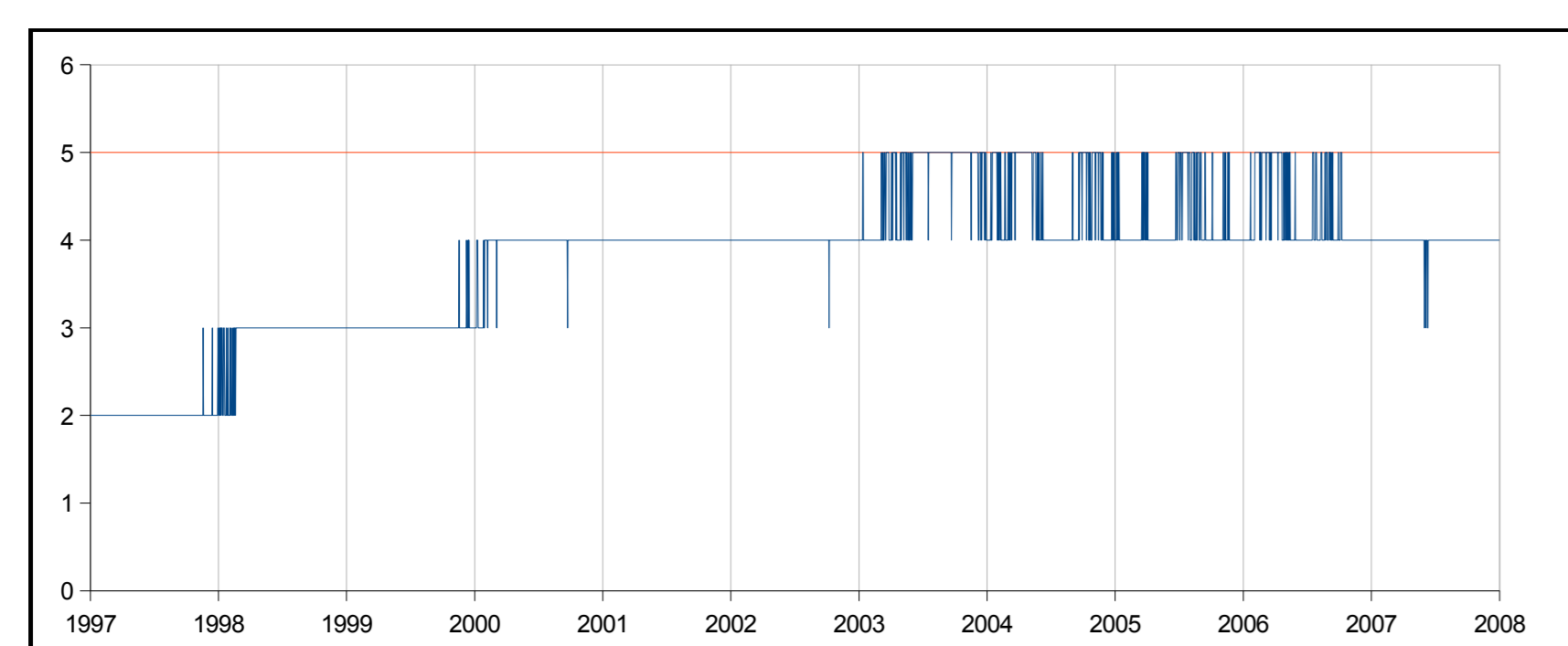

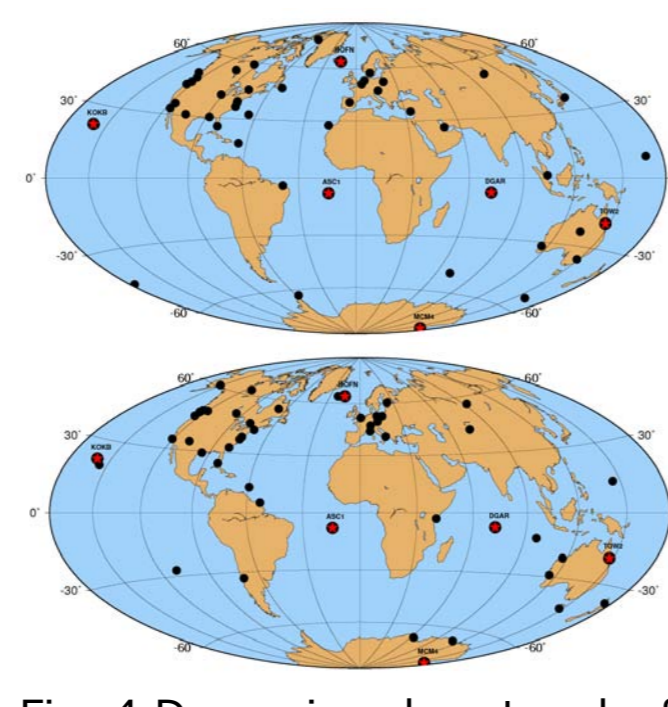Fig. 3 Number of static (red) and dynamic (blue) daily sub-networks

Fig. 4 Dynamic sub-networks for DOY 336 of 1997

In this work, static versus dynamic sub-network configurations were compared. All the available GPS data (225 stations for 11 years) were twice reprocessed with the same analysis strategy using these two approaches (more details at: *http://igscb.jpl.nasa.gov/ igscb/center/ analysis/ulr.acn*). We show the influence of the station distribution on the GPS processing quality by means of the greater number of observations, the improved estimated orbits and the effect on the reference frame realization.

② ☰ RESOLVED AMBIGUITIES IMPACT ☰

We extracted the percentage of double-differenced resolved ambiguities for each sub-network and then we computed the mean daily value for the static and dynamic approaches. The dynamic sub-networks showed a **noticeable improvement in the percentage of fixed ambiguities, up to 20%** (Figs. 5 and 6).
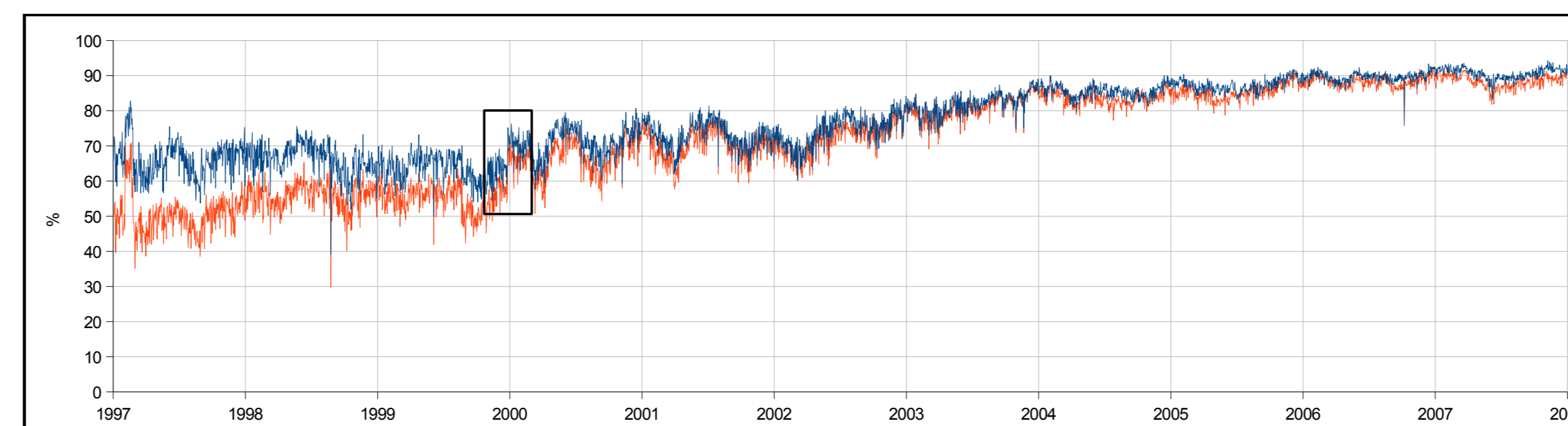

Fig. 5 Percentage of static (red) and dynamic (blue) resolved ambiguities
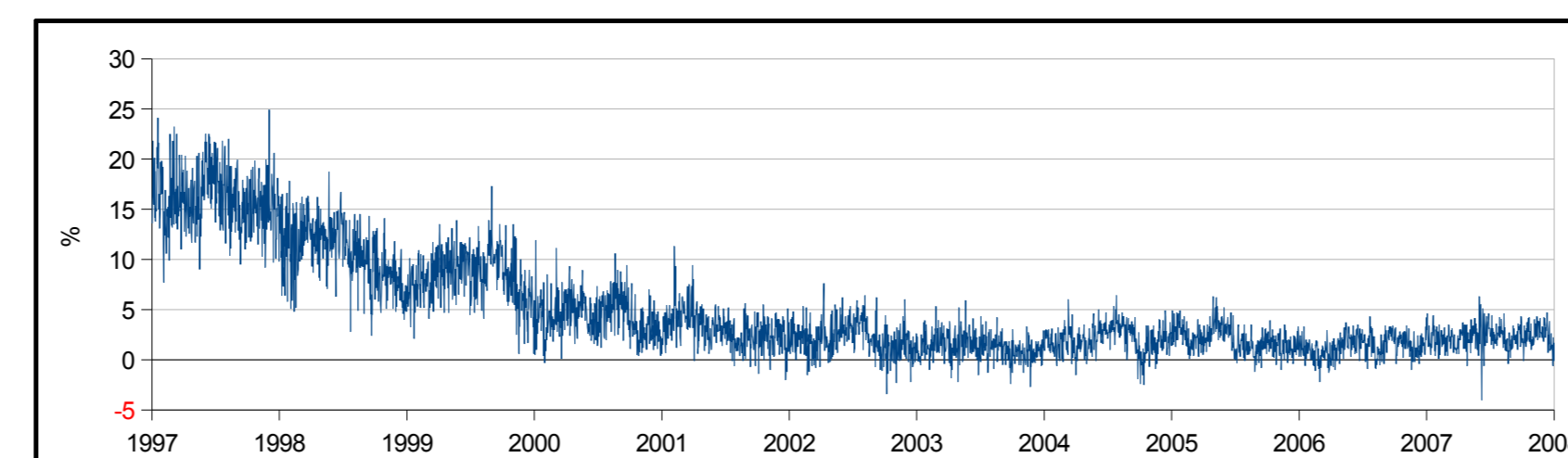

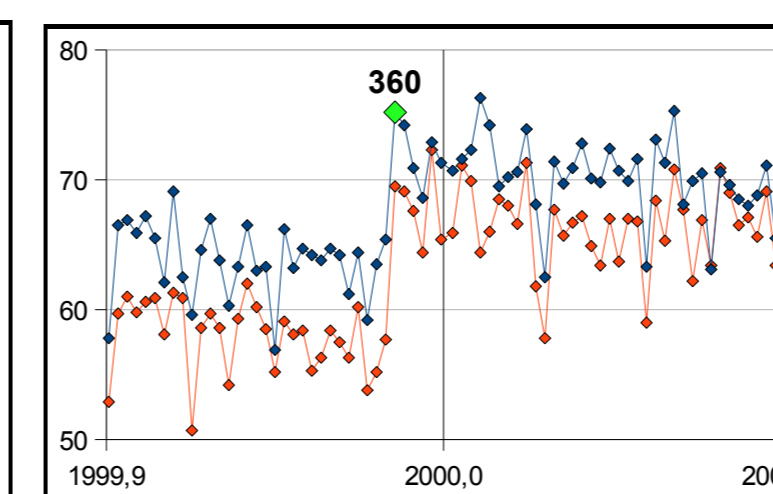Fig. 6 Difference in the percentage of resolved ambiguities (from Fig. 5)

Fig. 7 Zoom of Fig. 5

In 2000, we detected a discontinuity in the resolved ambiguities. A zoom (Fig. 7) revealed that the origin of the discontinuity was the starting point in the use of the Differential Code Bias (DCB) implemented in GAMIT software from December 26 1999 (DOY 360) onward. These DCB corrections are provided by the CODE IGS Analysis Center.

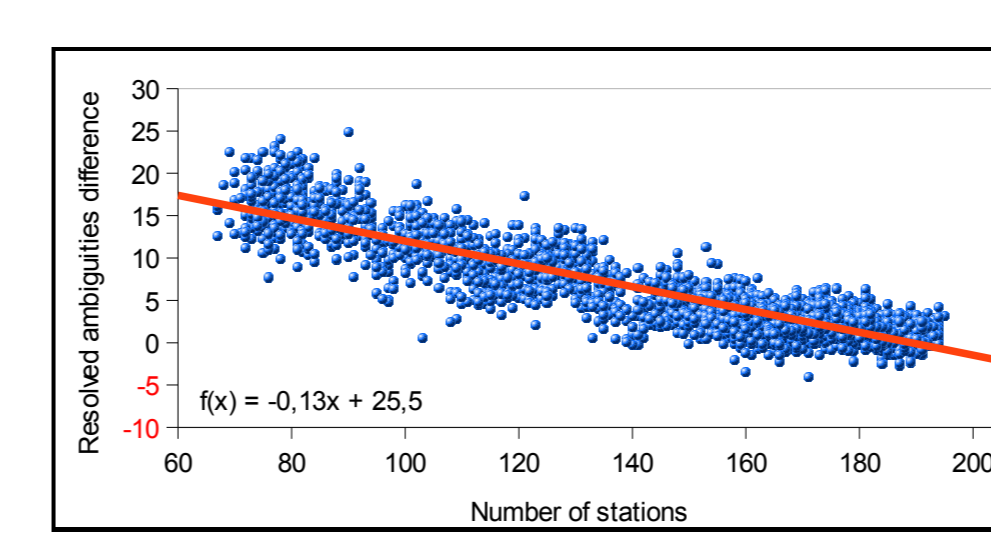Finally, Fig. 8 confirmed the role of the geometrical distribution of the stations.

Fig. 8 Correlation between number of stations and the difference of the resolved ambiguities

③ ⚽ REFERENCE FRAME IMPACT ⚽

For each approach, static and dynamic, daily solutions combined with GLOBK were stacked into weekly solutions. These weekly solutions were further stacked in one long-term solution using CATREF software. These stacked solutions were internally compared between them by a Helmert transformation of 14 parameters. (Figs. 12a and 12b). The impact of the dynamic sub-networks distribution on **vertical velocities WRMS reached 0.7 mm/year** in average, a very important issue for the TIGA Pilot Project objective.

Furthermore, the weekly repeatability (WRMS) w.r.t. the stacked solution were extracted for each solution (Fig. 14). The differences between them (Fig. 13) reached up to 2 mm.

	East	North	Up
Positions (mm)	1.0	0.9	2.6
Velocities (mm/yr)	0.3	0.3	0.7

Fig. 12a WRMS Dynamic/Static

	TX (mm)	TY (mm)	TZ (mm)	Scale (ppb)
	0.4	-0.2	-0.1	0.02
rates	-0.1	0.1	-0.1	0.02

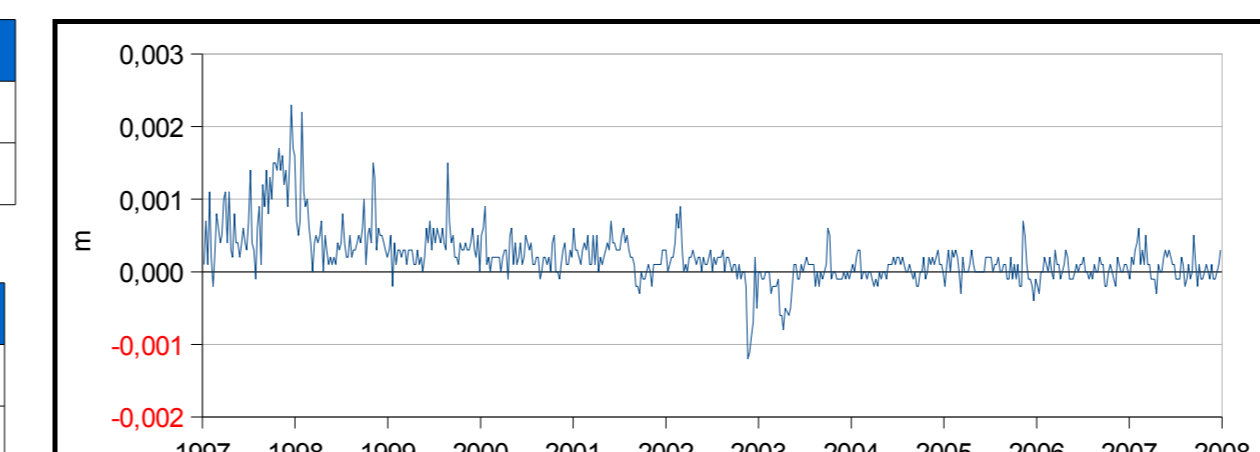Fig. 12b Transformation parameters Dynamic/Static

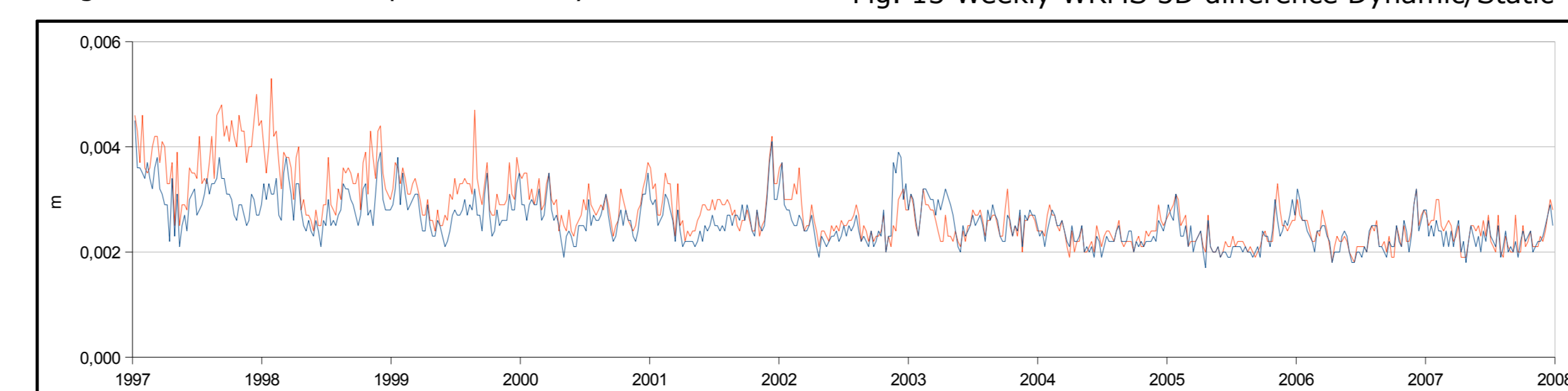Fig. 13 Weekly WRMS 3D difference Dynamic/Static

Fig. 14 Weekly WRMS 3D Dynamic (blue) and Static (red)

④ 🛰 ORBIT ESTIMATION IMPACT 🛰

For each sub-network, we estimated orbital parameters and then we combined these sub-network parameters using GLOBK to create a daily combined orbit. For each daily combined orbit, we estimated a Helmert transformation of 7 parameters (3 translations, 3 rotations and scale) between the static and the dynamic approach. The 3D RMS between them was extracted and plotted too (Fig. 11).

The greater number of resolved ambiguities of the dynamic approach back towards 1997 is transmitted into a **continuously greater RMS between the two estimated orbits, up to 3 cm**. The transformation parameters are almost negligible.
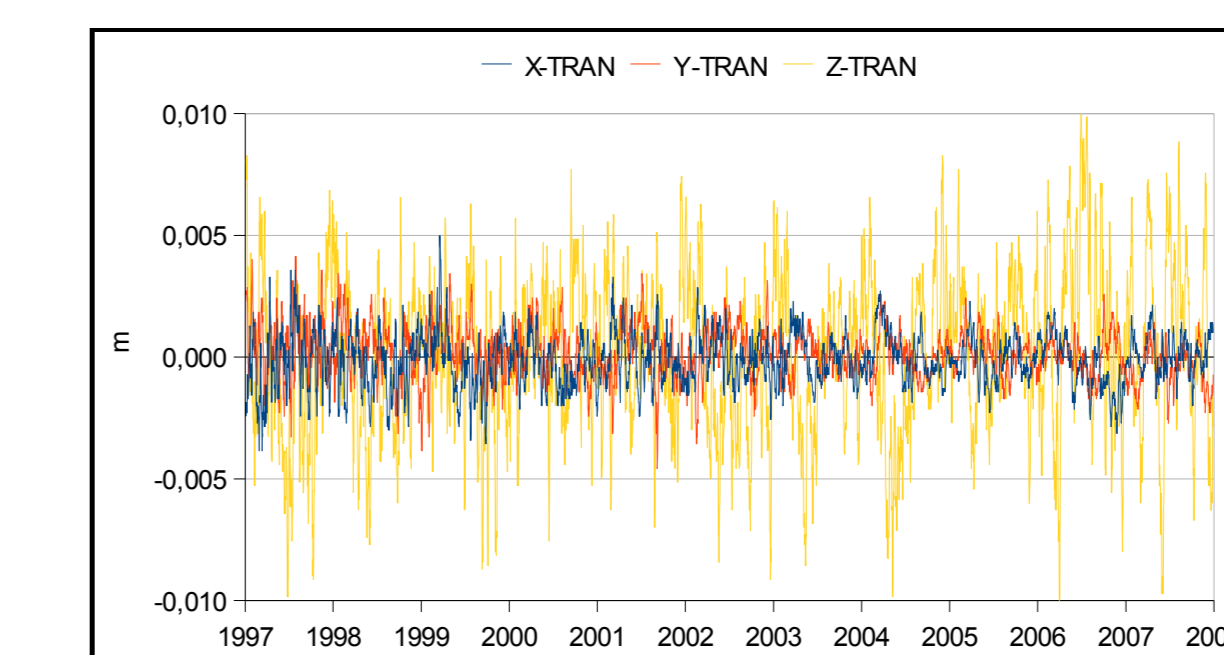

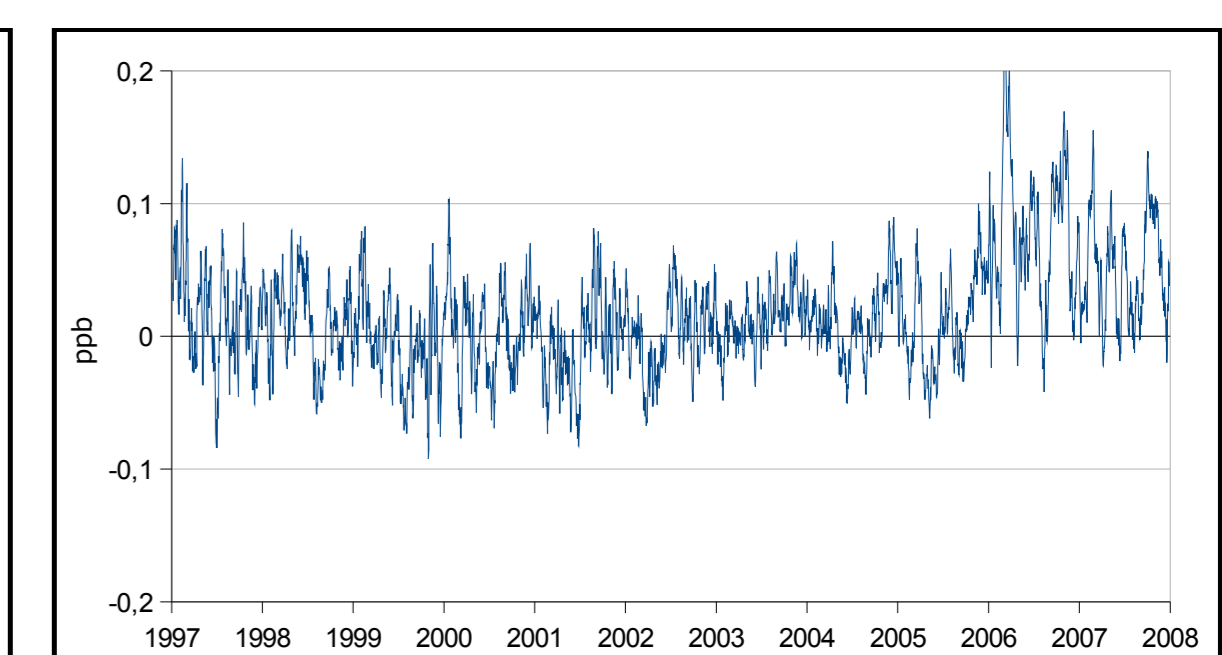Fig. 9 Orbit Translations (7-day moving average)

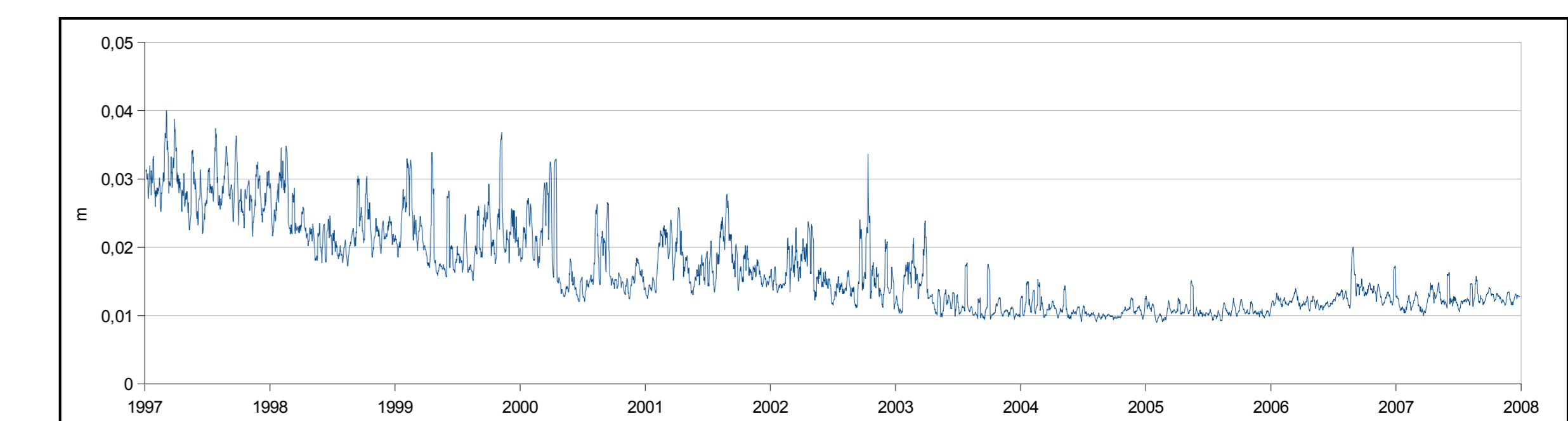Fig. 10 Orbit scale (7-day moving average)

Fig. 11 Orbit 3D RMS (7-day moving average)

⑤ 🔖 CONCLUSION 🔖

☞ The main improvement showed by this work is the increase of the available double-differenced observations, notably for the pre-2000 period up to more than 20%, using a geometrically-based daily distribution of stations, called dynamic sub-networks, in contrast to a classical static manually-selected sub-networks scheme.

☞ This greater number of double-differenced observations translates into an improvement of the estimated GPS parameters, like orbits, or an improvement of the reference frame implementation. Other parameters (not shown here) like tropospheric delays, satellite clocks (indirectly) or Earth Orientation Parameters are expected to be improved in the same way.

☞ The ULR TAC has never processed pre-1997 GPS using the static sub-networks scheme, due to the poor quality of the results. This new progress in the GPS processing strategy encourages us to reprocess additional 3 years (1994-1996), a very important issue within the framework of the TIGA Pilot Project and within the IGS re-analysis campaign.

☞ Another main issue found in this study was the impact of the use of the DCB corrections. At the end of 2008 (moment where all GPS data were analyzed), only DCB corrections for the post-2000 period were available. We discovered a noticeable jump of resolved ambiguities of 10% at this epoch. The fact that DCB corrections for the pre-2000 period (1994-2000) has been recently released by the CODE Analysis Center should further improve the results for that period, when GPS network was very sparse.